Development and characterization of a shape memory polymer composite actuator for morphing structures

Abdul Basit

Reference No. 12MULH1081 Year 2012

Ecole Doctorale ED-494 Jean-Henri Lambert

Université de Haute Alsace (UHA)

Laboratoire de Physique et Mécanique Textiles (LPMT)

A thesis submitted to fulfil the requirement for the degree of Doctor of Philosophy (PhD) in Mechanics

Submitted by: **Abdul Basit**

18 December 2012

Development and characterization of a shape memory polymer composite actuator for morphing structures

Développement et Caractérisation de composites à géométrie adaptative et à propriété de mémoires de formes

---

Jury Members

Prof. Dr. Jean François GANGHOFFER	Université de Nancy 1	Reviewer
Prof. Dr. Georges AKHRAS	Royal Military college of Canada	Reviewer
Prof. Dr. Christelle DELAITE	ENSCMu, UHA	Examiner
Prof. Dr. Emmanuel FOLTETE	Université de Dijon	Examiner
Prof. Dr. Bernard DURAND	ENSISA, UHA	Supervisor
Dr. Gildas L'HOSTIS	ENSISA, UHA	Co-supervisor
Mr. Fabrice LAURENT	UHA	Invited Member

Abstract

Shape memory polymers (SMPs) are the materials which can return to their original shape when a suitable stimulus (e.g. heat) is provided. These polymers are programmed through shape memory cycle that consists of two parts: programming part which gives shape memory effect (SME) i.e. temporary shape to the polymer and the recovery part which return it to its original shape. SMPs have low stiffness, therefore, produce large recoverable strains, but produce low recovery forces. However, SMP composites produce larger recovery forces as they are relatively rigid but have less recoverable strains. Moreover, strong shape memory actuators can be produced if two different effects can be combined in a single structure. An already active structure (e.g. shape memory alloys) can be embedded in SMP. Consequently, a strong coupled actuator can be obtained. In this work, the shape memory property of CBCM composite (an active composite that works on bimetallic affect) has been studied. CBCM stands for controlled behavior of composite material. CBCM activeness and its SM property has been coupled together to obtain a strong actuator. SM property has been obtained through thermo-mechanical programming at a temperature higher than glass transition temperature (Tg) of Epoxy resin used for its fabrication. The CBCM actuating properties have been studied through different one-step recoveries (unconstrained, constrained and recovery under load). Moreover, different asymmetrical CBCM composites have been developed by changing the position and orientation of the different layers used. These have been studied for their different actuation properties. Similarly, multi-step recoveries (unconstrained and constrained) have also been performed to show multi-step actuation capabilities in CBCM. The actuating properties of CBCM have also been compared with symmetrical composite (SYM) to show the advantage of coupled properties in CBCM. It has been found that CBCM has the ability to give high strain, high recovery forces. Also, it can recover under load and recover to its original position at the temperatures lower than the deforming temperature used in the programming cycle.

Acknowledgement

First of all, I want to express my deep gratitude to my supervisor Prof. Dr. ***Bernard DURAND****, and Dr.* ***Gildas LHOSTIS*** *(co-supervisor) for giving me the opportunity to develop this experience. I really appreciate their valuable guidance and advices throughout my thesis work. They motivated me in every way and put all their efforts to provide a favourable working environment. Without their contribution, it was impossible for me to accomplish my work. I express my heartiest gratitude to* ***Higher Education Commission (HEC) PAKISTAN*** *for financing me and providing me the opportunity to study abroad and develop new skills. I would also like to acknowledge all my country fellows in France especially in ENSISA (Sheraz AHMAD, Abher RASHEED, Arman SHAFI and Ahmad ALI). They were always there to share my joys and sorrows and to support me morally and spiritually. Last but not the least I am highly grateful to my* ***beloved family,*** *especially* ***my parents and my eldest brother*** *who supported me in every way throughout my career. They have always remained a constant source of encouragement and motivation for me.*

Dedication

I dedicate my thesis to my wonderful parents especially to my father

Important Nomenclature and Abbreviations

SMP	Shape Memory Polymer
SMA	Shape Memory Alloy
CBCM	Controlled Behavior of Composite Material
CBCM-SMPC	CBCM shape memory composite
SME	Shape Memory Effect
1W	One-way
2W	Two-way
Tg	Glass Transition Temperature
T_D	Deforming Temperature
Ta	Ambient Temperature
T_R	Recovery Temperature
$d_A (\varepsilon_A)$	Activation Displacement (Activation Deformation)
$d_F^I (\varepsilon_F^I)$	Initial Fixity Displacement (Initial Fixity Deformation)
$d_S (\varepsilon_S)$	Specific Displacement (Specific Deformation)
$d_{RA} (\varepsilon_{RA})$	Recovery Activation Displacement (Recovery Activation Deformation)
$d_{RF} (\varepsilon_{RF})$	Recovery Fixity Displacement “or Residual Displacement” (Recovery Fixity Deformation or Residual Deformation)
$d_{RT} (\varepsilon_{RT})$	Total Recovery Displacement (Total Recovery Deformation)
F_B	Blocking Force
F_T	Total Force
F_S	Force of Stabilization
F_E	Elastic Force

F_R	Recovery Force
F_{RES}	Residual Force
F_{RT}	Total Recovery Force
F_G	Given load during recovery under load
W_{RT}	Total Recovery Work
W_R	Work of Recovery
W_A	Work of Activation
W_G	Work under load during recovery under load

Résumé de mémoire de thèse en Français

Chapitre I. Introduction

Sous l'action d'un stimulus extérieur, les polymères à mémoire de forme (PMF) ou shape memory polymère (SMP) sont des matériaux qui peuvent revenir d'une position déformée à leur position d'origine. La plupart des SMP sont stimulés thermiquement. Pour obtenir cette propriété, l'élaboration d'un polymère à mémoire de forme, comporte deux étapes. L'étape de programmation durant laquelle le polymère est chauffé à une température dite de fixation, mis en forme puis refroidis, la forme temporaire est ainsi imposée et fixée. L'étape de recouvrance pendant laquelle après stimulation thermique à une température dite de recouvrance, le polymère recouvre sa configuration initiale.

Les principales propriétés des SMP sont leur faible densité, notamment comparée aux alliages métalliques à mémoire de forme (AMF) et leur capacité à recouvrir des fortes modifications géométrique (plusieurs centaines de pourcent). Cependant cette recouvrance ne peut se faire que pour un niveau de contrainte imposé faible 1 à 3 MPA comparé à celui obtenu pour les AMF de 0.5 à 1 GPA. Ce faible niveau de contrainte représente une limite des SMP pour des applications nécessitant une recouvrance de la géométrie tout en supportant un effort important. Par contre l'élaboration et la mise en forme de polymère à mémoire de forme sont classiques, et identiques à celles des autres polymères, car c'est l'étape ultérieure de programmation qui conduira aux propriétés de mémoire.

Pour surmonter le problème de recouvrance sous charge et d'augmenter ainsi les capacités d'actionnement des SMP, une solution consiste à renforcer le polymère de base par des particules élastiques ou par des renforts fibreux continus ou discontinus. On parlera alors de composite à mémoire de forme ou shape memory composites (SMC). Cependant l'augmentation de l'effort d'actionnement se fait au détriment de la recouvrance géométrique.

Les autres limitations des SMP ou des SMC sont principalement leur incapacité à recouvrir complètement leur géométrie initiale pour des températures de recouvrances inférieures à la température de fixation du cycle de programmation, et la recouvrance totale de la géométrie ne peut être obtenus sous chargement imposé. Ceci peut être complété par le fait que les structures obtenues uniquement à partir de SMP ou SMC ne possèdent pas lors de déformation flexionnelle, la propriété d'inversion de la courbure. Cette propriété peut être conférée uniquement par l'utilisation d'éléments intégrés de type alliage à mémoire de forme.

L'objectif de ce travail est de coupler dans une structure composite classique l'effet de mémoire du polymère avec des propriétés d'actionnement induite par une activation thermique de la structure. Cette propriété d'actionnement utilise l'effet M3C ou CBCM qui repose sur l'utilisation de l'asymétrie du composite lors d'une activation thermique. La démarche expérimentale mise en place permet de caractériser les différentes étapes clef du processus d'obtention de ce nouveau composite actif le CBCM-SMPC: activation de la structure non programmée, programmation de la structure et activation et recouvrance de la structure programmée. Pour caractériser les performances d'actionnement du CBCM-SMPC, l'ensemble des effets intervenants au cours de ces différentes étapes seront isolés et analysés. L'influence de la constitution de la structure composite sera également étudiée notamment au travers de son degré d'asymétrie. Enfin les propriétés de stabilisation des géométries temporairement fixées sont étudiées notamment dans le cas où une étape de relaxation des contraintes est introduite dans le cycle de programmation.

Chapitre II. Bibliographie positionnement du travail

Les matériaux intelligents sont des matériaux qui possèdent la capacité de changer leurs propriétés physiques sous l'action d'un stimulus extérieur. Les stimuli peuvent être la chaleur, la pression, un champ électrique ou magnétique. La réponse du matériau stimulé peut être le changement de sa forme, le changement de son comportement rhéologique (raideur, viscosité) ou la modification de propriétés internes comme les propriétés électriques (diélectrique, résistivité).

Les matériaux à mémoire de forme sont métalliques, matériaux à mémoire de forme (AMF ou SMA), ou polymérique, polymère à mémoire de forme (PMF ou SMP). A partir d'une géométrie initiale, ils ont la capacité de se déformer sous un chargement thermomécanique et de fixer une forme temporaire, puis sous l'action d'une activation thermique de revenir à leur géométrie initiale.

Depuis ces dernières années, de nombreux travaux ont porté sur les AMF. Cependant bien que possédant des propriétés de mémoire intéressante, tel que les efforts restituables, la généralisation de leur utilisation c'est heurtée notamment à leur masse, à leur cout de fabrication et à leur usinabilité.

Par palier ces inconvénients, des travaux ont portés sur la recherche et la mise au point de matériaux de substitution, en particulier les polymères à mémoire de forme. Contrairement aux AMF, différents stimuli peuvent être utilisés pour l'actionnement du SMP : un champ magnétique, l'humidité, la lumière, les infrarouges, mais le stimulus le plus utilisé reste la température.

Le fonctionnement des SMP n'est pas similaire à celui des SMA qui repose sur un phénomène de changement de phase. C'est l'existence dans la structure macromoléculaire du polymère de deux types de segments moléculaires (un souple et un rigide) qui va lui conférer cette propriété de mémoire. A température ambiante, la rigidité mécanique du polymère est donnée par les fortes propriétés élastiques des segments. A haute température, la rigidité du polymère soumis à un chargement mécanique est affectée par le mouvement Brownien des segments souples qui s'accentue. Durant le refroidissement sous maintient, ces segments souples se figent en position et assure le maintien d'une nouvelle position géométrique du matériau après la phase de déchargement. Sous l'action d'un nouveau stimulus thermique, l'augmentation rapide du mouvement brownien des segments souples, permet au matériau sous l'action des segments rigides de revenir dans sa position initiale.

Les principales étapes pour la réalisation d'une structure en polymère à mémoire de forme sont :

- La réalisation de la structure en SMP sous sa forme originale, puis chauffer cette structure de la température ambiante jusqu'au-delà de la température de transformation du polymère.
- Mettre en forme la structure maintenue à la température de transformation, par l'application d'un chargement mécanique
- Refroidir la structure jusqu'à la température ambiante, tout en la maintenant sous charge
- Décharger la structure afin d'obtenir la géométrie temporaire, c'est la dernière étape du cycle de programmation
- chauffer la structure au-delà de la température de la température de transition pour retrouver la géométrie initiale, c'est l'étape de recouvrance

Les différents polymères à mémoires de formes peuvent être caractérisé à partir le leur capacité lors de l'étape de recouvrance à retrouver différentes géométries mémorisées. On parlera d'effet unidirectionnel (1W effect) quand le polymère retrouve sa forme initiale à partir d'une ou de plusieurs géométries fixées et y reste même après une nouvelle activation. Pour l'effet bidirectionnel (2W effect) le polymère a la possibilité par activations successives d'évolué entre la géométrie initiale et la ou les géométries fixées (Figure 1). On parlera de dual shape quand le polymère possède deux géométries, sa géométrie initiale et une géométrie fixée, de triple shape dans le cas de deux géométries fixées, et de multi-shape pour un grand nombre de géométries fixées.

La propriété de triple Shape/1W effect, est illustré figure 2 et figure 3 dans le cas d'une structure laminée bicouche constitué de deux résines époxy possédant respectivement des températures de transition vitreuse distinctes. Un cycle de programmation constitué de deux chargement thermomécaniques conduit à l'obtention de trois géométries [41]. Après l'étape de recouvrance à 90°C la structure retrouve sa configuration initiale mais avec déprogrammation, c'est un 1W effect.

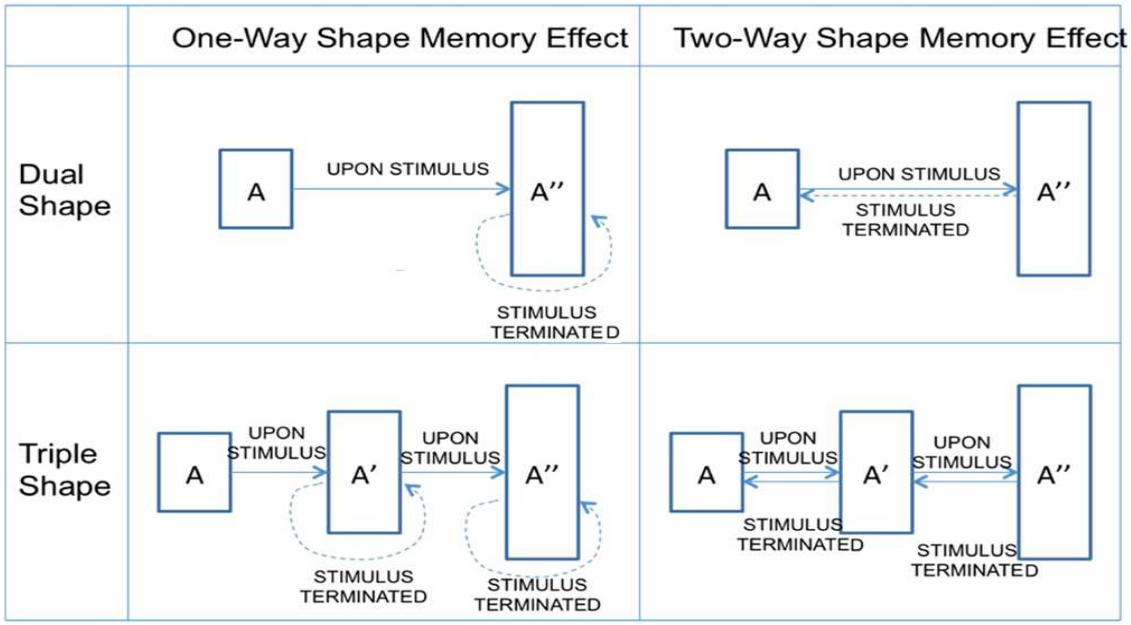

Figure 1 : Propriété de mémoire de forme pour un SMP [11].

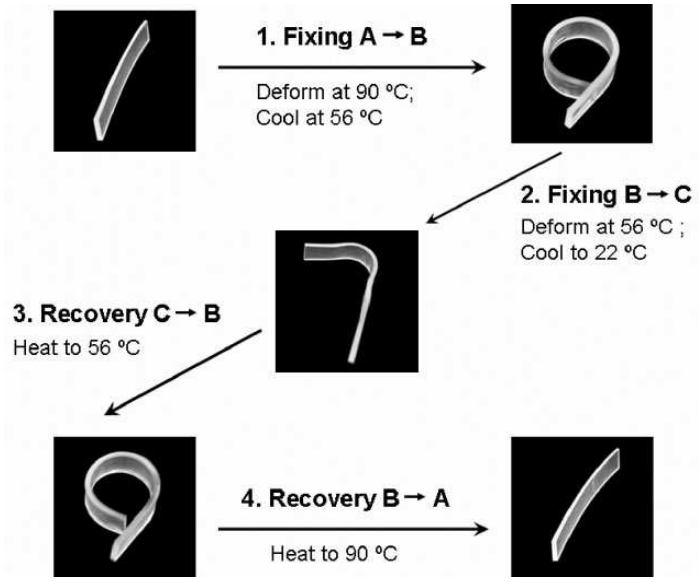

Figure 2. Géométries caractérisant la propriété de triple Shape [41]

La propriété de dual Shape/2W effect, est illustré figure 4 dans le cas d'une structure laminée pour laquelle l'effet bilame est amplifié par l'utilisation d'une couche en polymère à mémoire de forme [36]. Le polymère à mémoire de forme est réalisé à partir d'une résine polyuréthane qui a été pré étirée lors du cycle de programmation. L'activation thermique de la

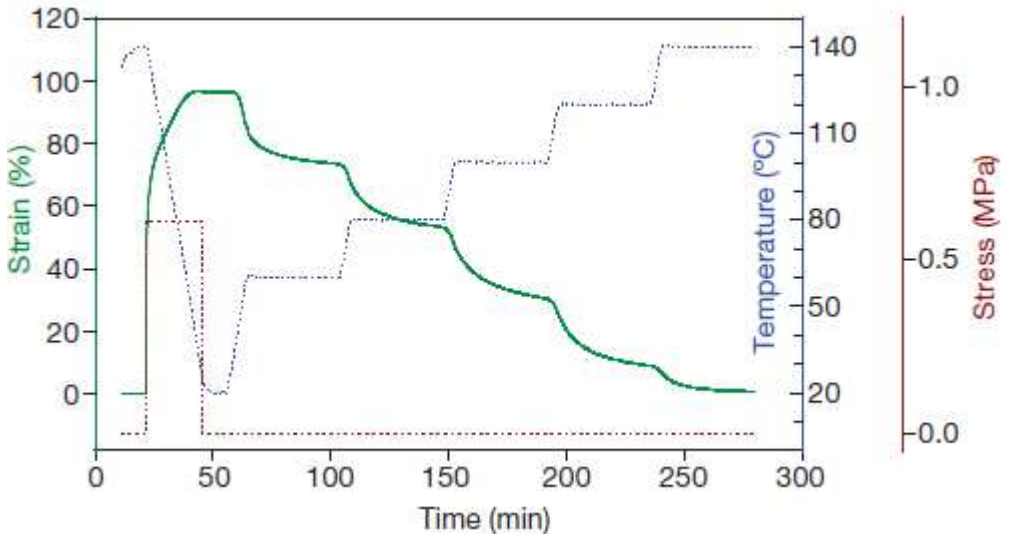

Figure 3. Evolution des grandeurs physiques associées à la propriété de Triple Shape.

structure active les propriétés de recouvrance du polymère à mémoire de forme, la structure fléchis, le substrat emmagasine une énergie de déformation, qui assure le retour dans la configuration initiale, correspondant à la mise sous tension de la couche en polymère à mémoire de forme. Le 2W effect repose donc sur la capacité lors de l'activation de la structure à emmagasiner au sein d'élément de la structure de l'énergie de déformation.

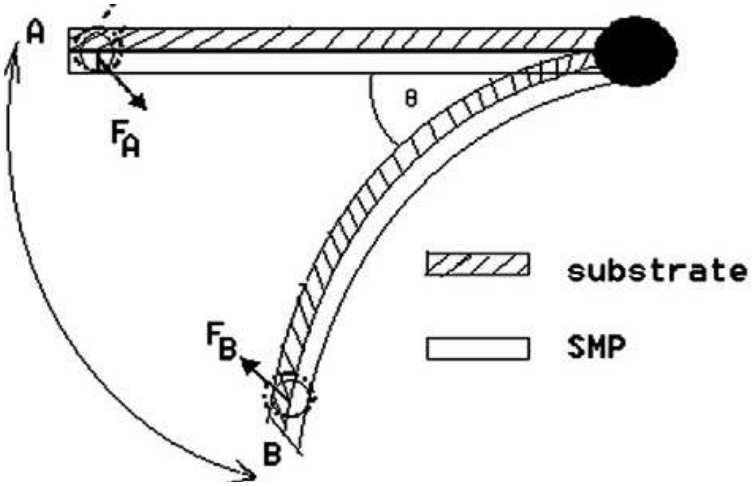

Figure 4. Propriété de 2W actuation [36]

Un composite à mémoire de forme (ou shape memory polymer composite, SMPC) est obtenu par la combinaison d'un polymère à mémoire de forme et d'un élément renforçant, renfort textile ou métallique. Dans le cas de renforts non métalliques ceux-ci peuvent être des particules telles que des micro ou nano-fibres ou des renforts continus. Ces renforts peuvent être

unidirectionnels ou bidirectionnels dans le cas de renforts tricotés ou tissés. L'ajout d'éléments renforçant dans un polymère à mémoire de forme conduit à une augmentation de sa rigidité. Concernant les propriétés de recouvrances, l'effort de recouvrance est augmenté au détriment de la déformation.

La température est des vecteurs privilégiés pour réaliser l'activation du SMP ou SMPC. Elle peut être également utilisée pour le développement d'actuateur thermique tel que le CBCM (Composite Material Controlled Behavior). Ce dernier est un composite thermiquement actif à géométrie adaptative ou morphing structure. Son fonctionnement repose sur des propriétés de gradient au sein de la structure composite. Ce gradient peut être matériel, différence de coefficient de dilatation entre les constituants, on parlera alors de simple effet ou effet température (figure 5). Mais il peut être également physique, distribution non constante de la température au sein du composite, on parlera alors de «double effet» ou «effet gradient». Double effet car dans ce cas la structure à la capacité de se déformer de part et d'autre de sa configuration initiale. Pour un composite laminé, le simple effet est obtenu pour une composition asymétrique de couches possédant des coefficients de dilatation différents, le double effet peut être obtenu avec une structure composite symétrique contenant une couche isolante, par exemple une structure sandwich.

La particularité du CBCM réside dans l'utilisation d'une couche thermiquement active qui a pour objectif de chauffer par effet Joules le composite. Le système d'actionnement est totalement intégré au composite qui devient ainsi un actionneur à part entière, et sa réponse c'est-à-dire son niveau de déformation est directement relié à l'intensité du courant parcourant la couche active.

Cette couche thermiquement active peut également être utilisée pour conférer à la structure composite des propriétés de mémoires. Ainsi grâce à un cycle de programmation, ces propriétés de mémoire seront naturellement couplées aux propriétés de changement de forme du CBCM, simple effet ou double effet.

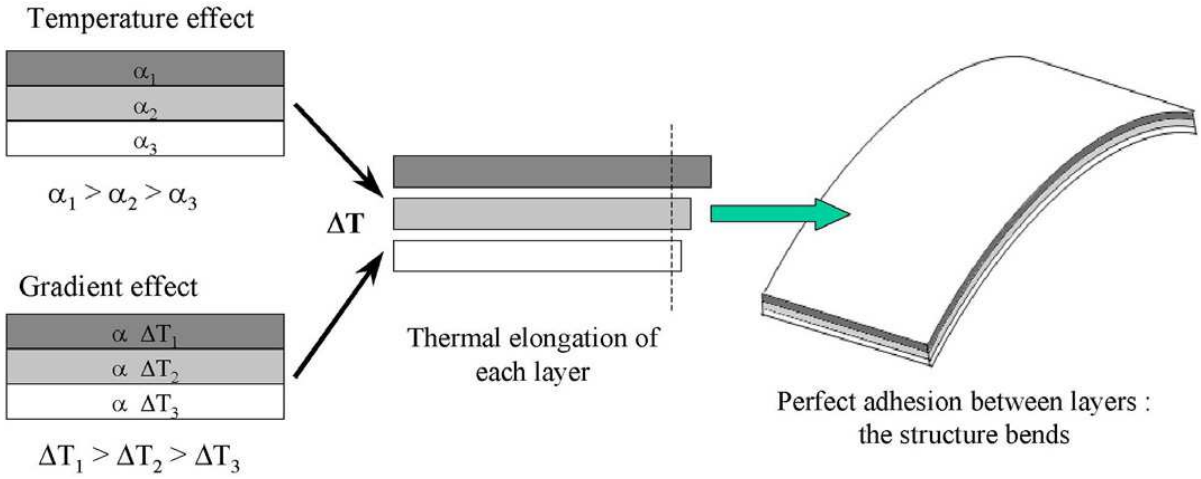

Figure 5. Principe du CBCM, effets gradient et température.

Chapitre III. Matériel et Méthodes

Dans ce travail, nous avons préparé des composites asymétriques avec effet CBCM (effet température) et comme référence, des composites de constitution symétrique (SYM). Les plaques composites de dimensions 395 × 12,5 × 2 mm^3 sont constituées deux couches de tissu de verre, de deux couches d'unidirectionnel de verre et deux couches de tissu d'aramide. Les composites ont été réalisé par moulage au contact avec mise sous pression dans le moule. Apres démoulage les pièces ont été étuvées suivant le cycle recommandé par le fabricant de résine. Ce cycle doit permettre d'obtenir une transition vitreuse de la matrice T_g=135°C.

Le test mécanique utilisé pour le cycle d'éducation et de recouvrance est un essai de flexion d'une plaque en appuis linéique sur deux de ces bords opposés (distance entre appuis L=300mm) et soumise en son centre à une force ponctuelle. Cet essai est réalisé avec une machine de traction MTS-20 équipée d'un capteur de 100N (précision de 0.01N) et commandée par le logiciel Testworks qui permet la mise en place de tout type de trajet de chargement.

Pour créer les propriétés de mémoires de formes, les plaques composites ont été soumises à un cycle thermomécanique de programmation ou d'éducation.

Ce cycle commence par une précontrainte de 0,3 N, la position correspondante (point A fig. 6) est prise comme position initiale pour toutes les mesures de déplacement. La plaque est ensuite chauffée à la température de déformation (T_D = 150 ° C) jusqu'à stabilisation thermique (800

secondes). La déformée de la plaque est caractérisée par le déplacement libre d_A donné par le point B.

Sur la plaque toujours à sa température de déformation on impose en son centre un déplacement spécifique ds = 25 mm (parcours BC). Ce déplacement a été préalablement définis pour assurer lors de la déformation aucune apparition de dommage de type délaminage.

Ce déplacement est maintenue pendant le refroidissement de la plaque par convection naturelle jusqu'à la température ambiante Ta (1000 secondes). Ceci se traduit par une diminution de l'effort mesuré au centre de la plaque (parcours CD). Après refroidissement, par un asservissement en force, la force est ramenée à la valeur de précharge de 0,3 N (DE). Cette position finale (point E) définie la déformée finale de la plaque après sa programmation, le déplacement correspondant est appelé fixité initiale ou déplacement initial fixé.

Sur cette plaque programmée, les propriétés de mémoires de formes sont ensuite investiguées. Trois types d'essais sont utilisés : deux essais standards de la littérature, l'essai de recouvrance sans contrainte « unconstrained recovery », l'essai de recouvrance sous contrainte « constrained recovery » et un essai que nous avons développé spécifiquement recouvrance sous chargement partiel « partial recovery under load ».

L'essai de recouvrance sans contrainte consiste à chauffer la plaque à une température de recouvrance T_R, plaque sur ces appuis et sans chargement extérieur autre que son poids. La quantité mesurée est le déplacement de recouvrance. Si la température T_R est égale à la température de déformation T_D on parlera de recouvrance unique « one-step recovery », si T_R est inférieure à T_D de recouvrance multiple « multi-step recovery ». Dans ce cas jusqu'à T_D, la plaque subit plusieurs cycles de chauffe à $T_R+\Delta T$, où ΔT est un incrément de température.

L'essai de recouvrance sous contrainte consiste à chauffer la plaque à une température de recouvrance T_R, plaque sur ces appuis et maintenue dans la position issue du cycle de programmation. La quantité mesurée est la force de recouvrance. Si la température T_R est égale à la température de déformation T_D on parlera de recouvrance unique « one-step recovery », si T_R est inférieure à T_D de recouvrance multiple « multi-step recovery ». Dans ce cas jusqu'à T_D,

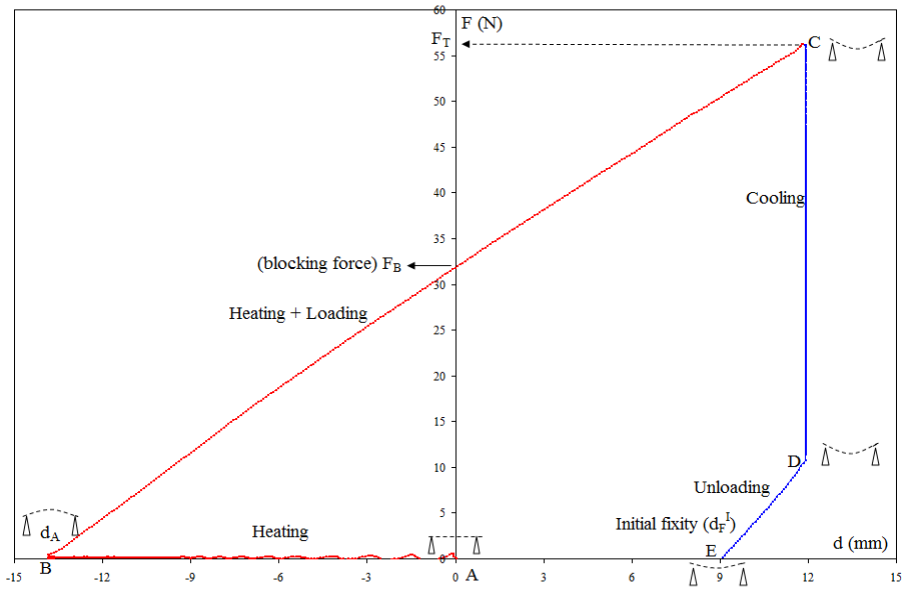

Figure 6. CBCM programming thermo-mechanical programming cycle

la plaque subit plusieurs cycles de chauffe à $T_R+\Delta T$, où ΔT est un incrément de température. A partir du produit du déplacement de recouvrance et de la force de recouvrances obtenus lors des essais précédents, il est possible de définir un travail de recouvrance. L'intérêt de l'essai de recouvrance sous chargement partiel est de pouvoir obtenir directement le travail de recouvrance. Cet essai est une combinaison des deux essais précédents, il consiste à chauffer la plaque à la température de recouvrance T_R, tout en maintenant par le système de régulation en force un effort fixé. Pour les composites asymétriques, si cet effort est l'effort de blocage, on a une mesure directe du travail de recouvrance uniquement due à la propriété de mémoire. L'effort de blocage est caractéristique d'une structure asymétrique et correspond à l'effort nécessaire pour maintenir la structure dans sa configuration initiale lors de son activation thermique.

Chapitre IV. Résultats et discussion

Ce chapitre est divisé en deux parties caractérisées par le type de recouvrance utilisé : recouvrance en une seule étape (one-step recovery) pour laquelle la température de recouvrance utilisée T_R est égale à la température de déformation T_D. Recouvrance en plusieurs étapes (multi-step recovery) pour laquelle la température de recouvrance prend successivement des valeurs comprises entre la température ambiante T_a et la température de déformation T_D.

Pour les plaques symétriques et CBCM, le recouvrement en une seul étape a été caractérisé pour les trois types de recouvrement, recouvrement sans et sous contrainte (unconstrained and constrained recovery) et recouvrement sous chargement partiel (partiel recovery under load). Pour le premier cycle de recouvrance sans contrainte à une température T_R=150°C, la plaque CBCM récupère 242 % du déplacement initial fixé, avec un déplacement de recouvrance total égal à d_{RT}=21,84 ± 1,26 mm (déformation de recouvrance associée ε_{RT}=7,28 % ± 0,42). Le résultat pour la plaque symétrique SYM est d_{RT}=9,15 ± 0,69 mm (ε_{RT}=3,05 ± 0,23 %) soit 100% du déplacement initial fixé. Cette différence entre les deux plaques CBCM et SYM s'explique pour le CBCM par l'addition à la propriété de recouvrance de la propriété d'activation, en effet on peut observer pour ce premier cycle de recouvrance que le déplacement initial fixé est recouvré pour une température égale à 90°C et non à 150°C comme la plaque symétrique.

Un résultat similaire est obtenus pour l'essai de recouvrance sous contrainte, à 150°C la force de recouvrance totale générée par le CBCM est égale à F_{RT}=48,54 ± 2,57N. Elle n'est que de 9,6 ± 0,33N pour la plaque SYM. Lors de nouveaux cycles de recouvrances (chauffe puis refroidissement), cet effort de recouvrance peut être de nouveau généré à une valeur identique. Cependant l'amplitude de cet effort est réduite car apparait lors du refroidissement une force résiduelle plus faible pour le CBCM que pour la plaque SYM.

Pour l'essai de recouvrance sous chargement partiel, après le premier cycle de recouvrance on peut observer une stabilisation des propriétés d'actuation des plaques CBCM et SYM. Cependant due à l'addition de la propriété de recouvrance avec celle d'actuation les performances du CBCM sont supérieures à celle de la plaque SYM. Une autre particularité que confère à la plaque CBCM l'addition des propriétés, est de pouvoir inverser sa courbure initiale sous charge. Ceci est impossible pour la plaque symétrique ou pour toute autre sorte de composite à mémoire de forme, c'est un résultat important de ce travail.

Une première étude portant sur les effets viscoélastiques lors du cycle de programmation nous ont conduit à intégrer dans ce cycle une étape de relaxation après le chargement sous température T_D (point C fig. 6). La durée de cette étape assure la stabilité de l'effort de

relaxation. Pour les plaques CBCM et SYM ayant subie ce nouveau cycle de programmation, les valeurs du déplacement initial fixé sont plus élevées que celle obtenus pour le cycle sans relaxation. Pour les trois tests de recouvrances les propriétés restent inchangées, même valeur de force de recouvrance et de déplacement de recouvrance. Par contre le déplacement initial étant plus grand, pour une température de recouvrance T_R égale à T_D, la géométrie initiale avant programmation n'est pas recouvrée, le déplacement de recouvrance total d_R^T est plus petit que le déplacement initial fixé. Il y a donc eu déformation permanente de la plaque lors du cycle de programmation. Cependant pour la plaque CBCM la géométrie initiale avant programmation peut être recouverte sous condition d'utiliser une température T_R supérieure à T_D ceci grâce à la partie CBCM de l'actionnement.

Dans cette partie l'influence sur les propriétés CBCM de l'organisation des renforts a été étudiée. En fonction de l'orientation des deux couches d'unidirectionnel de verre (UDV), quatre plaques CBCM ont été réalisées. La plaque CBCM classique (les deux couches d'UDV orientées à 90°suivant le sens transverse de la plaque), la $CBCM^{1/2}$ pour laquelle la seconde couche d'UDV est orientée dans le sens longitudinal (0°), la $CBCM_{1/2}$ pour laquelle la première couche d'UDV est orientée dans le sens longitudinal (0°), et la CBCM-L ou les deux couches d'UDV sont à 0°. Le déplacement libre obtenu lors du cycle de programmation (point B fig. 6) permet de classer ces plaques en fonction de leur asymétrie, et par ordre décroissant de l'asymétrie on obtient CBCM, $CBCM^{1/2}$, $CBCM_{1/2}$ et CBCM-L. On observe également que la valeur du déplacement initial fixé respecte également cet ordre. La géométrie fixée issue du cycle de programmation est donc directement reliée à l'asymétrie du composite, c'est un nouveau résultat de ce travail.

Pour l'essai de recouvrance sans contrainte, on obtient pour d_{RT} par ordre décroissant d'asymétrie les valeurs suivantes, d_{RT} = 21,84 ± 1,26mm, 18,54mm ± 0,12, 16,14 ± 0,12mm et 12,36 ± 0,39mm. Le déplacement total de recouvrance est directement dépendant de l'asymétrie. Après ce premier cycle de recouvrance (chauffe puis refroidissement), la nouvelle géométrie des plaques est proche de la géométrie initiale, on obtient par ordre décroissant d'asymétrie les valeurs suivantes pour le déplacement résiduel : 1,02 ± 0,3mm (11% du

déplacement initial fixé d_F^I), 0,96 ± 0,24mm (11% de d_F^I), 0,81 ± 0,18mm (11% de d_F^I) et 0,6 ± 0,15 mm (9% de d_F^I). Ces valeurs montrent qu'après le premier cycle de recouvrance les différentes plaques sont en parties déprogrammées, la géométrie initiale correspondant à une valeur nulle de d_F^I étant obtenue lors des cycles suivant.

Pour l'essai de recouvrance sous contrainte, la force F_{RT} générée par les différentes plaques CBCM suit également leur degré d'asymétrie: F_{RT}= 48.54 ± 1.57 N, 49.30 ± 0.93 N, 39.70 ± 0,8 N et 35,43 ± 0,81N. La force résiduelle après le premier cycle de recouvrance est inversement liée à l'asymétrie F_{RES} = 3,03 ± 0,96 N, 6,01 ± 0,5 N, 9,31 ± 0,57 et 12,87 ± N 0,64 N. L'existence de cette force ainsi que les résultats montrant la dépendance des différentes grandeurs caractéristiques des cycles de programmation et de recouvrance vis-à-vis de l'asymétrie n'ont jamais été montrées dans la littérature et sont un apport important de ce travail.

La seconde partie de ce chapitre porte sur l'essai de recouvrement en plusieurs étapes. Pour ces essais la température T_R varie progressivement de la température ambiante à la température de déformation T_D. Ainsi dans le cas du test de recouvrement sans contrainte, la géométrie initiale est recouvrée en plusieurs étapes, chacune de ces étapes étant associées à une configuration géométrique intermédiaire (Fig. 7). On peut observer la similitude de forme entre la courbe du déplacement de recouvrement et la température. Pour la première température de recouvrance T_R=80°C la plaque CBCM activée est revenue dans sa configuration initiale après refroidissement elle tend vers une nouvelle position géométrique. Pour les températures supérieure, on peut observer une inversion de la courbure qui sera maximale pour la dernière étape à une température T_R=150°C, pour laquelle la géométrie finale associée après refroidissement est proche de la géométrie initiale avant programmation. On montre également que les différentes positions géométriques lors de la chauffe ou du refroidissement ont une dépendance linéaire vis-à-vis de la température. La stabilité des configurations géométriques intermédiaires (après refroidissement) a été montrée par la répétition de cycle à une même température T_R.

Cette recouvrance pas à pas pour différentes valeurs de T_R, correspond à une déprogrammation progressive de l'effet mémoire obtenu lors du cycle de programmation. Ce processus n'est pas réversible il est impossible de revenir à une position associée à une température de recouvrement inférieure sans réinitialiser la plaque par un cycle de programmation.

Cette propriété est également présente pour la plaque SYM, par contre l'inversion de courbure observée pour le CBCM n'est pas réalisable. Pour le test de recouvrance sous contrainte la propriété de recouvrance multiple est également présente, dans ce cas la plaque génère un effort de recouvrance dépendant de la température. Par contre dans ce cas la plaque étant maintenue en position la déprogrammation ne se fait pas hormis la perte d'effort liée à l'existence de la force résiduelle.

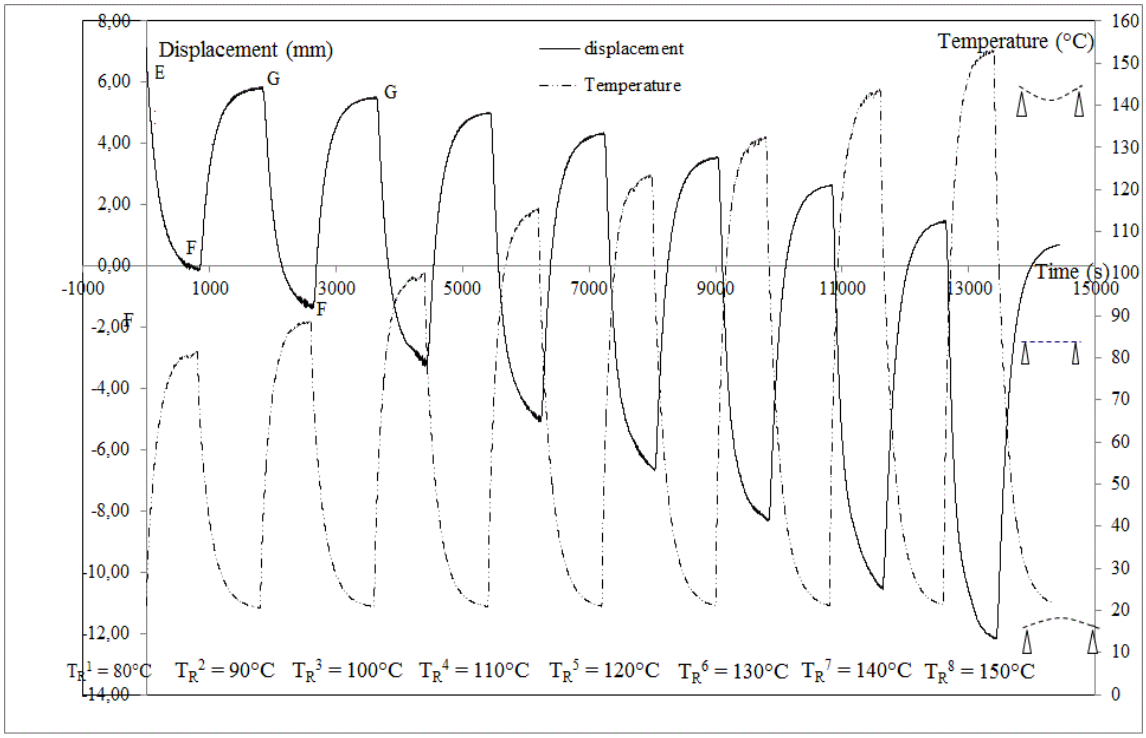

Figure 7 : Test de recouvrement multiple sans contrainte, plaque CBCM

Chapitre V. Conclusion

L'objectif de ce travail était de mettre en évidence le couplage ou non des propriétés de mémoire d'une matrice époxy avec les propriétés d'activation thermique de structure composite (effet CBCM). Ce couplage est réalisé de manière simple car sa mise en œuvre utilise un cycle classique d'éducation ou de programmation thermomécanique réalisé grâce au système

d'activation thermique (couche active) présent dans le composite et utilisé pour créer l'effet CBCM.

Plusieurs résultats non spécifiés dans la littérature ont été obtenus :

Lors du cycle de programmation, présence d'une force que l'on appelle de stabilisation lors du refroidissement de la structure maintenue déformée.

Lors de l'essai de recouvrance sans contrainte, on montre qu'il est possible de revenir à la configuration initiale de la structure (avant programmation) pour une température de recouvrance plus faible que la température de déformation utilisée lors de la programmation. Cette propriété non observé pour la structure symétrique est le résultat du couplage entre effet CBCM de la structure et propriété de mémoire de la matrice epoxy, l'importance de l'effet CBCM étant pour sa part lié au niveau d'asymétrie du composite.

Lors de l'essai de recouvrance sous contrainte, l'existence d'une force résiduelle après refroidissement a été mise en évidence.

L'essai de recouvrance sous charge a conforté les résultats liés au couplage effets mémoire et CBCM. Notamment par la propriété pour une structure CBCM programmée et soumise à un chargement mécanique, de revenir dans sa position initiale. Propriété que ne possède pas ou très peu les composite à mémoire de forme uniquement.

Enfin ces trois essais ont permis de caractériser et de séparer les différents travaux mécaniques, travail total, travail de recouvrement et travail d'activation CBCM.

L'étude de structures de dissymétrie différente, a permis de montrer que plusieurs grandeurs caractéristiques des propriétés de mémoire sont directement liées à l'asymétrie du composite. Une première approche de la caractérisation des propriétés viscoélastique réalisée notamment par l'insertion dans le cycle de programmation d'une étape de relaxation, a permis de mettre en évidence la stabilité ou non des structures programmées dans le temps.

Enfin l'utilisation de différentes valeurs de température pour la température de recouvrance, a mise en évidence la propriété de recouvrement en plusieurs étapes. C'est-à-dire la capacité pour la structure programmée de posséder différentes géométrie stabilisées entre la géométrie initiale et la géométrie fixée après le cycle de programmation.

L’ensemble de ces résultats montrent d’une part qu’il est possible à partir de ce couplage de développer des actionneurs continus à forte capacité d’actionnement. D’autre part les différentes grandeurs mécaniques que nous avons isolée expérimentalement tel que la force de stabilisation lors du cycle de programmation ou la force résiduelle lors de l’essai de recouvrement sous contrainte nous ont permis de proposer une explication basée sur la microstructure du composite et l’équilibre entre les effets des renforts et les propriétés de mémoire du polymère. Explications qui sont aujourd’hui à la base d’un travail de modélisation.

Table of Contents

List of Figures

List of Tables

Chapter I. Introduction

The Shape memory polymers (SMPs) are the materials which can return to their original position when a suitable stimulus is provided. Most of the SMPs work on heat stimulus. These polymers perform specific shape memory cycle which is composed of two parts: programming or fixing part which gives the temporary shape to the polymer and the recovery part which returns the polymer to its original shape.

1.1) Current research problems in SMPs and their composites

The shape memory polymers have high recoverable strain of several hundred percents and much lower density as compared to other shape memory materials i.e. shape memory alloys (SMA). Moreover, SMPs have easily adjustable material properties which can be easily produced and shaped by conventional polymer processing techniques. However, the mechanical properties of SMPs, in many cases, during the thermo-mechanical operation are not useable in certain applications. The SMPs have relatively low recovery stress, which is usually 1–3 MPa compared to 0.5–1 GPa for SMA. So, the relatively low recovery stress becomes a limiting factor in many applications, especially, in cases where SMP devices need to overcome a large resisting load during shape recovery. The SMPs and their composites cannot perform full recovery under any load. Therefore, it is the utmost requirement to develop a structure which can perform full recovery under a specific load.

For the improvement of low recovery force, two solutions are possible: making changes in the molecular structure of the polymer or incorporating the fillers externally which can enhance the properties. The second solution is mostly studied which results in the development of shape memory polymer composites in which nano-fillers such as nano-fibers, carbon nano-tubes, short fibers and even fabrics are being used. The SMPCs enhance the mechanical properties as well as are multifunctional. However, due to the addition of this reinforcement, elastic modulus increases which degrades the recoverable strains. Therefore, there is a need to develop such a structure which have optimum value for recovery stress and recoverable strains or which can produce an extra or additional strain that can compensate the reduced strain due to the addition of reinforcement.

The other problem is the recovery of the material to its original position at a temperature lower than its programming or deforming temperature. It is always desirable to recover the SM materials at a temperature lower than their programming temperatures so that they can be used in certain applications where high temperature is not preferable to use or cannot be used (medical applications). The conventional shape memory polymers and their composites can recover only to their original positions if recovery temperature is equal to its programming or deforming temperature, otherwise there will always be a residual strain after recovery. Therefore, it is always preferable to develop a structure that has the ability to recover at lower temperatures.

Mostly, SMPs and their composites have 1W shape memory effect which perform only one recovery after the programming cycle. They cannot perform second recovery cycle without the provision of second programming cycle. To make the SMPs to produce 2W shape memory effect, triple shape memory effect or multi shape memory effect, they need special programming during programming cycle or require to embed SMA or other elastic structures in the composite. It is always desirable to develop a structure which can perform the above mentioned shape memory effects without embedding external structures in the composites.

I.2) Objective of the thesis

It is already discussed that SMPs can give high strain but give less recovery forces during the recovery as these have less rigidity. However, shape memory composites can give high recovery forces but the recoverable strain is reduced as these are relatively rigid. Therefore, there is a need to develop a structure that can give high strain as well as can give high recovery forces. The development of such a structure is the main objective of this thesis.

The main objective of the thesis is to develop a shape memory polymer composite (SMPC) that can give high strain, can produce high recovery forces as well as can recover under load and can also recover to its original position at a temperature lower than the deforming temperature. For this, the objective is to couple the two properties: actuation property due to the asymmetry (CBCM-effect) and the actuation due to the shape memory property of the resin in the same structure i.e. CBCM-SMPC (CBCM stands for controlled behavior of composite material).

Furthermore, the objective is to study the different functionalities of the coupled structure and its comparison with the non-coupled structure i.e. SYM (the symmetrical composite). In addition, the objective is to understand the effect of position and orientation of different layers of reinforcement on the shape memory properties in CBCM-SMPC.

I.3) Outline of the thesis

Chapter I. Introduction

It describes the problems relating to shape memory polymers and their composites, the objective of the thesis and also the outline of the thesis.

Chapter II. Bibliography

This chapter explains SMPs classification, effect of reinforcement on SMPs, the research conducted for producing different shape memory effects in SMPs and their composites, applications of SMPs and their composites.

Chapter III. Materials and Methods

This chapter describes the experimental apparatus, materials for the fabrication of the composites and the characterization techniques used for this research.

Chapter IV. Results and Discussion

Chapter IV.1. One-step recovery

This section explains the behavior of the composites (CBCM and SYM) in one-step recovery (recovery temperature is given directly equal to programming or deforming temperature) for different recovery tests (unconstrained recovery, constrained recovery and recovery under load). Also, it illustrates the effect of stress relaxation during programming cycle on the shape memory properties of the composites. Moreover, this section elaborates the effect of changing the position and orientation of the different layers of a composite on its shape memory properties. For this, the unconstrained and constrained recovery tests have been performed.

Chapter IV.2 Multi-step recovery

In this section, multi-step recovery tests (unconstrained and constrained recovery) are performed. During multi-step recovery tests, the recovery temperature is gradually increased

from lower to higher temperature till the recovery temperature becomes equal to the programming or deforming temperature. At the end, the recovered work during multi-step recovery tests in reference to initial fixity is calculated. Also, the recovered work obtained at a recovery temperature equal to programming temperature during multi-step recovery is compared with the recovered work obtained from the one-step recovery.

Chapter V. Conclusion and perspectives

It gives a general conclusion for the results obtained in the thesis and the possible perspectives.

Chapter II. Bibliography

II.1) Introduction

This chapter starts with an introduction of smart materials and their structures. Then, the properties of shape memory polymers in comparison with shape memory alloys are discussed. After that, a brief background of shape memory polymers, their categorization (thermoplastic and thermoset with their brief comparison) are specified. The different techniques used to characterize shape memory polymers are also mentioned. Then, the typical shape memory cycle (along with its characteristic parameters) that is used to conduct thermo-mechanical programming and recovery of the shape memory polymers is explained. The different shape memory effects (1W, 2W, triple-way and multi-way) obtained due to thermo-mechanical programming in shape memory polymers are elaborated. The shape memory polymer composites along with their different types with respect to different reinforcements are also illustrated. In addition, the different shape memory effects (1W and 2W) that are produced in shape memory polymer composites are also described. At the end, the different applications of shape memory polymers and their composites are presented.

II.2 Smart materials and structures

"Smart materials are the materials which possess the ability to change their physical properties in a specific manner in response to a specific stimulus input."[1-2]

The stimuli (input) may be heat, pressure, electric and magnetic fields, chemicals etc. The response (output) may be the change in shape, change in rheological properties (stiffness, viscosity or damping) or change in internal electric properties like dielectric constant or resistivity etc. This smartness is programmed by changing the material composition, processing etc. to response for specific stimuli. Table II.1 gives the specific stimuli and their responses for the different smart materials [3].

From the smart materials, smart structures can be formed which can be divided into five levels of sophistication. The simplest level of smart structures is the sensory structures which can only sense the specific stimulus. The second level is the adaptive structures which have actuators to respond the specific stimulus. The third level is the controlled structures which perform

controlled functions with the help of integrated sensors and actuators. Similarly, the fourth level is the active structures which perform not only the controlled functions but also the structural functions. The last level is the intelligent structures that possess highly integrated electronic logics which provide intelligence to the structure. These sophistication levels are given in Figure II.1 for easy understanding [4-5].

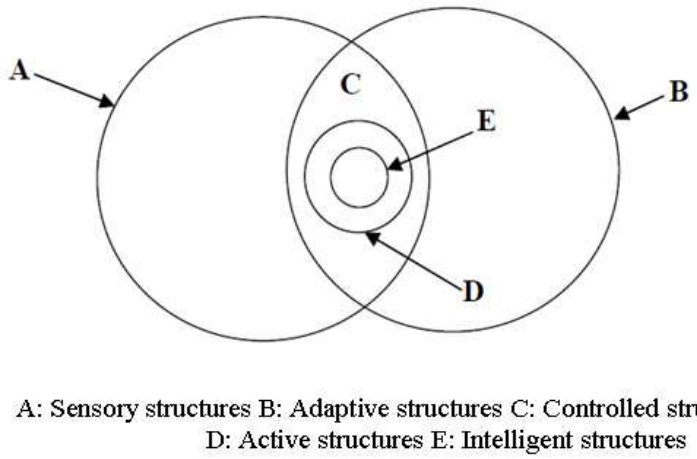

Figure II.1. Sophistication levels of smart structures [3, 6]

Smart Material	**Stimulus**	**Response**
Piezoelectric material	Stress	Electric charge
Magneto-strictive material	Magnetic field	Mechanical strain
Electro-rheological Fluid	Electric field	Change in viscosity
Optical fiber	Temperature, mechanical strain, Pressure	Change in opto-electric signals
SMA / SMP	Heat	Original memorized shape

Table II.1. Stimuli and responses of the smart materials [3]

II.3) Shape memory materials

Figure II.2 shows different shape memory materials out of which the mostly studied materials are SMAs and SMPs. They have the ability to deform and obtain the temporary shape and then on providing the heat stimulus returns to their permanent shape. These are the materials that include metals, ceramics and polymers. However, the most widely used shape-memory materials in recent years have been the shape-memory alloys (SMAs). The shape memory effect of SMAs depends on two stable crystal structures: a high temperature austenitic phase and a low temperature martensitic phase. The plastic deformations which are introduced during the low temperature phase are recovered elastically during the high temperature phase. As a result, SMA recovers and performs the shape recovery [8]. Currently, there are three major types of SMA systems, namely Cu-based (mainly CuAlNi and CuZnAl), NiTi-based, and Fe-based (e.g., FeMnSi, FeNiC and FeNiCoTi). The first two are more suitable for engineering applications, while the last one is traditionally seldom used [7].

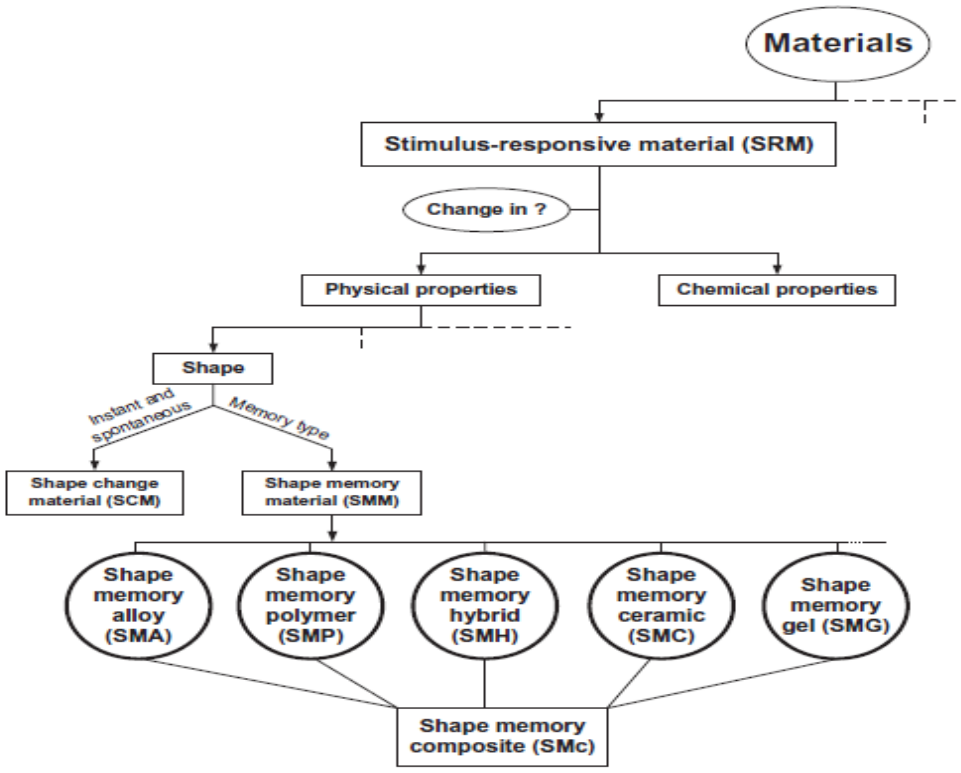

Figure II.2. Stimulus responsive materials and shape memory composites [7]

In literature, it is found that NiTi-based SMAs are more reliable and are highly biocompatible. The shape-memory effect in NiTi was discovered in 1963. After this discovery, the interest to use this in commercial applications was much increased. The reason behind was the specific properties (transition temperature close to body temperature, super elasticity, biocompatibility, and 2W shape-memory effect) that it possesses [9]. Apart from this, SMAs have some limitations and disadvantages. In Table II.2 the properties and limitations of SMAs have been compared with the SMPs. From Table II.2, it can be easily observed that the extent of deformation (%) of SMA is very less than SMP. Also, SMAs are heavy than SMPs, shaping is difficult, expensive and require higher temperatures for their fabrication.

Material Property	**Shape Memory Polymers**	**Shape-Memory Alloys**
Density/g cm^{-3}	1	6-7
Extent of deformation (%)	50-600	6
Stress required for deformation (MPa)	1–3	50–200
Stress generated during recovery (MPa)	1–3	150–300
Corrosion performance	Excellent	Excellent
shaping	easy	difficult
At low temperature	rigid	soft
At high temperature	soft	hard
Heat conductivity	Low	High
Biocompatibility and biodegradability	Can be biocompatible and/or biodegradable	Some are biocompatible (i.e. Nitinol), not biodegradable
Processing conditions	<200 °C, low pressure	High temperature (>1000 °C) and high pressure required
cost	Low	high

Table II.2. Properties of shape memory polymers and alloys [8, 10]

The various disadvantages and limitations of SMAs have given the opportunity for the development of alternative materials, especially the shape-memory polymeric materials.

II.4) Shape memory polymers

II.4.1) Background and definition

Shape-memory polymers (SMPs) are the materials which have the capability to respond for a specific stimulus by changing its shape from one form to the other. They can recover the mechanically induced strain. The molecular chains perform the active movements that enable the material to change its shape. Various stimuli can be used for the actuation of SMPs. These include magnetic filed, electric field, light, heat, moisture, infrared light etc. Out of these, heat stimulus is being mostly used nowadays. A SMP consists of two segments. One segment is soft while the other segment is hard. Hard segments have high elastic properties whereas the soft segments affect its elastic properties. At high temperature, the micro Brownian motion of soft segments increases and elasticity of the overall material decreases. On cooling, these soft segments become relaxed and frozen. Thus the material gets the new position. Then, if a suitable stimulus is provided to the material, the soft segments respond quickly and their micro Brownian motion increases again and the material returns to its original position called as shape recovery [8].

The first SMP was polynorborene with a Tg range of 35–40 °C developed by the French CdF Chimie Company and commercialized by the Japan Nippon Zeon Company in 1984. Then, in 1987 Kurare Corporation, Japan developed second SMP with Tg of −68°C. Similarly, third SMP named as Asmer was produced by Asahi Company, Japan with a Tg range of 60 to 90°C [11]. As SMPs show a variety of novel properties, they have been widely researched since the 1980s. In nineties Polyurethane based SMPs were developed which revolutionized the use of SMPs in many applications. Then, in 1997, SMP based composite was introduced to enhance the mechanical properties of the whole structure [12]. After that, based on the shape-memory effect, some novel multi-functional SMPs or nano SMP composites have also been proposed.

II.4.2) Categorization of shape memory polymers

SMPs are considered to be made up of net-points and molecular switches which can be formed through covalent bonds or intermolecular interactions. Depending on the nature of cross-linking, they can be called as chemically or physically cross-linked. The highly chemically cross-linked

SMPs are referred to as thermosets. These are chemically, thermally and mechanically stable. However, physically cross-linked SMPs are called as thermoplastics [9]. The network chains of SMPs can be either amorphous or crystalline. Hence, the transition temperature (Ttrans) for amorphous is glass transition temperature (Tg), whereas for crystalline, Ttrans is the melting temperature (Tm). Transition temperature (Ttrans) is the temperature at which the material changes from its one state to another state. It may be Tm or Tg. Tm is the temperature at which a material changes from solid to liquid state. In polymers, it is the peak temperature at which a semi-crystalline phase melts into an amorphous state. Similarly, Tg is the temperature beyond which a polymer turns from a hard, glass-like state to a rubber-like state.

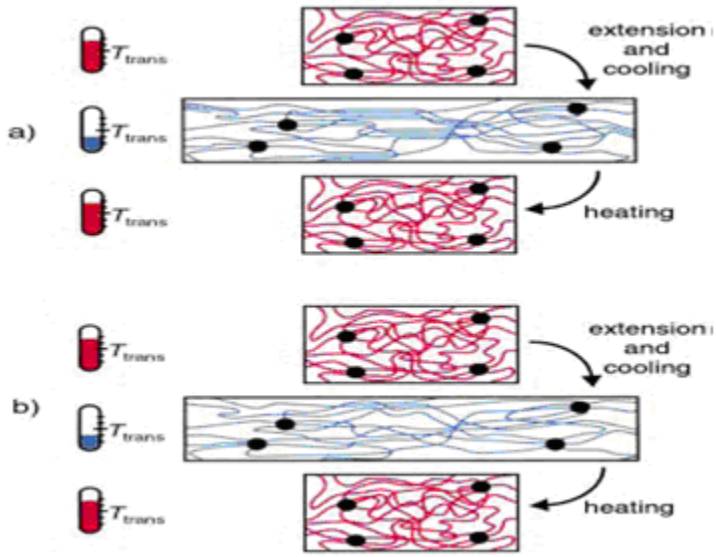

Figure II.3. Schematic representation of the molecular mechanism of the thermally induced shape-memory effect for a) a covalently cross-linked polymer with Ttrans = Tm, and b) a polymer network with Ttrans = Tg. If the increase in temperature is higher than Ttrans of the switching segments, these segments are flexible (shown in red) and the polymer can be deformed elastically. The temporary shape is fixed by cooling down below Ttrans (shown in blue). If the polymer is heated up again, the permanent shape is recovered [13]

If Ttrans is Tg, the micro Brownian motion of the network chains is frozen at temperatures below Tg, and is ‘‘switched’’ on at temperatures at or above Tg upon reheating. Similarly, if Ttrans is Tm, the switching segments crystallize at temperatures below Tm, and then recover their original shape at Tm or above. The molecular mechanism of thermally induced shape memory effect is given in Figure II.3.

More than twenty types of SMPs have been synthesized and widely researched in the recent years. Figure II.4 presents the classification scheme for existing polymer networks that exhibit the shape-memory effect.

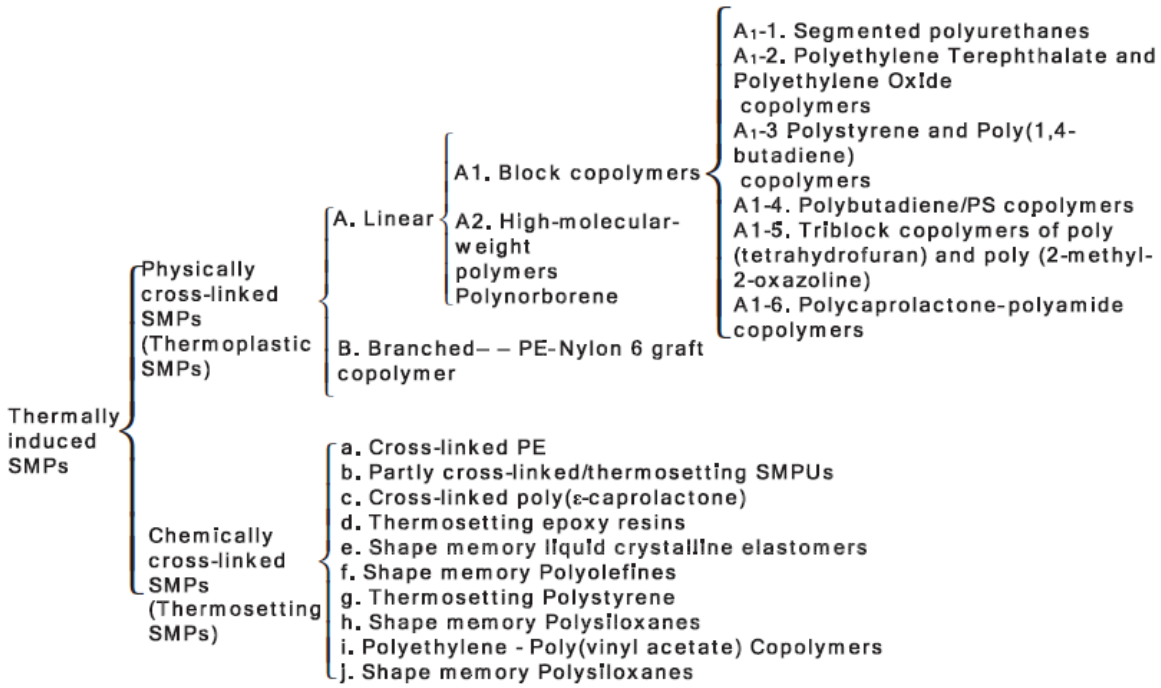

Figure II.4. Schematic of structural categorization of SMPs [11]

II.4.2.1) Thermoplastic shape memory polymers

Thermoplastic SMPs consist of two segregated domains. The domains which are related to highest thermal transition temperature are called the hard domains which function as physical net points. However, the domains related to relatively lower thermal transition temperatures are called as switching segments which work as the molecular switches [14]. Thermoplastics can be further classified into linear polymers [15-16], branched polymers [17] or complex polymers [9]. For thermoplastic polymer, polyurethane (PU) is mostly studied and used as SMP that

provides so many advantages over other SMPs. The advantages include a wider range of shape recovery temperature (from −30 to 70 °C), better biocompatibility and processing ability. The Tg of thermoplastic PU can be tailored from (-30 to 70 °C) by using different kinds of urethane ingredients (diisocyanate, polyol, and chain extenders) and by adjusting their molar ratios. For effective shape memory properties, the glassy hard segments must maintain the shape through chemical bonding along with physical cross-links whereas soft segments must have the mobility to absorb external stresses by unfolding and extending their molecular chains. If stress exceeds and breaks the interactions among hard segments, the shape memory would be lost and original position cannot be restored. Therefore, precise control of composition and structure of hard and soft segments is very important to satisfy the conditions required for certain applications [18].

II.4.2.2) Thermosetting shape memory Polymers

The thermosetting SMPs are covalently cross linked networks that possess chemically interconnected structures that determine the original macroscopic shape of SMPs. The switching segments of the chemically cross-linked SMPs are generally the network chains between the netpoints, and a thermal transition of the polymer segments is used as the shape memory switch. The chemical, thermal, mechanical and shape memory properties are determined by the reaction conditions, curing times, the type and length of network chains, and the cross-linking density. The two mostly used thermosets as SMPs are:

II.4.2.2.1) Thermosetting Styrene-based shape memory polymer

The Styrene-based SMP exhibit a cross-linked structure to exhibit the shape memory effect. The variety of methods to polymerize styrene and the wide availability of possible co-monomers enable these necessary features. Styrene can be polymerized through anionic, cationic, or free controlled radical polymerization methods. By controlling the cross-link densities and the rigidity of the polymer backbones, the styrene based SMPs show a tunable Tg, mechanical properties, and a good shape memory effect. Moreover, the styrene based materials show good reprogramming properties upon numerous shape recovery cycles, and excellent shape fixity and recovery ratios [11].

Zhang DW et al. investigated the influence of cross-linking degree on shape memory effect of styrene copolymer by altering the dosage of cross-linking agent. Tg increased from 35°C to 55°C followed by increasing the gel content from 0% to 35% through increasing the dosage of cross-linking agent from 0% to 1%. Furthermore, the SMP experienced good SME and the largest reversible strain of the SMP reached as high as 150% [19].

Bin Xu et al. studied the polystyrene based nano-composites using cross-linked polystyrene as a matrix and different nano-fillers (including alumina, silica and clay). They revealed that these nano-fillers enhance the thermal and shape memory properties of these nano-composites [20].

II.4.2.2.2) Thermosetting Epoxy shape memory polymer

In particular, epoxy SMP is a high-performance thermosetting resin possessing a unique thermo-mechanical property together with excellent shape-memory effect. In the case of SM epoxies, the transformational temperature is Tg. The crosslink density, a high chain flexibility and molecular mobility affect the performances of the epoxies. The permanent shape of epoxies is determined by the cross-links formed during the curing cycle whereas its temporary shape results from mechanical deformation performed on the curing samples at Tg. At a temperature higher than Tg, epoxies show elastic behavior. Therefore, in response to mechanical deformations, the more mobile polymer chains maintain maximum entropy and minimum internal energy, thus, allowing the conformational changes to occur. These conformational changes can be fixed with the subsequent cooling which results in temporary shape which can be recovered by heating it again [21].

Jinsong Leng et al. prepared the epoxy based resin with the linear monomer having an epoxy group number ratio of 1:1 in one molecule, a molecular weight ratio of 2:5 and a density ratio of 1:1. The linear monomer is composed of a long linear chain of C–O bonds. They found that the incorporated linear monomer results in an increase of C–O bonds in the whole network. With increasing linear monomer content, a decrease in Tg and an increase in elastic ratio can be observed for the polymers from DSC and DMA studies, respectively. The increase in linear monomer leads to decrease in crosslink density for the polymers. Finally, an investigation on shape recovery behavior reveals that each polymer shows a full recovery at a temperature equal

to or above Tg. Also, increasing the linear monomer content results in a decrease in both shape recovery ratio (below Tg) and shape recovery speed (at Tg) [22].

W.B. Song et al. prepared shape memory polymers by epoxy resin E-51 with varying content of curing agents of 4, 4-methylenedianiline (DDM) and m-phenylenediamine (m-PDA). They showed that all specimens fabricated in this study exhibit excellent shape fixture rate and recovery effect, but with different thermo-mechanical properties and critical transition temperatures. Also, the results show that a higher stiffness and critical transition temperature can be realized by increasing the content of curing agents [23].

II.4.2.3) A brief comparison between thermoplastic and thermoset SMPs

When compared with physically cross-linked SMPs, the chemically cross-linked SMPs often show less creep, thus the irreversible deformation during shape recovery is less. The chemically cross-linked SMPs usually show better chemical, thermal, mechanical and shape memory properties than the physically cross-linked SMPs. Moreover, these properties can be adjusted by controlling the cross-link density, curing conditions and curing times. The shape recovery ratio of the thermoplastic polyurethane SMP is usually in the range of 90-95%. The elastic modulus is between 0.5-2.5 GPa at room temperature. It is very sensitive to moisture. So, these are used at small scale such as for biomaterials and shape memory polymer textiles. However, the epoxy SMPs show better performance. The shape recovery is 98-100% while the elastic modulus is 2.5-5 GPa. Hence, generally these can also be used for structural materials, such as space deployable structures and automobile actuators [11].

II.4.3) Characterization techniques for shape memory polymers

II.4.3.1) Fourier transform infrared spectroscopy (FTIR)

FTIR stands for Fourier Transform Infra-Red, the preferred method of infrared spectroscopy. In infrared spectroscopy, IR radiation is passed through a sample. Some of the infrared radiation is absorbed by the sample and some of it is passed through (transmitted). The resulting spectrum represents the molecular absorption and transmission, creating a molecular finger-print of the sample. Like a finger-print, no two unique molecular structures produce the same infrared spectrum. This makes infrared spectroscopy useful for several types of analysis. It can also

identify unknown materials, determine the quality or consistency of a sample and determine the amount of components in a mixture [24].

FTIR spectrometry is often used to investigate the difference in structure of the networks in a molecule during the synthesis of an SMP [12, 22]. Raman spectroscopy and X-ray diffraction (XRD) are also used to determine the chemical structures.

II.4.3.2) Surface morphology detection.

Optical microscopy, scanning electron microscopy (SEM) and transmission electron microscopy (TEM) can be used to observe the surface morphology of SMPs or their composites. Optical microscope uses visible light along with system of lenses to magnify the images of small things. In SEM, the scattered electrons produce an image 300–600 times better than that of an optical microscope. TEM is a microscopy technique in which a beam of electrons is transmitted through an ultra thin specimen that interacts with the specimen. TEM has the ability to provide detail at the magnitude of about 1 nm [11].

II.4.3.3) Thermogravimetric analysis

Thermogravimetric Analysis (TGA) measures the amount and rate of change in the weight of a material as a function of temperature or time in a controlled atmosphere. Measurements are used primarily to determine the composition of materials and to predict their thermal stability at temperatures up to 1000°C. Thermal stability is vital to know as during shape recovery, recovery temperature must be less than its temperature of decomposition. Hence, it is the first tool before planning the shape memory process of the materials [25].

II.4.3.4) Differential scanning calorimeter

A DSC analyzer measures the energy changes that occur when a sample is heated, cooled or held isothermally, together with the temperature at which these changes occur. Generally, DSC is used to characterize the materials for their glass transition temperature, melting points and other material reaction characteristics such as specific heat, percent crystallinity, and reaction kinetics. For the SMPs, DSC is used to determine Tg during the transition process [26].

II.4.3.5) Dynamic mechanical analysis (DMA)

Dynamic mechanical analysis (DMA) is used to analyze and study the thermal and dynamic mechanical properties of the SMPs and their composites. DMA can be simply described as applying an oscillating force to a sample and analyzing the material's response to that force. From this, the properties like the tendency to flow (viscosity) from the phase lag and the stiffness (modulus) from the sample recovery can be calculated. These properties are often described as the ability to lose energy as heat (damping) and the ability to recover from deformation (elasticity).

In this technique, for a certain frequency, stress or strain is applied to the sample and its response is analyzed to obtain deformation and phase angle. This data is used to calculate complex modulus given by:

$E^* = E' + iE''$

where E' is the storage modulus and is a measurement of the recoverable strain energy. When deformation is small, it is approximately equal to the Young's modulus. E'' represents the loss modulus and is related to the hysterical energy dissipation. The phase angle (δ) is given by:

$\tan\delta = E''/E'$ [27]

II.4.4) Shape memory cycle

The shape memory cycle for SMPs can recover their original shapes after large deformation when subjected to an external stimulus, such as Joule heating, light, magnetism or moisture.

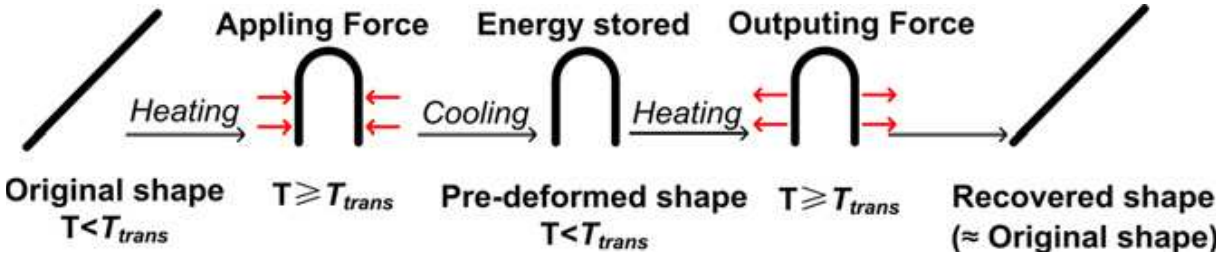

.

Figure II.5. Schematic of shape-memory effect during a typical thermo-mechanical cycle [11]

Among these SMPs, the thermo-responsive SMPs are most common. At a macroscopic level, as illustrated in Figure II.5, the typical thermo-mechanical cycle of a thermo-responsive SMP consists of the following procedure:

– Fabrication of the SMPs into an original shape

– Heating the SMP above the thermal transition temperature (Ttrans)

– Deformation of the SMP by applying an external force – cooling well below Ttrans

– Removal of the constraint to obtain a temporary pre-deformed shape and heating of the pre-deformed SMP again above Ttrans that results in the recovery of the SMP towards its original shape called as recovered shape.

The 3-D view (Force, Displacement, Temperature) of the SMP cycle is clearly shown in Figure II.6 The thermo-mechanical cycle is started by bringing the material at an elevated temperature above its Tg. Step 1 (path 1-2) shows deforming of the material to a specific deformation while the material is in rubbery state. The stress value at point 2 is denoted by F_{max}. Step 2 (path 2-3) shows the maintaining of this deformation while cooling the material at temperature lower than Tg. This step stores the strain in the material. Step-3 (path 3-4) is an unloading process at lower temperature which results in spontaneous spring-back. The stress is released and stress becomes zero. Normally, the fixed displacement is less than 100%. The corresponding strain at unloading is the amount of displacement fixed (d_F) in the material. At point 4, the temporary shape is fixed. The last step is the recovery step which can be divided into 2 paths: path (4-5a) and path (4-5b) which depends on the boundary conditions of the recovery. Path (4-5b) is the constrained recovery which is obtained by fixing the temporary or fixed position of the material when heated. This step records the generated forces during the recovery step and the curve comes very close to point 2. Similarly, path (4-5a) is the unconstrained recovery which is obtained by activating the material while allowing it to recover to its original position. The most of the displacement is recovered leaving behind the residual displacement which is used to determine the shape recovery. During unconstrained recovery the curve comes very close to point 1, the initial state of the material [28].

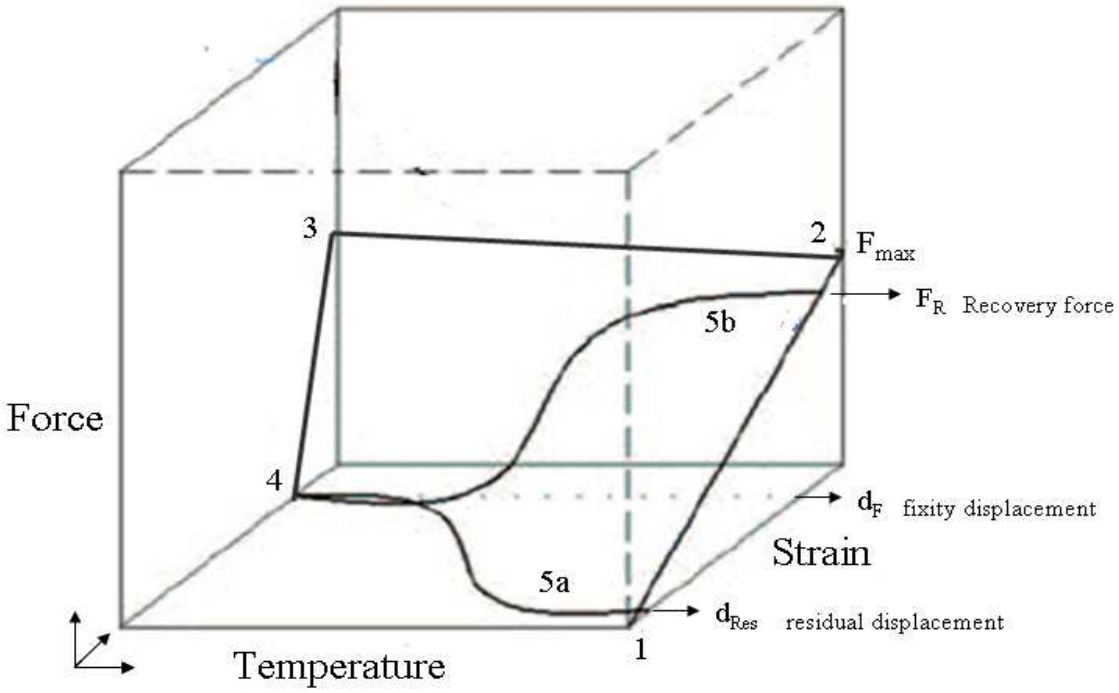

Figure II.6. Force–displacement–temperature diagram illustrating the typical only one thermomechanical cycle of a shape-memory polymer (reproduced from reference [28])

In addition to the 3-D view of thermo-mechanical cycle, 2-D view of thermo-mechanical cycle is also shown in Figure II.7 with multiple Y-axis (strain, stress and temperature) and x-axis (time). The points from 1 to 5 in Figure II.7 correspond to Figure II.6.

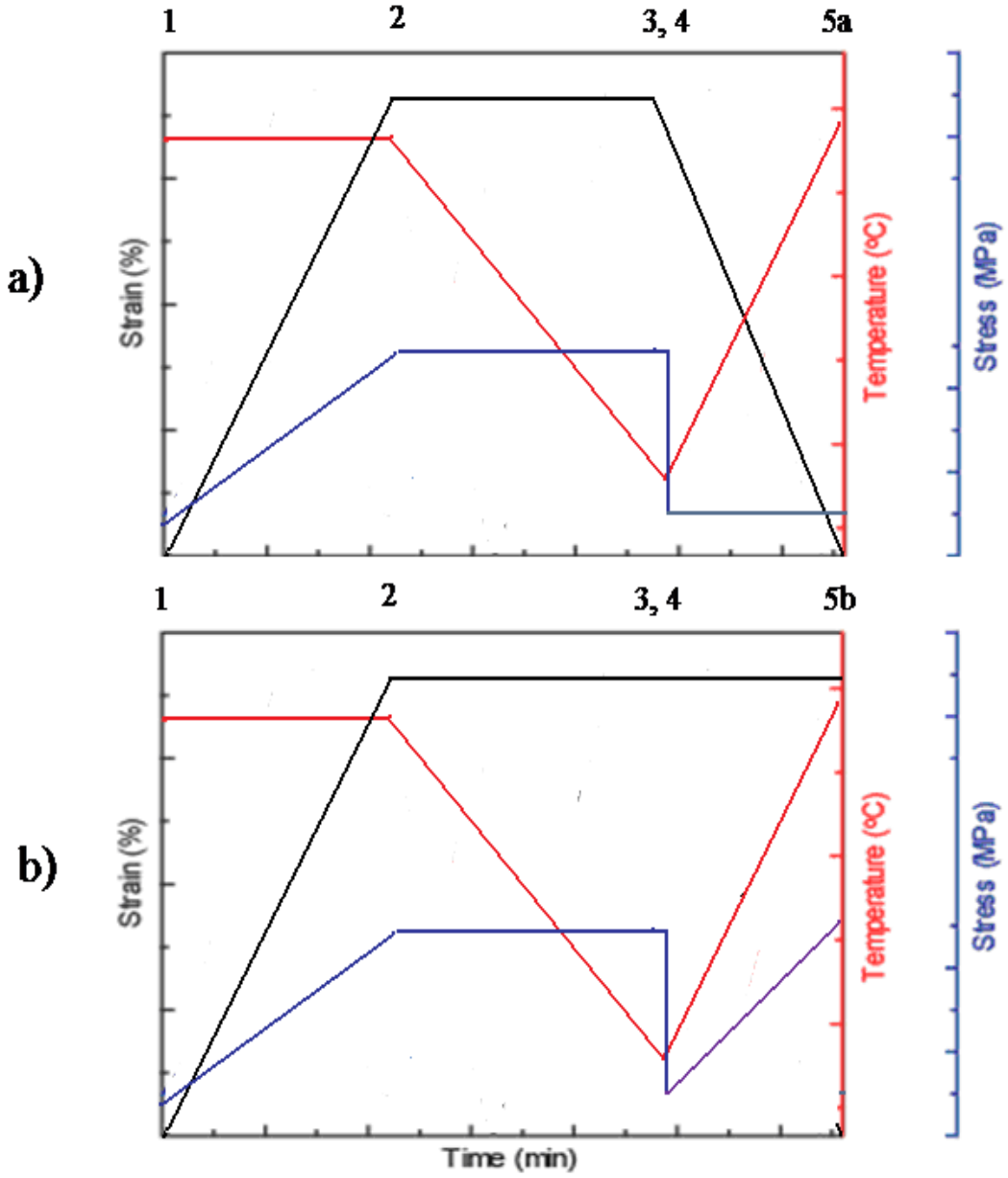

Figure II.7. a) Unconstrained recovery b) Constrained recovery; A representative 2-D plot for presenting cyclic thermo-mechanical testing results. The lines represent a hypothetically ideal SMP with 100% fixing ratio and 100% recovery ratio. (reproduced from [29])

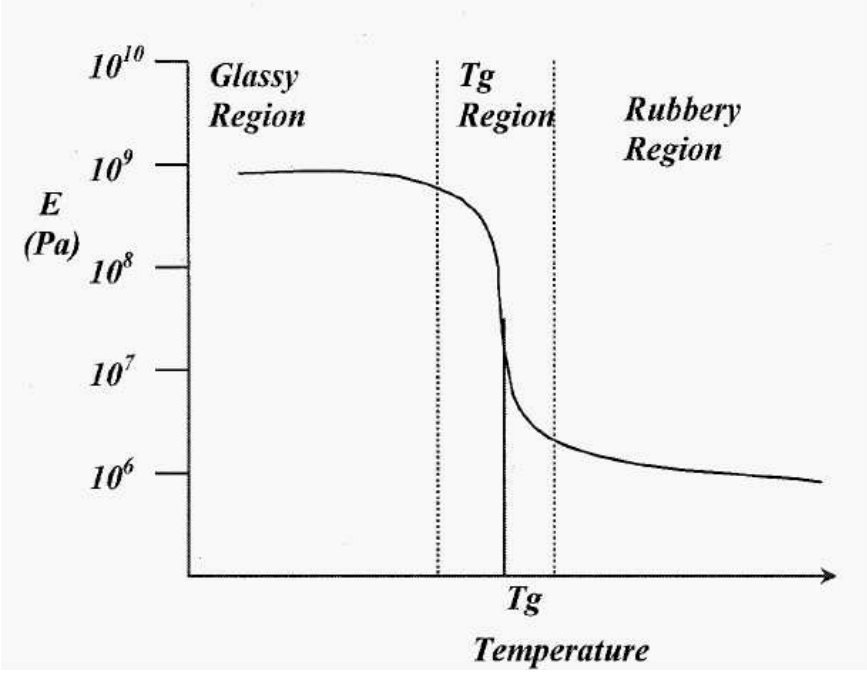

Figure II.8. Different regions during the heating of an amorphous polymer [30]

During the SM cycle, what happens to the molecular chains can be described from Figure II.8. The molecular chains undergo micro-Brownian movement above Tg (rubbery state) and the elastic modulus of the polymer material becomes low. In the rubbery state, the material can be easily deformed by the application of external force, and the molecular chains can be oriented in the direction of the applied force. When the temperature becomes below Tg and the deformation remains constant, the micro-Brownian motion becomes frozen and the chain orientation and deformation becomes fixed. When the material is heated above Tg, the micro-Brownian movement starts again, and the molecular chains lose their orientation and the material recovers its original shape [30].

II.4.5) SMP characteristic parameters during SM cycle

For the description of SM cycle of the polymers, there are certain terms which are very important and, therefore, must be defined separately for easy understanding of the cycle.

– **Shape fixing components:** These are the net points which are covalently cross linked bonded or physically formed (H-bonds or physical entanglement) in an SMP network which maintains the stability during the deformation and recovery process.

– **Shape switching components:** These are the polymeric chains in an SMP network that can switch from one state to another in response to the temperature change, which are responsible for the temperature-dependent deformation and recovery.

– **Shape deforming temperature:** It is the temperature at which the polymer is deformed to a certain strain to get the temporary shape. This temperature is very important as it affects the overall performance of the SMP. It may be equal, below or above Tg.

– **Fixing temperature:** It is the working temperature at which the temporary shape of a deformed SMP is fixed. For the glassy SMPs the fixing temperature is taken as 20°C less than the Tg. However, for the semi-crystalline SMPs, fixing temperature is the crystallization temperature which is less than the transition temperature, so generally these are cooled to 40°C less than the transition temperature.

– **Recovery temperature:** It is the temperature at which permanent shape is recovered. It may be called as Transformation or Switching Temperature or Response Temperature. Normally, it is the same temperature as the temperature of deformation during the first step of SM cycle generally taken as 20°C more than Tg.

– **Shape fixity:** Shape fixity characterizes the ability of an SMP to fix the strain imparted in the sample during the deformation step after subsequent cooling and unloading. R_F is determined as the ratio of the fixed displacement (d_F) to the maximum displacement (d_{max}) (see Figure II.6.) It is expressed as:

$$R_F = \frac{d_F}{d_{max}}$$

– **Shape recovery:** Shape recovery characterizes the ability of an SMP to recover the accumulated strain during the deformation step after subsequent cooling and unloading upon reheating to the rubbery state.

It may be defined in two ways. First way is the ratio between the recovered displacement and fixed displacement.

$$R_r = \frac{d_R}{d_F}$$

The 2nd way is the ratio between recovered displacement and the maximum displacement d_{max}.

$$R_r = \frac{d_R}{d_{max}}$$

– **Recovery speed:** Recovery speed can be defined as the percentage of recovery per unit time. This recovery speed is influenced by the recovery heating rate. Also, recovery speed increases if fixing is done at lower temperature during the programming cycle whereas recovery is done at higher temperature [31].

– **Shape memory cycle life:** The cycle life of an SMP is defined as the repeatability and durability of its SM properties over consecutive SM cycles. Therefore, the cycle life of an SMP defines the number of consecutive SM cycles it will be able to achieve without failure.

– **Shape memory cycle Time:** SMP cycle time corresponds to the time required for an SMP to be transformed from its permanent shape to its temporary shape and reversibly to its permanent shape during a single thermo-mechanical cycle. Therefore, the cycle time represents the overall time necessary for the programming of an SMP temporary shape and the recovery of its permanent shape [21, 29, 32].

II.4.6) Functionalities of SMPs (or their composites)

The different functionalities of SMPs are shown in Figure II.9. The different functionalities based on the direction of activation and deactivation of a SMP can be 1W-SME or 2W-SME. Similarly, based on the different shapes, dual shape or triple shape or even multi-shapes have been defined. In dual shape, the sample can have two shapes. In triple shape, it can have three shapes and, similarly, in multi-shapes, it can have many shapes.

For dual shape and 1W-SME, the samples become active on providing stimulus and get the other shape; however, when stimulus is removed, the sample maintains this position and cannot return to the initial position. For dual shape and 2W-SME, the samples become active on providing stimulus and get the other shape; however, when stimulus is removed, the sample

returns to the initial position. Hence, the sample can repeat this phenomenon on giving and removing the stimulus.

For triple shape and 1W-SME, the samples become active on providing stimulus and get the 1st shape. On further providing the stimulus, it gets the 2nd shape. However, when stimulus is removed, the sample maintains this position and cannot return to the 1st shape or initial position. In 2W-SME, the samples become active on providing stimulus and get the 1st shape. On further providing stimulus, it gets the 2nd shape. However, when stimulus is removed, the sample returns to the 1st shape and then to the initial position. Hence, the sample can repeat this phenomenon on the provision and removal of the stimuli.

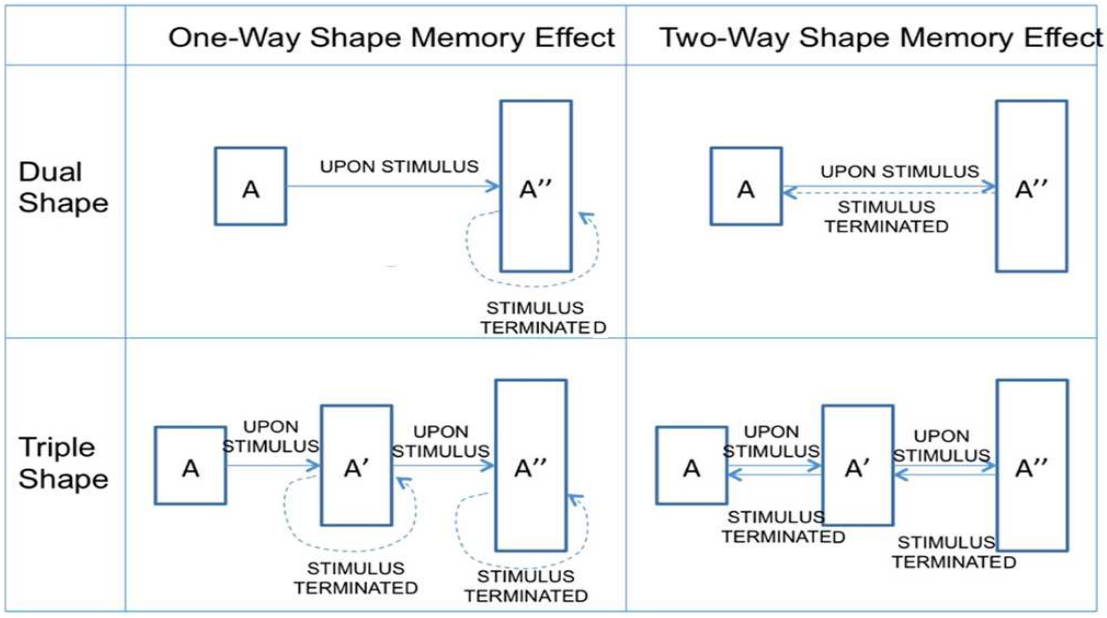

Figure II.9. Functionalities of SMPs or their composites [11]

II.4.7) Shape memory effects in SMPs

II.4.7.1) One-way and Two-way SME

The SM cycle can be divided into two steps: the programming step and the recovery step. Normally, for each recovery step there is a programming step before the recovery step. It means that it is not possible to get a recovery step without the programming step. The recovery is obtained in one direction that is terminated after its completion which means that it cannot go for a number of recoveries with a single programming. For more recoveries, it must be induced

the programming step in the material each time. Hence, the shape memory recovery in one direction is called 1W-SME. Contrary to this, if the material has the ability to go for a number of shape memory recoveries with only one programming step, then, it is called the 2W-SME. This means that the material has the ability to reverse its shape during heating and cooling [33-34].

The difference between 1W and 2W-SMEs is clearly shown in the Figure II.10 where T_H and T_L are temperatures greater than and less than the transition temperature of the material. The top arrow represents the 1W-SME while the circularly oriented arrows represent the repeatable, thermally controlled 2W-SME.

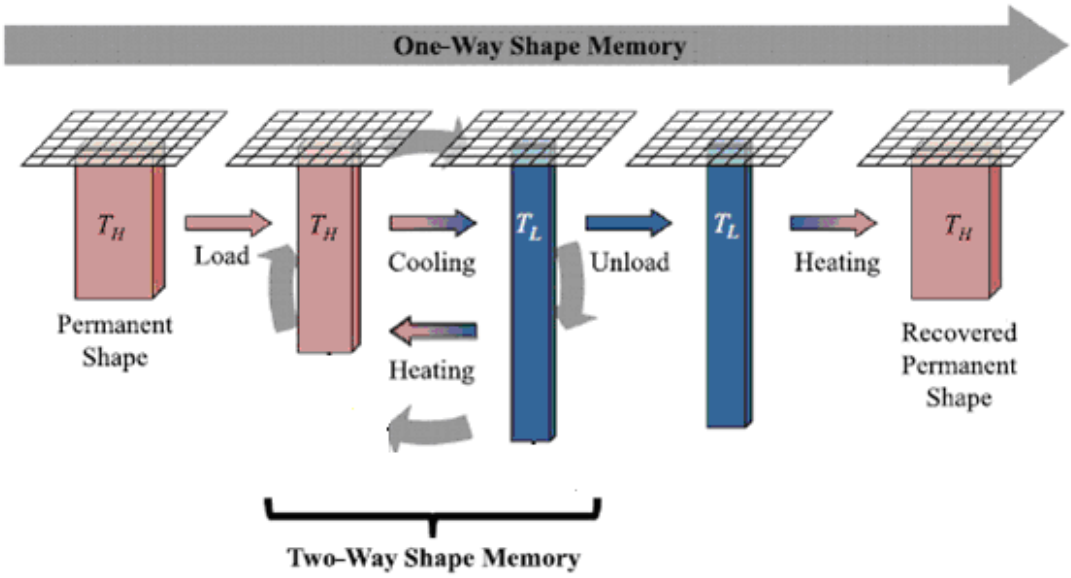

Figure II.10. 1W and 2W shape memory effects (reproduced from [34])

Similarly, 3D views of 1W and 2W-SMEs are demonstrated in Figure II.11. Figure (i) shows 1W recovery whereas (ii) shows the 2W-SME during recovery heating and cooling. This shows that 1W-SME requires another programming step for the second SME whereas 2W-SME performs reversible actuations and repeats number of recovery cycles having one position during heating and other position during cooling. The 2W effects of the shape memory materials function by their own distinctive mechanisms and actuations.

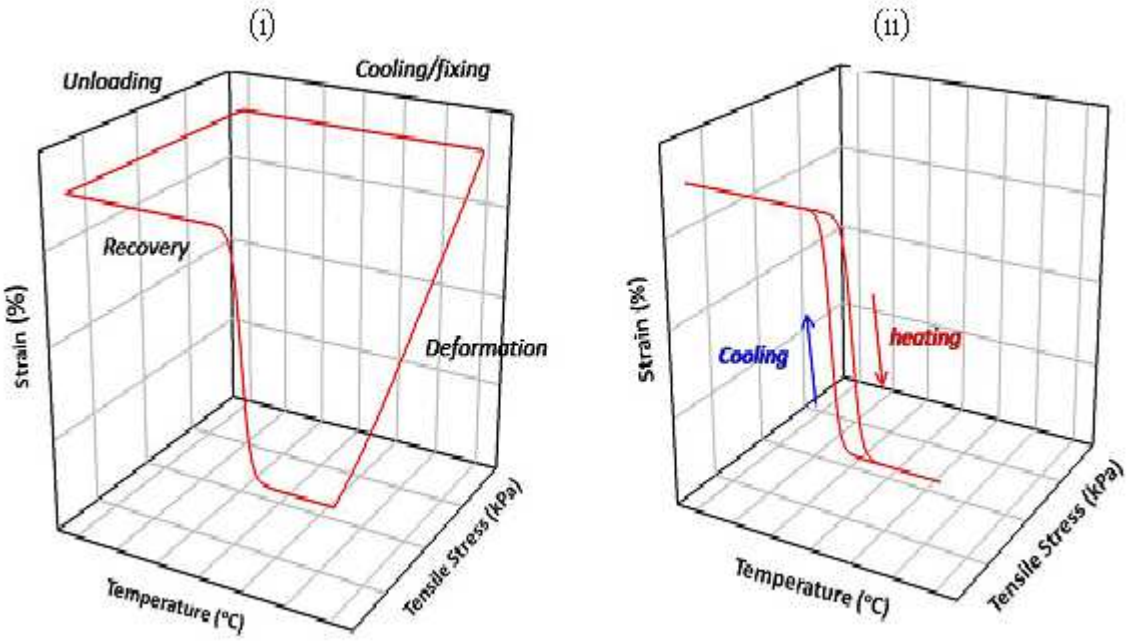

Figure II.11. Schematic illustrations of 1W and 2W shape memory cycles: (i) 1W shape memory cycle and (ii) 2W shape memory cycle [10]

Many efforts have been conducted to make SMPs having 2W-SME. *Chung et al.* have prepared cross-linked poly-cyclooctene (PCO) semicrystalline network samples by variation in the concentration of dicumyl peroxide (DCP) used as a thermal initiator and investigated the 2W shape memory behavior. Within this, when the material is heated above its transition temperature, load is applied to align the chains in the direction of the applied load. They have found that the cured PCOs undergo significant elongation in strain on cooling, producing crystalline domains and maintaining the temporary shape. The temporary shape can be recovered during contraction on heating under a constant load, thus, revealing novel dual shape 2W shape memory behavior in a polymer system. The crystallization process induces the strain increment while melting process induces contraction [35].

Westbrook et al. have achieved dual shape 2W-SME by embedding PCO-DCP (described by *Chung et al.)* strip in the polymer elastomeric matrix. The system thus performs 2-W actuation with the change in temperature without any need of an external load. The description of the system is shown in Figure II.12.

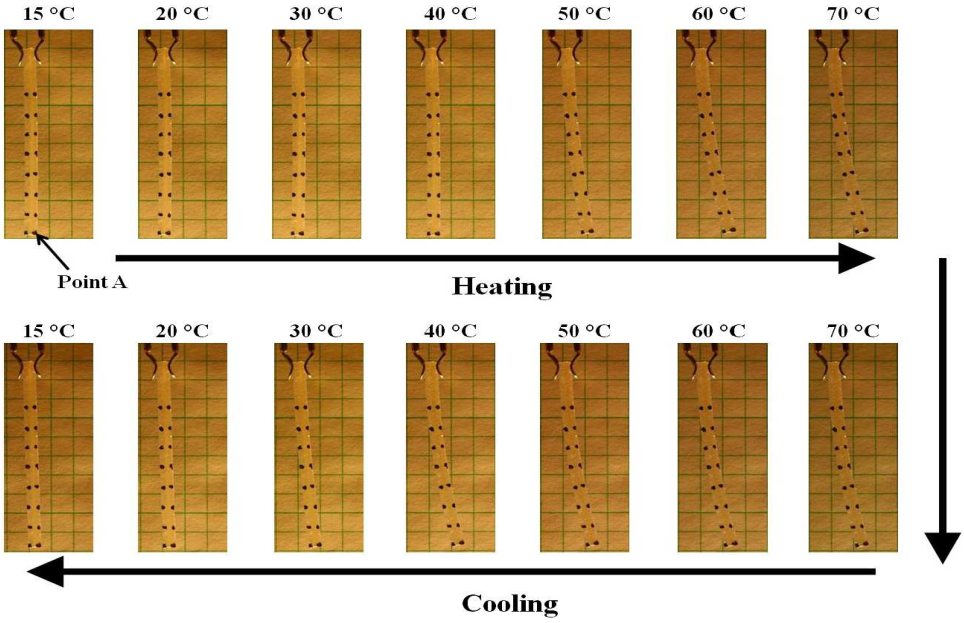

Figure II.12. 2W actuation [34]

Shaojun Chen et al. have prepared a laminate of PU shape memory layer with an elastic substrate layer of PU. They have observed the bending of the laminate upon heating; however, the reverse bending during cooling. During heating, the PU layer recovers and bends in one direction while during cooling, the elastic force of substrate layer bends the laminate in the reverse direction, thus, performing dual shape 2W-SME. In Figure II.13, the laminate is shown which goes from position A to position B when PU layer is recovered due to F_A during heating whereas during cooling, the elastic force of substrate layer brings the laminate very close to position A. Thus, this cycle continues performing 2W-SME [36].

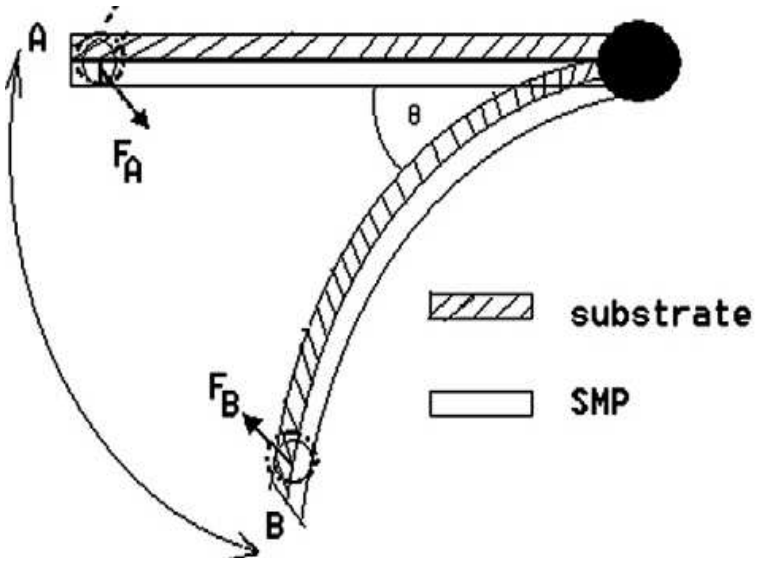

Figure II.13. 2W actuation in bilaminate [36]

Shaojun Chen et al. have prepared the laminated structures "the shape memory polyurethane based shape memory polymer composite" (SMPU-based-SMPC) by combining the pre-elongated SMPU film with the un-elongated elastic polymer film through physical combination of layer-by-layer. They have shown dual shape 2W-SME in these laminates. During heating, due to the restoring force of PU film, the laminate tends to recover, thus, bending in one direction occurs. However, during cooling, reverse bending occurs due to elastic force produced during recovery bending the structure in the other direction [36-37].

Tae-Hyung Kang et al. have fabricated a composite with PU based core and elastomeric based shell. Upon heating, the composite contracts due to the recovery force in the SMPU, simultaneously exerting a compressive force on the cured elastomer (see the arrow pointing in the right-hand direction in Figure II.14 (b). During subsequent cooling, the recovery force in the SMPU relaxes, due to the crystallites formed in the SMPU, but the compressive stress in the elastomer transforms into a tensile force, thus, bringing about crystallization induced elongation (see the arrow pointing in the left-hand direction in Figure II.14 (b)). As a result, the composites show net dual shape 2W-SME behavior under repeated heating and cooling without any external load involved [38].

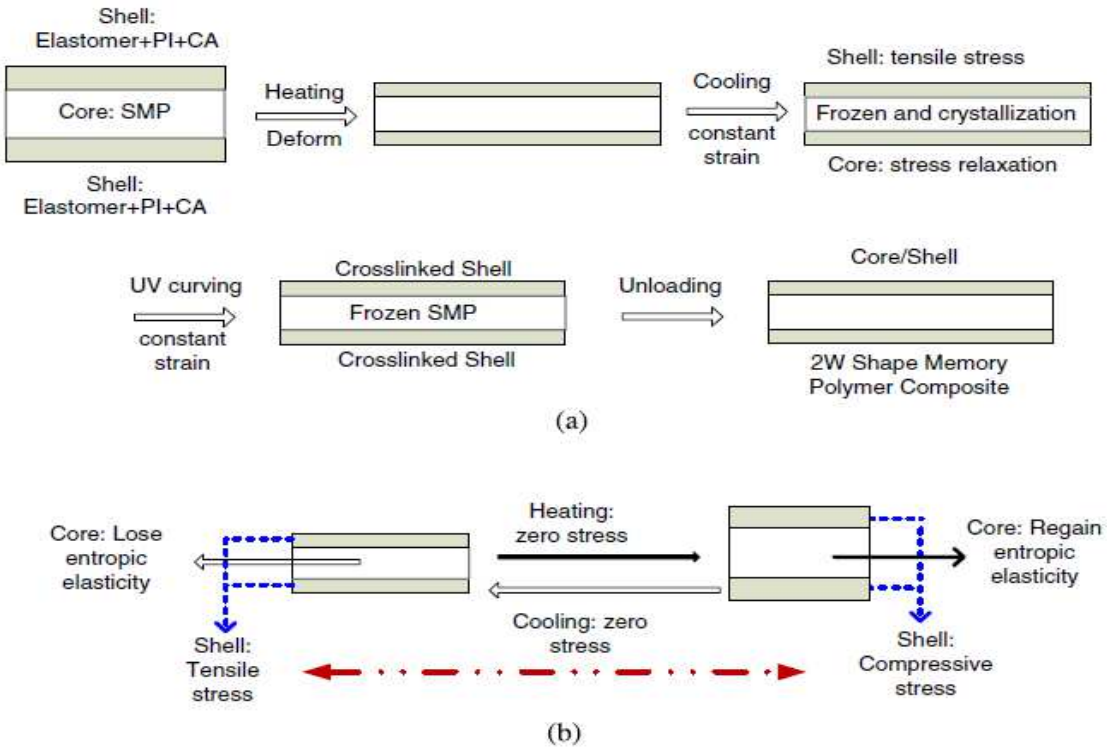

Figure II.14. Schematic diagrams for (a) manufacturing of 2W SMP composite and (b) explaining the 2W mechanism [38]

II.4.7.2) Triple shape memory effect

Triple Shape Memory effect **(**Triple-SME) refers to the phenomenon that a SMP can memorize two temporary shapes in a single shape memory recovery cycle. This effect is obtained through two-step programming. Many efforts have been conducted to make the materials having triple-SME with single or multi-step programming.

Marc Behl et al. have produced 1W triple-SME through one and two-step programming in AB polymer networks. The polymer consists of two different immiscible segments based on poly(ε-caprolactone) (PCL) and poly (cyclohexyl methacrylate) (PCHMA). The melting temperature for PCL is −10°C, the Tg of PCHMA is 70°C and 150°C has been chosen as a temperature above than Tg. It is possible to have triple-SME if the polymer is cooled from 150°C to 70°C which will allow the vitrification of PCHMA creating first switch segment. Similarly, second switching segment can be created if the polymer is cooled from 70°C to −10°C allowing the crystallization of the PCL. This process is shown in Figure II.15 a&b. However, they have

found that it is also possible to create switching segments through a single-step i.e. if the polymer is cooled directly from 150°C to −10°C shown by c in the Figure II.15. So, when the polymer is heated from −10°C to 70°C the first switching segment activates and recovers the polymer to the first position and further heating to 150°C activates the second switching segment, thus, recovering the original position of the polymer. Thus, they have produced triple-SME through a single-step programming [39].

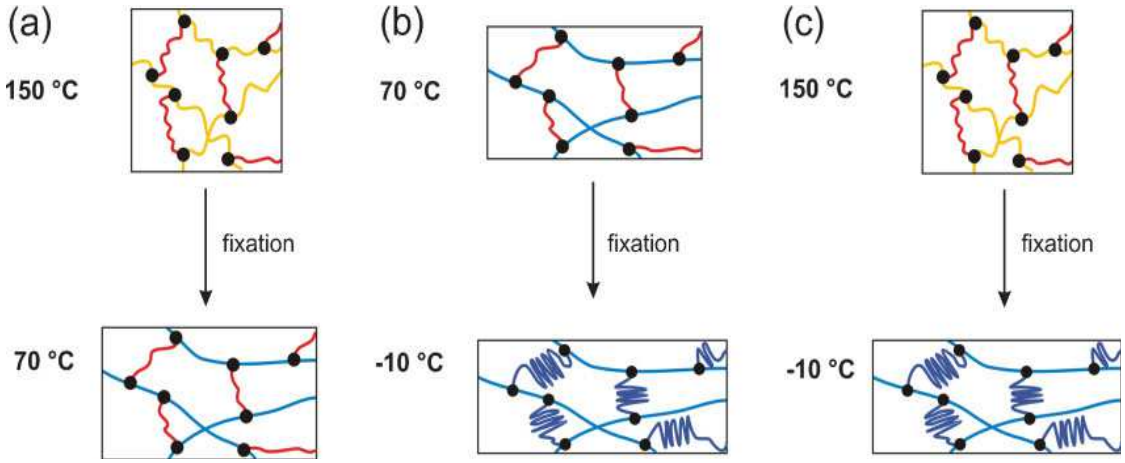

Figure II.15. (a&b) shows two-step whereas (c) shows single-step of programming [39]

Ingo Bellin et al. have obtained 1W triple-SME in multiphase polymeric networks consisting of (ε-caprolactone) (PCL) chain segments and poly(ethylene glycol) (PEG) side chains. They have conducted the same type of work as conducted by *Marc Behl et al.* They have used two types of programming: one-step programming and two-step programming. In two-step programming, the polymer was deformed first at 70°C and cooled to 40°C *(case I in Figure II.16)*, so, as to crystallize PCL chain segments. Then, again the polymer was deformed at 40°C and cooled to 0°C *(case II in Figure II.16)* so as to crystallize the PEG chain segments. In one-step programming, the polymer was deformed at 70°C and cooled to 0°C *(case III in Figure II.16)* in a single-step which gives the same effect as obtained in the two-step programming. Also, during recovery, the two types of programming give the triple-SME [40].

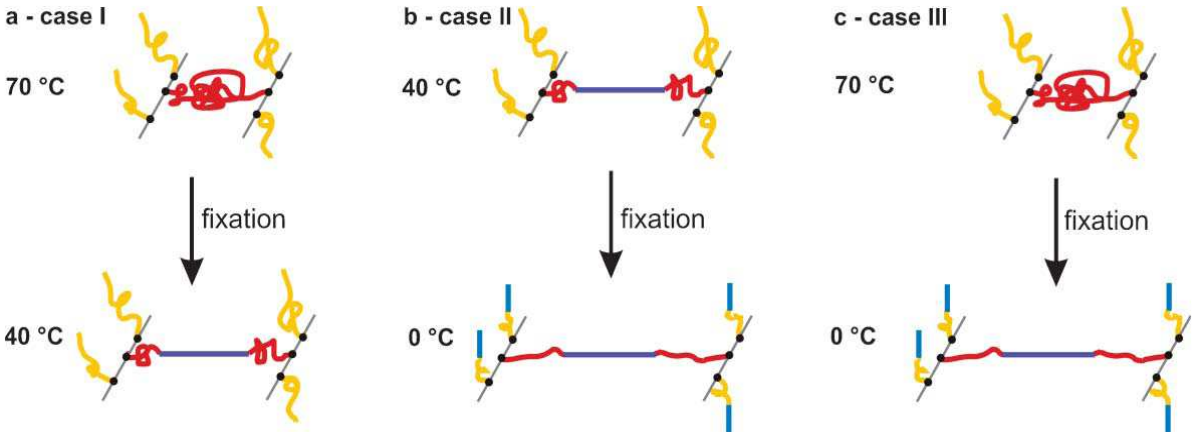

Figure II.16. (a&b) Two-step and (c) One-step programming for triple SME [40]

Tao Xie et al. have also obtained 1W triple SME in bilayers consisting of two epoxy layers with well separated value of Tg**.** They have also used the two step programming cycle and, similarly, recovery is also conducted in two steps shown in Figure II.17.

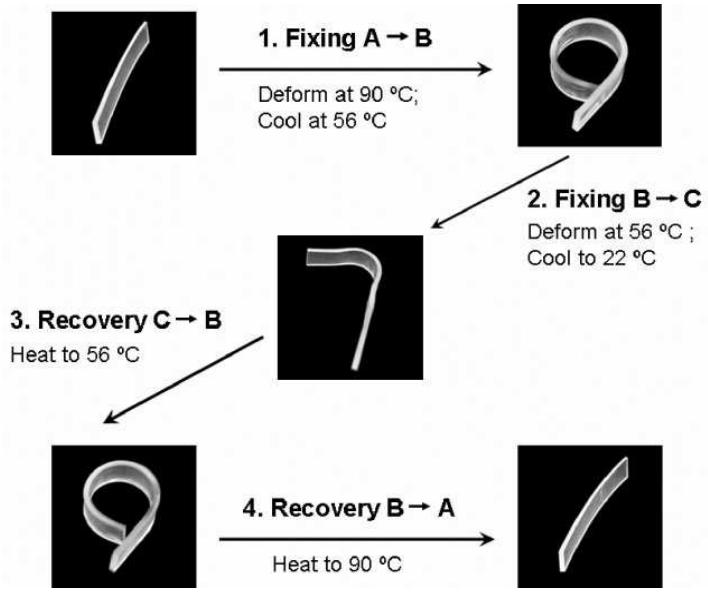

Figure II.17. Two-step programming for triple SME [41]

Thorsten Pretsch et al. have obtained 1W triple SME by two-step programming of the segregated polyurethane. During the programming, they deformed the material at 60°C and fixed the first deformation through soft segment crystallization by cooling to -20°C. They further deformed the material at −20°C and fixed this deformation by cooling it to −60°C. During the recovery, the material was first heated to 23°C to get the first recovery and then to

60°C to get the 2nd recovery. Thus, they have obtained two recovery responses with the two-step programming [42].

Junjun Li and Tao Xie have also obtained 1W triple-SME in Nafion obtained from DuPont by two-step programming. They deformed the material at 100°C and fixed at 60°C to obtain first fixing. The material was deformed further at 60°C and fixed at 20°C. The first recovery was obtained by heating to 60°C and similarly second recovery was obtained by heating to 100°C [43].

Similarly, *I. Bellin et al* have developed two polymer networks named as MACL and CLEG. They have demonstrated that with two-step programming and different combinations of shapes (e.g. shape A and shape B) it is possible to have a resulting "shape C" by adjusting specific parameters of the programming process [44].

Jose M. Cuevas et al. developed 1W triple-shape memory polymers by blending and cross-linking of the two semi-crystalline polymers (poly-cyclooctene, PCO, and polyethylene, PE). Through this, they have created two pronounced segregated crystalline domains within a covalently cross-linked network. Thus, by two-step programming, they have obtained triple-SME in the polymer blended structure [45].

II.4.7.3) Multi shape memory effect

Multi shape memory effect (multi-SME) is an effect in which the shape memory material has the ability to obtain number of positions during the recovery process with a mutli-step or a single-step programming. Some efforts have also been made to have multi-shape memory effect in the polymers.

Kolesov and Radusch have developed a SMP blended linear high-density polyethylene (HDPE), ethylene-1-octene copolymers (EOC), which can obtain 1W multi-shape memory effect if the blend is deformed by a multiple step programming and recovered properly. This multi-SME has been obtained through multiple crystallization and melting behavior of the material. Similarly, it is possible to obtain triple and quadruple SMEs with two and three-step programming respectively [46].

Similarly, Tao Xie has explored the SM properties of the PFSA, a commercial thermoplastic polymer with a polytetrafluoroethylene backbone and perfluoroether sulphonic acid side chains**.** The PFSA used in this study is Nafion, which has an equivalent weight (average molecular mass per mole of ionic groups in g mol^{-1}) of 1,000. It possesses a broad glass transition from 55 °C to 130 °C. He has obtained 1W triple and quadruple SMEs with special programming cycle and recovery.

The quadruple-shape memory effect for PFSA is demonstrated in Figure II.18. The permanent shape S0 is deformed at 140 °C and fixed at 107 °C to yield the first temporary shape S1, which is further deformed at 107°C and fixed at 68°C to yield the second temporary shape S2. Similarly, it is further deformed at 68°C and fixed at 20°C to get the third temporary shape. Upon reheating to 68 °C, the recovered first temporary shape S1rec is obtained. Further heating to 107 °C yields the second temporary shape S2rec. Similarly, further heating to 140°C yields the third temporary shape S3rec.

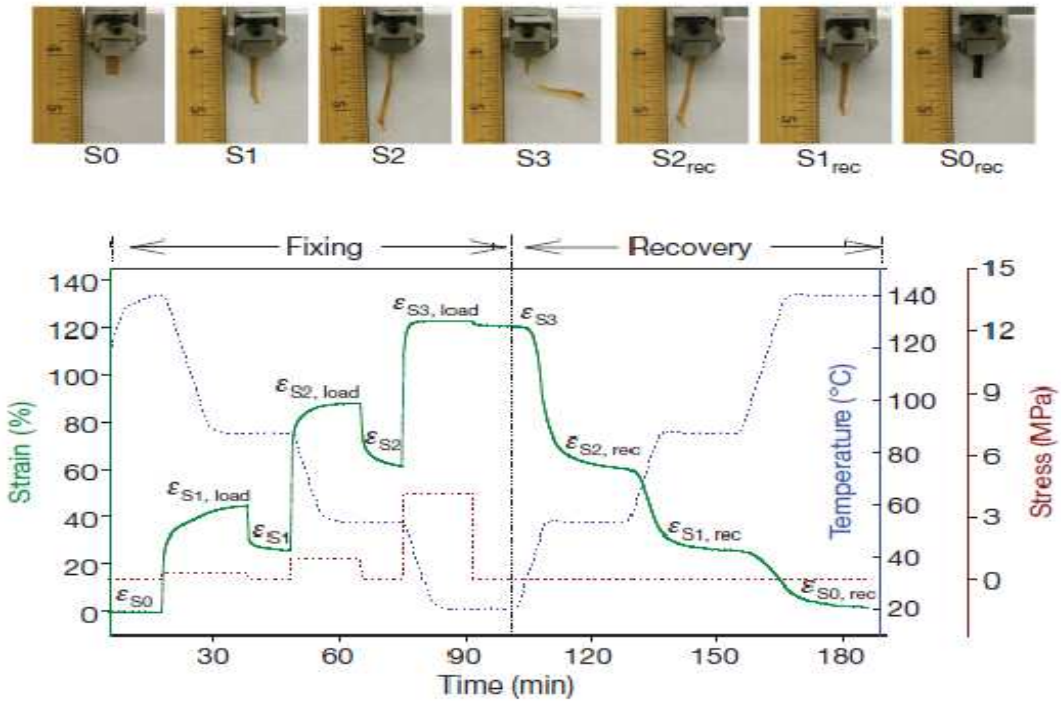

Figure II.18. Quadruple-shape memory effect [47]

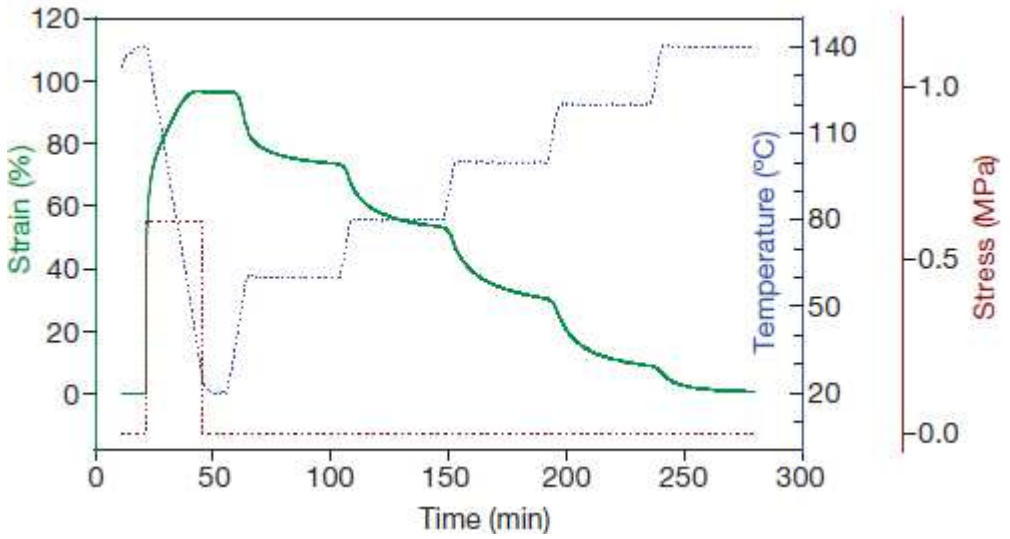

Figure II.19. Multi-shape memory effect through one-step programming [47]

Similarly, he has also obtained multi-SME with only one programming cycle by multi-step heating during the recovery process. It is shown clearly in the Figure II.19.

Kai Yu et al. have investigated the underlying physical mechanisms for the multi shape memory behaviors and the associated energy storage and its release by using a theoretical modeling approach. They have used multi-branch model similar to the generalized standard linear solid model (shown in Figure II.20) for visco-elasticity for a quantitative analysis. They have confirmed that the energy release during multi-steps is a complicated process [48].

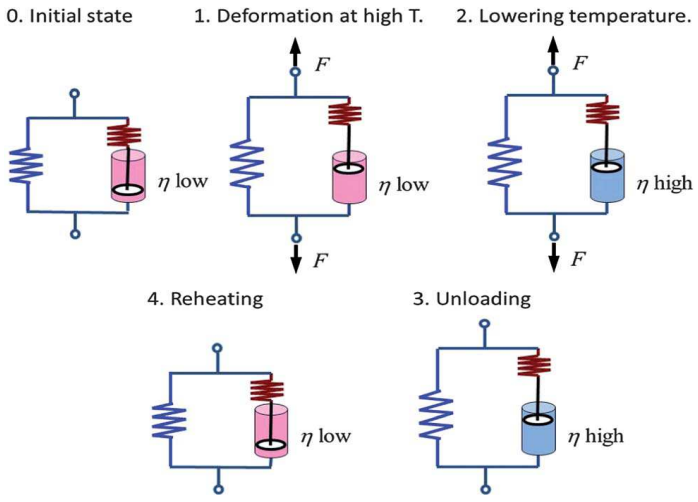

Figure II.20. Standard linear solid model that is used to illustrate the mechanism of shape memory effects in SMP. η represents viscosity [48]

Similarly, *Li Sun et al.* have demonstrated that through the programming, the thermo-responsive polymers can show multi shape memory properties. They have revealed the underlying mechanism of 1W triple and multi-SME in SMPs through experimentation and simulation. Furthermore, they have confirmed that the maximum stress is obtained during the recovery (constrained recovery), if the polymer is recovered at the temperature equal to the temperature at which the polymer was deformed during its programming [49].

II.5) Shape memory polymer composites

The light weight, low cost, easy processing and very high recoverable strain (several hundred percentages) compared to shape-memory metallic alloys (SMAs) (maximum 8%) and ceramics, make SMPs good candidates for many potential applications. However, the disadvantage of the SMPs is their lower stress recovery (3±2MPa) than the SMAs (0.5±0.25GPa) which limits their use in certain applications under constraint conditions [33].

The development of SMPCs provides the solution for this problem which makes them stronger enough to produce larger recovery stresses. Therefore, a lot of research efforts have been focused on increasing the naturally low stiffness and low recovery stress of SMPs through the development of composites, which incorporate shape memory polymer as the matrix material [18, 50-53].

The incorporation of reinforcement in any form increases the stiffness, strength and actuation stress of the composite structure [9, 13, 54-57]. The reinforcement may be nano- particles, chopped fibers of carbon, glass or Kevlar. Similarly, some fillers such as carbon black, carbon fibers or carbon nano-tubes can be added to the composite structure which enables the structure to activate through Joule's effect by providing electric current to the structure. Similarly, the SMPC containing magnetic particles, such as iron oxide or nickel zinc ferrite, could be inductively-actuated by exposure to an alternating magnetic field. The latter approach has the advantage of wireless/remote operation [58].

II.5.1) Types of shape memory polymer composites

II.5.1.1) Particle-filled shape-memory polymer composites

The SMPs filled with particles or short fibers come under this category. The filled particles may be carbon black, carbon nano-tubes, carbon nano-fibers, SiC, Ni, Fe3O4, clay, and short fibers may consist of short carbon fibers etc. The SMPs with these fillings increases the elastic modulus, or stiffness thus increasing the recovery stresses of the composite. However, SMPs filled with particles or short fibers are used as functional materials and not as structural materials. For example, electrically conductive carbon black, carbon nano-tubes, and chopped carbon fibers are incorporated into SMPs to develop electro-active SMPs [11].

II.5.1.2) Fiber-reinforced shape-memory polymer composites

The continuous reinforced SMPs are much stronger than the particle filled SMPCs showing improved mechanical properties such as in stiffness, strength and resistance against creep and relaxations. These improved properties make them capable for use in deployable structures such as in antennas, trusses and solar systems. The thermosetting SMPs with fiber reinforcement can be used as multifunctional composites as these have chemical, thermal stability as well as resistance against moisture [11].

II.5.2) Effect of reinforcement on shape memory effect of composites

In general, SMPs have low strength and stiffness that is why they have high elongation strain. The addition of reinforcement such as carbon nano-tubes, nano-fibers, fillers, fibers or fabric layers etc. increases the stiffness and strength of the structure. Such reinforcements influence the shape memory properties of the shape memory polymer composites. The increase in stiffness due to the reinforcement increases the elastic modulus of the structure. Hence, the instantaneous spring-back displacement increases during the programming cycle of the composite which results in decrease in overall fixity of the composite [59]. The fiber volume fraction of the reinforcement also affects the overall behavior of the shape memory composites. As fixity is obtained mainly due to the matrix in the composite, therefore, higher fiber volume fraction reduces the fixity of the composite. However, more fiber volume fraction increases the recovery of the composites as the elastic recovery of the reinforcement helps in the recovery of

the composites. As a result, residual strain decreases for the shape memory polymer composites with more fiber weight fraction. The residual strain decreases as a part of this residual strain is already recovered as spring-back recovery during the programming cycle [51]. A lot of study has been conducted to show the effect of different reinforcements on the shape memory properties of the composites which are explained ahead.

Ken Gall et al. have examined that the recoverability of the composite strongly depends on the presence of SiC particles. The addition of reinforcement decreases the unconstrained recoverable strain whereas it increases the recovery forces during constrained recovery. Furthermore, the hardness and modulus of the composite material can be tailored for a given application by altering the weight fraction of the SiC, or using alternative reinforcement materials/architectures [50].

I. Sedat Gunes et al. have studied the influence of Carbon black (CB) in polyurethane nano-composites. They have shown that the 3% loading of CB, starts to degenerate the shape memory properties whereas at 5% loading, its shape memory properties are completely destroyed due to its brittleness. They have found that CB nano-particles strongly deduce the crystallinity of soft segment of polymer due to which shape memory properties of the nano-composite are reduced [60].

Subrata Mondal et al. have found the optimized shape memory properties at 2.5 wt% of multi-walled carbon nano-tubes MWNT in the segmented polyurethane because this weight fraction gives enough stiffening effect to polymer chains [61].

J M Cuevas et al. have found similar kind of results by making glass fibers reinforced polyethylene composites. They have found that the addition of reinforcement increases the stiffness of the composite due to which recoverable strain decreases; however, the recovered force increases [62].

Masaaki Nishikawa et al. have studied the effect of fiber volume fraction, fiber aspect ratio, and fiber end position on the shape fixity and shape recovery of the composite. They have found that the fiber volume fraction, fiber length and fiber end positions greatly affects the shape fixity of the composites. Higher fiber volume fraction and large fiber length degrades the shape fixity as

the overall elasticity of the composite increases. Similarly, fiber end positions also affect the shape fixity and recovery ratios as the position of fiber ends influences the overall stiffness of the composite which ultimately degrades or improves the shape fixity and recovery ratios [59, 63].

Takeru Ohki et al. have predicted that there exists an optimum fiber weight fraction between 10 and 20 wt% to have an extremely low residual strain during cyclic loading. Furthermore, they have found that the recovery ratio is better for the composite with high fiber volume fraction; however, the recovery for the neat polymer also increases as the number of recovery cycles increases [51].

Similarly, *Takeru Ohki et al.* have also studied the relationship between fiber volume fraction and recoverability for discontinuous fibers reinforced SMPCs. The composite stiffness and recoverability depends strongly on the volume fraction of the discontinuous fibers. They have found that the addition of 50% chopped fibers increases the stiffness 4 times whereas decreases the recoverable strain 2.5 times [51].

Liang C et al. have demonstrated that the glass fibers and Kevlar reinforcements increase the stiffness of the SMP resins and reduce the recoverable strain levels [12].

Chun-Sheng Zhang et al. have studied the effect of carbon fabric reinforcement on the storage modulus and the recovery of laminates. They have found that the carbon fabric based laminate shows much higher storage modulus than SMP sheet. Similarly, recovery ratio of the SMP based laminate is found to be much larger than that of SMP sheet [64].

II.5.3) Shape memory effects in polymer composites

In Literature, multi-SME has not been reported in fiber reinforced SMPC; however, the 2W-SME and triple-SME has been rarely found.

Xiaofan Luo et al. have obtained 1W triple-SME through two-step programming in shape polymeric composites by incorporating non-woven thermoplastic fibers of a low melting temperature semi-crystalline polymer into a Tg based SMP matrix. One transition has been obtained from Tg of matrix and the second from the melting of the fibers which have been subsequently used for the fixing/recovery of two temporary shapes [65].

However, *Hirohisa Tamagawa et al.* have produced thermo-responsive 2W shape changeable polymeric laminate simply by attaching a resin plate to the fiber-reinforced polymer plate with instant glue. The bending of laminates is caused by the difference of coefficients of thermal expansion between the resin and fiber-reinforced polymer plates. The fiber-reinforced plate does not have a large thermal expansion or contraction. Such a difference between the thermal expansion of resin and fiber-reinforced polymer plates results in the bending [66].

Similarly, *H. Tobushi et al.* have used SMA as reinforcement in SMP for the fabrication of the shape-memory composite (SMC) that gives dual shape 2W-SME. They have used two kinds of SMA tapes showing SME and super-elasticity (SE). These two kinds of shape memorized round SMA tapes were arranged facing in the opposite directions. In Figure II.21, it is shown that the SMC belt is bent convexly downward (in the direction of the memorized round shape of the SE-SMA tape) using the recovery force of the SE-SMA tape at low temperature. However, it bends convexly upward (in the direction of the memorized round shape of the SME- SMA tape) using the recovery force of the SME-SMA tape at high temperature [67-68].

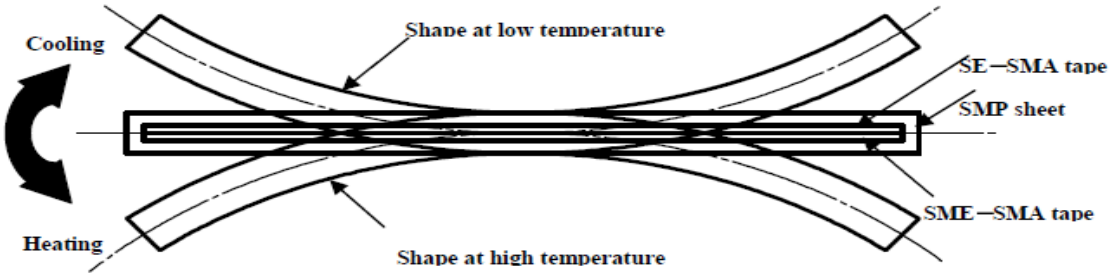

Figure II.21. 2W actuation in SMC belt [67-68]

Similarly, *H. Tobushi et al.* have produced a shape memory composite belt by using SMA wires and Polyurethane-SMP sheet matrix that performs the same type of dual shape 2W function. However, in this composite belt, first bending is performed by the SME of PU matrix during heating whereas the second bending is performed by the SMA wires during cooling [69-70].

In such type of composites, the main problem is the problem of adhesion between the SMA wires and the polymer matrix in a composite structure. A strong interfacial bond increases the

structural integrity of the composite. Due to the bad adhesion between SMA wires and polymer, the interface is not so strong which creates problems during the transfer of load or strain to the matrix. Similarly, the interfacial bonding between the SMA and polymer matrix is mechanical, not chemical bonding; however, by increasing the surface roughness of the wire bond strength can be increased [71].

Table II.3 describes the summary of the recent works regarding the different functionalities of the polymers or their composites.

Authors	**Type of programming**	**SMP/ SMPC**	**1W / 2W**	**SME**	**Type of actuation**	**Reference**
Chung et al.	One-step	poly-cyclooctene (PCO) semicrystalline network	2W	Dual-SME	bending	[35]
Westbrook et al.	One-step	poly-cyclooctene (PCO)	2W	Dual-SME	bending	[34]
Shaojun Chen et al.	One-step	PU/elastic laminate	2W	Dual-SME	bending	[36]
Shaojun Chen et al.	One-step	PU/elastic laminate	2W	Dual-SME	bending	[37]
Tae-Hyung Kang et al.	One-step	A composite PU based core and elastomeric based shell	2W	Dual-SME	Compression /elongation	[38]
Marc Behl et al.	One-step and two-step	poly(ε-caprolactone) (PCL) and poly (cyclohexylmethacrylate) (PCHMA).	1W	triple-SME	Compression /elongation	[39]
Ingo Bellin et al.	One-step and two-step	PCL/PEG	1W	triple-SME	bending	[40]
Tao Xie et al.	two-step	bilayers consisting of two Epoxy layers	1W	triple-SME	bending	[41]

Thorsten Pretsch et al.	two-step	segregated polyurethane	1W	triple-SME	bending	[42]
Junjun Li and Tao Xie	two-step	Nafion	1W	triple-SME	bending	[43]
I. Bellin et al	two-step	MACL and CLEG	1W	triple-SME	bending	[44]
Jose M. Cuevas et al.	two-step	PCO and PE	1W	triple-SME	bending	[45]
Kolesov and Radusch	Multi-step	Blended HDPE and EOC	1W	quadruple and Multi-SME	bending	[46]
Tao Xie	One-step and Multi-step	PFSA	1W	quadruple and Multi-SME	bending	[47]
Li Sun et al.	One-step	-	1W	Triple and multi-SME	-	[48]
Xiaofan Luo et al.	two-step	PCL and PEG	1W	triple-SME	bending	[49]
Hirohisa Tamagawa et al.	One-step	Composite laminate	2W	Dual-SME	bending	[50]
H. Tobushi et al.	-	SMA/SE-SMA composite	2W	Dual-SME	bending	[67]
H. Tobushi et al.	One-step	SMA/PU composite	2W	Dual-SME	bending	[68]

Table II.3. Summary of the recent works on SMPs and their composites

II.6) Applications of SMPs and their composites

The SMPs and their composites offer the possibility of their use in automotive, aerospace, building, electrical, optoelectronic, and especially in biomedical applications.

II.6.1) Biomedical applications

The review [29] gives comprehensive information about the applications of SMPs in medical field. Polyurethane-based SMP materials have great possibility of their use in biomedical field that include laser activated surgical tool to remove the blood clots, polymeric stents that overcomes the problems of metallic stents that are used presently [30]. For example, the use of

polymeric stent as a drug delivery system leads to significant reduction of restonosis and thrombosis. Also, polymeric stents are cost effective as compared to metallic stents. A polymeric stent made up of polyurethane used in constricted coronary blood vessels has been shown in Figure II.22 demonstrating the activation of the stent when temperature is provided to the stent.

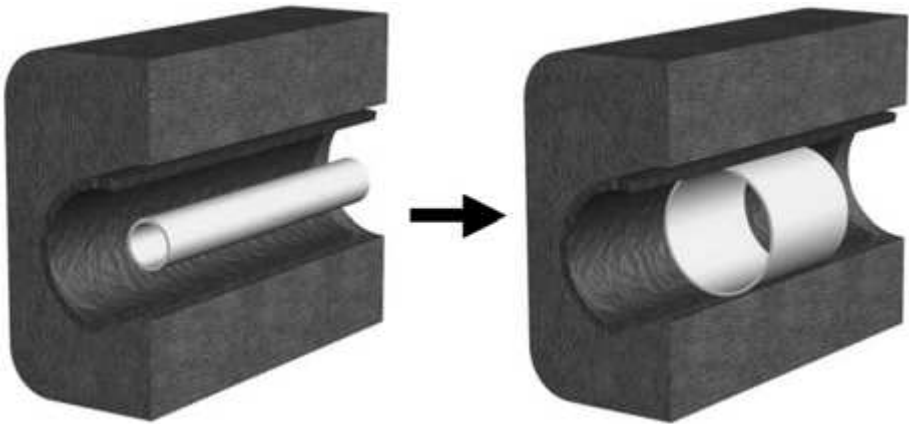

Figure II.22. Principle of the shape memory effect: prior to application (left); after reset (right) [72]

II.6.2) Other applications (deployable structures and actuators)

Some other interesting applications of SMPs and their composites are energy absorbing assemblies [73], tunable vehicle structures [74], releasable fastener systems [75], airflow control devices [76], adaptive lens assemblies [77], healable and structure health monitoring systems [78].

Figure II.23. Shape recovery process of a prototype of a deployable solar array actuated by an SMPC hinge [79].

Figure II.23 shows a prototype of a deployable solar array actuated by a carbon fiber reinforced hinge. It is bent to a storage angle of 90° by the application of an external force at 80°C. After fixing the deformed shape at room temperature, the hinge is heated again and the solar array is deployed from 90° to 0° in 80s [79].

Similarly, the sensing and actuating capabilities of SMPC integrated with hybrid filler of carbon black and chopped short carbon fibers (shown in Figure II.24) have been explored. The output recovery force produced by shape-memory effect of SMPC (electrically activated) is utilized and actuating capability is consequently demonstrated to actuate the motion of a table tennis ball [80].

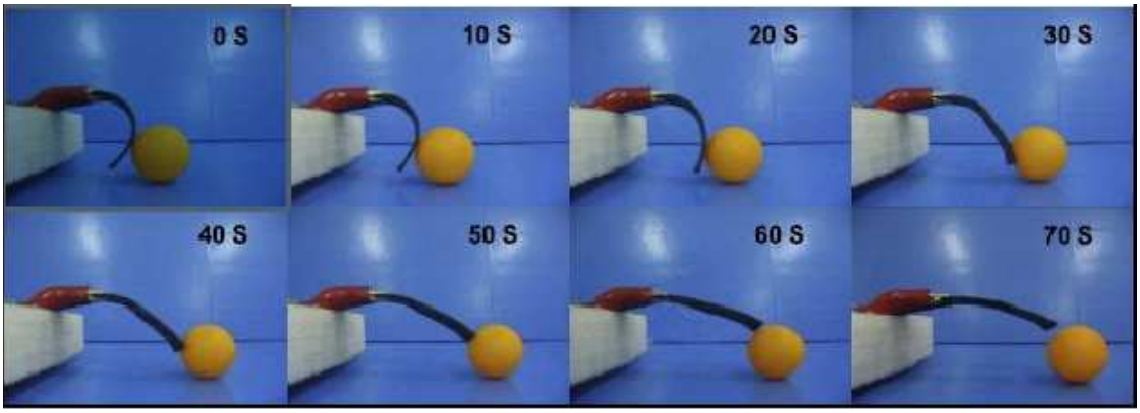

Figure II.24. Series of photographs showing SMC composite and actuating the motion of a table tennis ball. The permanent shape is a plane stripe of composite material and the temporary shape is deformed as a right-angle shape [80]

II.7) Conclusion

Generally, the particle and fiber reinforced SMPCs have been used for the study of SMPCs. The laminated SMPCs or fabric reinforced SMPCs have also been used to study the shape memory properties [79]; however, they are rare. In the present work, a thermosetting epoxy based laminated composite has been used for SM properties. This laminated composite has already been tested as an asymmetric active composite called as “controlled behavior of composite material” CBCM. This composite is similar to SMP laminated composites, in which Kevlar and glass fibers have been used in to investigate the mechanical and shape recovery properties of

thermoplastic SMPCs [64]; however, in this composite, the three types of laminates namely glass fabric laminates, Kevlar and unidirectional glass fiber laminates have been used.

Chapter III. Materials and Methods

III.1.) Introduction

In this chapter, the composite material along with its different constituents (reinforcement and matrix) is discussed. The matrix especially Epoxy polymer with some bibliography is elaborated that shows its use as a shape memory matrix in literature. Also, an introduction, principle and working of a CBCM composite are discussed. The different parameters to define an active composite are also illustrated. In the end, the different thermo-mechanical programming cycles are mentioned that have been used to induce the shape memory properties in the composites. Moreover, the different types of recoveries (unconstrained, constrained and recovery under load) that are usually performed to study the recovery of the induced shape memory property are presented.

III.2) Shape memory polymer composites, reinforcement and matrix

A composite material is a substance consisting of two or more materials, insoluble in one another, which are combined to form a useful engineering material possessing certain properties, not possessed by its constituents [81]. If a shape memory polymer is reinforced with any reinforcement, then it becomes a shape memory polymer composite.

III.2.1) Reinforcement for SMPC

The reinforcements that are used for any type of polymer composite (including shape memory polymer composites) are given below.

– Particles (particulate composites)

The particles are also used as reinforcement. The size of the particles varies from 10-100 nm. The shape of the particle may be spherical, ellipsoidal, polyhedral or irregular in shape. In particles reinforced composites, the bonding at the interface is very important. These particles increase the yield and tensile strength of the composite. The uniform distribution of these particles is necessary to bear most of the applied load [82].

– Fibers (fibrous composites)

The word fiber means a single, continuous material whose length is at least 200 times its width [81]. Glass fibers are the earliest known fibers used to reinforce materials. Ceramic and metal fibers were subsequently found out and put to extensive use, to render composites stiffer more resistant to heat. Fibers fall short of ideal performance due to several factors. The performance of a fiber composite is judged by its length, shape, orientation, and composition of the fibers and the mechanical properties of the matrix [82].

Fibers may be short fibers or long fibers. The short fibers are used as individual fibers; however, long fibers can be used in unidirectional or bidirectional.

• Unidirectional

Unidirectional reinforcements include tapes, tows, unidirectional tow sheets and rovings (collections of fibers or strands). Fibers, in this form, are all aligned parallel in one direction and uncrimped provide the highest mechanical properties. The composites, using unidirectional tapes or sheets, have high strength in the direction of the fiber. Unidirectional sheets are thin and multiple layers are required for most structural applications.

• Bidirectional

Mainly two types of bidirectional fabrics (shown in Figure III.1) are used to reinforce resins in a composite

✓ Woven

In woven fabrics, two sets of yarns are interlaced with one another at right angles. The lengthwise yarns are called as warp yarns whereas transverse yarns are called as weft yarns. The different interlacement of these yarns gives different types of weaves: Plain, Satin and Twill weaves.

✓ Knitted

The knitted fabrics are made by interlocking series of loops of one or more yarns. The two major classes of knitting are warp knitting and weft knitting. Knitting in which the yarns generally run lengthwise in the fabric is called warp knitting (e.g

tricot knitting) whereas knitting in which one continuous thread runs crosswise in the fabric making all of the loops in one course is called as Flat knitting.

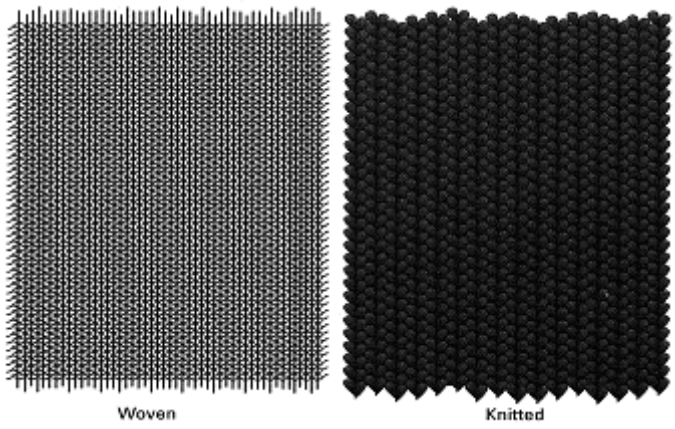

Figure III.1 Woven and knitted fabrics

III.2.2) Shape memory matrix

Various types of thermoplastic (e.g. polyurethane) and thermoset (e.g. styrene) shape memory polymers can be used as matrix for shape memory polymer composites. However, here, our concern is with the Epoxy shape memory polymer.

III.2.2.1) Epoxy as shape memory polymer

It has been already discussed in chapter I that Epoxy shape memory polymer is a good candidate to study the shape memory properties. Hence, the use of Epoxy resin as SMP can be found in literature. It is found that Epoxy has been used to study its shape memory properties along with various properties: mechanical, electrical, its stability in environment, thermo-mechanical cycling, etc.

Some have used the nano-particles as reinforcement to study its shape memory properties. For example, *Ken Gall et al.* [83] have used epoxy resin with 20wt% SIC nano-particles with an average diameter of 700 nm. They have studied the internal stress storage during the programming cycle and its release during the recovery process. Similarly, *Xiaofan Luo et al.* [84] have studied the actuation capabilities by incorporating continuous, non-woven carbon nano-fibers (CNFs) into an epoxy based SMP matrix. They have found that the resulting SMP composite increases the electrical conductivity, recovery stress and heat transfer.

Some have studied the various properties of Epoxy by its thermo-mechanical cycling. *Amber et al.* [85-86] have assessed the viscous effects during multiple shape-memory cycles of Veriflex-E, an epoxy-based, thermally triggered shape-memory polymer resin. They have investigated the effects of the deformation rate and hold times at elevated temperature on the shape-memory behavior. *Ingrid A. Rousseau* [87] has synthesized seven epoxy-amine polymers showing shape memory (SM) properties. They have found that the instantaneous response of tested epoxy-SMPs is independent on composition, structure, and mechanical properties; and the succession of multiple SM cycles does not affect the SM behavior of the 6 tested epoxies, the recovery speed increases with increasing crosslink density. They have confirmed the excellent SM behavior of the prepared epoxies. *Ingrid A. Rousseau et al.* [21] have prepared the epoxy SMP mixtures with three different di-amines as cross linkers. They have found that the SM performances are strongly affected by the strain dependent thermal expansion/contraction of the materials during thermo-mechanical cycling. Also, the networks with lower crosslink density, higher chain flexibility and/or mobility show reduced SM performances.

Some have studied its shape memory properties along with its mechanical properties. *Diane M. Feldkamp et al.* [88] have studied the range of deformability and high strength with intrinsically good thermal and chemical stability of epoxy based SMP networks. *Xuelian Wu et al.* [89] have synthesized three types of epoxy SMPs with various linear epoxy monomer contents and studied their mechanical properties. They have confirmed that the addition of higher linear monomer has a direct affect on Tg and mechanical properties and also show a quicker shape recovery speed. *Yuyan Liu et al.* [90] have prepared a series of organic-montmorillonite (OMMT) modified shape memory epoxy (SMEP) composites. They have found that the addition of OMMT improved the composites' toughness, tensile strength, transition temperature, and shape recovery speed, while shape recovery ratio remain unaffected. *V.A. Beloshenko et al.* [91] have studied the electrical properties of carbon containing epoxy compositions while realizing its shape memory effect. *Hua Deng et al.* [92] have prepared epoxy based SMP modified by flexible epoxy that decreases the transition temperature which improves the toughness properties while not effecting the shape memory properties of the overall epoxy system.

Some have studied its stability in environment along with other properties. *G. P. Tandon et al.* [28] have studied the durability of styrene- and epoxy-based shape memory polymer resin materials for morphing applications when exposed to service environment. They have further investigated the modulus in the rubbery and glassy state, stored strain, shape fixity, stress recovery ratio, and linear shape recovery. In addition, they have monitored changes in specimen color, weight, and dimensions along with onset of damage due to conditioning and subsequent thermo-mechanical cycling. Similarly, *Yuyan Liu et al.* [93] have prepared a series of shape memory epoxy resins by epoxy E-51 and varying content of curing agent DDM (4,4-diaminodiphenyl methane), through compression molding method for the purpose of application on space deployable structures. They have confirmed the excellent thermal, mechanical and shape recovery properties of the SMP epoxies.

Tao Xie et al. [94] have studied the tuning of the Tg of epoxy polymers by varying the crosslink density or chain flexibility of the systems. All the cross-linked epoxy samples show SMP characteristic terms of sharp transition temperatures and excellent shape fixity and recovery.

V. A. Beloshenko et al. [91] have studied the volume changes during the shape recovery in shape memory effect of the epoxy polymer composites with aggregated filler. Similarly, *V. A. Beloshenko* [95] have studied the increase in volume in the thermo-expanded graphite system during the shape memory effect of epoxy polymer.

Francisco Castro et al. [31] have studied the recovery of Epoxy-Based Shape Memory Polymers at higher and lower temperatures than the programming temperature. They have found that the recovery at higher temperature is far better than at lower temperature. Also, recovery at higher temperature yields the fastest recovery.

Similarly, some study has also been conducted on epoxy SMP foams. *Di Prima et al.* studied the shape memory properties of the epoxy shape memory polymer foams. They have showed that epoxy SM foams are capable of recovery from compressive strains of up to 90%; however, the compressive cyclic strain can damage the foam under certain temperatures and applied strains and the packaging temperature strongly affects the unconstrained shape recovery profile

[96-97]. Furthermore, they have developed a model to predict the effect of relative density on modulus [98-99].

In this work, Epoxy Epolam-2025 from the “Axson Technology” has been used as a matrix with an Hardener *{2,2'- dimethyl 4,4'- methylenebis (cyclohexylamine)}*.The mixing ratio is 28 grams of hardener per 100 grams of resin or 34 ml of hardener per 100 ml of resin at 25°C.

III.2.3) CBCM (An active composite)

It is an active composite that works on the principle of bimetallic effect. It uses the effect of different coefficients of thermal elongations in a given direction. Two effects can be obtained: First is called "single effect" or "temperature effect", and the second is called "double effect" or "gradient effect". The double effect has an advantage that it has the possibility to bend in one or two directions. The single effect is obtained in a laminate made of layers with different coefficients of thermal elongation in a given direction that results in bending of the plate (Figure III.2). The different coefficients can be obtained either by different materials or by different orientations of the reinforcement in the layers. Similarly, the double effect can be obtained with any composite structure containing an insulating layer, for example a sandwich structure. A gradient of temperature appears within the structure if one side is heated and insulation is provided between the two sides [100-101]. It also results in bending of the plate (Figure III.2).

Also, this active composite works on internal heat generation (Figure III.3). Heat is produced by using 8 carbon yarns as an active layer that is embedded in the composite. When electric current is provided by the electric generator then due to the Joule’s effect heat is produced which deforms the composite [102-111].

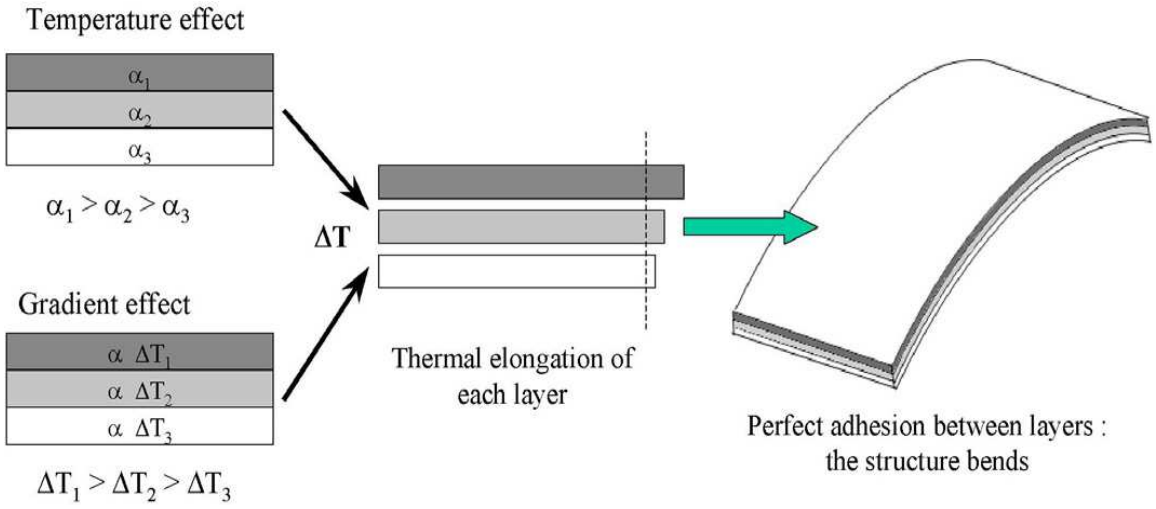

Figure III.2. Temperature and gradient effect [100]

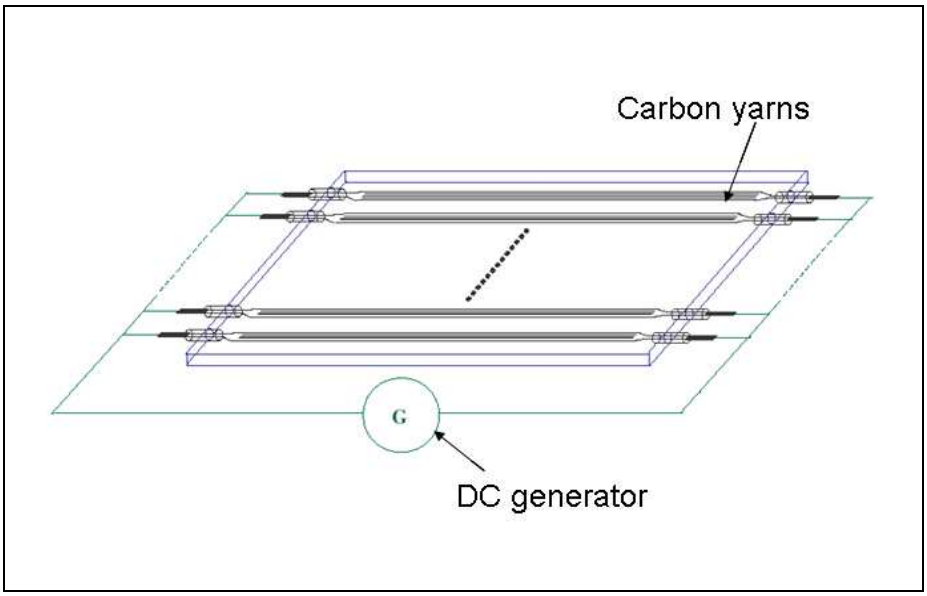

Figure III.3. Active layer used for internal heat generation in the composite plate

Also, CBCM can be compared with other smart materials very precisely. According to energy used and response time, it is very close to SMAs. However, as far as its mass mechanical work and operational system is concerned, it is similar to piezoelectric materials. Apart from this, it can be said that it is an independent structure which can work without the need of additional incorporated structures unlike others. This composite has already been tested as a smart or intelligent material when it is connected to the proportional–integral–derivative (PID) command and sensors (temperature and strain). Then the system can detect the variations in the

background and react accordingly. For example, it can maintain a specific strain when load increases or decreases by changing the input current [100].

III.3) SMPC manufacturing

III.3.1) Preparation of an active layer

The active layer has been prepared by cutting the 8 carbon yarns of the lengths equal to the composite plates i.e. 395 mm. These carbon yarns have been sewn in parallel on the already cut Kevlar fabric in a way that the two yarns have the equal distance between them. Then, the thin copper plates have been glued, transversally to the sewn yarns, on the two sides of the Kevlar fabric. Then, the ends of sewn carbon yarns have been glued on the fixed copper plates with conducted epoxy resin. Thus, the active layer is prepared.

III.3.2) Constitution of composite plates

The different types of composite plates ($395\times12.5\times2$ mm^3) have been manufactured to study different things. The different types of asymmetric composite plates called as CBCM composites have been fabricated. CBCM stands for "composite behavior of composite material". A symmetric composite (SYM) is also made. The detail of organization of each composite plate is given in Table III.1. In addition, the description of each constitutive layer is given in Table III.2.

Composite plate type	organization
CBCM	$(2D^G)_2/(90^G)_2/A_L/(2D^A)_2$
$CBCM^{1/2}$	$(2D^G)_2/(90^G)_1/(0^G)_1/A_L/(2D^A)_2$
$CBCM_{1/2}$	$(2D^G)_2/(0^G)_1/(90^G)_1/A_L/(2D^A)_2$
CBCM-L	$(2D^G)_2/(0^G)_2/A_L/(2D^A)_2$
SYM	$(2D^G)_1/(90^G)_1/(2D^A)_1/A_L/(2D^A)_1/(90^G)_1/(2D^G)_1$

Table III.1. Organizations of different composite plates

Name	Description	Gsm (g/m^2)
$2D^G$	Balanced weaved glass fabric	196
$2D^A$	Balanced weaved aramid fabric	173
90^G	Transversal unidirectional glass fibers	588
0^G	Longitudinal unidirectional glass fibers	588
A_L	Active layer of 8 carbon yarns	--

Table III.2. Description of each constitutive layer

All the layers with the given dimensions are cut and then placed in the mold according to the geometry of the final composite plate. If there are six layers to form a composite, at first, two layers are put and then about one third of the prepared mixture (Epoxy resin + hardener) is poured. Then, again two layers are put and again one third of the prepared is poured. Then, again 2 layers are put and the remaining one third of the prepared mixture is poured. Then, the four pieces of required thickness are placed on the four sides of the lower part of the mould so as to give the thickness to the composite plates equal to the piece used. Then, the upper part of the mould is put on the lower part of the mould and the whole mould is placed in the compression machine for compression molding.

III.3.3) Compression molding

Compression molding is a technique in which resin along with the curing agent, filler and reinforcement is placed in the mould which is then placed under pressure in the compression machine (shown in Figure III.4). The applied pressure causes the resin to flow in the mould. This flow affects the orientation of the reinforcement. The resin system is given enough time so that the cross-linking level can reach to the required level. The molded products are then removed from the mould. The post curing is carried out in a heated oven where maximum level of cross linking is done. The resultant, compression molded samples possess properties including high rigidity and strength (tensile, compression, impact) and good surface properties (smoothness, paintability) [81].

Figure III.4. Machine for compression molding

The mold (shown in Figure III.5) has two parts lower part and upper part. Both are made up of steel. The dimensions of the mold are 400×400 mm^2. The lower part of the mold has four bars which can be opened with screws to remove the prepared composite plates. The upper surface of the lower part and lower surface of the upper part of the mold are polished with wax,

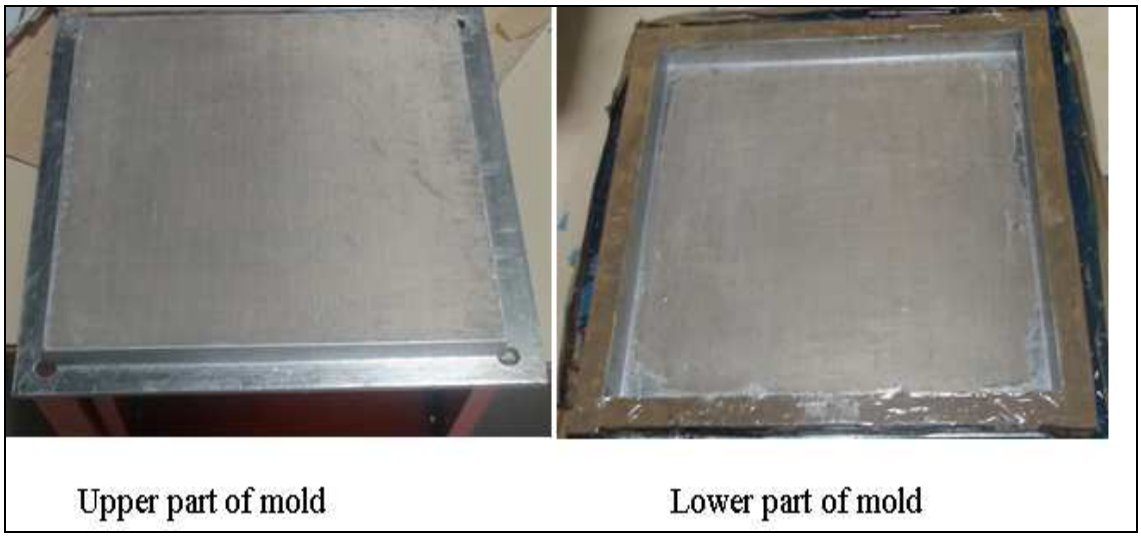

Figure III.5. Mold

so, that the resin cannot stick to the surfaces of the mold. In this way, the composite plates are very easy to remove from the mold.

III.3.4) Curing cycle

After the fabrication of the composite plates, they have been cut and then cured in the oven for polymerization. The curing cycle has been followed as recommended by the manufacturers to obtain the Tg of 130°C. Then the oven is switched off and the composite plates are taken out after cooling.

III.4) Experimental techniques

III.4.1) CBCM and SMPC mechanical characterization

III.4.1.1) Apparatus

The mechanical characterization is based on a three point bending test (Figure III.6), the composite plate is placed on the two supports which are (L = 300 mm) apart. A tensile machine MTS-20 is used for all tests. Thanks to “Test-works software”, different programs are used in order to control the specific tests necessary to characterize the activation and shape memory properties of the SMPC. A load cell of 100 N (accuracy of 0.01) is used and the accuracy of the tensile machine crosshead is also 0.01.

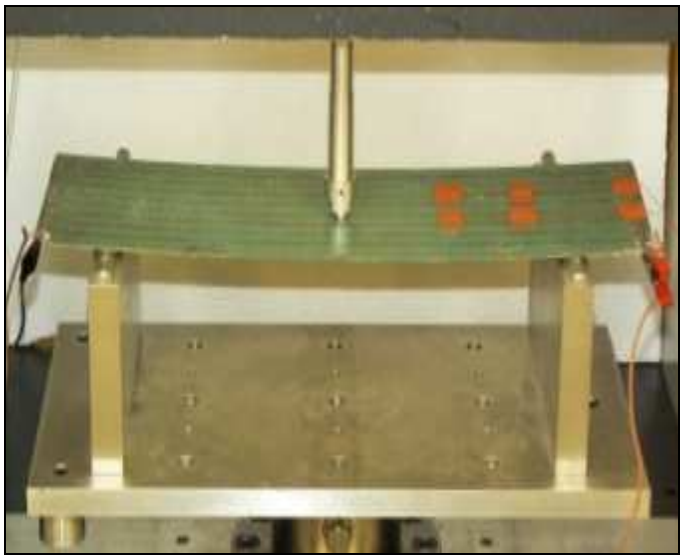

Figure III.6. Three-point bending setup in MTS machine

For the temperature measurement, thermocouples of type K are used. As all the composite plates used in this work have an active layer of eight carbon yarns, so, for each test, one thermocouple is put on the carbon yarn whereas the second thermocouple is put in between the two carbon yarns. Both the thermocouples are put on the upper side of the composite plate. The temperature for the thermocouple on the carbon yarn is always greater than the second one. These thermocouples are connected to DAQ system which works with the Labview software. Hence, different temperatures are visible in Labview software which can be exported to Excel sheets.

III.4.1.2) CBCM activation property

The composites are characterized through free displacement and blocking force tests [112-113]. Free displacement test can be defined as the maximum displacement of the composite attained from its initial position when it is activated to a specific temperature. The free displacement of CBCM composite increases with high temperature and vice versa. This free displacement also depends on the construction of the composite whether the unidirectional glass fibers (UD layer) are transversally or longitudinally placed. The composite with UD layer of transversal fibers have more free deflection as the fibers are not directly involved in the overall mechanical strength and rigidity structure of the composite. However, UD layer with longitudinal fibers

have less free deflection as the rigidity increases with the direct involvement of the fibers in the mechanical strength of the composite. Free displacement is a measure of activated displacement at higher temperature in reference to the initial position at ambient temperature. The composite plate is allowed to move freely under free conditions (no load is applied). It gives instant response when temperature is increased from the ambient temperature. The plate gets heated to a certain temperature and thus it deforms giving a certain displacement which is the characteristic value of free displacement at that temperature. This displacement is fully controllable with the temperature. It will be high at higher temperature and vice versa. Figure III.7 explains the set up for performing the free displacement test.

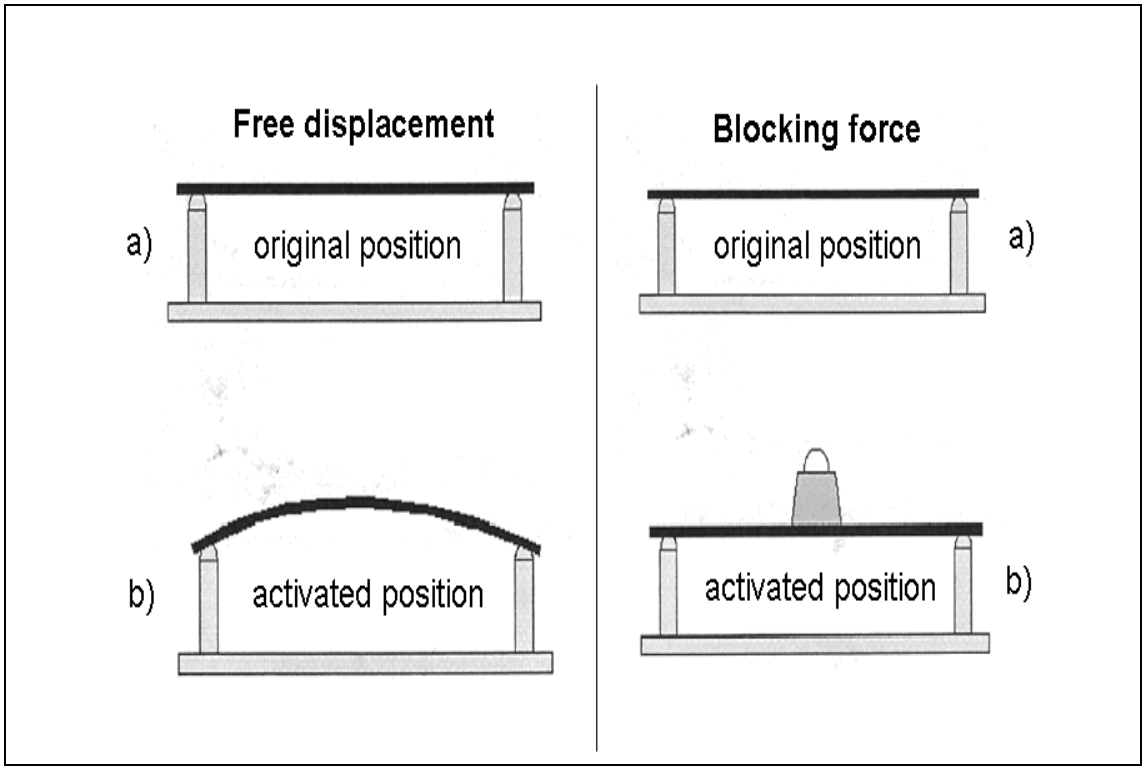

Figure III.7 Description of free displacement and blocking force

Similarly, blocking force test can be defined as maximum force generated when heated the active structure while keeping it blocked at its original (at a specific temperature). The blocking force increases with the increase of temperature as the free displacement increases and thus more force is required to bring the structure at its initial position. In the same way, the blocking force for the composite with transversal fibers in the UD layer is more than the composite with

longitudinal fibers in the UD layer as the latter has more free displacement although former has more rigidity. Blocking force (Figure III.7) is a measure of a force which is generated by blocking the initial position of the composite plate when it is activated by providing a temperature higher than the ambient temperature. Force is generated when the composite plate is activated by providing a certain temperature and the measured value of force will be the characteristic value of blocking force at that temperature. Blocking force increases with the increase in temperature. The different blocking forces can be measured at different temperatures. Blocking force increases with the increase of temperature showing that composite plate gets more activated at high temperature.

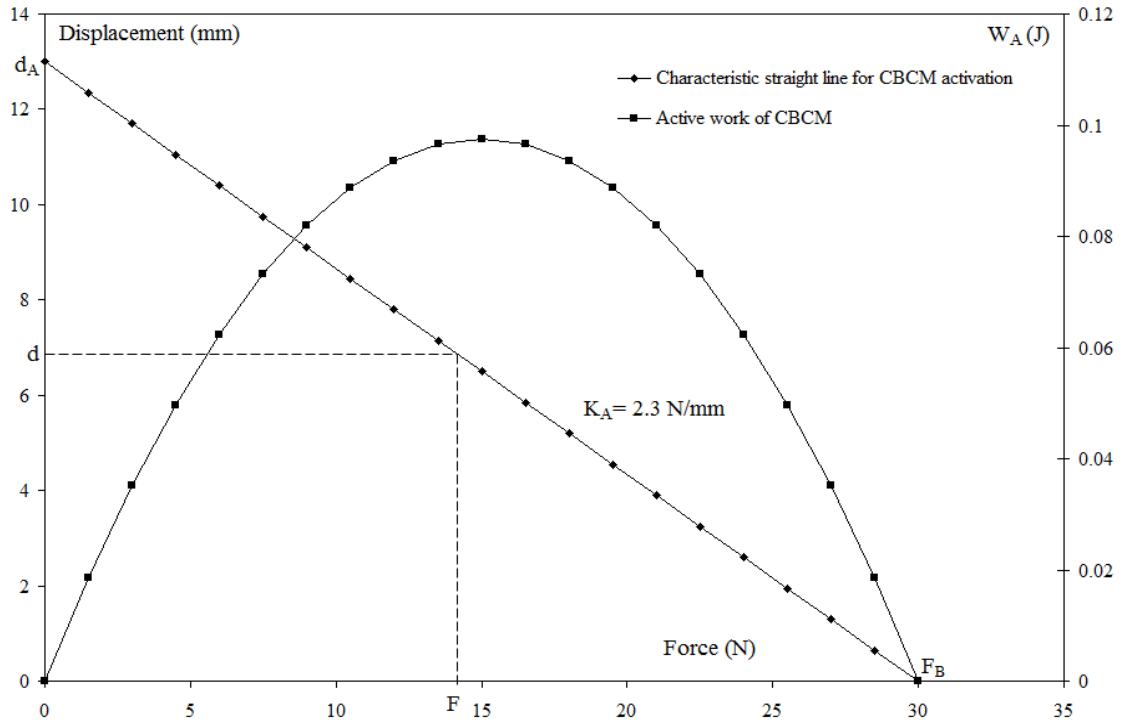

Figure III.8. CBCM characteristic straight line and the corresponding work performed at a certain temperature

For an active composite, it is usual to define a characteristic straight line using the free displacement and blocking force at a certain temperature. In Figure III.8, a characteristic line and an active work (Eq. 1) are shown which are drawn by free displacement and the corresponding blocking force.

$$W_A = F\,d = F\,d_A\,(1-\frac{F}{F_B}) \quad \text{with } d = d_A(1-\frac{F}{F_B}) \quad \text{and } F \in [0, F_B] \tag{1}$$

The maximum work W_A^{max} will be equal to $\frac{F_B d_A}{4}$

This characteristic line and the corresponding work performed are given for a CBCM active composite if it has a free displacement of 13 mm with blocking force of 30 N at a certain temperature. Similar type of curves can be drawn for a number of temperatures from ambient to high temperatures.

III.4.1.2.1) Functionality of CBCM (non-programmed)

The functionality of CBCM can be explained from Figure III.9. In this figure, when CBCM is heated to high deforming temperature (T_D) from the ambient temperature (T_a), CBCM is activated and changes its position from A to B. On cooling again to T_a, CBCM returns back to position A from position B (returning back to its original position). As a result, CBCM performs 2W actuation during heating and cooling.

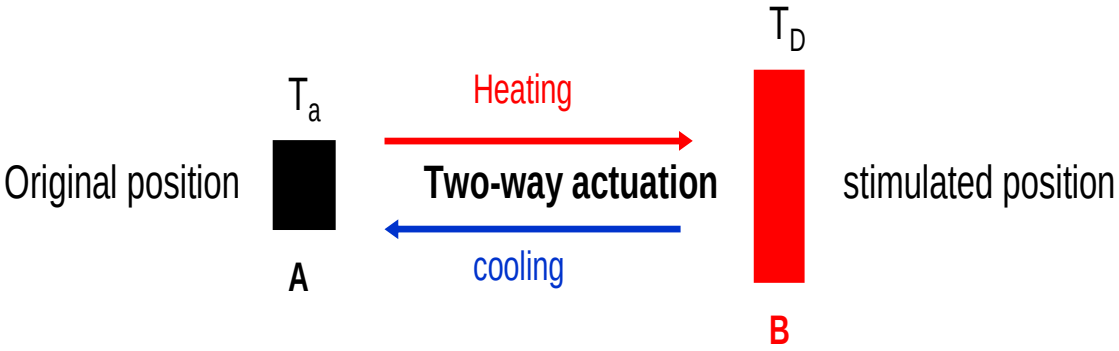

Figure III.9. Functionality of CBCM (non-programmed)

III.4.1.3) SMPC property

For the characterization of shape memory properties of the composites, at first, the programming cycles are performed to induce a temporary shape or initial fixity. This temporary shape or initial fixity is then recovered by performing different recoveries. The different programming cycles and recoveries are explained ahead. The programming cycles can be of two types: Normal programming and stress relaxation programming. The only difference between

these two programming cycles is the addition of a step of stress relaxation for a certain time in stress relaxation programming.

Before the programming, the preliminary tests of limiting force (F_{Lim}) and limiting displacement (d_{Lim}) have been carried out to know the F_{Lim} and d_{Lim} for the composite plate so as to ensure the integrity of the composite plate during the thermo-mechanical testing. The limit force and the corresponding displacement which correspond to the loss of linearity of the response curve have been obtained. In order to ensure the plate integrity, the value of the total displacement used for the programming cycle is approximately equal to the corresponding average displacement of the average limit force minus the standard deviation. The values of F_{Lim} and d_{Lim} for CBCM and SYM are given in Chapter IV.

III.4.1.3.1) SMPC programming

III.4.1.3.1.1) Normal programming cycle

The thermo-mechanical cycle consists of two parts: programming cycle and recovery cycle. Programming cycle gives the temporary shape to the material whereas recovery cycle recovers the temporary shape to original shape. The programming cycle starts with the preloading of 0.3 N, and the corresponding position is taken as initial position for all displacement measurements. The plate is then heated to the deforming temperature (T_D = Tg + 20°C i.e. 150°C) until the thermal stabilization (800s) and the plate gets free displacement d_A ($\varepsilon_A = \frac{d_A}{L}$) shown by AB for CBCM (Figure III.10). Then a specific deformation is applied $\varepsilon_S = \frac{d_S}{L}$, where d_S = 25 mm (BC) is the prescribed displacement. d_S is the determined displacement for which no damage (e.g. delamination) occurs to the plate. This deformation is maintained and the plate is allowed to cool for 1000 seconds to return at the ambient temperature (Ta) shown by CD. After cooling, the force is reduced to 0.3 N (DE) equal to pretension. At this point, the final position (E) obtained is the initial fixity displacement (d_F^I) or the initial fixity deformation ($\varepsilon_F^I = \frac{d_F^I}{L}$) that gives the initial fixity or initial shape memory of the plate.

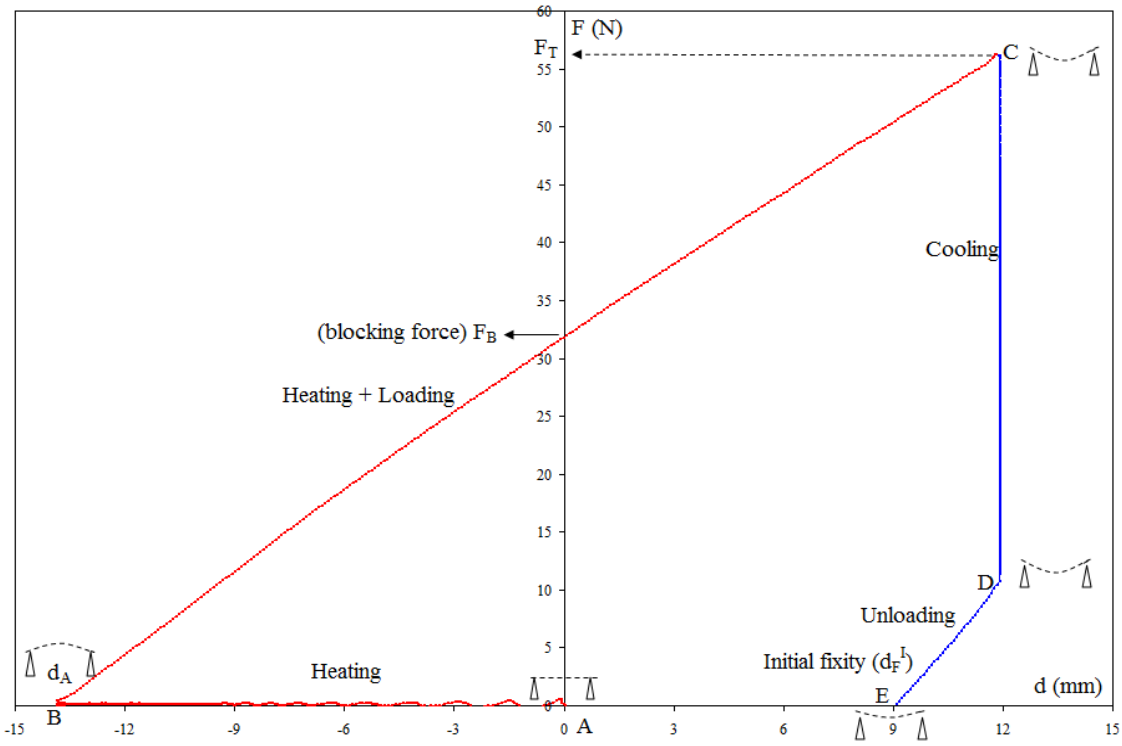

Figure III.10. Normal CBCM thermo-mechanical programming cycle

III.4.1.3.1.2) Stress relaxation programming cycle

The stress relaxation programming for CBCM is shown in Figure III.11. It is different from

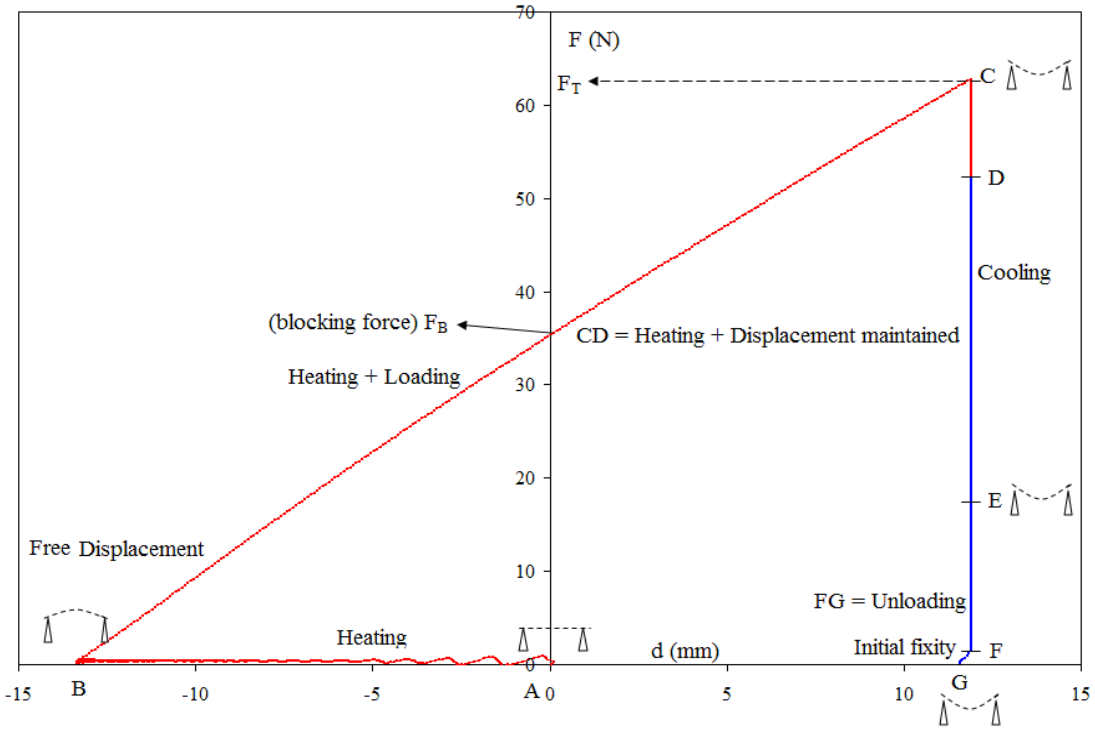

Figure III.11. CBCM stress relaxation thermo-mechanical programming cycle

normal programming as in this programming, heating and displacement is maintained for 4 hours shown by CD. The maintaining of displacement for 4 hours is the step that is added in normal programming which is the only difference between the normal programming and stress relaxation programming. This step affects the initial fixity shown by G.

III.4.1.3.2) SMPC recovery

After the step of thermo-mechanical programming, various recoveries are possible to obtain depending on the requirements, conditions and the applications. The recovery acts according to the condition applied. The recoveries may be under free condition (unconstrained recovery), under constrained condition (constrained recovery), and under a specific load (recovery under load).

III.4.1.3.2.1) Unconstrained recovery

It is one of the classical tests used to characterize the recovery properties of the programming structures. Unconstrained recovery is a type of recovery in which the external stresses are removed and the sample is allowed to recover the induced strain under free condition. Unconstrained recovery is analogous to free displacement. With the increase of temperature, the strain is gradually recovered. After the shape recovery, the remaining displacement is called residual strain. Recovered strain is defined as the initial fixity strain minus the residual strain. The recovery displacement can be measured for two kinds of recovery cycles:

First one is the one-step recovery cycle in which the recovery temperature (T_R) is equal to the deforming temperature (T_D) i.e. T_R=150°C. During unconstrained recovery, 3 recovery cycles (heating + cooling) are provided. During the 1st recovery cycle, the total recovery displacement (d_{RT}) with the associated deformation (ε_{RT}) is measured by the addition of recovery of initial fixity displacement (d_F^I) and activated recovery displacement (d_{RA}) with the associated deformations of ε_F^I and ε_{RA} respectively. After cooling, a residual displacement, called the fixity displacement (d_{RF}) with the associated deformation of ε_{RF} is also measured.

Second one is the multi-step recovery in which several successive temperatures (from 80 to 150°C) are given with an increment of 10°C. The time for heating for each T_R is 800 seconds. Cooling to ambient temperature for 1000 seconds is also provided in between the two T_R. As

CBCM is an active composite which shows active displacement when heated (the active displacements of non-programmed CBCM at different temperatures from 80°C to 150°C are also measured). Therefore, the actual recovered displacement d_R and the corresponding deformation (ε_R) at each T_R are calculated by taking the difference of total recovered displacement d_{RT} (ε_{RT}) and the free displacement d_A (ε_A) produced by CBCM-effect.

III.4.1.3.2.2) Constrained recovery

The second classical test is the test of constrained recovery in which the initial fixity strain is blocked and the gradually increasing recovery forces are generated with the increase of temperature. Constrained recovery test is analogous to blocking force test. Constrained recovery consists of measuring the total recovery force F_{RT} for two kinds of recovery cycles: One-step recovery cycle in which the recovery temperature (T_R) is equal to the deforming temperature (T_D) i.e. T_R=150°C and multi-step recovery cycle in which several successive T_R are used from 80°C to 150°C with an increment of 10°C. For the multi-step recovery cycle, first heating is conducted for 800 s to stabilize the temperature to 80°C; however, time for the onward heating for each T_R is 500 s. No cooling is performed between the two T_R because the objective is just to record the generation of different forces during the activation (heating) of the composites. For CBCM, the actual recovered force (F_R) at each T_R is calculated by taking the difference of the total measured recovery force (F_{RT}) and the force (F_B) produced by CBCM-effect.

III.4.1.3.2.3) Recovery under load

It is a type of test in which recovery is conducted under a certain load. In this test, sample plate is allowed to move but under a certain load. Normally, for the shape memory materials like any active composite, a value of total recovery force (F_{RT}), is taken from constrained recovery and value of total recovery displacement d_{RT} is taken from unconstrained recovery and work W_{RT} [114] is calculated by taking the half product of total recovered force and total recovered displacement given by Eq. 2.

$$W_{RT} = \frac{1}{2} F_{RT} d_{RT} \tag{2}$$

As a result, it is possible to draw a theoretical characteristic straight line and a curve of work performed (similar to CBCM shown in Figure III.9) by using the recovery force and the recovery displacement produced during the recovery process. However, it is possible to draw an experimental straight line and corresponding curve of work performed by performing the different recoveries under different loads. It may be called as partial recovery under load. This type of recovery applies to all types of shape memory materials. The recovery under load is a test in which recovery work can be measured directly. The value of load during the recovery gives the value of force whereas the recovered displacement under this load gives the value of displacement, the product of which gives the recovered work W_G.

In this test, at the beginning, a first step of constrained recovery is used until the load becomes equal to the given force (F_G). Then, unconstrained recovery step is used, but F_G is maintained by using the control system of the machine. The plate can be deformed and reaches at the end of the heating a position characterized by the recovery displacement under load d_{RT}^{L}. So, the recovered mechanical work is given by Eq. (3) [115]

$$W_G = F_G d_{RT}^{L} \tag{3}$$

However, to study the shape memory properties under load for the active structures like CBCM, the test of recovery under load is very useful as it gives a direct measure of work performed for a recovery close to full recovery to its original position. To measure this work, the recovery under load is conducted at a load equal to its F_B. Under this load, CBCM can recover close to its original position thus giving a direct measure of a work performed during full recovery by replacing F_G by F_B given by Eq. 4

$$W_B = F_B d_{RT}^{L} \tag{4}$$

Contrary to the above equation (Eq. 4), to measure the recovered work W_R, the active work W_A performed by non-programmed CBCM is given by Eq. 5, must be subtracted from the total work calculated from Eq. 2 by using unconstrained recovery and constrained recovery

$$W_A = \frac{1}{2} F_B d_A \tag{5}$$

So, the recovered work W_R is given by Eq. 6

$$W_R = W_{RT} - W_A \quad (6)$$

Therefore, the test of recovery under load is well adapted for CBCM to measure the recovered mechanical work during the full recovery from the temporary position or initial fixity to its original position.

It is to be noted that all the deformations and forces are the averages of last 50 values calculated when the temperature is stabilized during heating and cooling respectively. Also, in reference to initial position of the composites, the negative values show upward deformation; however, positive values show downward deformation. All the values of displacements and the corresponding deformations are measured from the initial position. Each deformation (%) can be converted into displacement in millimeter by multiplying it by 3.

III.4.2) Epoxy physico-chemical characterization

III.4.2.1) Differential scanning calorimeter (DSC)

In order to analyze thermal transitions of Epoxy resin and hardener, DSC Q-200 of TA instruments has been used that is shown in Figure III**.**12. It is used with "TA universal analysis "software". The analysis is conducted on two consecutive heating and cooling cycles from − 80°C to 150°C. The rate of increase and decrease of the temperature is 10º C / min under the constant flow of 50 ml/min of nitrogen gas. The samples having weight of 3-8 mg are put into Aluminum capsules and also an empty capsule is put each time as a reference.

The curves of DSC for Epoxy resin and Epoxy cross-linked composite are given in Appendix-A.

Figure III.12. DSC

III.4.2.2) Thermo-gravimetric analysis (TGA)

It is a type of testing that is performed on samples to determine changes in weight in relation to change in temperature and thus it is possible to measure the temperature of degradation and

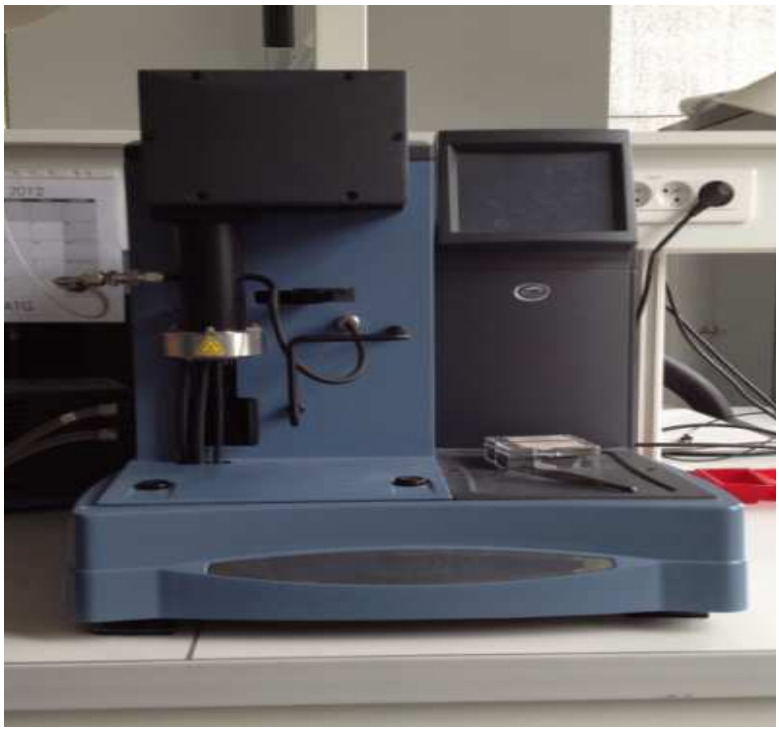

Figure III.13. TGA

thermal kinematics of the solids. The thermal stability of Epoxy resin and the harder has been studied by using TGA (Q-500 of TA instruments) shown in Figure III.13. A sample of 8 -10 mg is placed in a platinum pan. Then, the loss of mass is observed by increasing the temperature from 20^{o} C to 900^{o} C at a rate of 10^{o} C /min in nitrogen atmosphere. The TGA curve for Epoxy resin is given in Appendix-A.

III.4.2.3) Infra-red spectroscopy

An attenuated total reflection accessory operates by measuring the changes that occur in a totally internally reflected infrared beam when the beam comes into contact with a sample (indicated in Figure III.14).

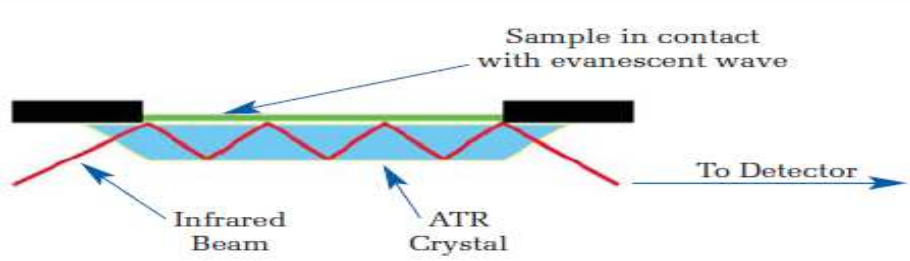

Figure III.14. A multiple reflection ATR system

An infrared beam is directed onto an optically dense crystal with a high refractive index at a certain angle. This internal reflectance creates an evanescent wave that extends beyond the surface of the crystal into the sample held in contact with the crystal. It can be easier to think of this evanescent wave as a bubble of infrared that sits on the surface of the crystal. This evanescent wave protrudes only a few microns (0.5 μ - 5 μ) beyond the crystal surface and into the sample. Consequently, there must be good contact between the sample and the crystal surface. In regions of the infrared spectrum where the sample absorbs energy, the evanescent wave will be attenuated or altered. The attenuated energy from each evanescent wave is passed back to the IR beam, which then exits the opposite end of the crystal and is passed to the detector in the IR spectrometer. The system then generates an infrared spectrum [116].

Infrared Brüker Vertex 70-ATR (shown in Figure III.15) has been used for the analysis of Epoxy resin and the hardener. For the analysis, 1 or 2 drops of the sample has been put on the

crystal of Zinc Selenide (ZnSe) and then infra-red beam has been passed through the sample. The ATR spectrums for Epoxy resin and hardener are given in Appendix-A.

Figure III.15. Infra-red Brüker Vertex 70-ATR

III.4.2.4) Nuclear resonance magnetic spectroscopy (NMR)

Nuclear magnetic resonance spectroscopy is an analytical chemistry technique that is used in quality control and research for determining the content and purity of a sample as well as the molecular structure. For example, NMR can analyze the mixtures containing known compounds. For known compounds, NMR can either be used to match against spectral libraries or to infer the basic structure directly. Once the basic structure is known, NMR can be used to determine the molecular conformation in solution as well as studying the physical properties at the molecular level such as conformational exchange, phase change in solubility and diffusion etc. The principle behind NMR is that many nuclei have spin and all nuclei are electrically charged. If an external magnetic field is applied, an energy transfer is possible between the base energy to a higher energy level (generally a single energy gap). The energy transfer takes place at a wavelength that corresponds to radio frequencies and when the spin returns to its base level, energy is transmitted and processed in order to yield an NMR spectrum for the nucleus concerned [117].

Figure III.16. Bruker 300 ultraShield

"Bruker 300 UltraShield" (shown in Figure III.16) that operates at 300MHz has been used for NMR ^{1}H analysis of the Epoxy and hardener. The samples have been prepared by dissolving the materials (epoxy or hardener) in deuterated Dimethyl sulfoxide (DMSO) at a concentration of 3% by mass for NMR ^{1}H. Deuterated DMSO an isotopologue of DMSO, $(CH_3)_2S=O$) having a chemical formula $(CD_3)_2S=O$) in which the hydrogen atoms ("H") are replaced with their isotope deuterium ("D"). Pure deuterated DMSO shows no peak in ^{1}H NMR spectroscopy so is commonly used as an NMR solvent; however, commercially available samples are not 100% pure and a DMSO quintet peak is observed in the regions 2.54 ppm for ^{1}H NMR. The NMR ^{1}H spectrum for Epoxy resin is given in Appendix-A.

Chapter IV. Results and Discussion

IV.1) One-step recovery

When CBCM is programmed through a shape memory cycle, it gets a shape memory property. In this property, CBCM gets fixed and gets a temporary shape. This shape may be recovered in one step recovery in which a temperature equal to T_D is directly given to return back CBCM to its original position. This type of one-step recovery can be demonstrated by the Figure IV.1.1. In this figure, after programming, CBCM gets an initial fixity called as the temporary shape. This initial fixity is shown by A‴. On heating at a recovery temperature T_R equal to T_D, it is activated and changes its position from A‴ to B. On cooling, it returns back to its original position A (the position before the start of the test). Its return to original position demonstrates that the shape memory property is disappeared from it. On heating again to T_D, it is activated again and changes its shape from A to B. After that, on heating and cooling continuously, it can perform 2W actuation.

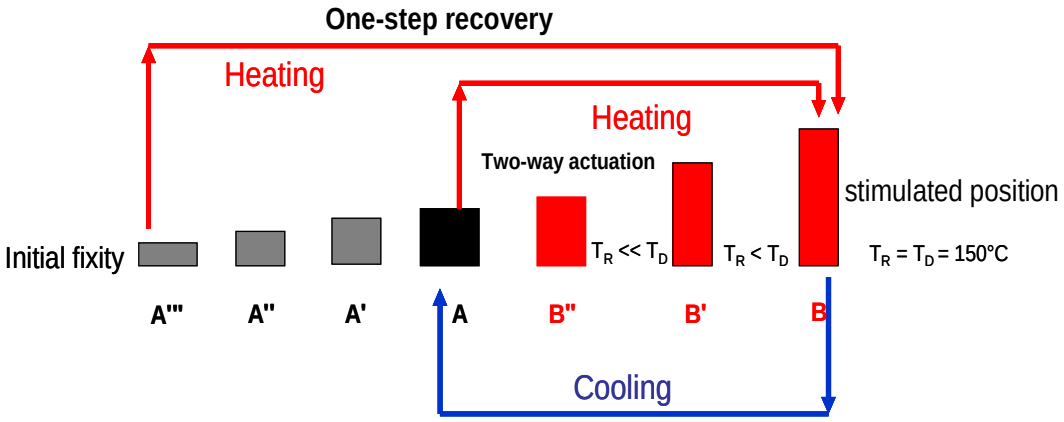

Figure IV.1.1. A model for one-step recovery for CBCM (programmed)

IV.1.1) Introduction

In this section, different one-step recoveries (unconstrained, constrained, and recovery under load) are studied. For each type of recovery, three composite plates are used on which three tests, one on each composite plate, are conducted. For all the recoveries, the same three plates are used. After performing the tests for one type of recovery tests (e.g unconstrained) on each plate, the plates have been put free for at least three days and then the 2nd type of recovery tests

(e.g. constrained) is performed. This is done so as to remove all the internal or residual stresses from the plates induced due to the previous testing.

At first, for CBCM, the normal programming cycle with different recoveries (unconstrained, constrained and recovery under load) and then stress relaxation programming cycle with different recoveries (unconstrained and constrained) are studied. Similarly, for SYM, the normal programming cycle with different recoveries (unconstrained, constrained and recovery under load) and then stress relaxation programming cycle with different recoveries (unconstrained and constrained) are studied. Also, SYM has been compared with CBCM. Furthermore, at the end, the effect of position and orientation of unidirectional glass layers on the shape memory properties of different asymmetric composites has been studied. For this, the unconstrained and constrained recoveries have been performed. It is to be noted that the different recoveries have been performed immediately after the programming cycle (i.e. there is no time delay between the recoveries and the programming cycles).

IV.1.2) CBCM

By the preliminary tests of bending at T_D (3 samples of CBCM and SYM plates) until fracture shown in Figure IV.1.2, the limit force and the corresponding displacement which correspond to the loss of linearity of the response curve, have been obtained. In order to ensure the CBCM plate integrity, the value of d_S is approximately equal to the corresponding average displacement of the average limit force minus the standard deviation. For CBCM plates, the average values of the limit force and the corresponding displacement are equal to 61.75±1.42N and 27.29±1.89 mm respectively.

IV.1.2.1) CBCM normal programming cycle

A three-point bending test has been chosen to characterize the behavior of the composite structure. The plates are supported by two rigid cylinders placed (L = 300 mm) apart. The thermo-mechanical cycle (Figure IV.1.3) starts with the pretension of 0.3 N at the start of each test. Then the plate is heated for 800 seconds. The initial displacement for CBCM (free displacement d_A is equal to 13.47 mm) shown by AB. During 800 s of heating, the deforming temperature (T_D) is stabilized (Tg + 20°C). When temperature is stabilized, load is applied to

get the specific bending deformation $\varepsilon_S = \frac{d_S}{L}$ where d_S = 25 mm, the total prescribed displacement (BC). All the deformations presented in this chapter are calculated in this manner. This displacement is the maximum displacement that can be obtained without any damage (e.g. delamination) to the plates. This deformation is maintained and cooled for 1000 s to get the

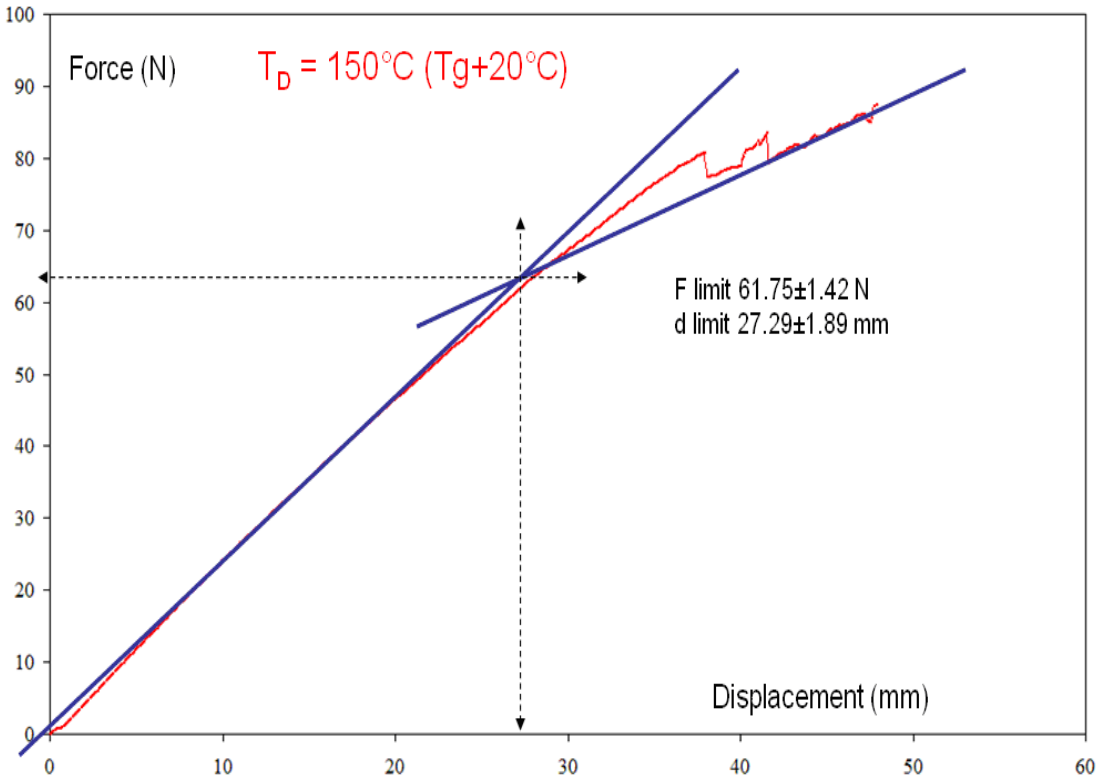

Figure IV.1.2. Determination of the limit force for CBCM

ambient temperature (CD). When the plate becomes cooled, load is reduced to the pretension of 0.3 N (DE). Here, at point E, initial fixity is obtained. The fixing or programming cycle is thus completed. This programming cycle is called normal programming cycle as the step of stress relaxation is not used after the step of loading (point C).

The two parts of the programming cycle can be explained in terms of different forces acting during the cycle. The total force F_T (A-A_2) is the sum of two forces: the blocking force F_B (A-A_1), corresponding to the active part. The force F_I (A_1-A_2) is imposed to reach the prescribed displacement d_S = 25mm. Similarly, during cooling, the total force F_T (C-C_3), is the combination of three forces: the blocking force F_B (C-C_1), the force F_S (C1-C2) called as force of stabilization,

and the elastic force F_E (C_2-C_3). The blocking force F_B disappears simply due to the cooling of the composite and F_E is restituted force during the elastic recovery (DE) to the preloaded position. F_E is the result of the equilibrium of the whole structure during the unloading step. The fixity d_F^I is linked to the value of F_S. For more F_S, more will be the fixity and vice versa. So, the values of F_S and d_F^I characterize the internal mechanical work stored in the composite structure after the programming cycle.

All the characteristic values of the programming cycle are given in Table IV.1.1. For d_F^I and F_S, it is observed that d_F^I is 36% of d_S and F_S is 25% of F_T. Also, d_F^I is 68% of d_A and F_S is 45% of F_B.

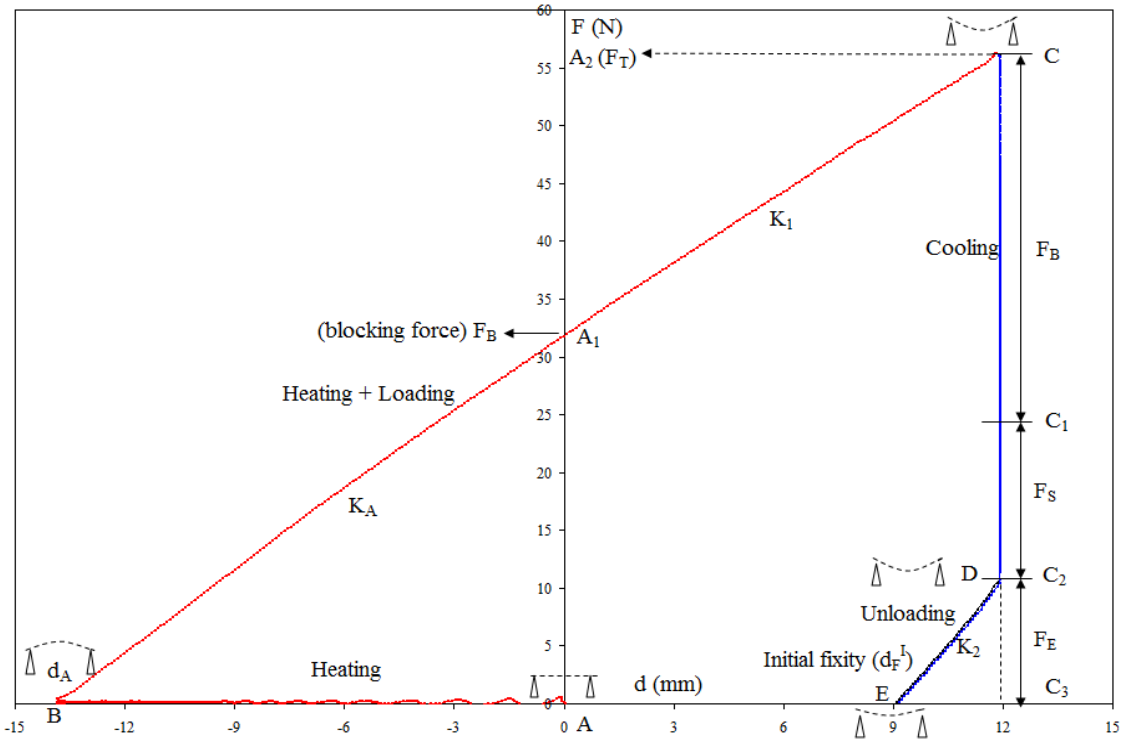

Figure IV.1.3. Thermo-mechanical programming cycle for CBCM

For this kind of composite structures, the use of the rigidities which appear during the programming cycle is a convenient characterization of the structure behavior. The structural characteristics have an influence on several phenomena like: the loss of matrix stiffness versus temperature, the new organization of the polymer after the programming or the geometrical rigidity induced by the structure curvature that may change during the activation. K_A and K_1 are

the characteristic behavior of the non-programmed composite plate at T_D. The rigidity K_2 (DE) during unloading is the characteristic of the programmed composite plate at ambient temperature ($T_{a)}$. It can be compared to the non-active rigidity K_{NA} that is the characteristic of the non-programmed composite plate at T_a. The level of internal stress in the composite plate induced by its new shape (d_F^I) leads to the value of K_2 higher than K_{NA} (Table IV.1.1).

Characteristic values	CBCM
d_A (mm)	−13.47±0.75
F_B (N)	31.48±1
K_A (N/mm)	2.33±0.1
F_T (N)	57.70±1.94
K_1 (N/mm)	2.2±0.24
F_S (N)	14.31±2.06
F_E (N)	11.91±1.62
d_F^I (mm)	9.18±0.63
K_2 (N/mm)	4.28±0.39
K_{NA} (N/mm)	3.34±0.36

Table IV.1.1. Characteristic values of the programming cycle; K_A is the active rigidity; K_1 is the rigidity for second part of deformation; K_2 is the rigidity at ambient temperature after programming cycle; K_{NA} is the rigidity at ambient temperature without programming cycle

IV.1.2.2) Recoveries

IV.1.2.2.1) Unconstrained recovery

The test of unconstrained recovery (Figure IV.1.4) has been performed at recovery temperature (T_R) equal to 150°C. During the 1st recovery cycle, as compared to d_F^I, CBCM recovers 242% with the total recovery displacement (d_{RT}) of 21.84±1.26 mm during heating with the associated deformation (ε_{RT}) of 7.28 % ± 0.42. d_{RT} is the sum of d_F^I and d_{RA}. d_{RA} is an active recovery displacement of the programmed CBCM during the recovery with the associated recovery deformation (ε_{RA}). After cooling, the fixity position of the plate is close to the initial position (before the programming cycle) and the residual displacement is equal to d_{RF} = 1.02 ± 0.3 mm

(11 % of d_F^I). So, after one-step unconstrained recovery cycle, the plate is largely deprogrammed. The comparison between the value of d_{RT} = 21.84±1.26 mm and the sum of d_F^I and d_A ($d_F^I + d_A$ = 22.65±1.38 mm) shows that the value of the free displacement (CBCM-effect) remains the same before and after the programming cycle.

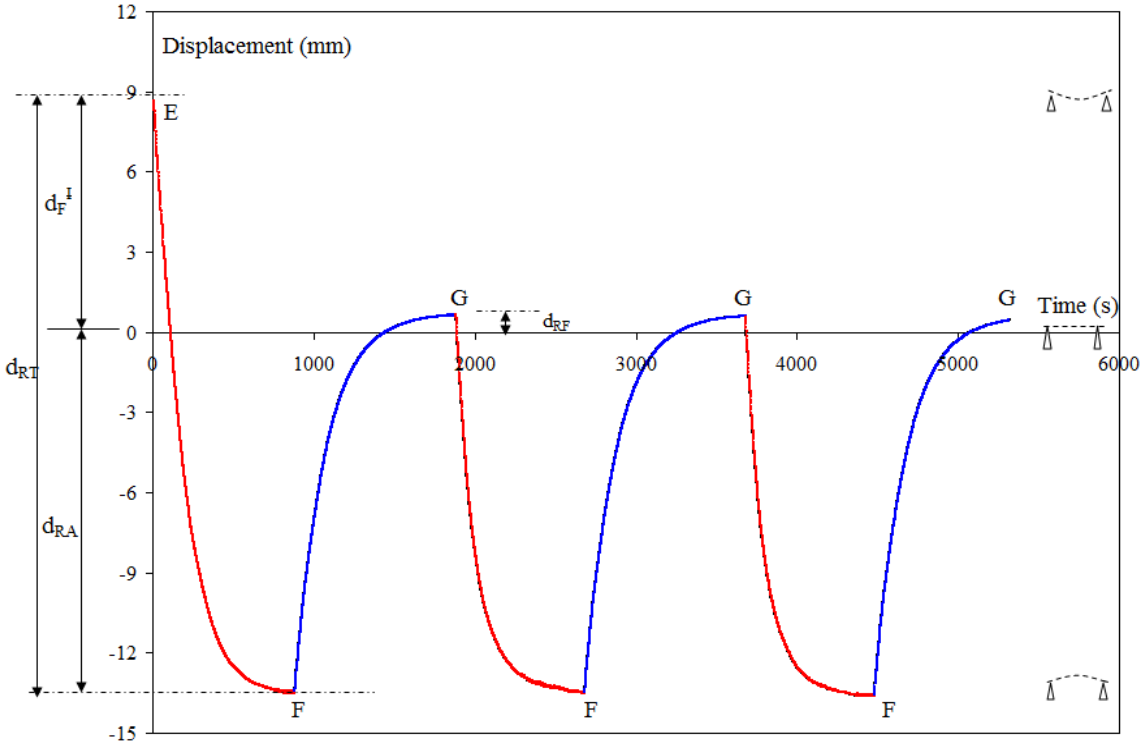

Figure IV.1.4. Characteristic unconstrained recovery curve of CBCM; E = initial fixity (d_F^I = 9.21±0.63 mm); EF, GF = Heating to T_D (i.e. = 150°C; FG = Cooling to Ta (i.e. = 22°C)

The recovery displacement of the 1st recovery cycle for CBCM is shown as a function of temperature in figure IV.1.5. For CBCM, a recovery close to 100% is obtained at 90°C which proves that full recovery is possible at a T_R much lower than T_D. However, it is not possible for the conventional SMPs and their composites as described by *Castro et al.* [31, 118]. It is mainly due to the presence of CBCM-effect in the CBCM composite which helps during recovery and makes the composite to recover at lower temperature. Although, for CBCM, this 242% recovery is possible only for 1st recovery cycle; however, this higher displacement cannot be obtained by "CBCM composite without SM programming". Hence, by introducing SME in an asymmetrical composite like CBCM composite, the reduced recoverable strains due to its high rigidity is

compensated by its activated displacement. As a result, the increase in overall activation is a major advantage gained by combining the two effects namely SME and CBCM-effect in the same structure. To characterize the return to initial position and the 2W property of the CBCM, the average activation and fixity deformations (ε_{RA} and ε_{RF}) of the recovery cycles for CBCM are given in Table IV.1.2.

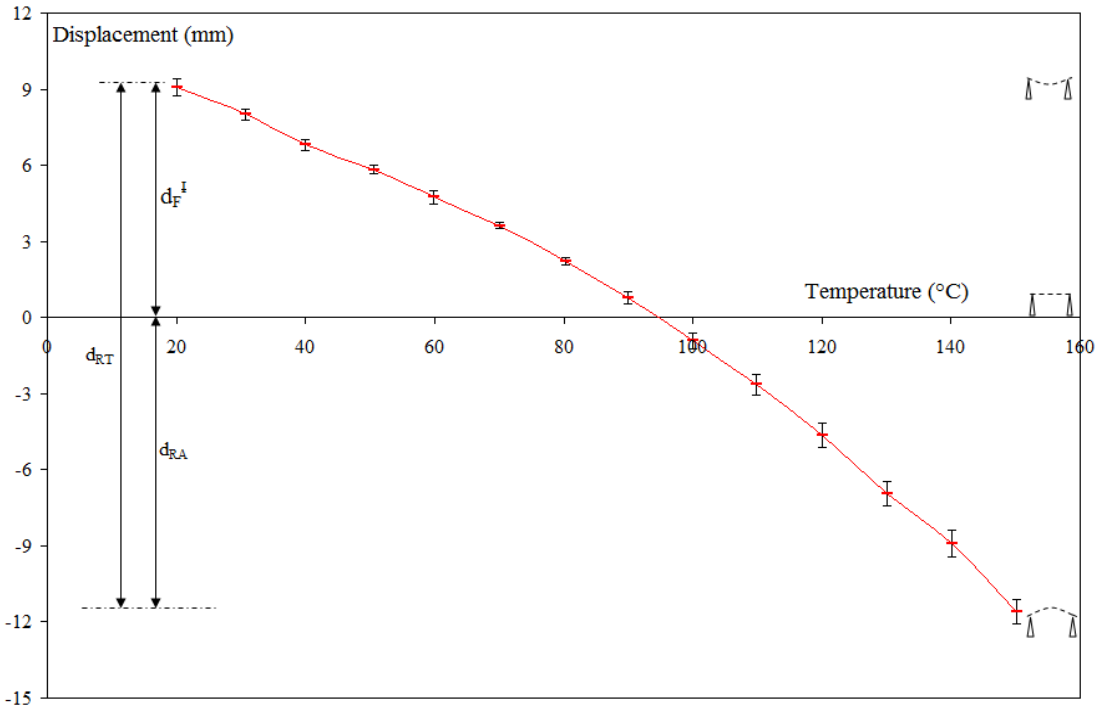

Figure IV.1.5. Unconstrained recovery of CBCM at different temperatures during the 1st recovery cycle; (d_F^I = 9.21±0.63 mm)

Composite plate	Deformations	Recovery cycles		
		1	2	3
CBCM	d_{RA} (mm)	−12.63 ± 0.86	−12.93±0.78	−12.96±0.66
	ε_{RA} (%)	−4.21 ± 0.29	−4.31±0.26	−4.32±0.22
	d_{RF} (mm)	1.02 ± 0.3	0.78±0.39	0.66±0.45
	ε_{RF} (%)	0.34 ± 0.1	0.26±0.13	0.22±0.15

Table IV.1.2. Unconstrained recovery activations and fixities during the 3 recovery cycles, ε_F^I = 3.07±0.21% or d_F^I = 9.21±0.63 mm

ε_{RA} is the activated recovery deformation during heating (point F) and ε_{RF} is the recovery deformation during cooling (point G). It can be observed that with the successive recovery cycles, the value of d_{RF} decreases (may be due to successive deprogramming) and the plate comes more close to its initial position.

IV.1.2.2.2) Constrained recovery

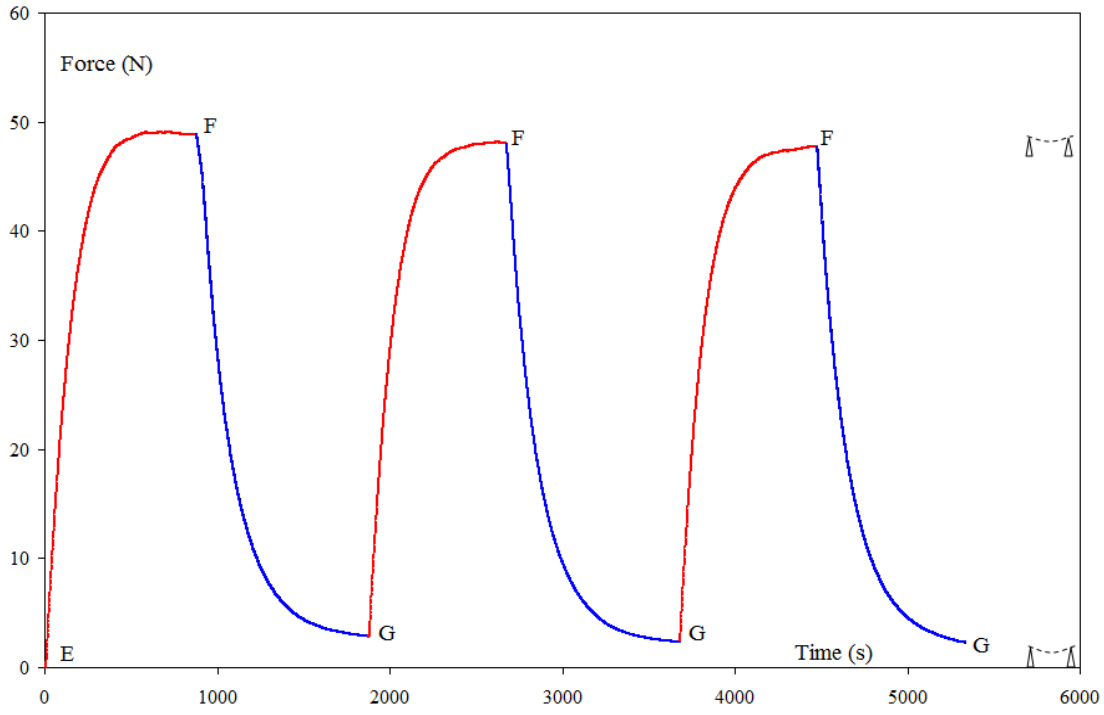

Figure IV.1.6. Constrained recovery curves for CBCM; E = d_F^I = 9.12 ±0.3mm; EF, GF = Heating to T_D (i.e. = 150°C; FG = Cooling to Ta (i.e. = 22°C)

During constrained recovery, Figure IV.1.6 shows the generation of forces during the recovery. During the heating of first recovery cycle (EF), the F_{RT} is 48.54 ± 2.57 N (Table IV.1.3), which is 84% of the total force (F_T = 57.70±1.94 N) required to deform during programming of the CBCM. F_{RT} is stabilized during the heating of the other two recovery cycles (Table IV.1.3).This shows high level of recovery force. The combined recovery force for CBCM plate is developed due to the two effects (CBCM-effect and SME). The force F_B for CBCM produced due to CBCM-effect is 31.48±1 N. So, F_R during heating of first cycle for CBCM is 17.06±0.57 N

whereas F_R is the difference of F_{RT} and F_B. Also, F_R gained during the recovery is 29% of its F_T and 54% of its F_B.

Compared to the unconstrained recovery test, during this test, the fixity is maintained, so, there is no movement of the plate and only the force is recovered. This test shows a difference between the average force F_S acting during the programming cycle and F_R during the recovery. Indeed, the standard deviations associated to these forces do not conclude the equality of these two forces. Moreover, after cooling a residual force F_{RES} (point G) appears that will induce a deformation if the composite plate is unloaded. The initial fixity is changed and the plate has a new position of equilibrium. F_{RES} for CBCM is 3.03N (Table IV.1.3) which is 6% of the force produced during heating (F_{RT} = 48.54N) ensuring that the major part of the recovery force is always available during heating.

Composite Plate	**Forces (N)**	**Recovery Cycles**		
		1	2	3
CBCM	F_{RT}	48.54 ± 2.57	47.77 ± 2.37	47.44 ± 2.33
	F_{RES}	3.03 ± 0.96	2.51 ± 0.87	2.23 ± 0.94
	$\delta F = F_{RT} - F_{RES}$	45.51±3.53	45.26±3.24	45.21±3.27

Table IV.1.3. Constrained recovery forces for CBCM; $\varepsilon_F^I = 3.04 \pm 0.1$

IV.1.2.2.3) Recovery under load

The test of recovery under load has been performed for CBCM composite. The representative curve of recovery under load ($F_G = F_B$) is shown in Figure IV.1.7 in which displacement is given as a function of time. The curve is made of two parts: a part of recovery under load (EH) and a part of functioning under load (HL). In the first part, (EF) corresponds to the step of constrained recovery. When the recovery force F_R becomes equal to given load (F_B), the plate is free to move under F_B (FG). At point (G), it returns close to initial position by performing total recovery displacement (d_{RT}^L = 7.8±0.64 mm) under a load equal to F_B with the associated deformation (ε_{RT}^L) of 2.6±0.21 %. This verifies the definition of the blocking force F_B of an activated CBCM plate without programming i.e. F_B is the maximum load that the beam can support while maintaining its initial configuration. So, along the path EG, all the mechanical

work stored in the structure is restored and the corresponding mechanical work W_B = 0.24±0.02 J (Eq. 4 in Chapter II) is an appropriate measurement. The path GH corresponds to the cooling of the plate and the corresponding displacement d_{RF}^{L} = 13.29 ± 0.21 mm is the displacement under load. The part of functioning under load (HL) highlights the actuation property of programmed CBCM plate under load. The CBCM-SMPC is able to perform 2W-SME under a load (equal to F_B) during the recovery cycles; however, the curvature of the composite changes and it works in a new framework compared to the programming cycle.

The value of W_B = 0.24±0.02 J obtained by recovery under F_B is comparable to the precedent value of W_R (0.31±0.06 J) obtained (by Eq. 6 in chapter III) from unconstrained and constrained recovery tests. For the characterization of the recovery mechanical work, this result shows the equivalence of these two approaches and consequently it is the main interest of the test of recovery under load. The test of recovery under load is the characterization of the whole properties of the SMPC by only one test: free displacement and the blocking force are defined during the programming step and the recovery mechanical work is obtained during the recovery step.

Similar types of recoveries under different loads (F_G) are also performed for CBCM. The results of these recoveries are given in Table IV.1.4. The curves for these recoveries under different loads are given in Appendix-B; however, a representative curve under (F_G = 10 N) is shown in Figure IV.1.8. The total deformations recovered under different loads (ε_{RT}^{L}) are calculated for the recovery cycles by adding or subtracting the recovery activations under load (ε_{RA}^{L}) and the recovery fixities under load (ε_{RF}^{L}) depending on the extent of recovery (see Table IV.1.4).

In an unconstrained recovery, at 150°C, the plate becomes totally deprogrammed at the end of the first recovery cycle. As a result, for the subsequent cycles, CBCM has only the CBCM-effect and there is no recovery displacement due to the SME for the second and third cycle. However, for the recovery under load, this is not the case as during the cooling of the first cycle, there is a memory effect due to the load, and of course a value of fixity is obtained that is different from the initial fixity. During the subsequent cycles, the total recovery displacement

combines the CBCM-effect and SME which give the stabilized positions during heating and cooling. The results show that for CBCM, during the recoveries under different loads, there is a

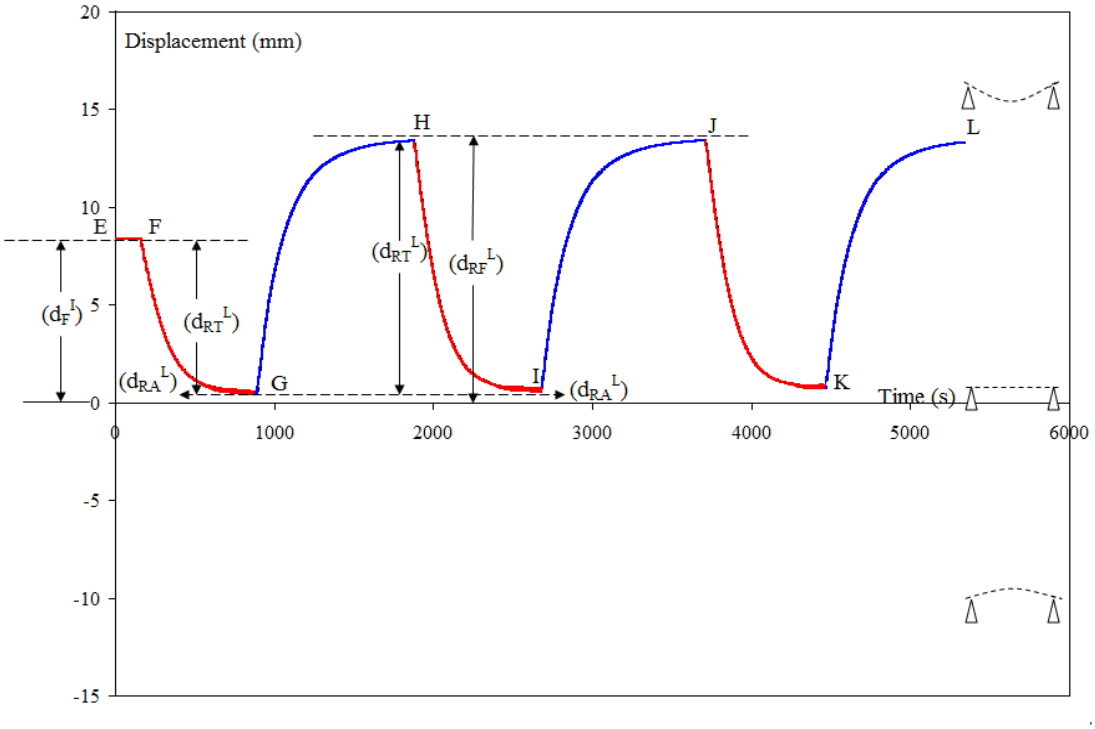

Figure IV.1.7. Recovery under load ($F_G = F_B$) for CBCM; cycle 1 = EFGH; cycle 2 = HIJ; cycle 3 = JKL; E = d_F^I = 9.01± 0.4 mm; EFG, HI, JK = Heating to T_D (i.e. = 150°C; GH, IJ, KL = Cooling to Ta (i.e. = 22°C)

great difference between heating and cooling deformations which is mainly due to its CBCM-effect. From Table IV.1.4, it can be observed that as F_G increases, ε_{RA}^L decreases whereas ε_{RF}^L increases. Also, ε_{RT}^L decreases as F_G increases during the recovery heating of 1st recovery cycle. For the other recovery cycles, ε_{RT}^L remains almost same for each F_G (Table IV.1.4.).

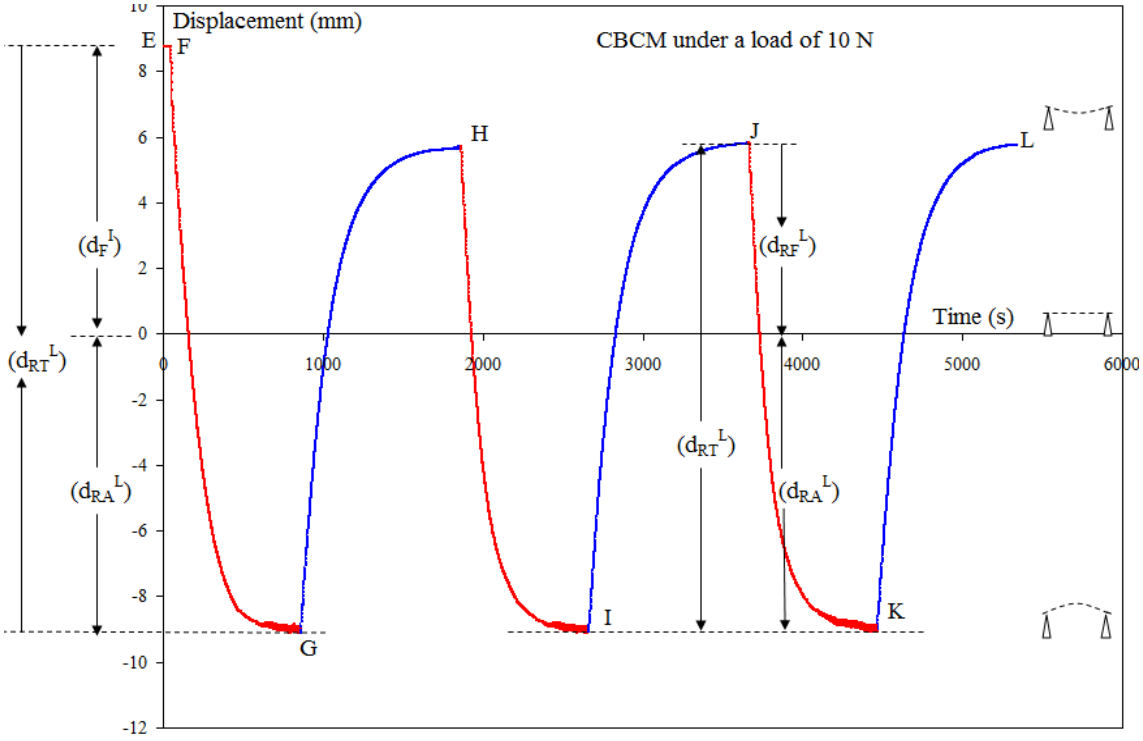

Figure IV.1.8. Recovery under load (F_G = 10 N) for CBCM; cycle 1 = EFGH; cycle 2 = HIJ; cycle 3 = JKL; E = d_F^I = 8.8± 0.45 mm; EFG, HI, JK = Heating to T_D (i.e. = 150°C; GH, IJ, KL = Cooling to Ta (i.e. = 22°C)

In chapter II, the characteristic straight line and the active rigidity (K_A) for the characterization of an active structure has been presented. Similarly, to characterize the shape memory properties of a structure, it is also possible to draw the characteristic line of its total recovery with the corresponding rigidity (K_{RT}). For the SMP composites (Figure IV.1.9), this line is defined from the displacement obtained from the unconstrained recovery test d_{RT} and the force obtained from the constrained recovery test F_{RT}. The experimental values obtained from different tests under different F_G are in accordance with the characteristic straight line.

As we know that the total recovery of the programmed CBCM is a combination of CBCM-effect and SME, therefore, in reality, the total recovery characteristic line obtained from F_{RT} and d_{RT} is also the combination of characteristic line of CBCM activation obtained from d_A and F_B and characteristic line of the recovery of the shape memory part obtained from d_R and F_R. If the hypothesis of separation between the two effects is used, Figure IV.1.10 (a) shows for F_G = 10N < F_B, the construction of the total recovery characteristic line from d_A, F_B, d_R and F_R. If load F_G

is considered completely compensated by the CBCM-effect with a corresponding displacement d_A^{10}, the SME remains totally available and is characterized by d_R. So, the total displacement d_{10} is the sum of d_A^{10} and d_R. For $F_G = 40N > F_B$ (Figure IV.1.10 (b)), the load is not compensated by the CBCM-effect, no displacement is induced by this effect because F_G is greater than F_B. The SME has to be compensated a force equal to $(F_G - F_B)$, so, it induces a displacement called as d_{40}. Also, if we know the two characteristic curves for SME and the effect of actuator, here CBCM, it is possible to reconstruct the characteristic curve for the structure having these two effects.

F_G (N)	Deformations (%)	Recovery cycle (i)			
		0	1	2	3
10	$(\varepsilon_{RA}^{L})_i$	0	−3.1±0.04	−3.2±0.07	−3.25±0.04
	$(\varepsilon_{RF}^{L})_i$	2.93±0.15	1.65±0.05	1.69±0.07	1.74±0.04
	$(\varepsilon_{RT}^{L})_i = (\varepsilon_{RF}^{L})_{i-1} + (\lvert\varepsilon_{RA}^{L}\rvert)_i$	0	6.03±0.19	4.85±0.12	4.94±0.11
20	$(\varepsilon_{RA}^{L})_i$	0	−1.46±0.09	−1.52±0.04	−1.55±0.09
	$(\varepsilon_{RF}^{L})_i$	2.86±0.09	2.58±0.11	2.71±0.07	2.79±0.05
	$(\varepsilon_{RT}^{L})_i = (\varepsilon_{RF}^{L})_{i-1} + (\lvert\varepsilon_{RA}^{L}\rvert)_i$	0	4.32±0.18	4.10±0.15	4.26±0.16
25	$(\varepsilon_{RA}^{L})_i$	0	−0.7±0.09	−0.84±0.11	0.87±0.12
	$(\varepsilon_{RF}^{L})_i$	2.9±0.08	3.6±0.1	3.74±0.08	3.8±0.11
	$(\varepsilon_{RT}^{L})_i = (\varepsilon_{RF}^{L})_{i-1} + (\lvert\varepsilon_{RA}^{L}\rvert)_i$	0	3.6±0.17	4.44±0.21	4.61±0.2
30	$(\varepsilon_{RA}^{L})_i$	0	0.27±0.09	0.33±0.1	0.35±0.08
	$(\varepsilon_{RF}^{L})_i$	3.01±0.11	4.43±0.07	4.53±0.09	4.62±0.07
	$(\varepsilon_{RT}^{L})_i = (\varepsilon_{RF}^{L})_{i-1} - (\lvert\varepsilon_{RA}^{L}\rvert)_i$	0	2.74±0.20	4.13±0.17	4.18±0.17
40	$(\varepsilon_{RA}^{L})_i$	0	1.63±0.11	1.67±0.17	1.69±0.21
	$(\varepsilon_{RF}^{L})_i$	2.96±0.1	5.9±0.19	5.94±0.20	5.99±0.21
	$(\varepsilon_{RT}^{L})_i = (\varepsilon_{RF}^{L})_{i-1} - (\lvert\varepsilon_{RA}^{L}\rvert)_i$	0	1.33±0.21	4.23±0.36	4.25±0.41

Table IV.1.4. CBCM recovery under different loads; $((\varepsilon_{RF}^{L})_0 = \varepsilon_F^{I})$

From characteristic straight line characterized by d_{RT} and F_{RT} (Figure IV.1.9), the corresponding theoretical work W_G performed during the recovery can be defined as the product of the force F and the displacement d given by Eq. (7).

$$W_G = F_G d_{RT}^{\ L} = F_G d_{RT}\left(1 - \frac{F_G}{F_{RT}}\right) \quad \text{with } d_{RT}^{\ L} = d_{RT}\left(1 - \frac{F_G}{F_{RT}}\right) \text{ and } F_G \in [0, F_{RT}] \qquad (7)$$

Note that this work is equal to zero when the force is equal to F_{RT} or when the displacement is equal to d_{RT}. Moreover, it exhibits a maximum work, (Figure IV.1.11), corresponding to the capability of maximum of recovery given by $\frac{F_{RT} d_{RT}}{4}$.

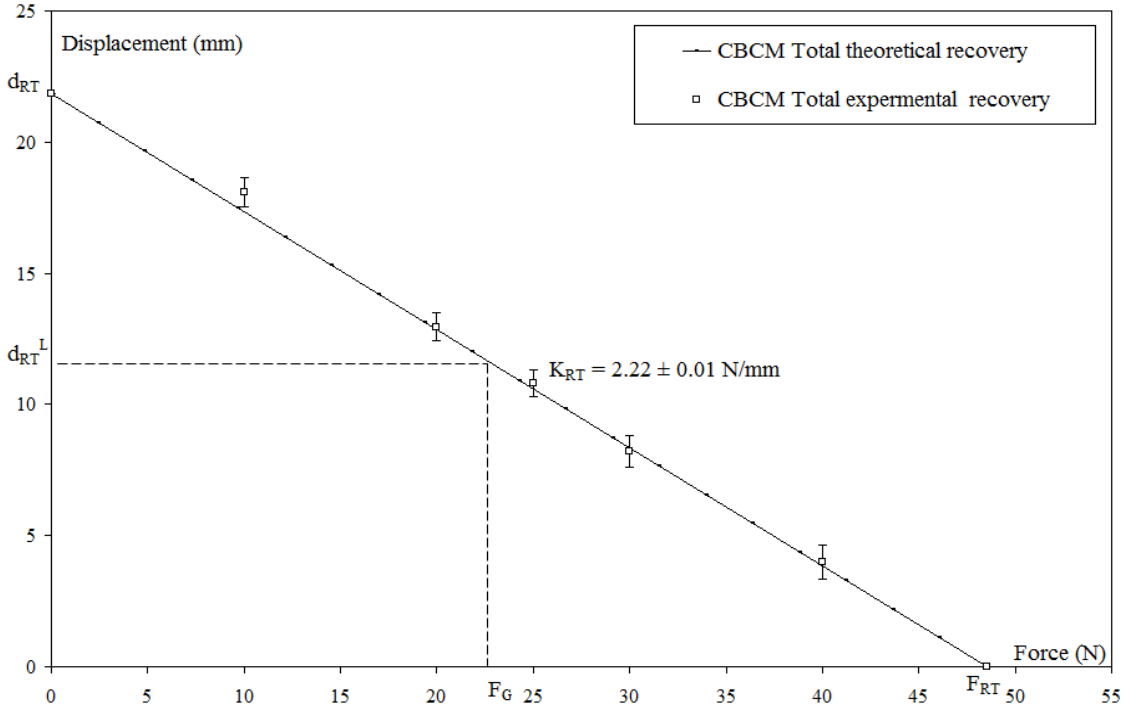

Figure IV.1.9. Recovery displacements under different loads by CBCM

During recovery cycle (EFG) and for different loads F_G, the experimental work W_G is calculated by Eq. 3 given in chapter III. W_G is in accordance (Figure IV.1.11) with the "theoretical" value of W_G calculated by Eq. 7. Figure IV.1.11 also shows that the maximum experimental work (W_G^{Max}) performed (0.27 ± 0.012J) is close to the maximum value of "theoretical" value (0.26 ± 0.03 J).

Similarly, work for CBCM activation (W_A) and CBCM-SMPC recovery (W_R) are given in Figure IV.1.11. From this figure, it can be clearly observed that W_G is much larger than W_A and W_R. The maximum values W_A and W_R are 0.1 J and 0.035 J respectively. W_G^{Max} is 2.6 times higher than the maximum value of W_A whereas it is 7.4 times higher than the maximum value of W_R. This confirms the advantage of coupling the CBCM-effect and SME in the same structure.

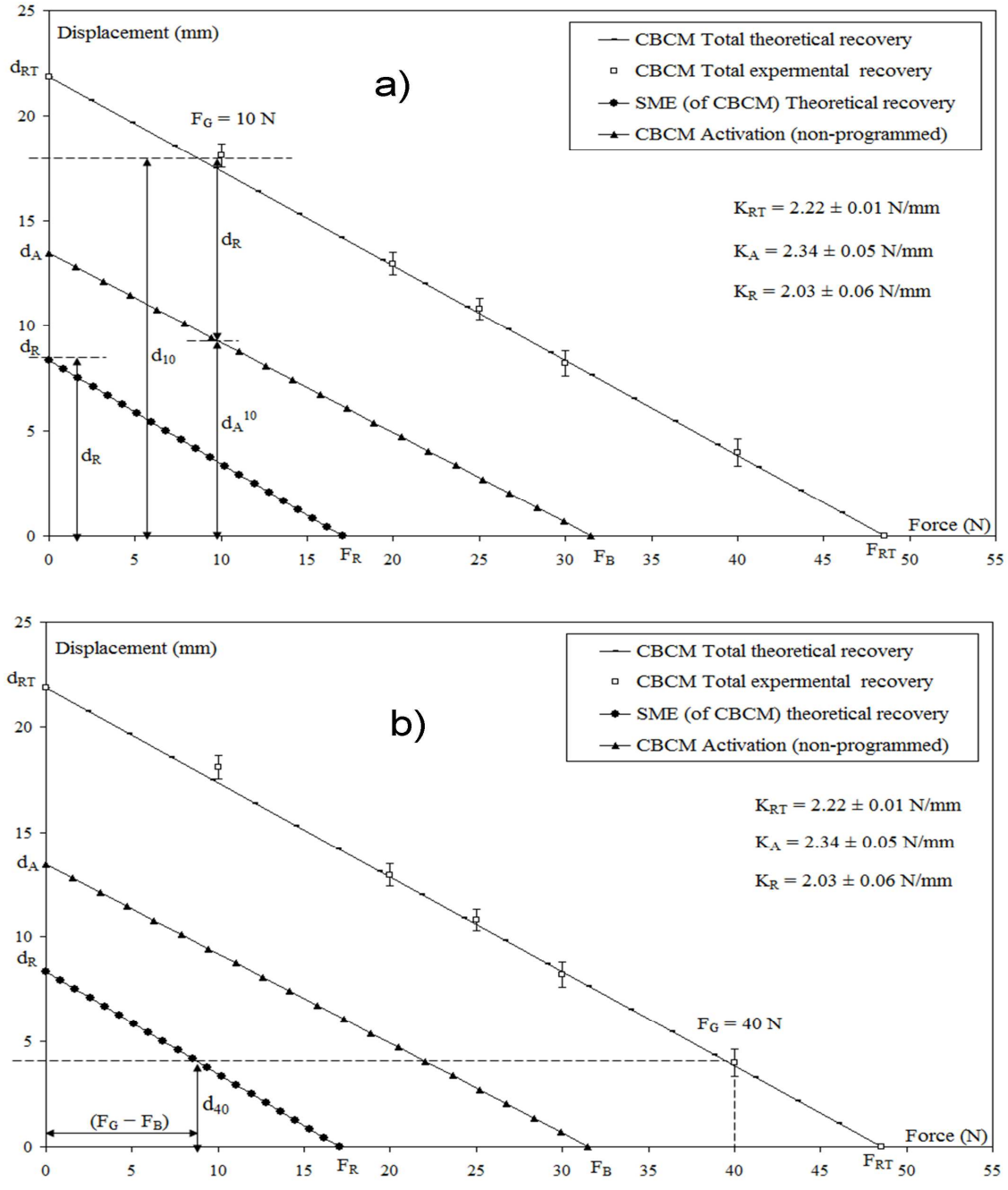

Figure IV.1.10. (a) d_{RT} under F_G = 10 N; (b). d_{RT} under F_G = 40 N

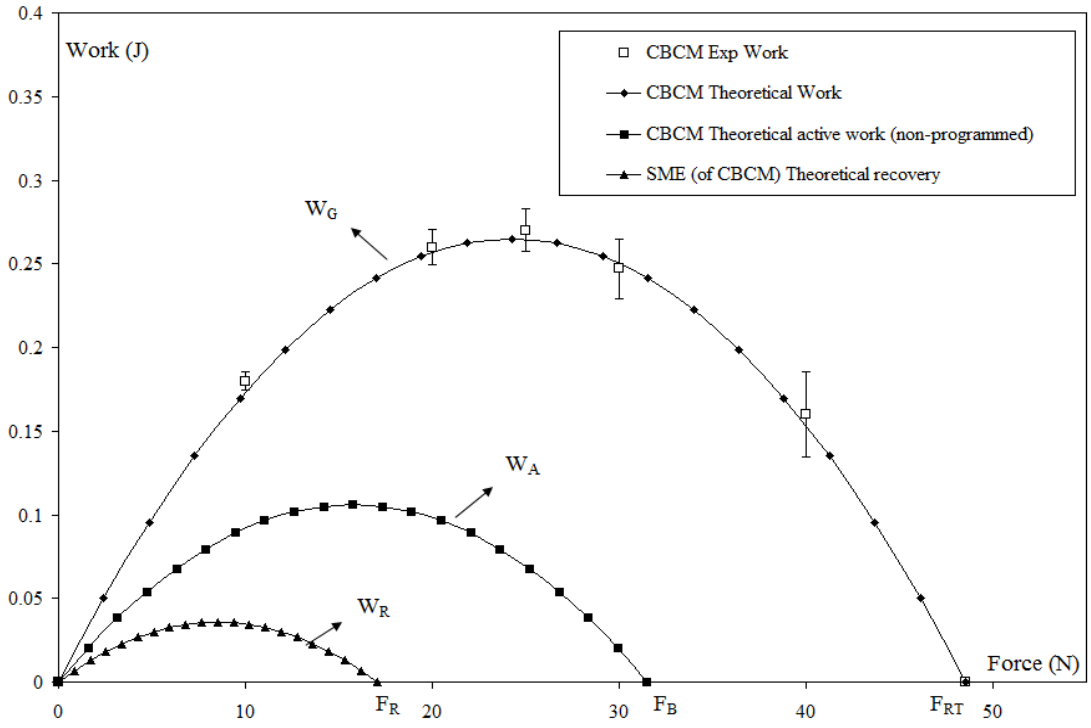

Figure IV.1.11. Work performed under different loads during recovery by CBCM

IV.1.2.3) CBCM stress relaxation programming cycle

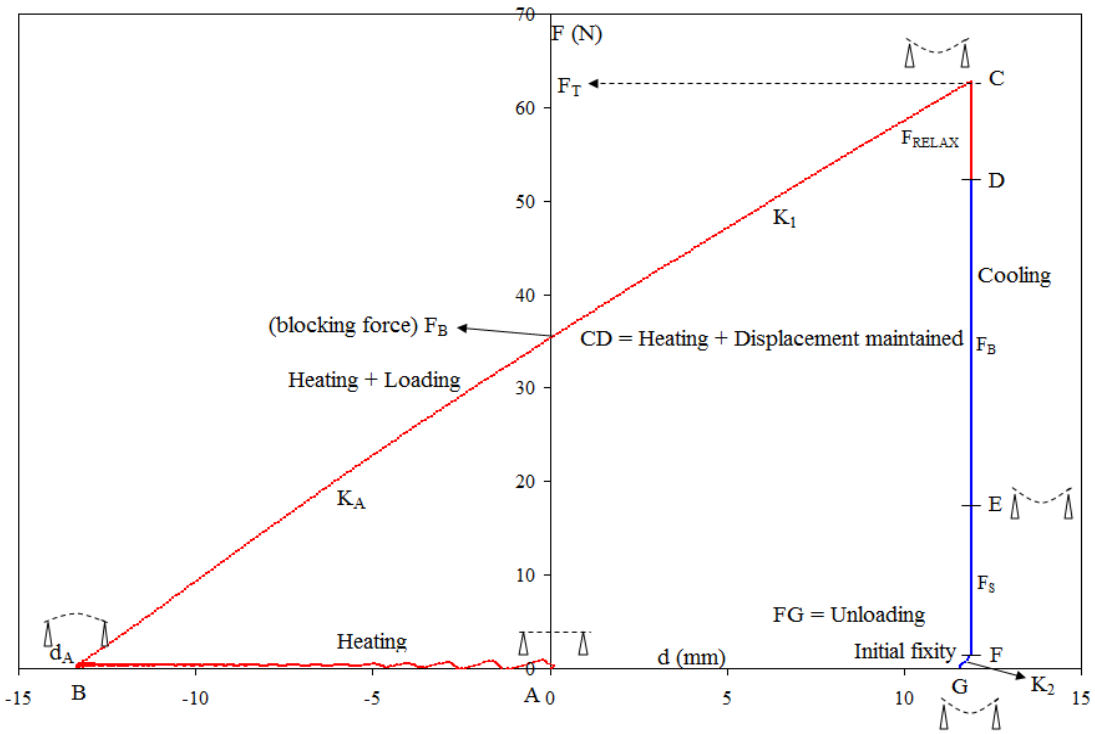

Figure IV.1.12. CBCM stress relaxation thermo-mechanical programming cycle

The stress relaxation programming for CBCM is shown in Figure IV.1.12. This programming is different from normal programming as in this programming, heating and displacement is maintained for 4 hours. It is the necessary time which ensures the complete stress relaxation (CD) taken from the work of *Tobushi et al.* [119] in which they have used various time periods for stress relaxation. Figure IV.1.13 shows the corresponding characteristic curve for the force as a function of time during the programming cycle given in Figure IV.1.12.

Characteristic values	**CBCM**
d_A (mm)	−13.05±0.45
F_B (N)	33.2±0.8
K_A (N/mm)	2.54±0.3
F_T (N)	61.7±1.1
K_1 (N/mm)	2.25±0.25
F_{RELAX} (N)	11.9±0.42
F_S (N)	15.1±0.37
F_E (N)	1.5±0.24
d_F^I (mm)	11.49±0.48
K_2 (N/mm)	2.94±0.21
K_{NA} (N/mm)	3.34±0.36

Table IV.1.5 Characteristic values of programming cycle for CBCM with stress relaxation

It clearly shows the disappearance of a force called as F_{RELAX} during the step of stress relaxation (CD). All the characteristic values for the stress relaxation programming cycle are given in Table IV.1.5. For d_F^I and F_S, it is observed that d_F^I is 45% of ds and F_S is 24% of F_T. Also, d_F^I is 88% of d_A and F_S is 45% of F_B. This shows that the step of stress relaxation affects the initial fixity as well as the rigidity K_2. It gives 24% more d_F^I than with the normal programming cycle; however, K_2 decreases and is 32% less than the normal programming cycle. The rigidity K_2 after the programming cycle is comparable to the K_{NA}. This decrease in rigidity is in accordance with the stress relaxation. d_F^I increases as there is a decrease in F_E and some force as F_{RELAX} disappears from the composite plate during the stress relaxation. Also, if the standard deviations of each characteristic value are observed, it is found that these are less than the standard deviations with the corresponding characteristic values of normal programming cycle. This

shows that with stress relaxation programming, the composite plate tends to stabilize and thus give less variation.

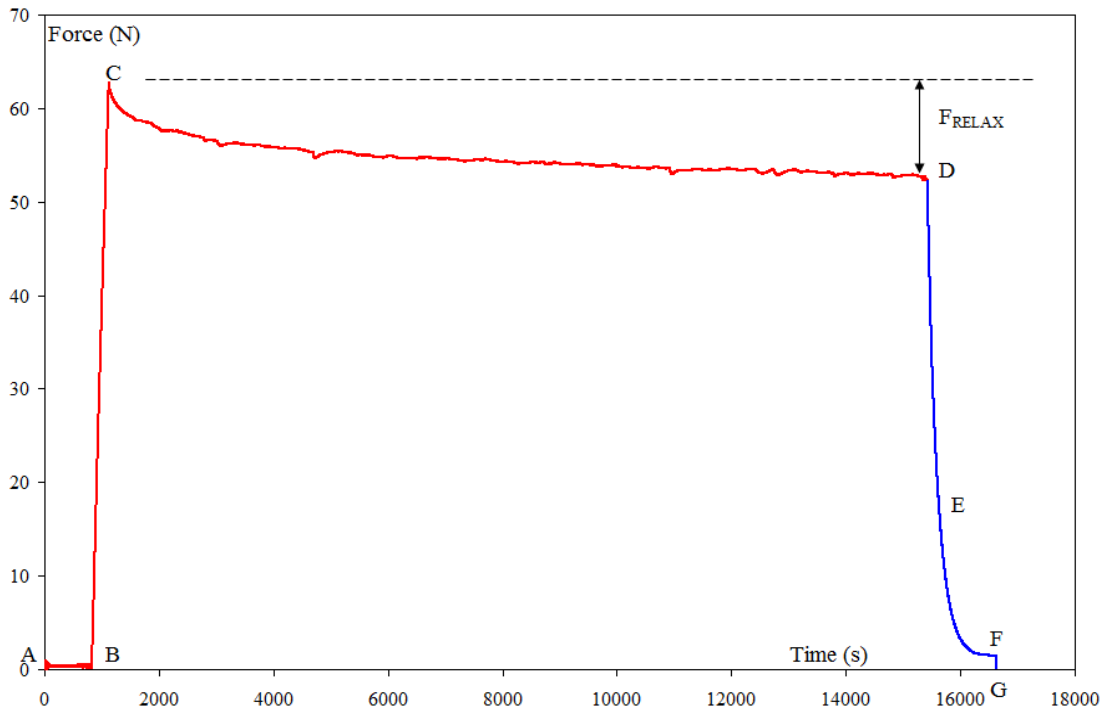

Figure IV.1.13. CBCM stress relaxation thermo-mechanical programming cycle

IV.1.2.4) Recoveries

IV.1.2.4.1) Unconstrained recovery

Figure IV.1.14 shows the unconstrained recovery for 5 recovery cycles. The first 3 cycles are performed at T_R of 150°C that is equal to T_D; however, 4th cycle is at T_R of 160°C and the 5th cycle is at T_R of 170°C. After each given T_R, cooling is also performed. After the first cooling, it can be clearly observed from the Figure IV.1.14 and Table IV.1.6 that the composite plate has a residual strain (d_{RF}). This residual strain is more than the residual strain for normal programming cycle. This residual strain is induced in the composite due to the effect of stress relaxation performed during the programming cycle. This residual strain decreases as the composite is reheated at the same T_R for more than one cycle. However, this residual strain decreases further as T_R is increased to 160°C and then 170°C. This demonstrates that with the addition of step of stress relaxation in the programming cycle, the residual strain is observed which is named as irrecoverable residual strain by *Tobushi et al.* [119]. They have demonstrated

that this residual strain is irrecoverable and it gives a new geometry to the composite plate. However, in this work, it is shown that it is recoverable if the composite plate is reheated at T_R

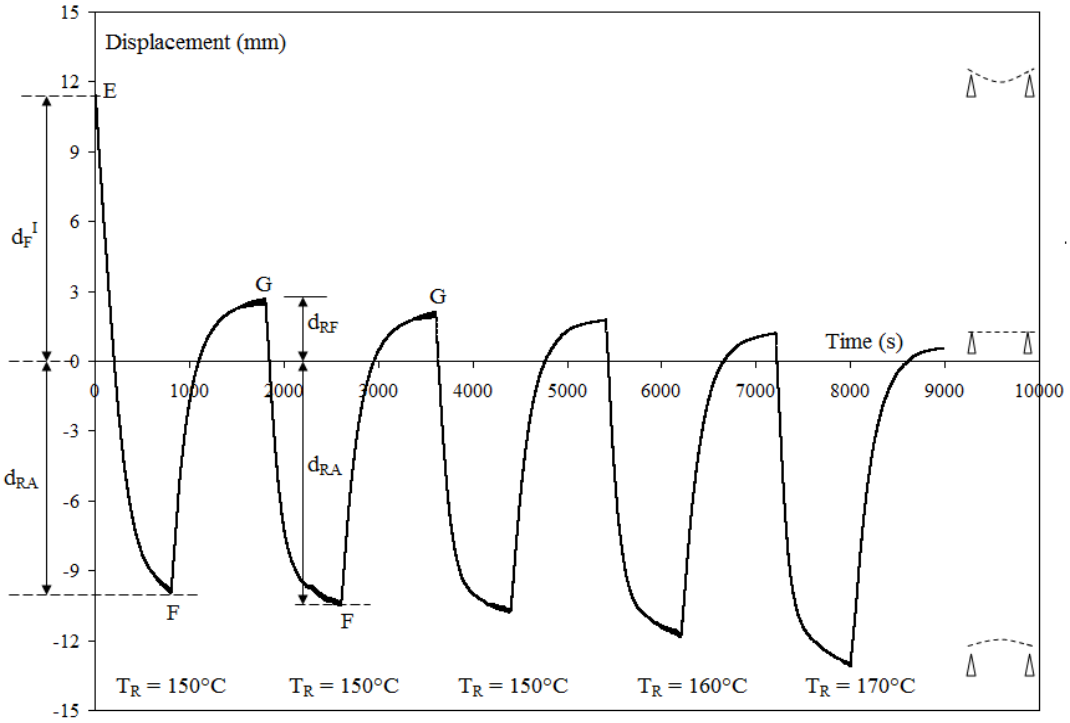

Figure IV.1.14. CBCM unconstrained recovery with stress relaxation programming; EF, GF = Heating; FG = Cooling to Ta (i.e. = 22°C)

higher than T_D. Although, this residual strain decreases if more than one cycle at T_R equal to T_D is given; however, it decreases significantly at T_R higher than higher T_D.

Furthermore, as we know that the initial fixity increases with stress relaxation programming; however, there is a decrease in ε_{RA}. Hence, the total recovery activation with stress relaxation programming (ε_{RT} = 7.23 ± 0.42 %) remains the same as compared to total recovery activation (ε_{RT} = 7.28 ± 0.29 %) with normal programming. This shows that stress relaxation has no effect on the overall performance of recovery activation.

Composite plate	Deformations (%)	Recovery cycles				
		1	2	3	4	5
		150 (°C)	150 (°C)	150 (°C)	160 (°C)	170 (°C)
CBCM	ε_{RA}	−3.4±0.13	−3.9±0.37	−4.08±0.44	−4.4±0.45	−4.7±0.39
	ε_{RF}	1.03±0.17	0.82±0.2	0.68±0.16	0.51±0.14	0.32±0.14

Table IV.1.6. Recovery deformations for CBCM during unconstrained recovery with stress relaxation programming; ε_F^I = 3.83±0.16 %

IV.1.2.4.2) Constrained recovery

Similarly, Figure IV.1.15 and Table IV.1.7 demonstrate the generation of recovery force during recovery cycles at T_R = 150°C. It can be observed that during the successive recovery cycles, F_{RT} tends to increase. Similarly, F_{RES} also tends to increase with the cooling associated to T_R. If F_{RT} generated during constrained recovery with stress relaxation programming is compared to normal programming, it can be observed that they are almost equal. F_{RT} generated at 150°C, during 3rd recovery cycle, with normal programming is 47.44 ± 2.33N and with stress relaxation programming is 47.35 ±0.44. This shows that the stress relaxation effect has no effect on the performance (generation of recovery force) of CBCM.

Composite plate	Force (N)	Recovery cycles		
		1	2	3
		150 (°C)	150 (°C)	150 (°C)
CBCM	F_{RT}	46.44±0.47	47.10±0.26	47.35±0.44
	F_{RES}	1.98±0.09	2.08±0.13	2.20±0.22
	$\delta F = F_{RT} - F_{RES}$	44.46±0.56	45.02±0.39	45.15±0.66

Table IV.1.7. Recovery forces for CBCM during constrained recovery with stress relaxation programming; ε_F^I for CBCM 3.73±0.32

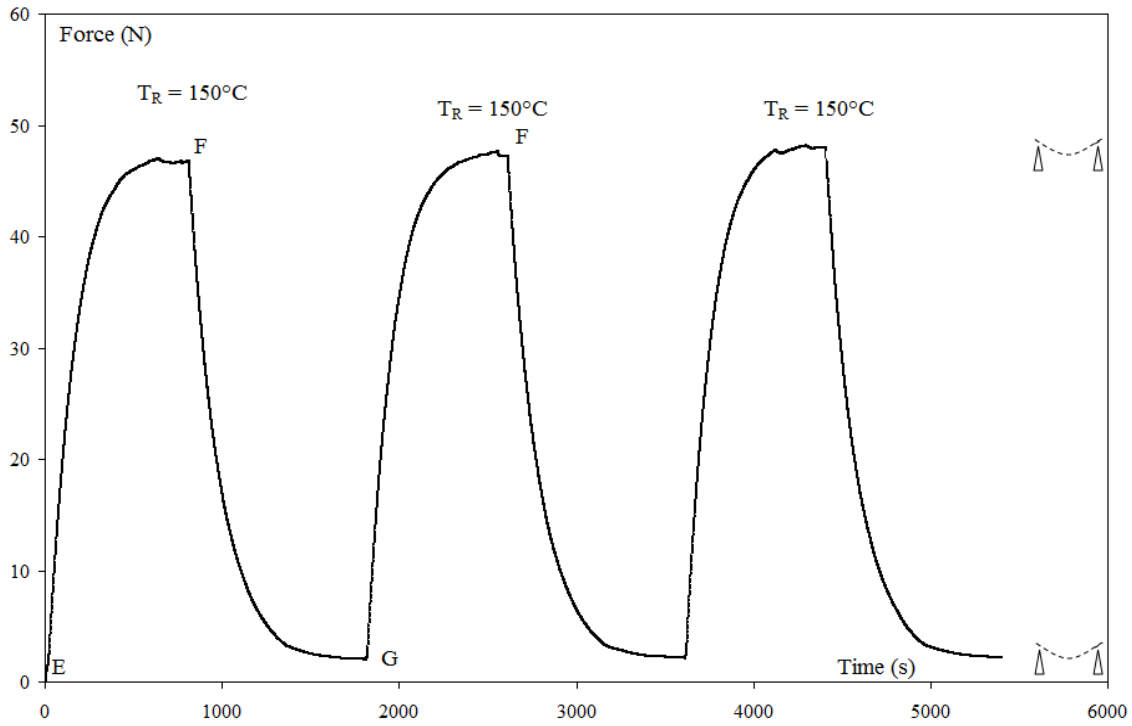

Figure IV.1.15. Constrained recoveries for CBCM and SYM; E = Initial fixity, EF, GF = Heating to T_D (i.e. = 150°C; FG = Cooling to Ta (i.e. = 22°C)

Similarly, F_R obtained from 1st recovery cycle is 13.24±0.35 N. If F_R is compared with F_S, it is observed that F_R is less than F_S (15.1±0.37 N) that shows that due to the disappearance of F_{RELAX} from the composite during stress relaxation programming, it gives a lesser value of F_R.

IV.1.2.4.3) Characteristic straight line and corresponding work

Figure IV.1.16 demonstrates the characteristic straight line drawn from d_{RT} obtained from unconstrained recovery and F_{RT} obtained from constrained recovery of the 3rd cycle at 150°C from the Tables IV.1.6 and IV.1.7 respectively. Similarly, the theoretical recovered work W_G is also given that corresponds to the characteristic line. The maximum theoretical recovered work W_G^{max} obtained is 0.25 ± 0.02 J. It can be assumed that the experimental and theoretical W_G are in accordance as it is already explained in section IV.1.2.2.3. Also, it is found that K_{RT}, during the recovery, with normal programming cycle and with stress relaxation programming cycle is also same that also shows no effect of stress relaxation on the overall performance of CBCM. Hence, it is clear that the performance of the CBCM-SMPC actuator remains unchanged by the

introduction of a step of stress relaxation in the programming cycle. However, only the initial fixity and the geometry after the unconstrained recovery are changed.

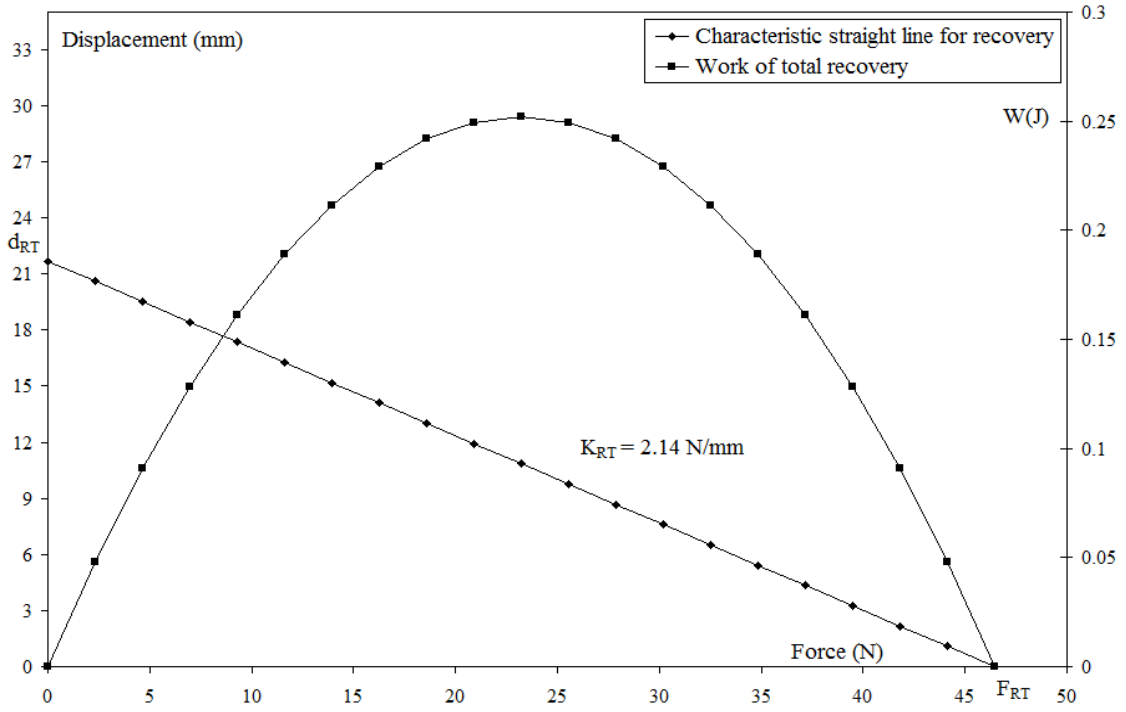

Figure IV.1.16. Characteristic straight line and corresponding work for CBCM recovery at 150°C with stress relaxation programming

IV.1.2.5) CBCM initial fixity stabilization

To observe at ambient temperature Ta, the influences of the stress relaxation step on the stabilization of initial fixity d_F^I, two virgin plates programmed by a programming cycle with and without stress relaxation step are tested. This test is carried out just after the programming cycle, and during this test, the preload of 0.3N is maintained, by the PID control of the cross head of the tensile testing machine. The plate displacement versus time is represented in Figure IV.1.17. Two different responses can be observed. After 10,000 s (2.7h), the stabilization of the plate with stress relaxation step is obtained and the loss of displacement is equal to 0.6 mm, 5% of d_F^I. For the other plate without stress relaxation step, the displacement stabilization cannot be observed even after 43,000 s and the loss of displacement is equal to 0.64mm, 6.7% of the

initial fixity. In this case, a long-term stabilization of the plate may be possible but with a significant loss of d_F^I.

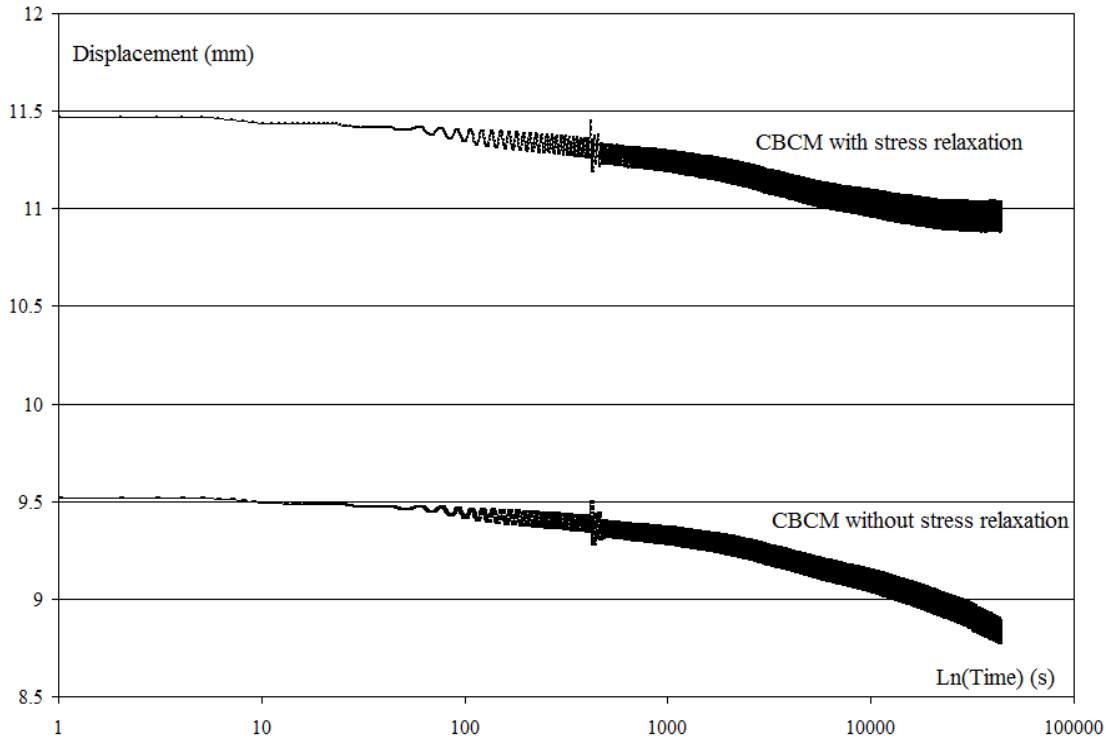

Figure IV.1.17. Visco-elastic effect for CBCM

IV.1.3) SYM

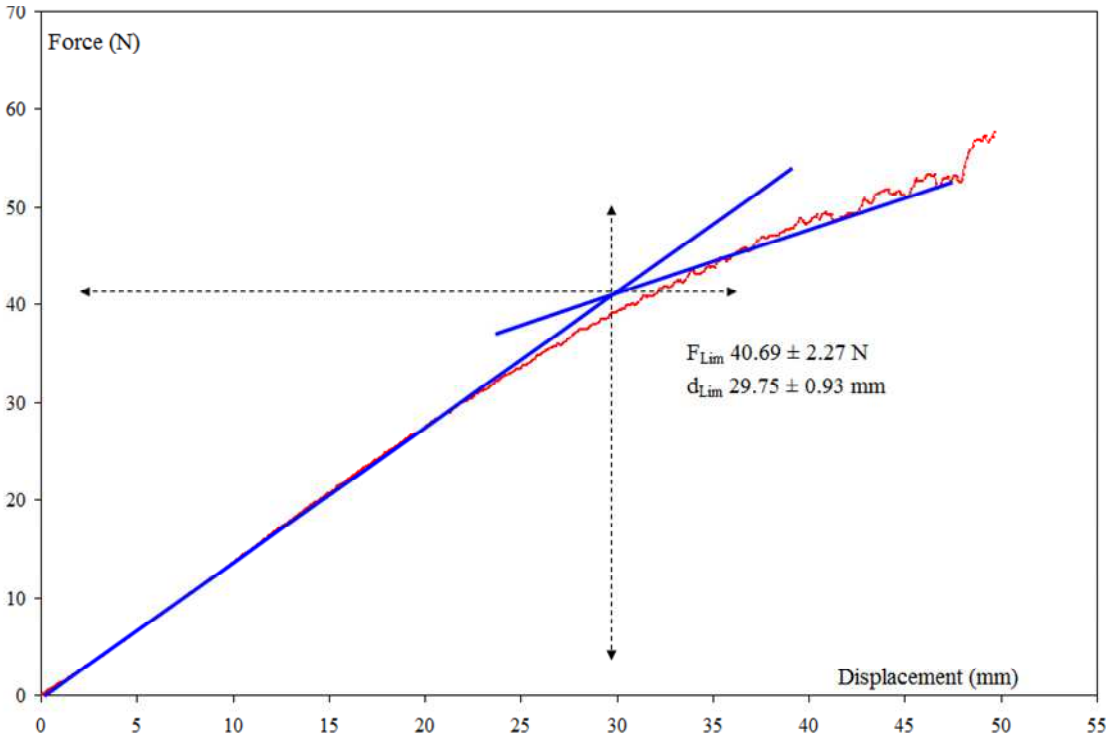

Figure IV.1.18. Determination of limit force for SYM

By the preliminary tests of bending at T_D (3 samples of SYM plates) until fracture as shown in Figure IV.1.18, the limit force and the corresponding displacement which correspond to the loss of linearity of the response curve, have been obtained. In order to ensure the SYM plate integrity, the value of d_S is approximately equal to the corresponding average displacement of the average limit force minus the standard deviation. For SYM plates, the average values of the limit force and the corresponding displacement are equal to 40.69±2.27N and 29.75±0.93 mm respectively.

IV.1.3.1) SYM normal programming cycle

Figure IV.1.19 represents the programming cycle for SYM. All the characteristic values for the SYM normal programming cycle are given in Table IV.1.8. Actuation properties (d_A and F_B) are also produced during heating, because due to the manufacturing process, the SYM composite plates have an unsymmetrical gradient property (through the thickness) that is not easily controllable especially for the high temperatures. However, d_A and F_B are less as compared to the CBCM. The prescribed displacement d_S (including d_A) leads to a F_T equal to 33.44 N, 56% lesser than the CBCM one. During cooling, the small value of F_B is retrieved and F_S is 500% smaller than the CBCM corresponding value. This difference of F_S between SYM and CBCM shows that this stabilization force is linked to different phenomena which appear during the cooling under load. Indeed, due to the stress field through the thickness of the composite and according to the shape memory property of the epoxy resin, the polymer network fixes a new configuration different to the initial one. During cooling, the rearrangement of the polymer network induces dilatation effect (due to SME) which is added to the thermal dilatation effect. F_S combines the dilatation effect of each layer which results in the coupling of dilatation effects between the resin and the reinforcement. F_S is linked to the residual stress in the composite and is a measure of the interaction between the resin and the nature of the reinforcement, and characterizes the asymmetry of the composite structure.

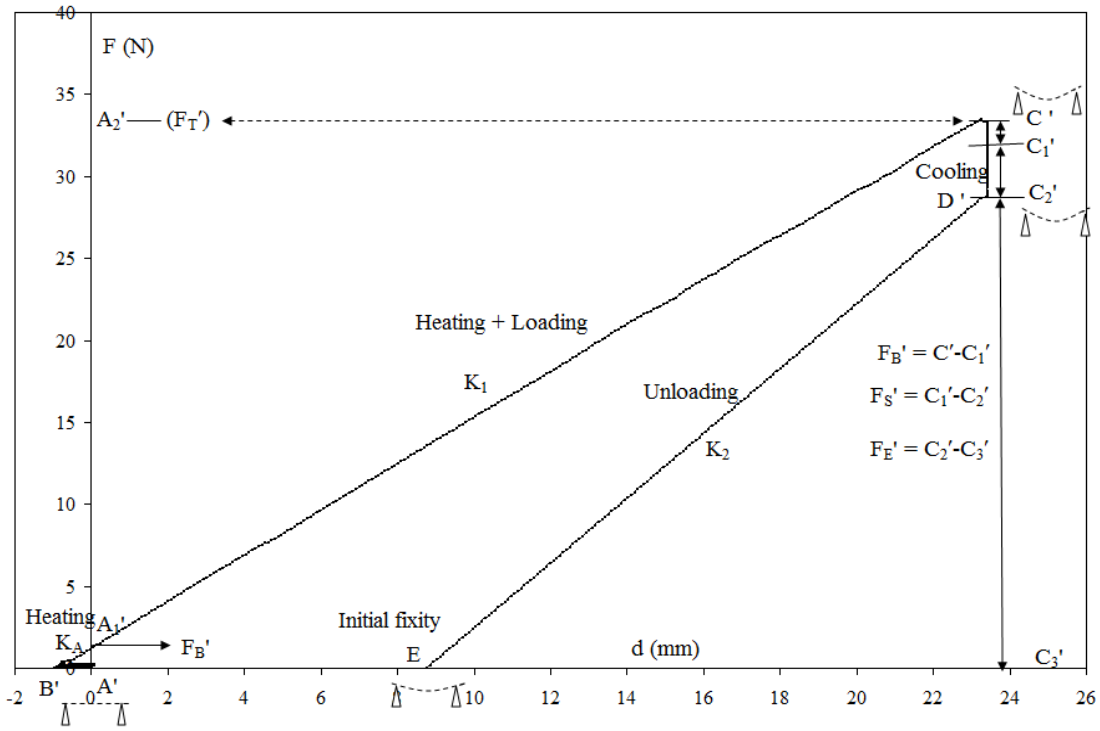

Figure IV.1.19. Normal SYM thermo-mechanical programming cycle

Characteristic values	SYM
d_A (mm)	−0.93±0.3
F_B (N)	1.1±0.12
K_A (N/mm)	1.18±0.2
F_T (N)	33.44±0.9
K_1 (N/mm)	1.37±0.1
F_S (N)	2.88±1.1
F_E (N)	29.46±1.3
d_F^I (mm)	8.64±0.2
K_2 (N/mm)	1.98±0.32
K_{NA} (N/mm)	1.8±0.14

Table IV.1.8. Characteristic values for SYM normal programming cycle

Compared to the CBCM, the rigidity K_2 close to K_{NA} is smaller, ratio of 2.16. For all the characteristic values of the programming cycle, the standard deviations of all are lesser than the CBCM ones. The value of F_E and a lower initial fixity d_F^I, highlight the lower level of internal stress for the SYM plate, compared to the CBCM.

IV.1.3.2) SYM recoveries

IV.1.3.2.1) Unconstrained recovery

The test of unconstrained recovery (Figure IV.1.20) shows that at T_R equal to 150°C, during the 1st recovery cycle, SYM gives 100% recovery with d_{RT} of 9.15±0.69 mm with the associated deformation (ε_{RT}) of 3.05±0.23%. In comparison, CBCM recovers 242% with the d_{RT} of 21.84±1.26 mm during heating and ε_{RT} of 7.28 % ± 0.42.

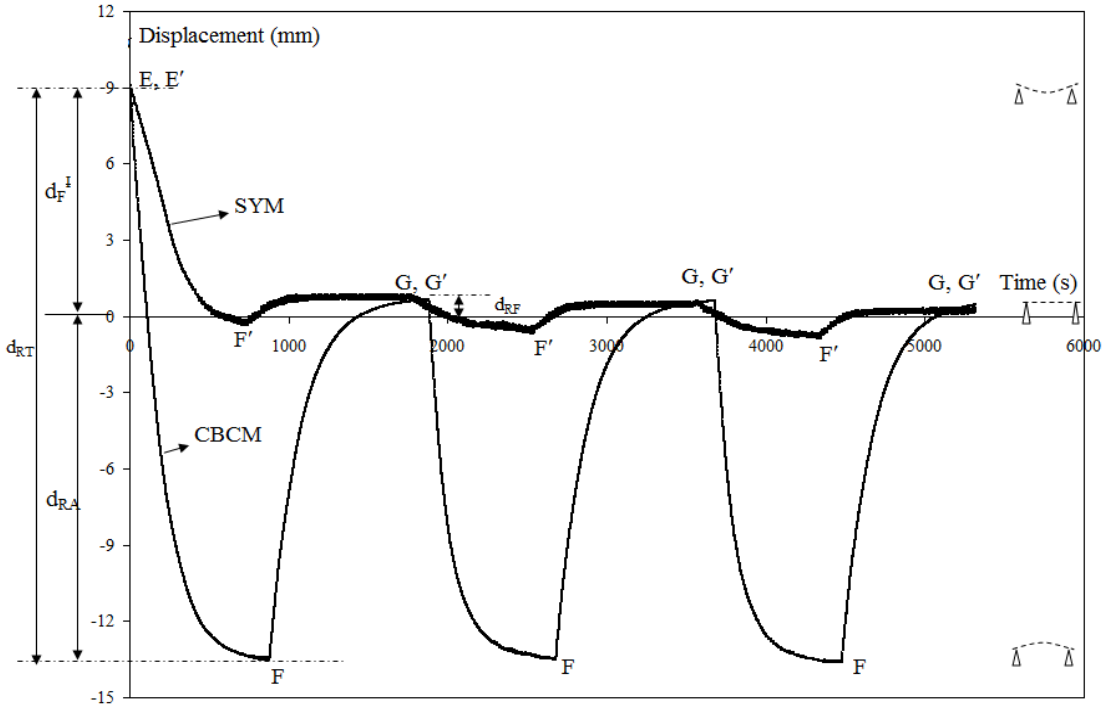

Figure IV.1.20. Unconstrained recovery of CBCM and SYM; E, E′= initial fixities; d_F^I = 9.21±0.63 mm for CBCM and d_F^I = 9.09±0.39 mm for SYM; EF, GF = Heating to T_D (i.e. = 150°C; FG = Cooling to Ta (i.e. = 22°C)

The recovery displacement of SYM and CBCM as a function of temperature, during heating of the 1st recovery is shown in Figure IV.1.21. The full recovery of SYM plate is obtained at T_D; this result is in accordance with the description given by *Castro et al.* [31, 118] that full recovery at a temperature lower than T_D is not possible for the conventional SMPs and their composites. In comparison, CBCM gives full recovery at a temperature close to 90°C. So,

CBCM plate has the capability to change the curvature during the unconstrained recovery.

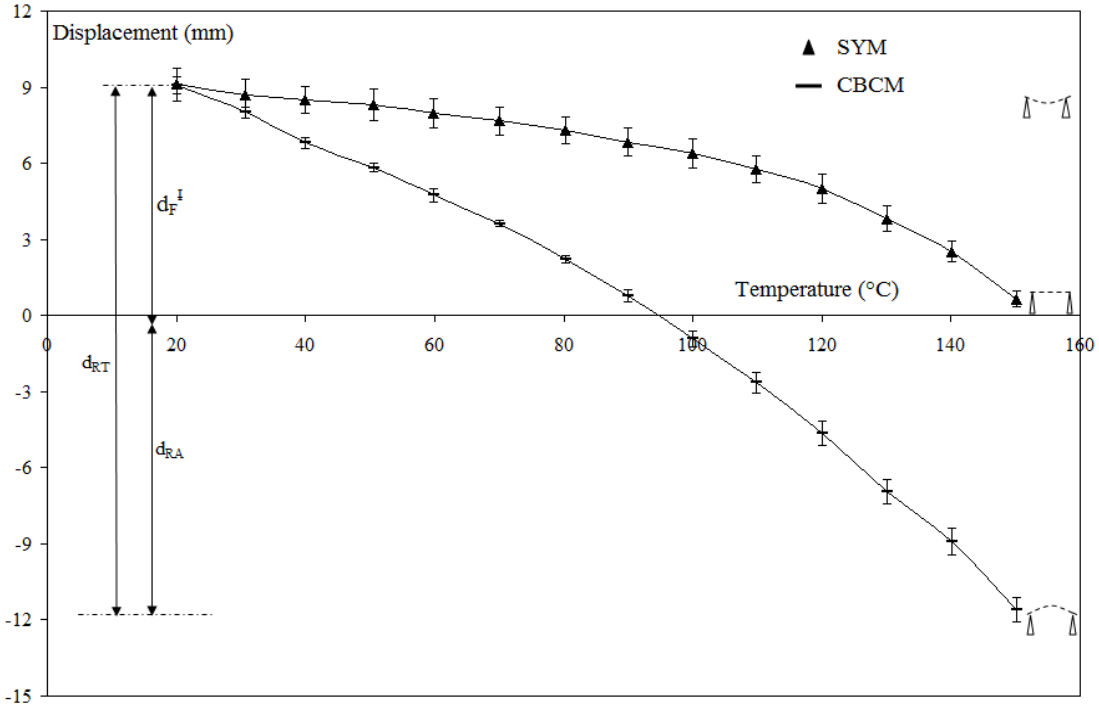

Figure IV.1.21. Unconstrained recovery of CBCM and SYM at different temperatures during 1st recovery cycle; d_F^I = 9.21±0.63 mm for CBCM and d_F^I = 9.09±0.39 mm for SYM

Compared to the SYM plate, this result highlights the major advantage induced by the coupling between the SMP (i.e. SME) and CBCM properties, the ability to obtain large actuation property. To characterize the return to initial position, the average activation and fixity deformations (ε_{RA} and ε_{RF}) for three recovery cycles are given in Table IV.1.9. ε_{RA} is the activated recovery deformation (point F, F′) during heating and ε_{RF} is the recovery deformation during cooling (point G, G′). In Figure IV.1.20, the cooling of 1st recovery cycle (FG, F′G′) shows the return of the composite plates to their initial positions demonstrating that the fixities due to the SMEs are recovered and thus disappear during the heating of 1st recovery cycle. For the cooling of other recovery cycles particularly after the cooling of the 3rd cycle (Table IV.1.9), CBCM has ε_{RF} = 0.22±0.15 % and SYM has ε_{RF} = 0.13±0.08 %.

Composite plates	Deformations (%)	Recovery cycles		
		1	2	3
SYM	ε_{RA}	−0.02 ± 0.1	−0.09±0.11	−0.14±0.09
	ε_{RF}	0.21 ± 0.12	0.15±0.1	0.13±0.08
CBCM	ε_{RA}	−4.21 ± 0.29	−4.31±0.26	−4.32±0.22
	ε_{RF}	0.34 ± 0.1	0.26±0.13	0.22±0.15

Table IV.1.9. Unconstrained recovery activations and fixities during the 3 recovery cycles, ε_F^I = 3.07±0.21 for CBCM and ε_F^I = 3.03±0.13 for SYM

IV.1.3.2.2) Constrained recovery

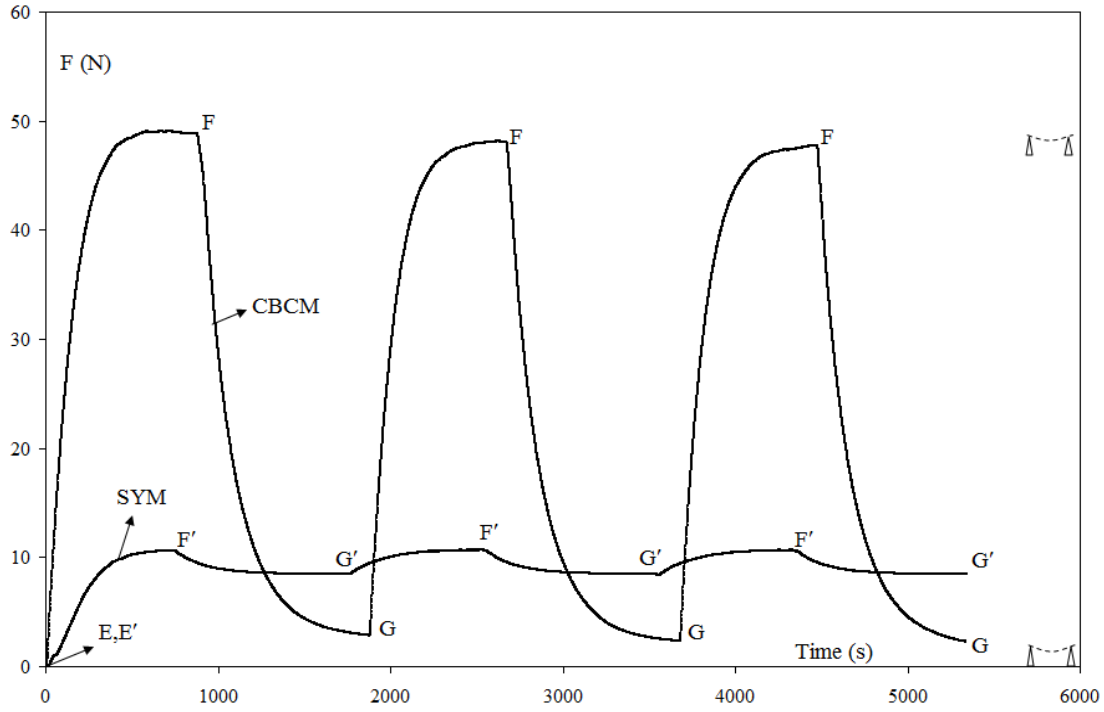

Figure IV.1.22. Constrained recovery curves for CBCM and SYM; E = Initial fixity; EF, GF = Heating to T_D (i.e. = 150°C; FG = Cooling to Ta (i.e. = 22°C)

In Figure IV.1.22, the total recovery force F_{RT} is 10.6 N, that is only 30.7% of F_T = 34.02 N±1.14, the force required to deform the SYM plates during the programming cycle. In comparison, F_{RT} for CBCM plates is 48.54 ± 2.57 (84% of F_T = 57.70±1.94). The blocking force F_B for SYM is 1±0.3 N (31.48±1 N for CBCM). As we already know that F_R is the difference of F_{RT} and F_B, therefore, F_R produced during heating of 1st recovery cycle for SYM is 9.6± 0.33N

(17.06±1.57 for CBCM). For comparable values of initial fixity d_F^I (9.12 ± 0.3 mm for SYM and 8.64 ± 0.3 mm), F_R of CBCM is 77% more than F_R of SYM (Table IV.1.10). However, the ratios between F_R and F_T are close to each other; 0.28±0.02 for SYM and 0.29±0.03 for CBCM. For SYM, at the cooling of 1st recovery cycle, F_{RES} is 8.45 N which is 80% of F_{RT} during heating (10.6N). Therefore, on successive heating, only 20% of the forces will be available. In comparison, F_{RES} for CBCM is 3.03N which is 6% of F_{RT} (48.54N), so, 94% of the recovery force remains constant for SYM and CBCM (Table IV.1.10). At point G, if the plates are unloaded, δF will induce a deformation which will lead to a new position of equilibrium corresponding to a new value of the fixity. δF can also give some information regarding the interaction between the reinforcement and the polymer. For the successive three cycles, $\delta F = F_{RT} - F_{RES}$ which characterizes the level of the Indeed, at the end of the programming cycle, the fixity shape is obtained because of equilibrium between the deformation energy of the reinforcement and the polymer.

The polymer can be considered as a lock which maintains the reinforcement in position and gives the fixity shape characterized by F_S and d_F^I. During the heating step of the constrained recovery, the level of the stress field and the reinforcement-polymer interaction affect the property of the polymer rearrangement and modify the equilibrium between the deformation energy of the reinforcement and the polymer. After cooling, the consequence is the existence of the residual force. A new equilibrium between the deformation energy of the reinforcement and the polymer is established.

Composite plates	Force (N)	Recovery Cycles		
		1	2	3
CBCM	F_{RT}	48.54 ± 2.57	47.77 ± 2.37	47.44 ± 2.33
	F_{RES}	3.03 ± 0.96	2.51 ± 0.87	2.23 ± 0.94
	$\delta F = F_{RT} - F_{RES}$	45.51±3.53	45.26±3.24	45.21±3.27
SYM	F_{RT}	10.6 ± 0.22	10.65±0.24	10.63 ± 0.27
	F_{RES}	8.45 ± 0.19	8.44±0.16	8.46 ± 0.2
	$\delta F = F_{RT} - F_{RES}$	2.15±0.41	2.21±0.11	2.17±0.47

Table IV.1.10. Constrained recovery forces for CBCM and SYM; ε_F^I = 3.04 ± 0.1 % for CBCM and ε_F^I = 2.88 ± 0.1 % for SYM

IV.1.3.2.3) Recovery under load

The representative curve of recovery under load of 8 N (and a compared CBCM curve under 10N load) is shown in Figure IV.1.23 in which displacement is given as a function of time. For SYM, 8 N is the maximum load under which the performed work has been measured. Similar

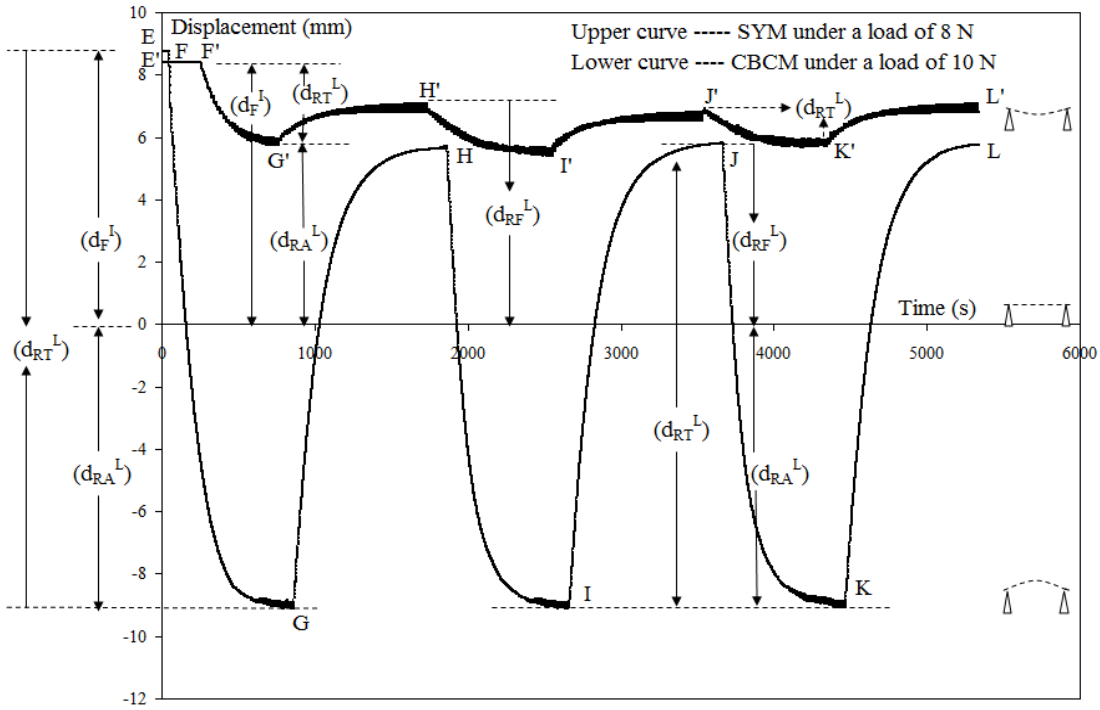

Figure IV.1.23. Recovery under load for CBCM and SYM.; E, E´= initial fixities; cycle 1 = EFGH; cycle 2 = HIJ; cycle 3 = JKL; EFG, HI, JK = Heating to T_D (i.e. = 150°C; GH, IJ, KL = Cooling to Ta (i.e. = 22°C)

types of recoveries under different loads are also performed and the results of these recoveries are given in Table IV.1.11 (the corresponding curves are shown in Appendix-B). In comparison to CBCM, for SYM, the blocking force is small and can be neglected. For this reason, SYM

F_G (N)	Deformations (%)	Recovery cycle (i)			
		0	1	2	3
2	$(\varepsilon_{RA}{}^{L})_i$	0	0.40±0.09	0.42±0.05	0.41±0.08
	$(\varepsilon_{RF}{}^{L})_i$	2.70±0.11	0.68±0.05	0.68±0.07	0.69±0.03
	$(\varepsilon_{RT}{}^{L})_i = (\varepsilon_{RF}{}^{L})_{i-1} - (\lvert\varepsilon_{RA}{}^{L}\rvert)_i$	0	2.3±0.2	0.26±0.1	0.27±0.15
4	$(\varepsilon_{RA}{}^{L})_i$	0	1.01±0.1	0.99±0.04	1.03±0.03
	$(\varepsilon_{RF}{}^{L})_i$	2.80±0.1	1.34±0.05	1.33±0.03	1.43±0.06
	$(\varepsilon_{RT}{}^{L})_i = (\varepsilon_{RF}{}^{L})_{i-1} - (\lvert\varepsilon_{RA}{}^{L}\rvert)_i$	0	1.79±0.2	0.35±0.09	0.3±0.06
5	$(\varepsilon_{RA}{}^{L})_i$	0	1.51±0.12	1.49±0.11	1.52±0.08
	$(\varepsilon_{RF}{}^{L})_i$	2.99±0.06	1.66±0.13	1.68±0.07	1.7±0.1
	$(\varepsilon_{RT}{}^{L})_i = (\varepsilon_{RF}{}^{L})_{i-1} - (\lvert\varepsilon_{RA}{}^{L}\rvert)_i$	0	1.48±0.18	0.17±0.24	0.16±0.15
6	$(\varepsilon_{RA}{}^{L})_i$	0	1.60±0.09	1.63±0.05	1.62±0.06
	$(\varepsilon_{RF}{}^{L})_i$	2.76±0.12	1.94±0.05	1.95±0.03	1.97±0.02
	$(\varepsilon_{RT}{}^{L})_i = (\varepsilon_{RF}{}^{L})_{i-1} - (\lvert\varepsilon_{RA}{}^{L}\rvert)_i$	0	1.16±0.21	0.31±0.1	0.33±0.09
8	$(\varepsilon_{RA}{}^{L})_i$	0	1.95±0.11	1.84±0.07	1.85±0.07
	$(\varepsilon_{RF}{}^{L})_i$	2.65±0.09	2.31±0.05	2.24±0.1	2.30±0.04
	$(\varepsilon_{RT}{}^{L})_i = (\varepsilon_{RF}{}^{L})_{i-1} - (\lvert\varepsilon_{RA}{}^{L}\rvert)_i$	0	0.7±0.20	0.47±0.12	0.39±0.17

Table IV.1.11. SYM recovery under different loads; $((\varepsilon_{RF}{}^{L})_0 = \varepsilon_F{}^{I})$

under a load, has not the ability to return to its initial position, thus, the active displacement is between the initial fixity ($d_F{}^{I}$) and the initial position (Figure IV.1.23). The total deformations recovered under different loads ($\varepsilon_{RT}{}^{L}$) are calculated for the recovery cycles by adding or subtracting the activations under load ($\varepsilon_{RA}{}^{L}$) and the fixities under load ($\varepsilon_{RF}{}^{L}$) depending on the extent of recovery (see Table IV.1.11).

It can be clearly observed that after the partial recovery of the initial fixities, SYM tends to stabilize under load and this stabilization can be obtained for a number of cycles. Compared to CBCM (Table IV.1.4) the deformation $\varepsilon_{RT}{}^{L}$ for SYM is smaller. This is due to the high actuation capability of CBCM under load and especially the ability to change its curvature

during its actuation (deforms upward during heating and deforms downward during cooling in reference to its initial position).

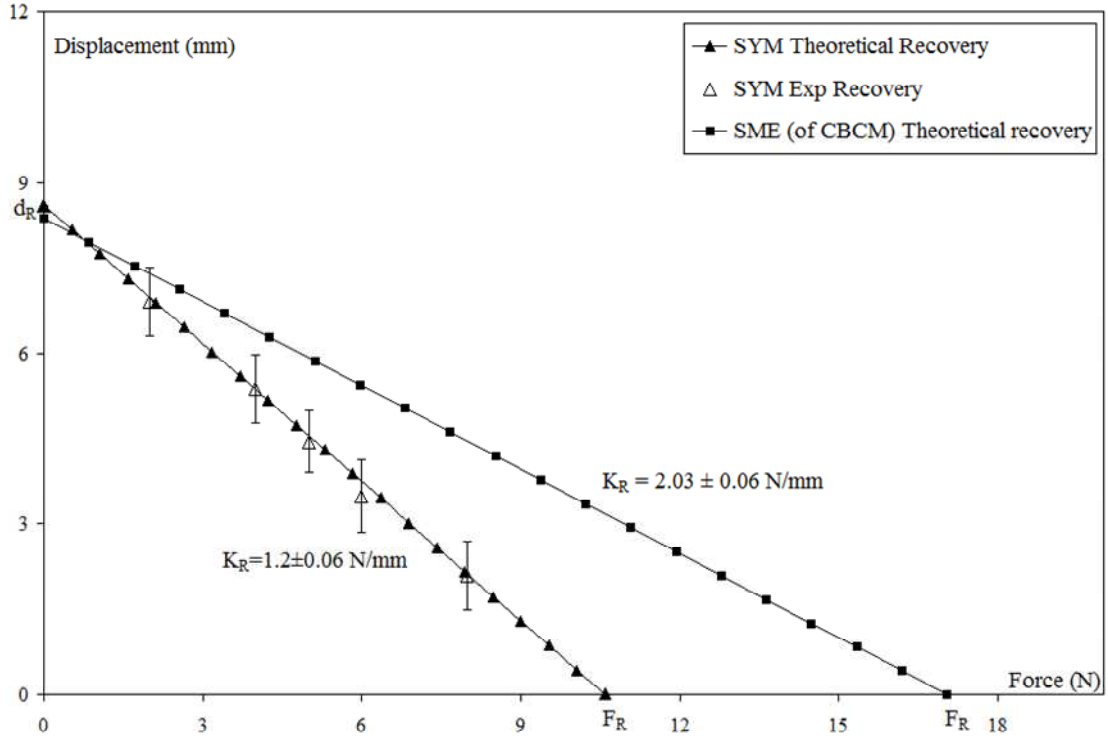

Figure IV.1.24. Recovery displacements under different loads by CBCM and SYM

Figure IV.1.24 shows the characteristic straight lines for SYM and CBCM obtained from the unconstrained recovery displacement d_{RT} and the force F_{RT} obtained from the constrained recovery test. For SYM, the actuation properties can be neglected with respect to SME of the polymer, so $F_R = F_{RT}$ and $d_R = d_{RT}$. As explained for CBCM previously, for SYM, the experimental values obtained under different F_G are also in accordance with the characteristic straight line, characterized by a rigidity K_R equal to 1.2 N/mm (K_R=2.03N/mm for CBCM). The two d_R (for SYM and CBCM) are close together; however, for F_R, a difference can be observed. Like the results obtained for F_S, the greater value of F_R may be induced by the asymmetry of CBCM.

Figure IV.1.25 shows the corresponding theoretical work W_R (Eq. 7) restituted during the recoveries. As explained for CBCM previously, for W_G, the theoretical and experimental values (Eq. 3 chap. II) are also in accordance. For SYM, the experimental maximum work W_R is given by load of 5 N (0.022 J). If the maximum theoretical work W_R of CBCM (0.035J) is compared

with maximum theoretical W_R of SYM (0.022 J), then it can be observed that W_R for CBCM is 1.6 times higher than W_R of SYM. Hence, it also confirms that even W_R of CBCM is higher than W_R of SYM. This leads to the development of a powerful CBCM shape memory actuator.

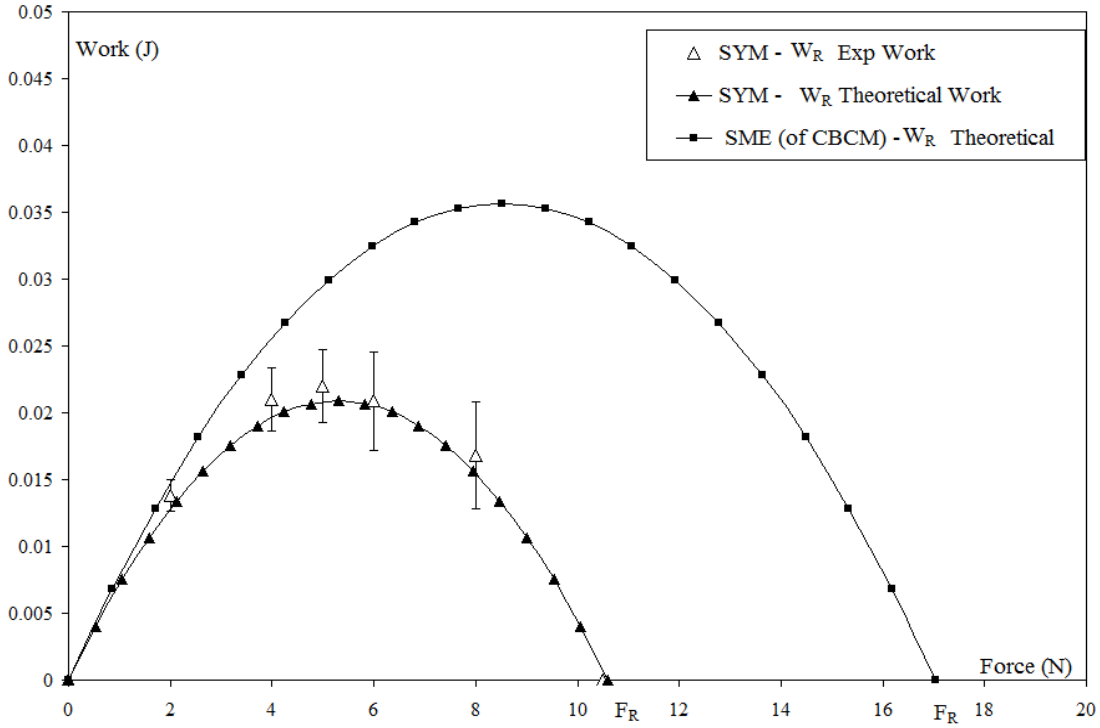

Figure IV.1.25. Works performed under different loads during recovery by CBCM and SYM

IV.1.3.3) SYM stress relaxation programming cycle

Figure IV.1.26 shows the stress relaxation programming cycle with a stress relaxation step of 4 hours. The evolution of F_{RELAX} (2.23±0.45 N) during the step of stress relaxation is shown by (CD) in Figure IV.1.27. However, for CBCM, F_{RELAX} is equal to 11.9±0.42 N. All the characteristic values for this programming cycle are given in Table IV.1.12. The results for SYM during unconstrained recovery and constrained recovery tests are given in Appendix- C.

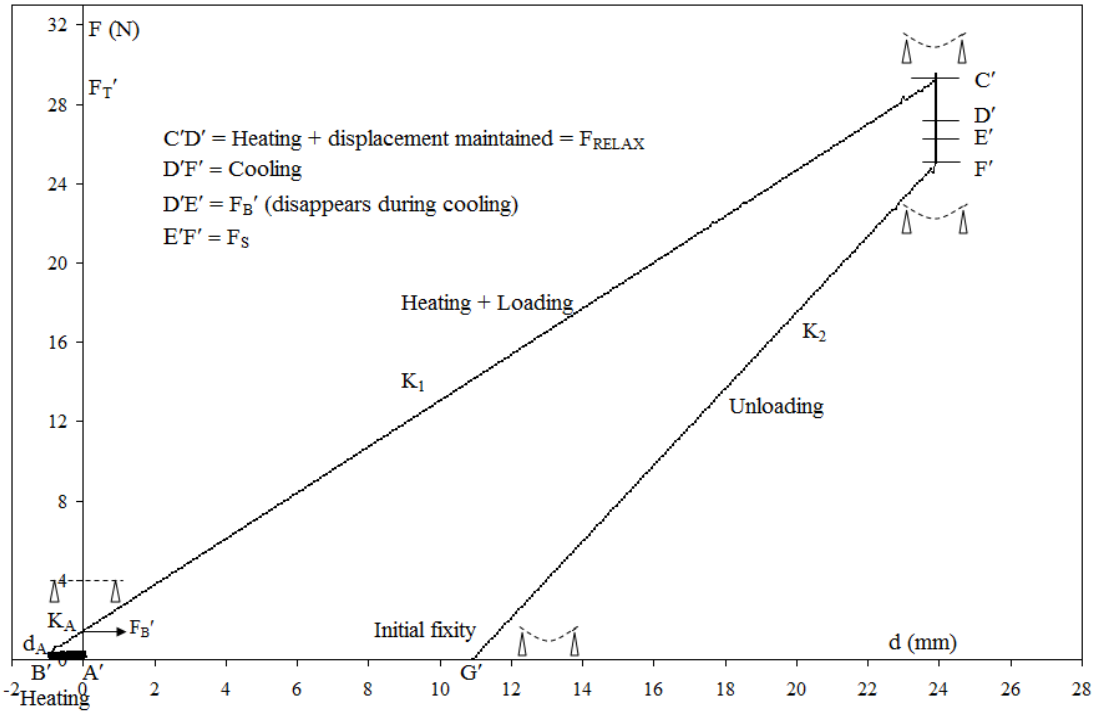

Figure IV.1.26. SYM stress relaxation thermo-mechanical programming cycle

The results for the recovery tests for SYM during normal programming cycle and with stress relaxation programming are found to be in accordance as in case of CBCM with normal programming cycle and stress relaxation programming cycle.

The stress relaxation programming cycle does not affect the overall performance of SYM as in the case of CBCM. Like CBCM, and compared to the SYM with normal programming cycle, the step of stress relaxation has the same results, decrease the force F_S (2.3%) and F_E (4.5%), and increase of the initial fixity d_F^I (25%). The rigidity K_2 close to K_{NA} is found to be the same as with normal programming cycle.

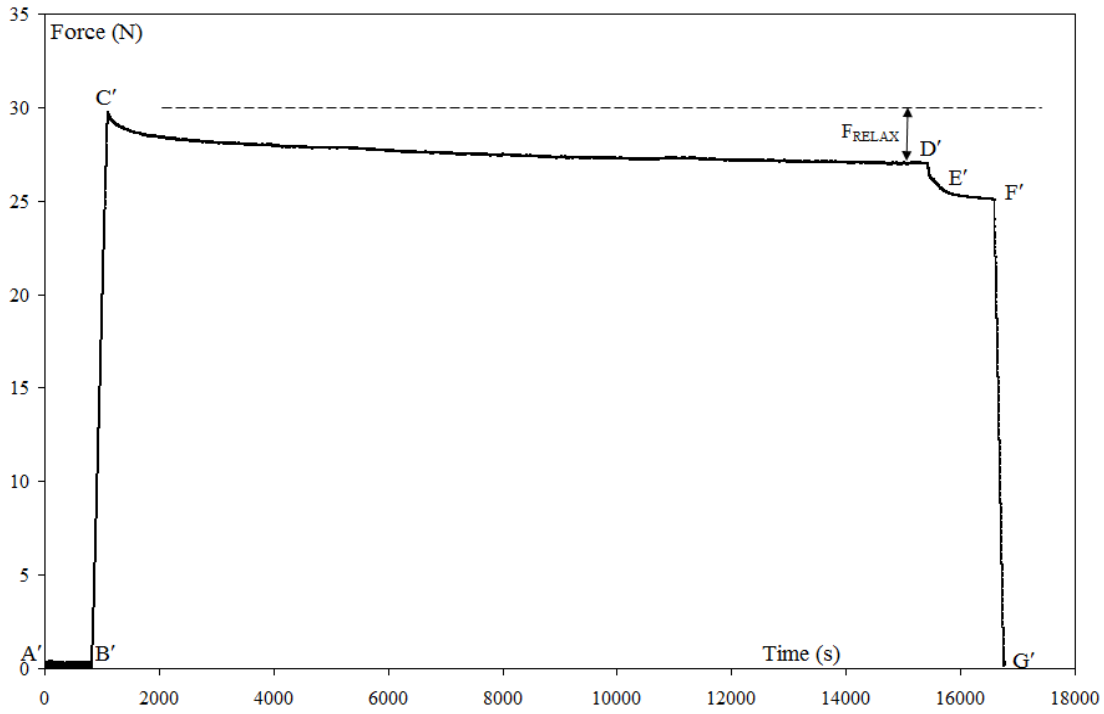

Figure IV.1.27. Force as a function of time during the SYM stress relaxation thermo-mechanical programming cycle

Characteristic values	SYM
d_A (mm)	−0.86±0.33
F_B (N)	1.01±0.21
K_A (N/mm)	1.06±0.18
F_T (N)	29.43±1.3
K_1 (N/mm)	1.03±0.1
F_{RELAX} (N)	2.23±0.45
F_S (N)	1.54±0.27
F_E (N)	24.6±0.75
d_F^I (mm)	10.8±0.35
K_2 (N/mm)	1.86±0.12
K_{NA} (N/mm)	1.8±0.13

Table IV.1.12. Characteristic values for SYM with stress relaxation programming

IV.1.3.4) SYM initial fixity stabilization

The SYM initial fixity function of time and at Ta is observed after the two different programming cycles, with and without the stress relaxation step (Figure IV.1.28). Unlike CBCM, the step of stress relaxation does not lead to a stabilization of the fixity. After 12 hours, the decrease in fixity is 21% without stress relaxation programming; however, the decrease in fixity is 16.3 % with stress relaxation programming. For SYM, a long-term stabilization of the plate may be possible but with a significant loss of d_F^I.

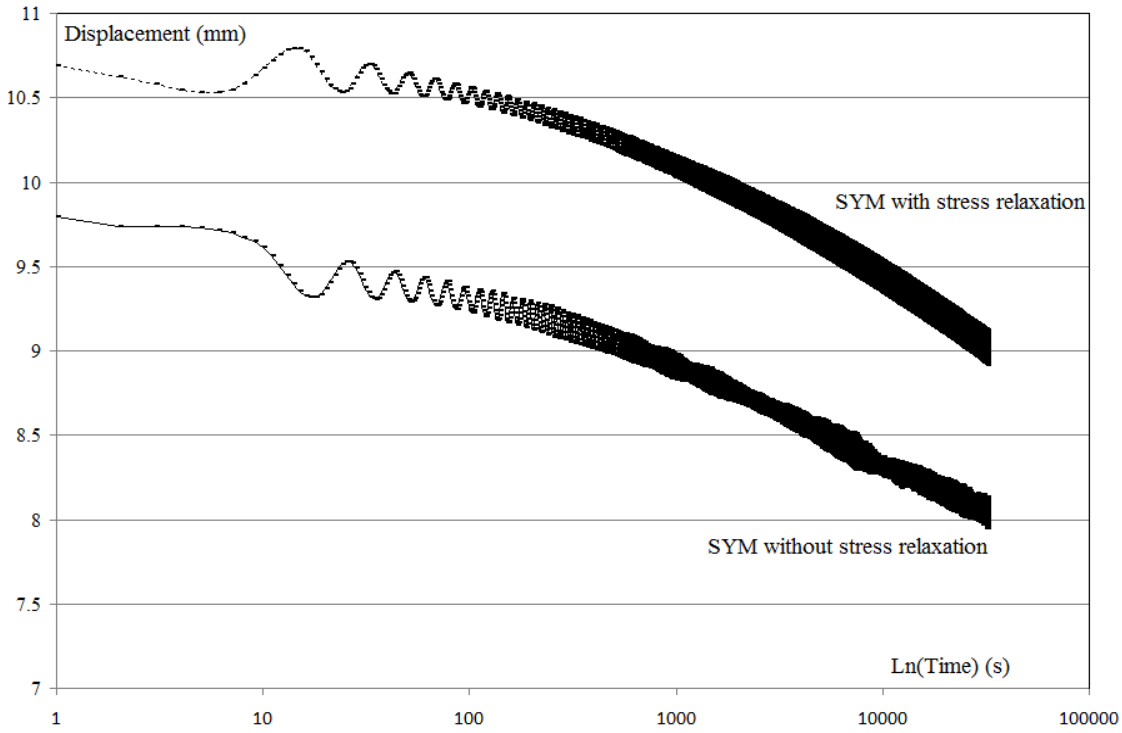

Figure IV.1.28. Visco-elastic effect for SYM

IV.1.4) Summary (CBCM and SYM)

From the macroscopic characterization, an explanation can be proposed but it is necessary to make a point on the main results (Table IV.1.13).

- For the two kinds of programming cycles, with and without stress relaxation step, SYM and CBCM plates have the same prescribed displacement d_S (active displacement d_A is counted in this prescribed displacement).

Characteristic values	CBCM	SYM	CBCM relax	SYM relax
F_T (N)	57.7±1.94	33.44±0.9	61.7±1.1	29.43±1.3
F_B (N)	31.48±1	1.1±0.12	33.2±0.8	1.01±0.21
F_{RELAX} (N)	–	–	11.9±0.42	2.23±0.45
F_S (N)	14.31±2.06	2.88±1.1	15.1±0.37	1.54±0.27
F_E (N)	11.91±1.62	29.46±1.3	1.5±0.24	24.6±0.75
d_A (mm)	−13.47±0.75	−0.93±0.3	−13.05±0.45	−0.86±0.33
d_F^I (mm)	9.18±0.63	8.64±0.2	11.49±0.48	10.8±0.35

Table IV.1.13. Main values of the macroscopic characterization

- For CBCM and SYM, the corresponding d_F^I are comparable, ratio of 1.06 from average values, the same for the two kinds of cycles.

- Compared to SYM, the total force F_T corresponding to d_S is higher for the CBCM, ratio of 2.09 and 1.72 for the programming cycle, with and without the step of stress relaxation respectively. This difference is due to the CBCM-effect and the value of the blocking force F_B.

- At the deforming temperature T_D=150°C, and compared to the SYM, the CBCM is more affected by the stress relaxation effect; F_{RELAX} is higher for the CBCM with the ratio of 5.3.

- During cooling, similar to F_B during heating, a difference between CBCM and SYM is obtained for the stabilization force F_S; ratio of 9.8 and 4.96 during the programming cycles, with and without the step of stress relaxation respectively.

- The elastic force F_E highlights the main difference of behavior between CBCM and SYM plates. For the two plates, the step of stress relaxation induces a decrease of F_E but differently; ratio of 0.83 for SYM and 0.12 for CBCM. For the CBCM with stress relaxation step, the value of F_E is equal to 2.4% of F_T. For SYM, the corresponding value is equal to 83.5% of F_T.

The step of the loading at F_T with T_D=150°C, leads to a deformation of the structure but also to a new configuration of the polymer network. This configuration is linking to the polymer mobility in the composite structure under F_T and consequently to the interaction between the polymer and the reinforcement.

The stress relaxation step at T_D leads to a reorganization of this loaded configuration. This reorganization is linked to the value of F_T and to the polymer/reinforcement interaction.

During cooling F_B disappears and F_S appears. Like F_B, this stabilization force is characteristic of the asymmetry of the composite and can be comparable to dilation effects due to the polymer reorganization during the cooling. For CBCM and SYM and for the two kinds of programming cycles, the values of F_S are the same respectively (if the standard deviations are taken in account). So, the stress relaxation step does not affect the value of F_S. F_E is the result of the equilibrium of the whole structure during the unloading step, equilibrium between the deformation energy of the reinforcement and the polymer which has a configuration different to the initial one after the cooling.

It has been already explained (in section IV.1.3.2.2) that the polymer may be considered as a lock which maintained the reinforcement in position and gives the fixity shape characterized by d_F^I. It appears that the maintaining of this initial fixity is linked to the value of F_E compared to F_T. This ratio may define the limit between the reversible strain and the existence of an irreversible strain in the constrained composite. This irreversible strain is linked to the ability of the polymer to maintain d_F^I under the forces induced by the elastic return of the reinforcements.

IV.1.5) Different asymmetric composite plates

The precedent results have shown the influence of the coupling between the matrix and the reinforcement on the actuation and shape memory properties of the thermally active plates. In this part, the influence of position and orientation of the unidirectional glass layers on different properties are studied. Figure IV.1.29 shows the organization of different composite plates.

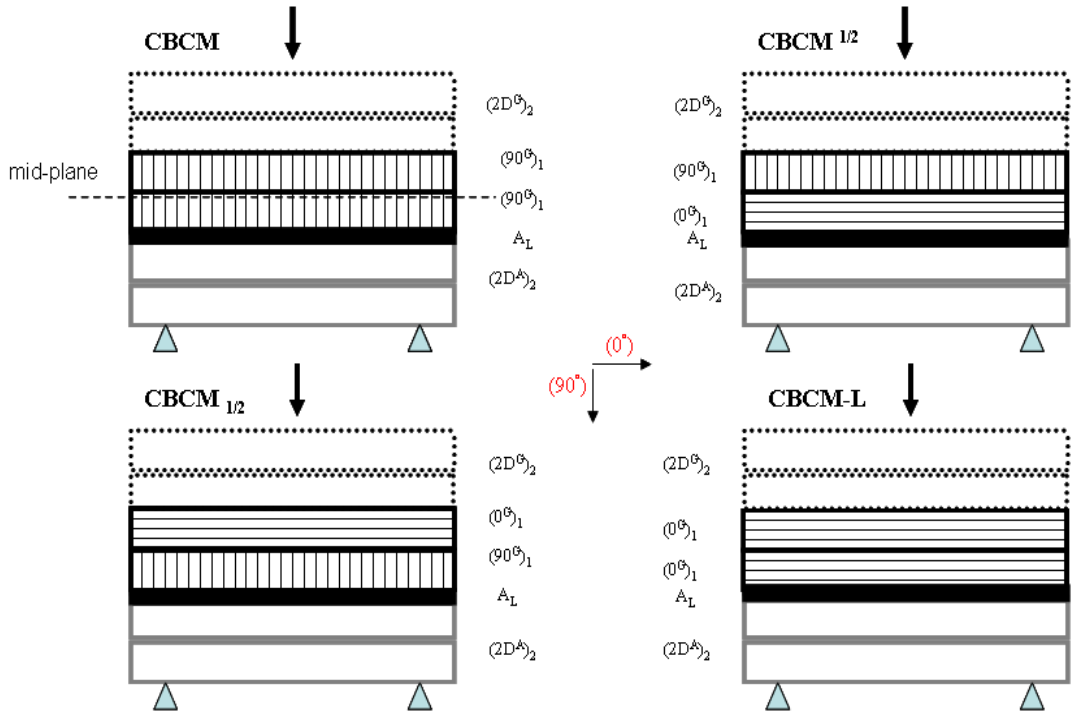

Figure IV.1.29. CBCM organization, longitudinal direction of the plate (0°) and transversal direction (90°). Layer thickness $2D^A$=0.5mm, A_L=0.1mm, $0^G/90^G$=0.7mm and $2D^G$=0.25mm

IV.1.5.1) Normal programming cycle

Normal programming cycles as explained in previous sections are performed for different composites. All the characteristic values for different composites are given in Table IV.1.14 and the curves of programming cycles for different composite plates are given in Appendix D.

CBCM that has already been tested and compared with CBCM-L at a temperature less than Tg [101] in which CBCM gives high actuation properties in terms of free displacement (d_A) and blocking force (F_B). In the previous results, CBCM at a deforming temperature T_D (i.e. 150°C), the results have been verified at a temperature higher than Tg. However, the maximum value of F_B is obtained for $CBCM^{1/2}$ (Table IV.1.14). This result may be explained by two effects: the thermal activation and the loss of mechanical properties of the matrix because of the heat and more particularly for T_D=150°C. These effects can be different depending on the reinforcement organization in the structure and particularly the orientation of the glass unidirectional layer.

Characteristic values	Composite plates			
	CBCM	$CBCM^{1/2}$	$CBCM_{1/2}$	CBCM-L
d_A (mm)	−13.47±0.75	−11.64±0.27	−9.57±0.57	−6.81±0.35
F_B (N)	31.48±1	34.90±0.14	27.57±0.6	23.5±0.61
K_A (N/mm)	2.33±0.1	2.99±0.06	2.88±0.15	3.4±0.12
F_T (N)	57.70±1.94	66.61±1.06	69.37±0.81	74.80±0.86
K_1 (N/mm)	2.2±0.24	2.25±0.08	2.45±0.1	2.67±0.05
F_S (N)	14.31±2.06	9.86±0.49	6.87±0.8	5.92±0.5
F_E (N)	11.91±1.62	21.85±0.81	34.93±0.67	45.38±0.75
d_F^I (mm)	9.18±0.63	8.25±0.42	7.08±0.48	6.42±0.54
K_2 (N/mm)	4.24±0.39	3.79±0.13	3.7±0.1	3.6±0.18
K_{NA} (N/mm)	3.34±0.36	3.6±0.37	3.76±0.1	4.1±0.13

Table IV.1.14. Characteristic values of different composites during their programming cycles

For the unidirectional glass layer along the transversal direction, the greater properties of dilation are along the longitudinal direction, but in this direction, the loss of rigidity of the matrix is also high. The competition between these two effects explains the greater value of F_B for $CBCM^{1/2}$, as for the combination of these two unidirectional layers, the bottom layer at 0° decreases the loss of rigidity while maintaining good properties of dilatations for the two layers. For the two other composites ($CBCM_{1/2}$ and CBCM-L), the two unidirectional layers give lesser values of d_A and F_B due to a greater rigidity K_1 at T_D and K_{NA} at Ta.

For a given temperature, the asymmetry of the composite may be defined by the plate curvature and the value of the corresponding displacement d_A. Thus, CBCM and CBCM-L appear to be the most and the least asymmetrical composites respectively. For the different composites, the evolution of F_S is in accordance with the evolution of d_A. This result confirms that F_S is induced by the composite asymmetry and can be used to characterize the level of the asymmetry. Due to the lower value of F_E (elastic force responsible for the spring-back of the composite) and despite the lower value of the total force F_T, the maximum value of F_T minus F_E is obtained for the CBCM. The direct consequence of this result is given by the value of d_F^I, CBCM has the maximum value of the initial fixity displacement d_F^I.

The variation of the rigidity K_2 defined by d_F^I and F_E versus the asymmetry is in accordance with d_F^I and F_S, K_2 is more for more asymmetry. K_2 reflects the level of internal stress in the composite after the programming cycle. So during recovery, the maximum recovery properties (d_R and F_R) will be given by the CBCM.

IV.1.5.2) Recoveries

IV.1.5.2.1) Unconstrained recovery

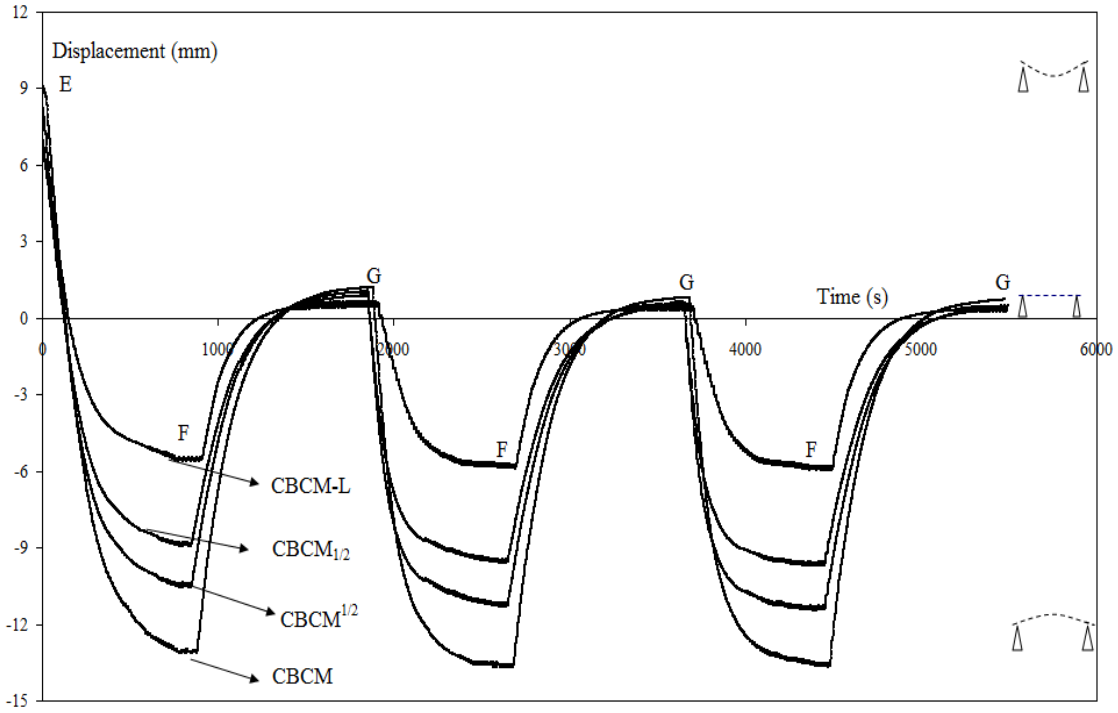

Figure IV.1.30. Unconstrained recovery for different CBCM; E= Initial fixities; EF, GF = Heating to T_D (i.e. = 150°C; FG = Cooling to Ta (i.e. = 22°C); d_F^I for CBCM, CBCM$^{1/2}$, CBCM$_{1/2}$, and CBCM-L are 9.18±0.63 mm, 8.25±0.42 mm, 7.08±0 .48 mm and 6.42±0.54 respectively

The representative curves of unconstrained recoveries for different composites are shown in Figure IV.1.30 and the values are given in Table IV.1.15. During 1st recovery heating, the d_{RT} for CBCM, CBCM$^{1/2}$, CBCM$_{1/2}$, and CBCM-L are 21.84±1.26 mm, 18.54±0.12 mm, 16.14±0.12 mm and 12.36±0.39 mm respectively. The values of d_R for CBCM, CBCM$^{1/2}$, CBCM$_{1/2}$, and CBCM-L are 8.37±0.51 mm, 6.9±0.15 mm, 6.7±0.45 mm and 5.55±0.15 mm

respectively. After 1st cooling, the fixity positions of the plates are close to the initial position (before the programming cycle) and the residual displacements (d_{RF}) for CBCM, $CBCM^{1/2}$, $CBCM_{1/2}$, and CBCM-L are equal to 1.02 ± 0.3 mm (11 % of d_F^I), 0.96 ± 0.24 mm (11 % of d_F^I), 0.81 ± 0.18 mm (11 % of d_F^I) and 0.6 ± 0.15 mm (9 % of d_F^I) respectively.

So, after one-step unconstrained recovery cycle, the plates are largely deprogrammed. For the other two recovery cycles, d_{RF} decreases that demonstrates that the composites are successively more deprogrammed. Also, they show only the activation due to their asymmetries as SMEs disappear after the 1st recovery cycle. The unconstrained recoveries for the composite plates also demonstrate that CBCM has highest displacement recovery as it gives highest free displacement and the initial fixity. The d_{RT} and the d_{RF} is more for the plate having more asymmetry. Also the rigidities of the plates (K_1, K_{NA}) have a direct effect on the residual displacements after recovery. More the rigidity less will be the residual displacement that demonstrates that high rigidity makes the composite plate to return close to its initial position after cooling.

Composite plates	Deformations (%)	Recovery cycles		
		1	2	3
CBCM	ε_{RA}	−4.21±0.29	−4.31±0.26	−4.32±0.22
	ε_{RF}	0.34±0.1	0.26±0.13	0.22±0.15
$CBCM^{1/2}$	ε_{RA}	−3.43±0.1	−3.67±0.15	−3.74±0.07
	ε_{RF}	0.32±0.08	0.25±0.07	0.21±0.05
$CBCM_{1/2}$	ε_{RA}	−3.02±0.12	−3.04±0.07	−3.07±0.04
	ε_{RF}	0.27±0.06	0.22±0.04	0.17±0.05
CBCM-L	ε_{RA}	−1.98±0.07	−2.03±0.06	−2.09±0.04
	ε_{RF}	0.20±0.05	0.16±0.05	0.11±0.04

Table IV.1.15.Unconstrained recoveries of the composites; d_F^I for CBCM, $CBCM^{1/2}$, $CBCM_{1/2}$, and CBCM-L are 9.21±0.63 mm, 8.25±0.42 mm, 7.08±0.4 8 mm and 6.42±0.54 respectively

IV.1.5.2.2) Constrained recovery

The representative curves of constrained recoveries for different composites are given in Figure IV.1.31. F_{RT} is the sum of F_B and F_R and due to F_B, the maximum value is given by the

CBCM$^{1/2}$. However, like the recovery displacement d_R, the recovered force F_R is maximum for

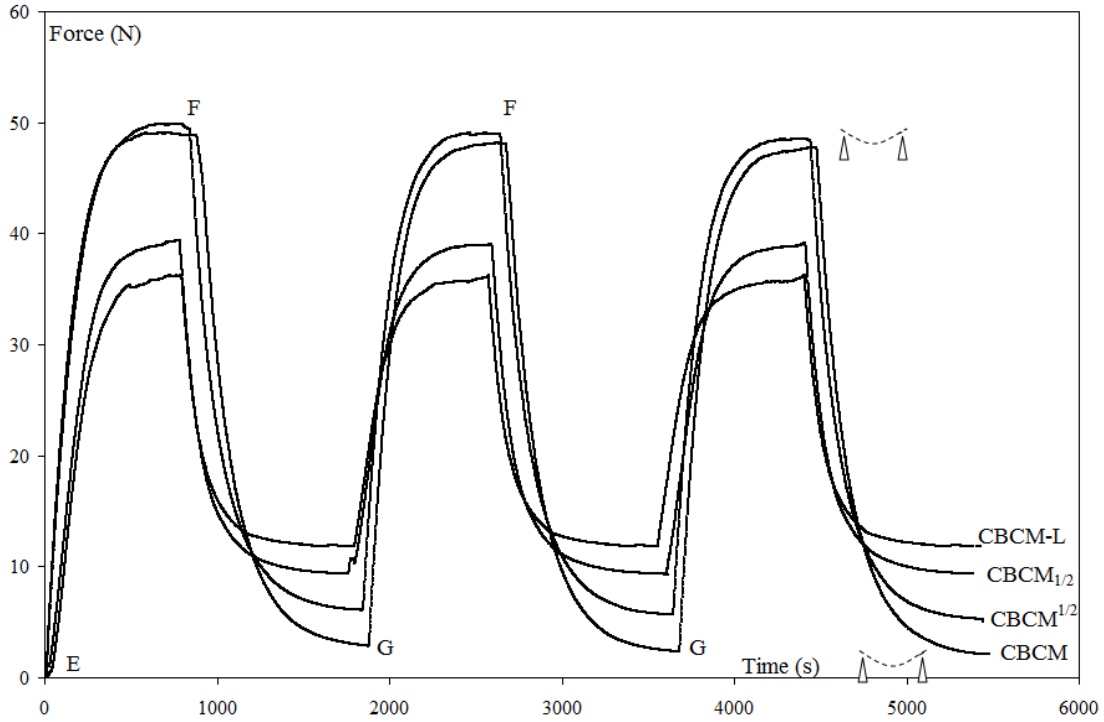

Figure IV.1.31. Constrained recovery (F_{RT}) for different CBCM composite; E= Initial fixities; EF, GF = Heating to T_D (i.e. = 150°C; FG = Cooling to Ta (i.e. = 22°C); d_F^I for CBCM, CBCM$^{1/2}$, CBCM$_{1/2}$, and CBCM-L are 9.12±0.3 mm, 8.25±0.42 mm, 7.08±0. 48 mm and 6.42±0.54 respectively

CBCM. The values of F_R for CBCM, CBCM$^{1/2}$, CBCM$_{1/2}$, and CBCM-L are 17.06±0.57 N, 14.4±0.54 N, 12.1±0.2 N and 11.88±0.2 N respectively. The variation of F_R is in accordance with the variation of d_F^I, F_S and K_2. After the cooling of the first recovery, a residual force F_{RES} remains. More the plate is rigid (K_1, K_{NA}), more is F_{RES}. Along the successive recovery cycles, the maximum value of δF (Table IV.1.16) which characterize the strength of the actuation is obtained for CBCM.

In section IV.1.3.2.2, for the SYM plates compared to CBCM ones, a hypothesis was proposed to explain the existence of F_{RES}. During the recovery heating of the constrained recovery, the level of the stress field and the reinforcement-polymer interaction affect the property of the

polymer rearrangement and modify the equilibrium between the deformation energy of the reinforcement and the polymer.

Composite plates	**Force (N)**	**Recovery cycles**		
		1	2	3
CBCM	F_{RT}	48.54±1.57	47.77±1.37	47.44±1.33
	F_{RES}	3.03±0.96	2.51±0.87	2.23±0.94
	$\delta F = F_{RT} - F_{RES}$	45.51±0.61	45.26±0.5	45.21±0.39
$CBCM^{1/2}$	F_{RT}	49.30±0.93	48.71±0.84	48.30±0.7
	F_{RES}	6.01±0.5	5.57±0.3	5.16±0.45
	$\delta F = F_{RT} - F_{RES}$	43.29±0.43	43.14±0.65	43.14±0.25
$CBCM_{1/2}$	F_{RT}	39.70±0.8	39.37±0.9	39.13±0.95
	F_{RES}	9.31±0.57	8.83±0.52	8.73±0.61
	$\delta F = F_{RT} - F_{RES}$	30.39±0.23	30.54±0.38	30.4±0.34
CBCM-L	F_{RT}	35.43±0.81	34.98±0.97	34.60±0.48
	F_{RES}	12.87±0.64	12.47±0.45	12.23±0.77
	$\delta F = F_{RT} - F_{RES}$	22.56±0.17	22.51±0.52	22.37±0.29

Table IV.1.16. Forces produced during constrained recoveries of different composites

This hypothesis is confirmed by the values of F_{RES} obtained for the different asymmetrical composites. During the recovery heating to T_R = 150°C and cooling to Ta, the plate remains fixed and immoveable. So, F_{RES} is linked to the ability of the polymer (at T_R) to reorganize and return to its initial configuration (before the programming cycle).

- If the polymer can rearrange and recovers to its initial configuration, the equilibrium between the deformation energy of the reinforcement and the polymer is largely modified, the value of F_{RES} is high, and δF will be low (close to zero).
- If the polymer cannot rearrange to its initial configuration, the equilibrium between the deformation energy of the reinforcement and the polymer change to a smaller extent. So, the polymer again acts as a lock and thus will maintain the reinforcement position. Hence, F_{RES} is low and δF will be high.

The polymer rearrangement is linked to the level of stress in the polymer, and consequently to the stress transfer between fiber and matrix in the layers and at the interfaces. For the unidirectional layers of CBCM, the flexural stress is distributed mainly on the polymer, thus,

limiting its ability to reorganize. For the other composites, more is the rigidity (K_1, K_{NA}), more the flexural stress will be supported by the fibers, and more the polymer can rearrange during the recovery heating in the composite structure. Thus, the equilibrium between polymer and reinforcement is modified, the plate is partially deprogrammed and the strength of the actuation is less.

IV.1.5.2.3) Characteristic straight lines and theoretical work

The different characteristic straight lines (Figure IV.1.32, Figure IV.1.33, Figure IV.1.34) summarize the overall results for the different composites. These curves highlight the high actuation performances of CBCM especially the greatest properties of recovery properties due to SME of the matrix.

In Figure IV.1.34, the rigidity K_R of SYM uniquely for SME is least as SYM has least F_R. So, comparing to SYM, the different asymmetric composites give high actuation properties. Hence, it can be concluded that the asymmetry of the composite has an influence on the actuation property induced by the SME.

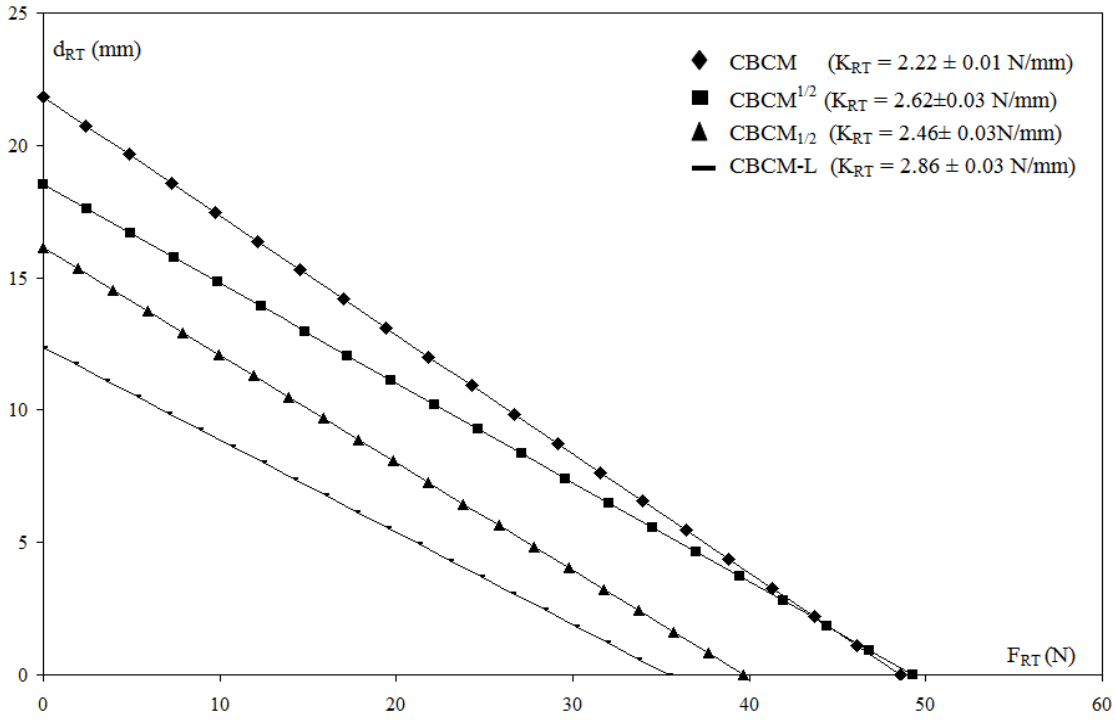

Figure IV.1.32. Corresponding characteristic straight lines of d_{RT} and F_{RT} for different composites

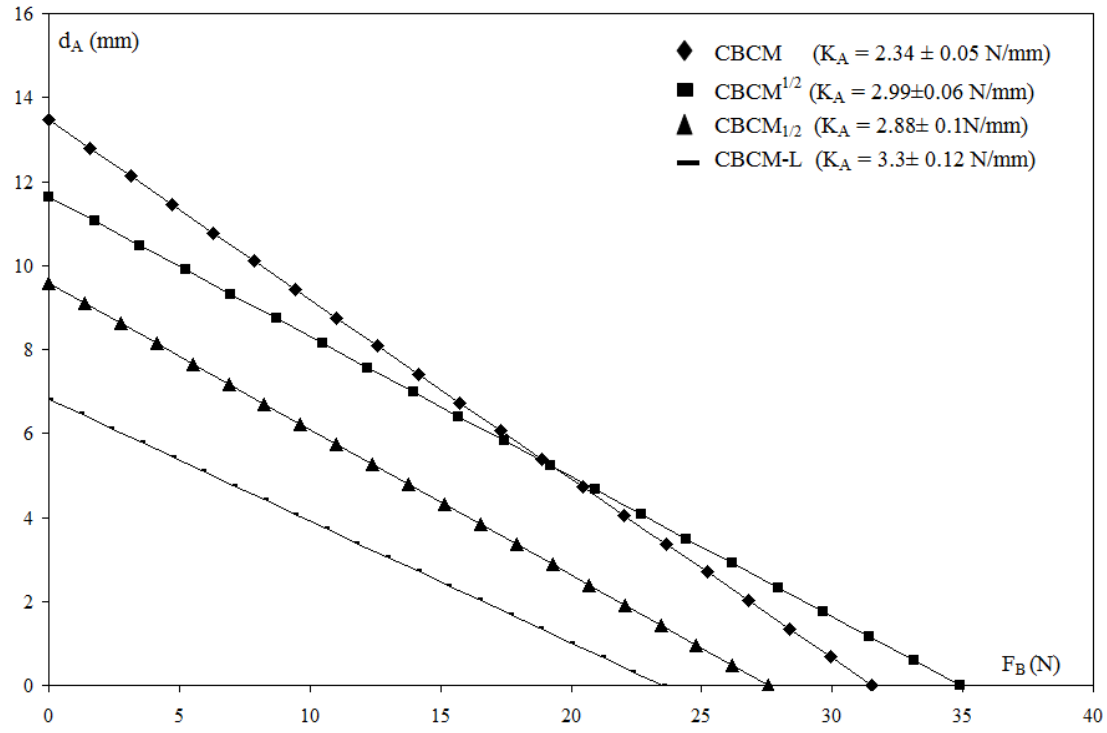

Figure IV.1.33. Corresponding characteristic straight lines of d_A and F_B for different composites

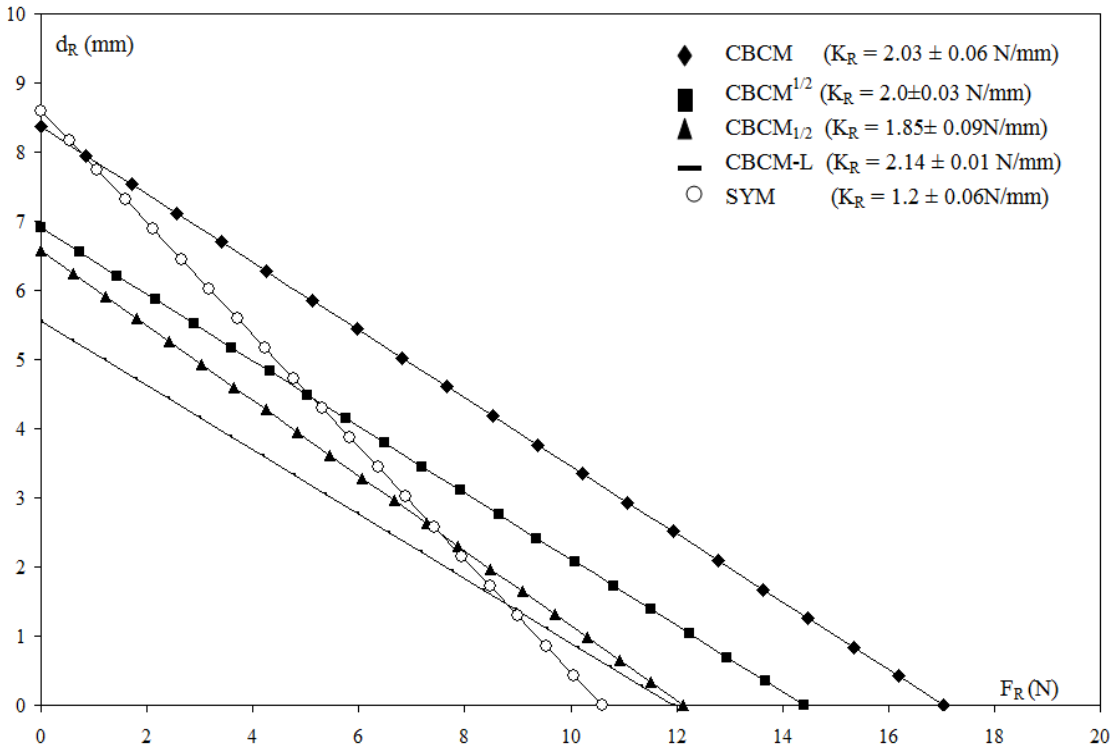

Figure IV.1.34. Corresponding characteristic straight lines of d_R and F_R for different composites

For the SME, the maximum work calculated by F_R and d_R for CBCM, $CBCM^{1/2}$, $CBCM_{1/2}$, CBCM-L and SYM are 0.035 J, 0.0248 J, 0.02 J, 0.016 J and 0.02 J respectively. It can be observed that the work induced by SME is the least for CBCM-L; however, for SYM and $CBCM_{1/2}$, it is equal. This shows that for the SME, the rigidity K_{NA} can limit these effects.

Composite plates	Theoretical W_G^{max} (J)
CBCM	0.265
$CBCM^{1/2}$	0.228
$CBCM_{1/2}$	0.16
CBCM-L	0.1
SYM	0.02

Table IV.1.17. Theoretical maximum work obtained from F_{RT} and d_{RT} for different composites

However, if the maximum work (Table IV.1.17 and Figure IV.1.35) given by d_{RT} and F_{RT} is observed, it is found that it is maximum for CBCM and minimum for SYM as CBCM has highest CBCM-effect and SYM has no CBCM-effect.

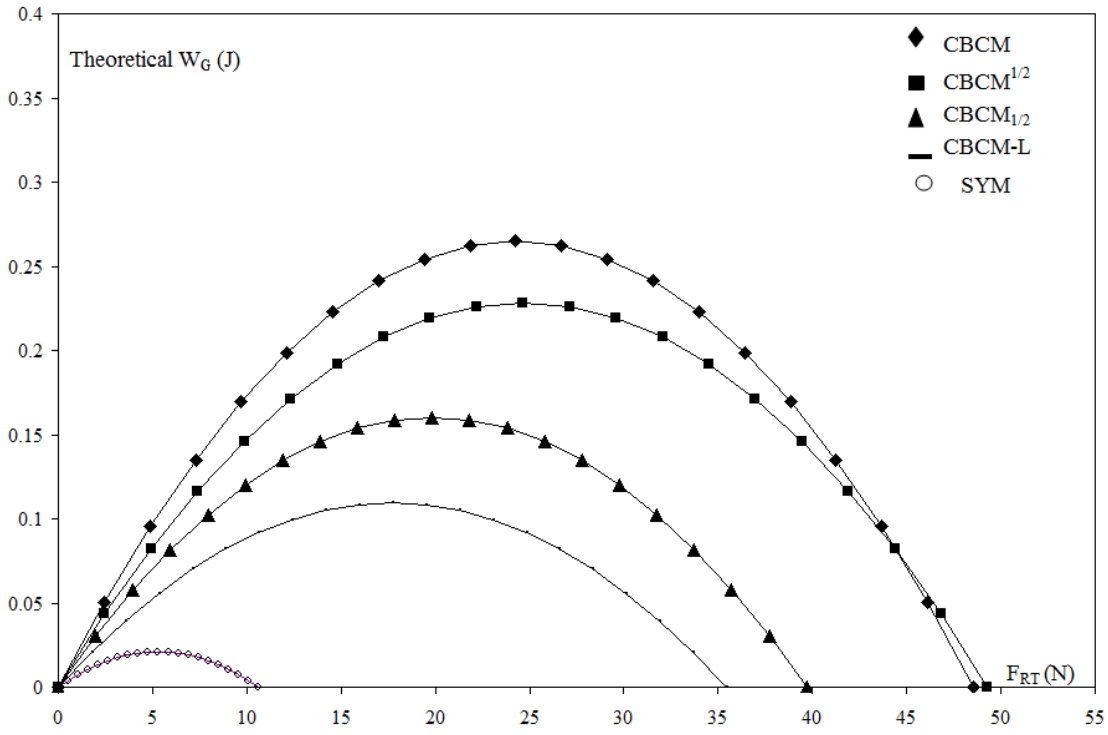

Figure IV.1.35. Theoretical work for different composites

IV.1.6) Conclusion

At recovery heating, during the unconstrained recovery of CBCM with normal programming cycle, it is found that a large activated displacement is obtained. This displacement is the

combination of two displacements: a displacement obtained due to the SME and the displacement obtained due to CBCM-effect. During this recovery displacement, it is observed that CBCM recovers to its original position (initial position before the start of the test) at 90°C (a temperature lower than the deforming temperature T_D). This is not the case with SYM (without CBCM-effect) as it recovers to its original position at a temperature equal to T_D. Full recovery at a temperature lower than T_D is not possible for SYM. Moreover, SYM has less overall activated displacement during unconstrained recovery as the recovery displacement produced is only due to the SME. At recovery cooling, both CBCM and SYM come to their initial positions which show that these are largely deprogrammed at heating during unconstrained recovery.

At recovery heating, during constrained recovery, CBCM produces a total recovery force that is also the combination of the two forces: a force produced due to the CBCM-effect whereas the other force is produced due to the SME. However, for SYM, less force (as compared to CBCM) is produced as this is a force produced only due to the SME. During cooling, a residual force is obtained both for CBCM and SYM; however, for SYM, it is more than CBCM. Furthermore, it is observed that during successive recovery cycles, the different forces (total recovery force produced during heating and residual force during cooling) are stabilized.

During recovery under load, it is observed that CBCM has the ability to recover close to its original position even under a load equal to its F_B. Also, recovery under load gives direct measure of the recovered work of CBCM during the recovery as CBCM-effect is compensated by the load. Moreover, CBCM can recover beyond its original position at loads less than its F_B. However, SYM cannot recover to its original position under any load.

The stress relaxation during the programming cycle does not affect the overall performance of the composite; however, it increases its initial fixity. Also, the initial fixity is more stabilized with the step of stress relaxation than with the normal programming cycle.

During the study of the effect of change in position and orientation of unidirectional glass layers in the composite, it is observed that the change in position and orientation of unidirectional glass layers changes the asymmetry of the composite. This change in asymmetry actually affects

all the characteristic parameters of the composite. It changes not only the free displacement and blocking force but also changes the shape memory properties of the composite. The initial fixity is degraded as the rigidity increases with the change of position and orientation of unidirectional glass layers in the composite. As a result, the recovered work is also affected. It is found that the composite having more asymmetry gives higher actuation properties than other composites.

IV.2) Multi-step recovery

In multi-step recovery (Figure IV.2.1), the programmed CBCM recovers from its initial fixity (A‴) to its original position (A) in a number of steps. In multi-step recovery, during the 1st step , if CBCM is heated at a recovery temperature that is much less than $T_{D,}$ then, it will activate to B″. On cooling, CBCM will come back to the initial fixity and will get a position (A″) different from the initial fixity. Similarly, if CBCM is heated to another temperature that is less than T_D, CBCM will be activated to another position (B′). On cooling, CBCM will also come back to initial fixity; however, it will get another position (A′) that will be different from the initial fixity (A‴) and 1st position (A″). This different position is due to a part of recovery during the heating at this temperature. Now, if CBCM is heated to a temperature T_D equal to 150°C, CBCM will get a new activated position (B) different from the previous activated positions. On cooling, CBCM will return to original position (A) and then CBCM can perform cycling activation and deactivation showing that the initial fixity induced due to the programming is disappeared from CBCM due to the recovery heating. Therefore, in multi-step recovery, contrary to one-step recovery, the initial fixity can be recovered in a number of steps by having different activated and deactivated positions.

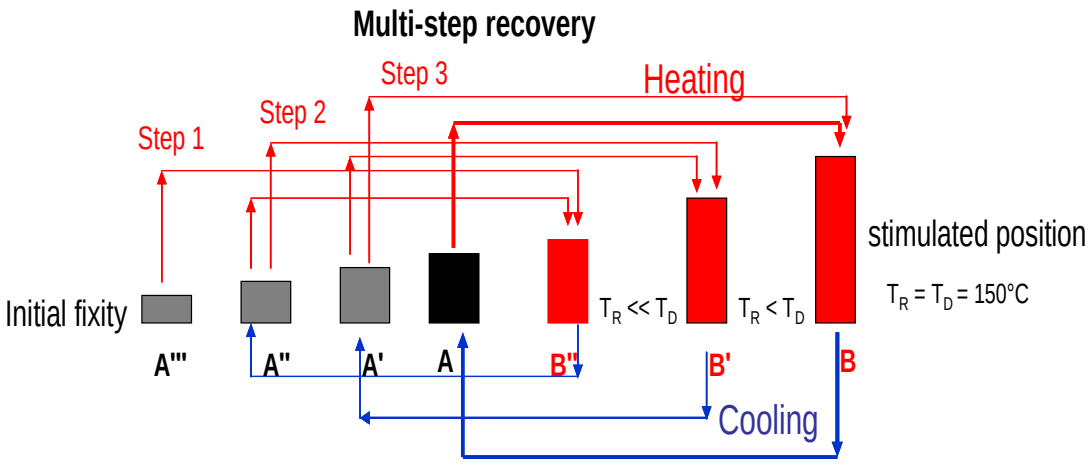

Figure IV.2.1. A model for multi-step recovery of CBCM

IV.2.1) Introduction

In this section, mainly, the multi-step unconstrained and constrained recoveries for CBCM and SYM are demonstrated. For each composite plate used, three successive tests (one after the other) for each recovery have been conducted on the same plate. In unconstrained recovery test, multi-step unconstrained recoveries are explained. It is further explained that the recovery displacement during multi-step recovery is fully controllable with T_R. The stabilization of recovery displacement with the provision of same T_R for multiple cycles is also explained. The constrained recovery test gives the measure of the generation of recovery forces at different T_R.

IV.2.2) Normal programming cycles

IV.2.2.1) CBCM programming cycle

Figure.IV.2.2 shows the programming cycle for CBCM. It is the same type of programming cycle without the stress relaxation step as explained in the previous sections. Table IV.2.1 gives the characteristic values for CBCM programming cycle.

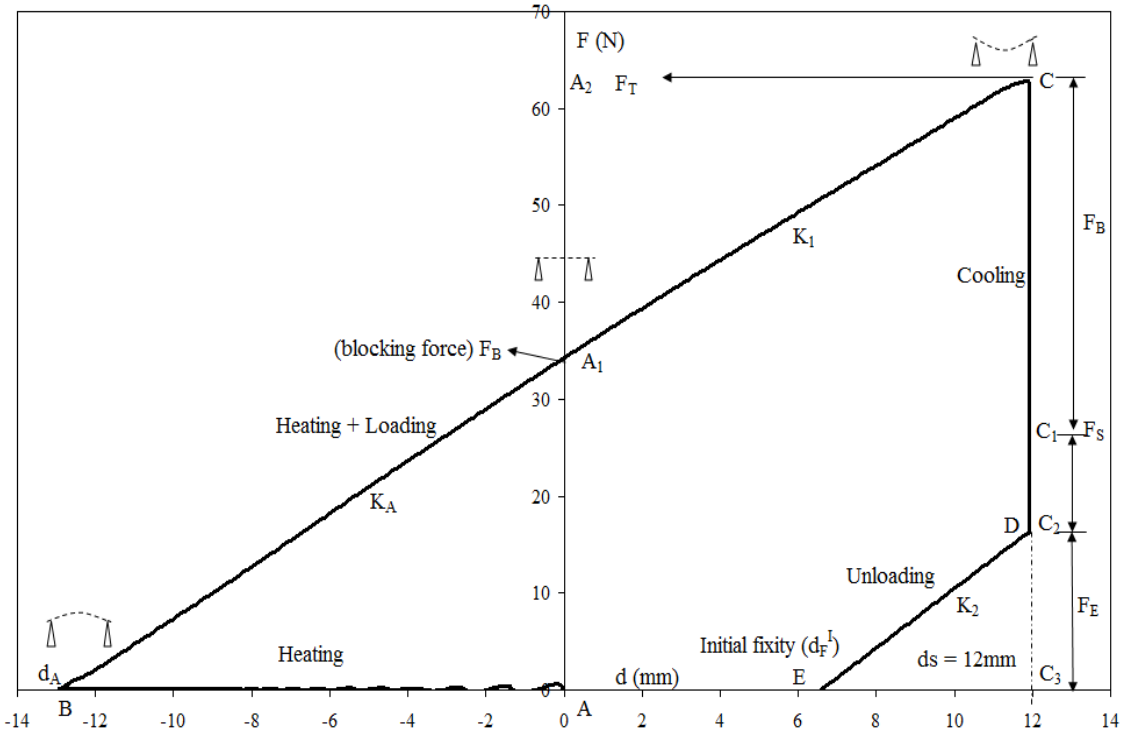

Figure IV.2.2. CBCM fixing or programming cycle

Characteristic values	CBCM
d_A (mm)	−12.87±0.45
F_B (N)	36.5±2.6
K_A (N/mm)	2.83±0.1
F_T (N)	63.2±3.97
K_1 (N/mm)	2.2±0.13
F_S (N)	11.1±1.1
F_E (N)	15.6±2.8
d_F^I (mm)	6.9±0.48
K_2 (N/mm)	3.05±0.12
K_{NA} (N/mm)	3.7±0.06

Table IV.2.1. Characteristic values of CBCM programming cycle

It is to be noted here that the successive tests (3 tests for each recovery) have been performed successively one after the other (programming + recovery) on the same composite plate. The composite plate is not allowed to relax during the successive testing.

IV.2.2.2) SYM programming cycle

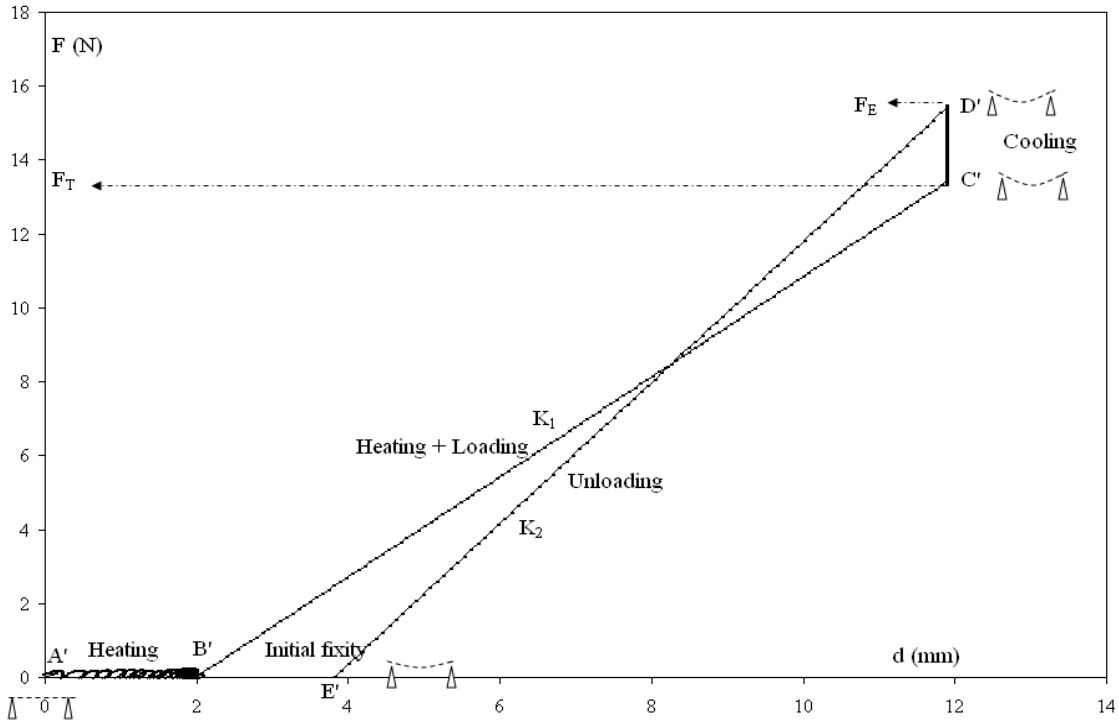

Figure IV.2.3. 2nd SYM programming cycle

The programming cycle for SYM is shown in Figure IV.2.3. Due to gradient property which appears during the manufacturing process, the activation property (AB) can be observed at a temperature equal to 150°C. Here, the direction of activation is downward (taken as positive) contrary to the previous activation of SYM. This type of activation is observed if SYM is placed on three point bending test as obtained from the manufacturing process. As direction of d_A is downward so F_B and K_A do not exist. SYM is deformed to d_S = 12 mm comparable to CBCM as the initial position is taken as the reference point for ds both for SYM and CBCM. In reality, SYM is deformed (BC) less than CBCM (when initial position is taken as a reference point). During the cooling step (CD), an increase in force is observed as the activation for SYM disappears. After cooling, a step of unloading (DE) is performed that gives an initial fixity (d_F^I) at point E. In this programming cycle, as the overall deformation is lesser than the previous SYM programming, so, it gives less d_F^I. All the characteristic values for this type of SYM programming are given in Table IV.2.2.

Characteristic values	**SYM**
d_A (mm)	1.89±0.45
F_B (N)	–
K_A (N/mm)	–
F_T (N)	14.15±0.2
K_1 (N/mm)	1.4±0.02
F_S (N)	–
F_E (N)	15.9±0.48
d_F^I (mm)	3.81±0.33
K_2 (N/mm)	1.93±0.03
K_{NA} (N/mm)	1.8±0.14

Table IV.2.2. Characteristic values of SYM programming cycle

IV.2.3) Multi-step recoveries

IV.2.3.1) Multi-step unconstrained recovery

Figure IV.2.4 shows the multi-step recovery for CBCM and SYM [120] at different recovery temperatures (T_R). For CBCM, during multi-step recovery, the value of d_F^I = 7.29±0.9 mm with associated ε_F^I= 2.43±0.3 %. During multi-step recovery, in contrast to one-step recovery, d_F^I or ε_F^I can be recovered in more than one step by providing different T_R less than

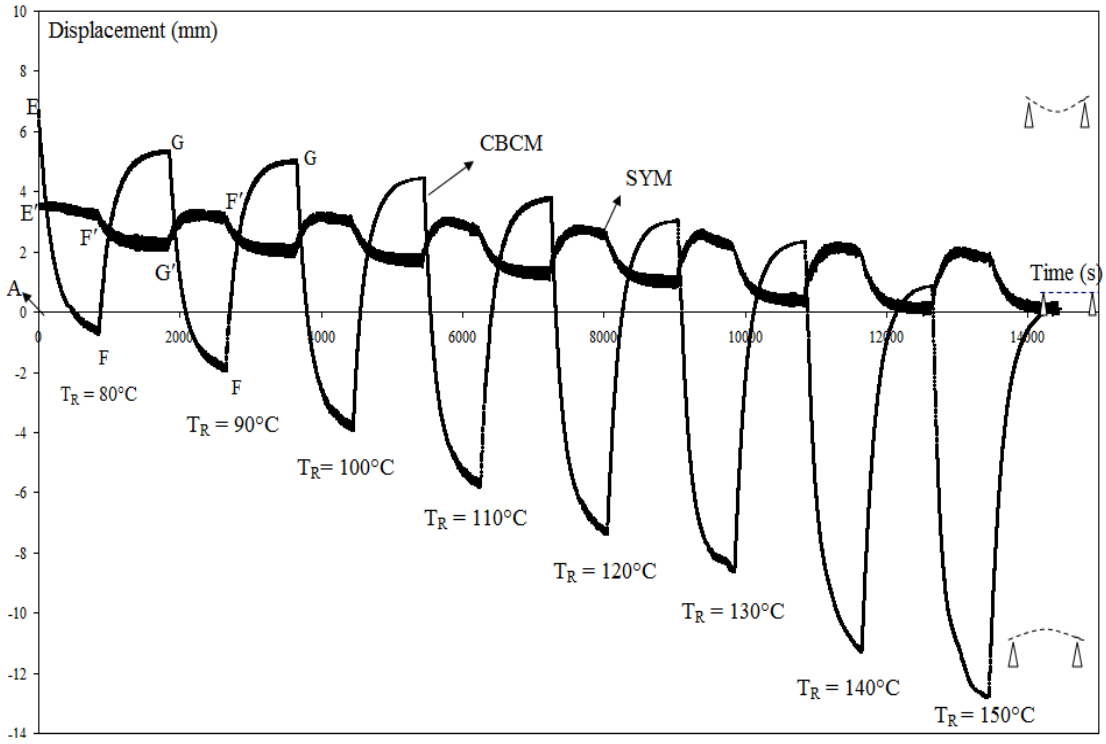

Figure IV.2.4. Multi-SME of CBCM and SYM; A = Initial position before the start of test; For CBCM {AE = d_F^I; EF, GF = Heating during recovery; FG = Cooling during recovery; AF = d_{RA}; AG = d_{RF}}, For SYM {AE′= d_F^I; E′F′, G′F′= Heating during recovery; F′G′= Cooling during recovery; AF′= d_{RA} for SYM; AG′= d_{RF}}

T_D. For the first recovery temperature (at T_R=80°C), CBCM recovers (EF) to its original position and tends to become flat due to the CBCM-effect whereas upon cooling (FG) it returns back close to its initial fixity due to the SME of the composite but to a lesser fixity deformation (ε_{RF} = 1.99 %) than the initial fixity ε_F^I. This loss in fixity deformation is due to the heating at T_R of 80°C where a part (0.44 % of ε_F^I) of the initial fixity deformation is restored (Table IV.2.3) at

cooling. This shows that, a deformation of 0.44 % is recovered during the first recovery step. This phenomenon continues till T_R of 150°C at which CBCM recover completely. Similarly, for SYM, the initial fixity deformation (1.26 ± 0.11 %) can be recovered in many steps by providing T_R from 80°C to 150°C. The different values corresponding to the different T_R are given in the Table IV.2.4. At cooling associated to T_R=80°C, SYM recovers to fixity deformation 0.82 % which is also lesser than ε_F^I (1.26 %). Therefore, the composite plates get certain ε_{RF} (fixities at cooling) and ε_{RA} (activations during heating) for each T_R whereas ε_{RF} decreases and ε_{RA} increases as the T_R increases. For CBCM, the curvature of the composite plate changes for ε_{RF} and ε_{RA} during each T_R thus showing the 2W-SME (Figure IV.2.4); however, SYM cannot change its curvature during its multi-step recovery and always remains lower in reference to initial position during recovery heating and cooling. Furthermore, the total recovered deformation (ε_{RT}) is calculated for both CBCM and SYM by taking the difference of initial fixity deformations (ε_F^I) and ε_{RA} for each T_R (see Table IV.2.3 and Table IV.2.4). It can be observed that CBCM shows higher activations than SYM during the multi-step recovery at

Deformations (%)	**T_R (°C)**							
	80	90	100	110	120	130	140	150
ε_{RA}	0.03±0.33	−0.39±0.36	−0.95±0.39	−1.60±0.4	−2.15±0.3	−2.72±0.32	−3.49±0.24	−4.06±0.23
ε_{RF}	1.99±0.31	1.89±0.33	1.73±0.34	1.48±0.33	1.23±0.28	0.92±0.92	0.51±0.51	0.25±0.26
$\varepsilon_{RT} = \varepsilon_F^I - \varepsilon_{RA}$	2.40±0.63	2.82±0.66	3.38±0.69	4.03±0.7	4.58±0.6	5.15±0.62	5.92±0.54	6.49±0.54
ε_A	−2.14±0.15	−2.41±0.21	−2.82±0.27	−3.2±0.11	−3.47±0.15	−3.71±0.11	−3.99±0.12	−4.31±0.08
$\varepsilon_R = \varepsilon_{RT} - \lvert\varepsilon_A\rvert$	0.26±0.48	0.41±0.45	0.56±0.42	0.83±0.58	1.11±0.45	1.44±0.51	1.93±0.42	2.18±0.46

Table IV.2.3. CBCM multi-step unconstrained recovery, The initial fixity (ε_F^I) = 2.43±0.3 %

different T_R. In addition, to calculate the recovered deformation (ε_R) for CBCM-SMPC, free deformation (ε_A) at different temperature from 80 to 150°C (see Figure IV.2.5) obtained from non-programmed CBCM is subtracted from ε_{RT}. The values of ε_R for CBCM-SMPC are given in Table IV.2.3.

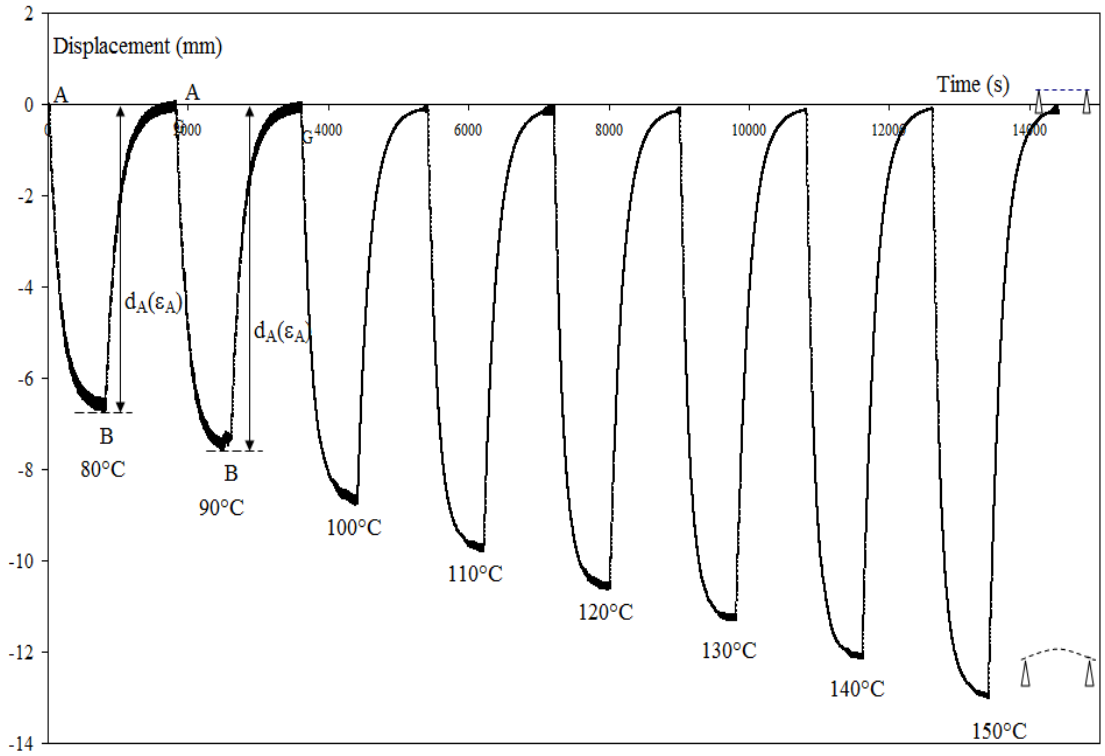

Figure IV.2.5. d_A for non-programmed CBCM at different temperatures from 80°C to 150°C; A = initial position; AB = heating, BA = cooling

Deformations (%)	**T_R (°C)**							
	80	90	100	110	120	130	140	150
ε_{RA}	1.14±0.12	1.11±0.16	1.07±0.14	0.98±0.14	0.91±0.11	0.80±0.16	0.7±0.12	0.64±0.09
ε_{RF}	0.82±0.11	0.75±0.11	0.66±0.12	0.52±0.11	0.4±0.07	0.24±0.11	0.09±0.1	0.01±0.07
$\varepsilon_{RT} = \varepsilon_R = \varepsilon_F^I - \varepsilon_{RA}$	0.12±0.01	0.15±0.05	0.19±0.03	0.28±0.03	0.35±0.03	0.46±0.05	0.56±0.05	0.62±0.02

Table IV.2.4. SYM multi-step unconstrained recovery, $\varepsilon_F^I = 1.26±0.11$

For SYM, ε_{RT} is equal to ε_R as here, the evolution of initial fixity is being examined by recovery heating and cooling, so, the value of free deformation (ε_A) has no effect during the recovery.

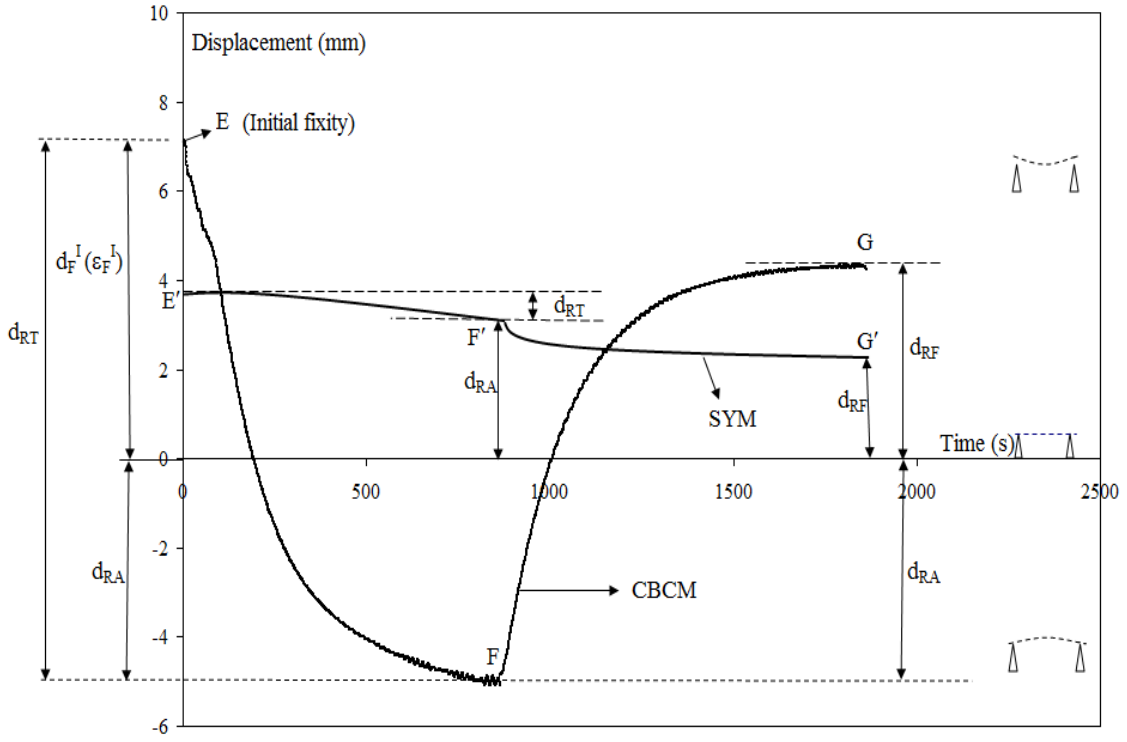

Figure IV.2.6. Evolution of initial fixity at a certain T_R for CBCM and SYM

To study the evolution of deformations during unconstrained multi-step recovery at different T_R in reference to the initial fixity (Figure IV.2.6), the recovery fixity ratios r_F and recovery activation ratios r_A are calculated by Eq. 8. So a linear dependence of r_F and r_A versus T_R can be observed (Figure IV.2.7 &8).

$$r_F = 1 - \frac{\varepsilon_{RF}}{\varepsilon_F^I} \quad \& \quad r_A = 1 + \frac{\varepsilon_{RA}}{\varepsilon_F^I} \qquad \text{for CBCM}$$

$$r_F = 1 - \frac{\varepsilon_{RF}}{\varepsilon_F^I} \quad \& \quad r_A = 1 - \frac{\varepsilon_{RA}}{\varepsilon_F^I} \qquad \text{for SYM} \qquad (8)$$

For CBCM and SYM, the slope "a" of the corresponding curve characterizes the multi-shape property of the plate and indicates the step-wise recoveries from the initial fixity during heating and cooling. The slope "a" for r_A is 2.45×10^{-2} °C^{-1} for CBCM and is 6.1×10^{-3} for SYM). Similarly, the slope "a" for r_F is 9.5×10^{-3} °C^{-1} for CBCM and is 9.8×10^{-3} for SYM.

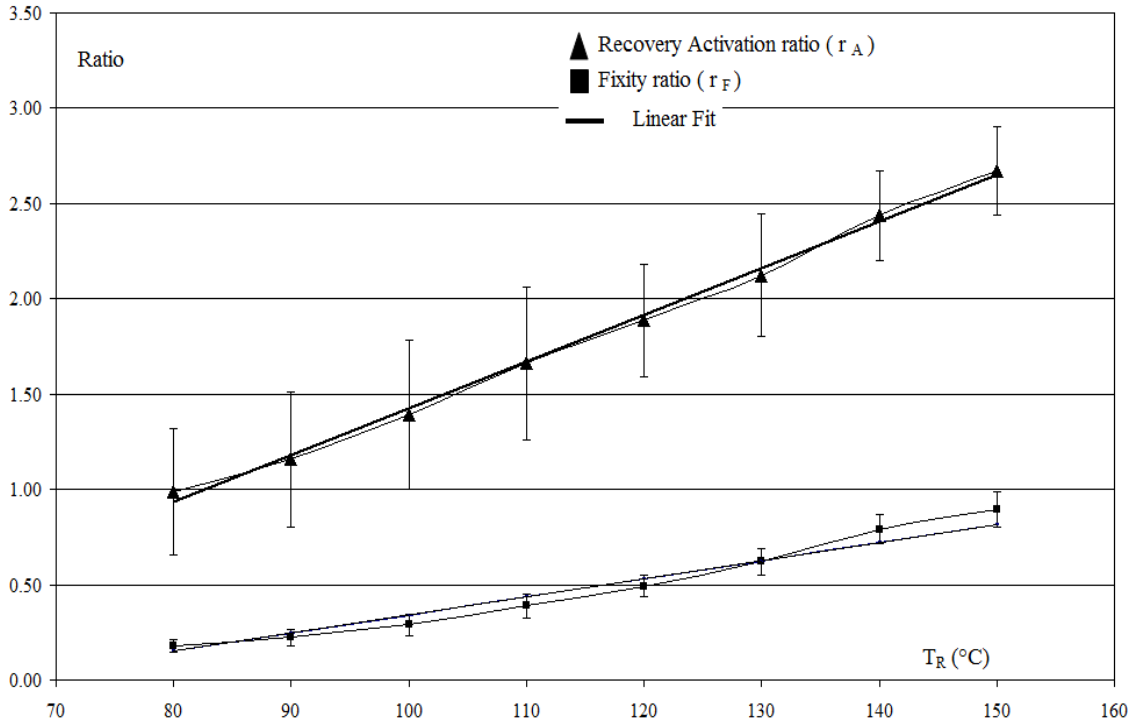

Figure IV.2.7. CBCM recovery activation ratio and fixity ratio in function with T_R

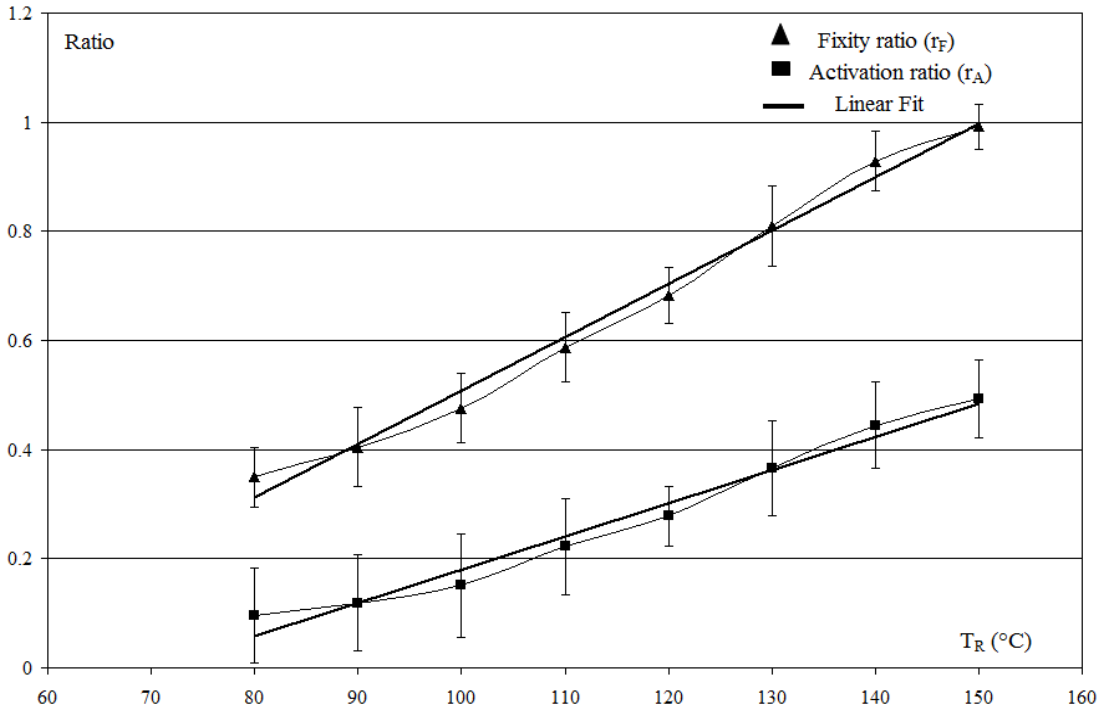

Figure IV.2.8. SYM recovery activation ratio and fixity ratio in function with T_R

IV.2.3.1.1) Stabilization properties at a certain T_R

To investigate the stabilization of ε_{RA} and ε_{RF} for a certain T_R, six recovery cycles at T_R of 80°C (Figure IV.2.9) are provided. Table IV.2.5 gives the recovery values that show that ε_{RA} and ε_{RF} change during first 3 recovery cycles but after 3rd cycle, ε_{RA} and ε_{RF} tend to stabilize. For CBCM, the average values for ε_{RA} and ε_{RF} during the first 3 recovery cycles at 80°C are − 0.09 ± 0.06 % and 1.85 ± 0.04 %. Similarly, the average values for ε_{RA} and ε_{RF} during the last 3 recovery cycles at 80°C are − 0.18 ± 0.01 % and 1.78 ± 0.01 %. Similarly, for SYM, the average values for ε_{RA} and ε_{RF} during the first 3 recovery cycles at 80°C are 0.82 ± 0.01 % and 0.85 ± 0.02 %. Similarly, the average values for ε_{RA} and ε_{RF} during the last 3 recovery cycles at 80°C are 1.15 ± 0.01 % and 0.82 ± 0.01 %. This shows the high level of stabilization as number of recovery cycles increase.

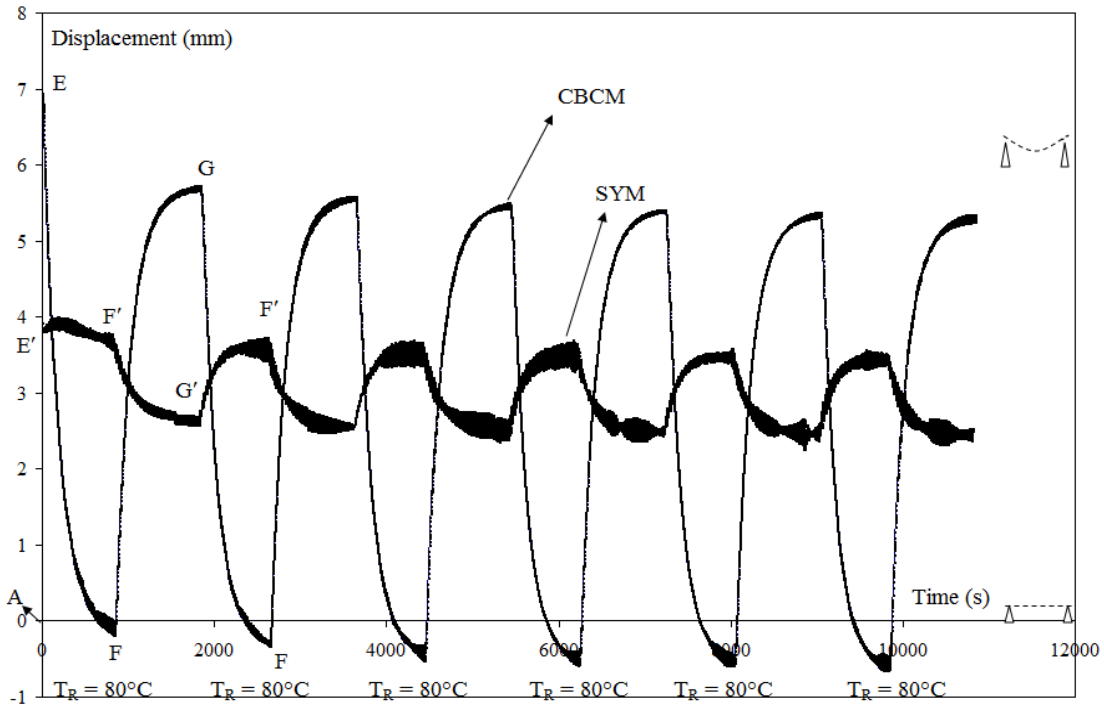

Figure IV.2.9. 2W-SME at T_R = 80°C; A = Initial position before the start of test; For CBCM {AE = d_F^I; EF, GF = Heating during recovery; FG = Cooling during recovery; AF = d_{RA}; AG = d_{RF}}, For SYM {AE′= d_F^I; E′F′, G′F′= Heating during recovery; F′G′= Cooling during recovery; AF′= d_{RA} for SYM; AG′= d_{RF}}

Composite plates	Deformations (%)	Recovery cycles (at T_R = 80°C)					
		1	2	3	4	5	6
CBCM	ε_{RA}	−0.03±0.28	−0.10±0.28	−0.14±0.29	−0.17±0.29	−0.18±0.31	−0.19±0.3
	ε_{RF}	1.89±0.33	1.85±0.33	1.82±0.33	1.79±0.34	1.78±0.33	1.76±0.34
SYM	ε_{RA}	1.23±0.11	1.19±0.11	1.17±0.11	1.16±0.12	1.15±0.12	1.14±0.12
	ε_{RF}	0.88±0.11	0.85±0.11	0.84±0.12	0.83±0.12	0.82±0.11	0.81±0.12

Table IV.2.5. ε_{RA} (%) during heating at T_R = 80°C and corresponding ε_{RF} (%) after cooling for the 6 recovery cycles. For CBCM, ε_F^I = 2.31±0.31 whereas for SYM, ε_F^I = 1.3±0.11

Similarly, the recovery of the composites have also been investigated by heating them for certain number of cycles at a certain T_R i.e. 80°C and then increased the T_R to 90°C (Figure IV.2.10). The different values of ε_{RA} and ε_{RF} (Table IV.2.6) show that composites respond immediately for a different fixity and activated position when a higher T_R is provided even if it is heated at lower T_R for certain number of cycles. Thus the composite plates adjust themselves according to the new T_R. For CBCM, for the 3 recovery cycles at 80°C, the average values for the ε_{RA} and ε_{RF} are − 0.30 ± 0.08 % and 1.62 ± 0.05 %. Similarly, for the 3 recovery cycles at 90°C, the average values for the ε_{RA} and ε_{RF} are − 0.86 ± 0.04 % and 1.45 ± 0.04 %.

For SYM, for the 3 recovery cycles at 80°C, the average values for the ε_A and ε_F are 1.09 ± 0.03 % and 0.76 ± 0.02 %. Similarly, for the 3 recovery cycles at 90°C, the average values for the ε_{RA} and ε_{RF} are 1.04 ± 0.02 % and 0.68 ± 0.02 %. It confirms the adaptability of the composites for a change in given T_R (which tends to stabilize if a same T_R is provided for multiple cycles).

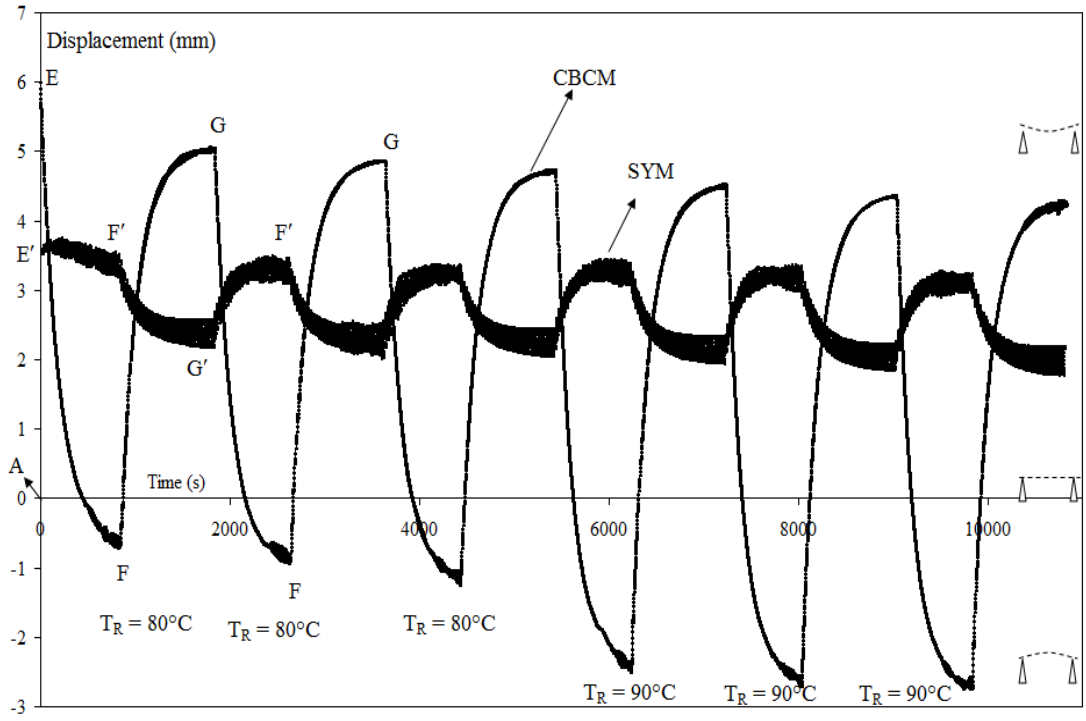

Figure IV.2.10. CBCM and SYM recovery at T_R = 80°C and T_R = 90°C; A = Initial position before the start of test; For CBCM {AE = d_F^I; EF, GF = Heating during recovery; FG = Cooling during recovery; AF = d_{RA}; AG = d_{RF}}, For SYM {AE′= d_F^I; E′F′, G′F′= Heating during recovery; F′G′= Cooling during recovery; AF′= d_{RA} for SYM; AG′= d_{RF}}

Composite plates	**Deformations (%)**	**Recovery cycles**					
		T_R = 80°C			T_R = 90°C		
		1	2	3	1	2	3
CBCM	ε_{RA}	−0.21±0.17	−0.29±0.17	−0.38±0.16	−0.81±0.17	−0.87±0.18	−0.89±0.14
	ε_{RF}	1.67±0.13	1.62±0.14	1.57±0.14	1.49±0.14	1.45±0.14	1.41±0.14
SYM	ε_{RA}	1.13±0.04	1.09±0.03	1.07±0.04	1.07±0.04	1.04±0.04	1.02±0.04
	ε_{RF}	0.79±0.05	0.76±0.05	0.75±0.05	0.71±0.05	0.69±0.05	0.66±0.07

Table IV.2.6. ε_{RA} (%) and corresponding ε_{RF} (%) after heating (at T_R = 80°C and at T_R = 90°C) and after cooling for the 3 cycles. For CBCM, ε_F^I = 2.07±0.12. For SYM, ε_F^I = 1.21±0.06

The fixity gained during the step of programming is recovered in several steps by providing lower T_R. This enables the composite to obtain several fixities and activations during cooling and heating respectively. Each T_R defines a new activated position during heating and a new

fixity during cooling. Thus, it is possible to obtain infinitive number of activated positions between the activated position at T_R of 80°C and the activated position at T_R of 150°C by providing infinitive T_R between 80°C and 150°C. Similarly, it is possible to obtain infinitive number of fixities between the initial fixity and the initial position of the composite plate by cooling the composite plate for infinitive number of T_R.

It thus confirms the adaptability of the composite by carefully changing the T_R. The different ε_{RA} and ε_{RF} controlled by T_R perform 2W-SME and the multi-SME during heating and cooling respectively. However, for a certain T_R, ε_{RA} and ε_{RF} start stabilizing after 3 cycles. Hence, the combination of CBCM-effect and SME confirms the fabrication of 2W-SM actuator that can also change its curvature in the same recovery cycle of heating and cooling.

IV.2.3.2) Multi-step constrained recovery

During multi-step recovery, the recovery force increases with the increase of T_R. The curve for total recovery forces (F_{RT}) for CBCM is shown in Figure IV.2.11 and the values of F_{RT} are given in Table IV.2.7. Also, the curve for different blocking forces (F_B) at different temperatures is shown in figure IV.2.12 whereas the values are given in Table IV.2.7. As F_{RT} is the combination of F_B and F_R, so F_R obtained at different T_R produced due to the SME are calculated by taking the difference of the F_{RT} and F_B.

Force (N)	**T_R (°C)**							
	80	90	100	110	120	130	140	150
F_{RT}	22.4±0.51	25.47±0.49	29.72±0.48	34.25±0.37	38.11±1	41.85±1.31	45.75±0.73	48.88±0.89
F_B	21.25±0.64	23.2±0.42	25.65±0.74	28.6±0.55	30.65±0.59	32.65±1.12	34.05±0.51	35.58±0.88
$F_R = F_{RT} - F_B$	1.15±0.13	2.27±0.07	4.05±0.25	5.65±0.18	7.46±0.41	9.5±0.1	11.7±0.22	13.32±0.1

Table IV.2.7. T_R and their corresponding CBCM recovery forces

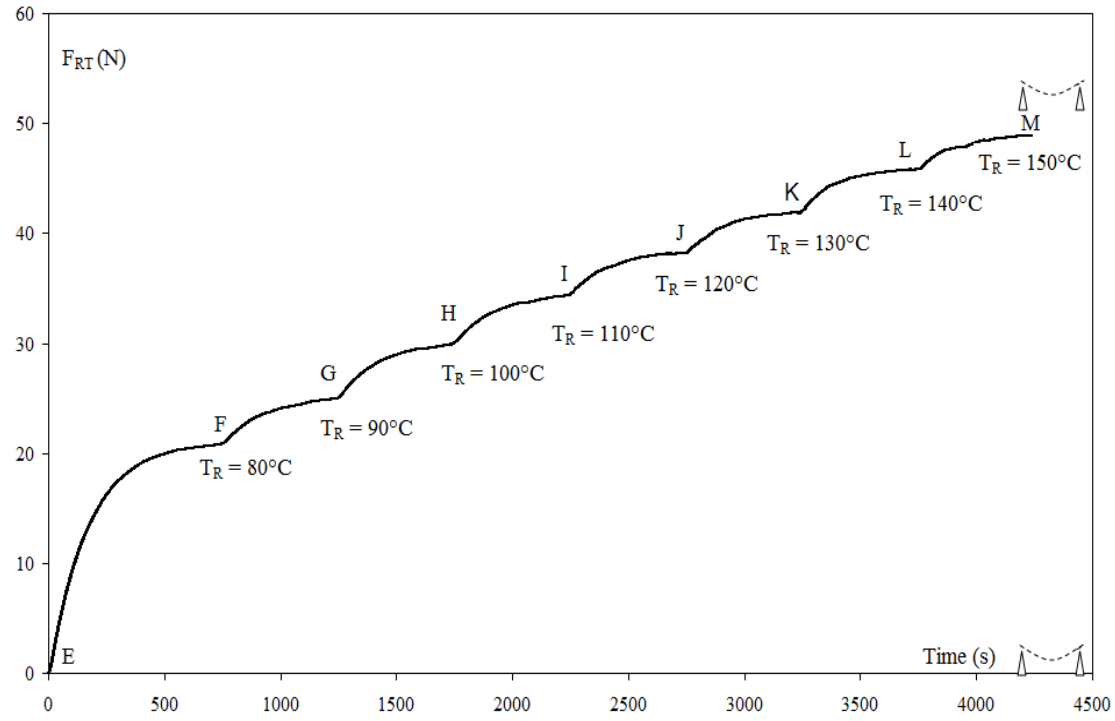

Figure IV.2.11. Multi-step constrained recovery (F_{RT}) at different T_R for CBCM

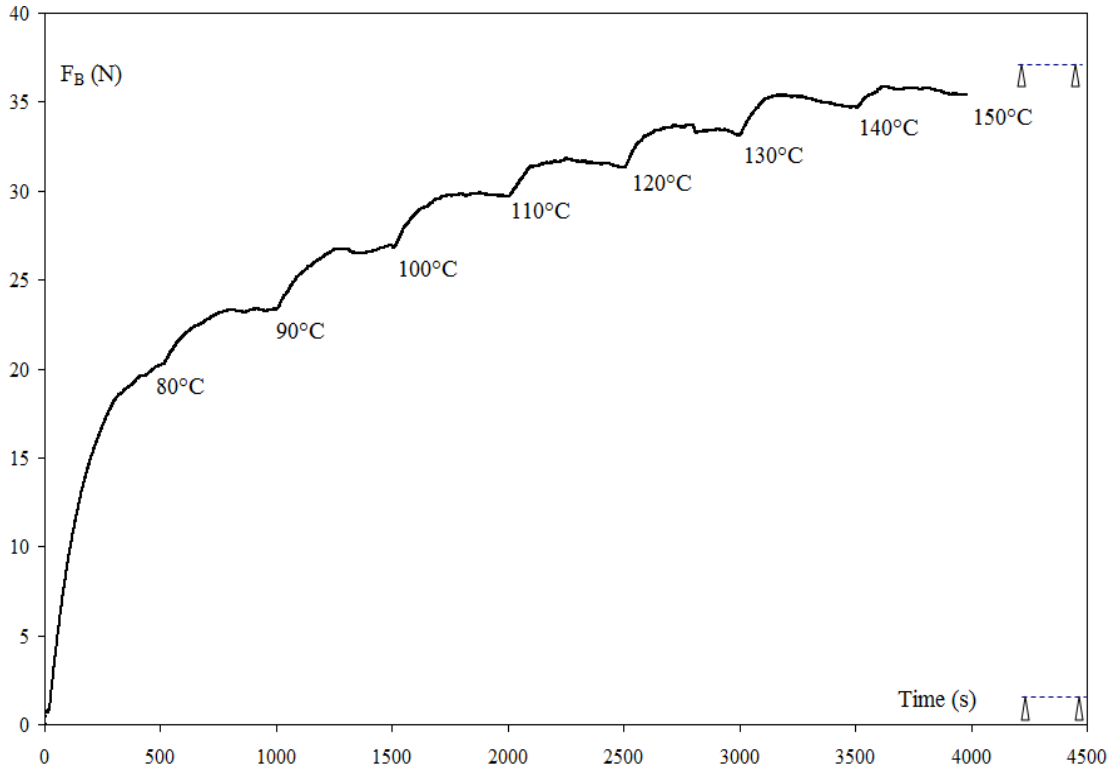

Figure IV.2.12. Non-programmed CBCM blocking forces (F_B) at different temperatures

Similarly, the curve for recovery forces for SYM at T_R is shown in figure IV.2.13 and the values are given in Table IV.2.8.

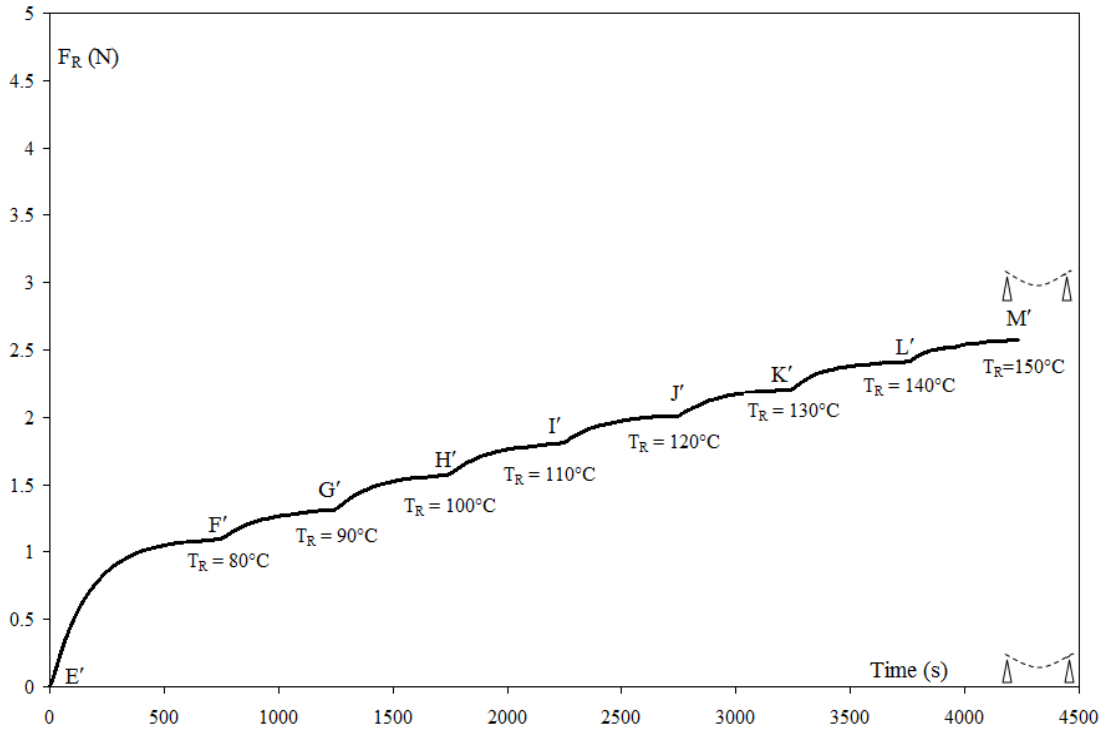

Figure IV.2.13. SYM multi-step recovery forces at different T_R

Force (N)	**T_R (°C)**							
	80	90	100	110	120	130	140	150
F_R	1.12±0.15	1.32±0.14	1.59±0.14	1.84±0.17	2.02±0.11	2.22±0.12	2.38±0.13	2.45±0.14

Table IV.2.8. T_R and their corresponding SYM recovery forces

According to the variation of F_R (different forces acting during the multi-step recovery), a linear dependence versus the recovery temperature T_R can be observed for both CBCM and SYM (Figure IV.2.14. and Figure IV.2.15 respectively). For CBCM, the slope "a" for F_{RT}, F_B and F_R is 7.8×10^{-3}, 4.3×10^{-3} and 3.6×10^{-3} respectively. For SYM, the slope "a" for F_R is 0.4×10^{-3}. It is already discussed that instead of one-step recovery at a T_R equal to T_D, multi-step recovery can be performed by providing various T_R lower than T_D. During recovery, for CBCM, the work recovered (W_R) during one-step recovery (unconstrained and constrained) calculated by Eq. 6 is 0.27±0.02 J. Similarly, for SYM, in one-step recovery, W_R is $2.3\times10^{-3} \pm 3.67\times10^{-4}$ J.

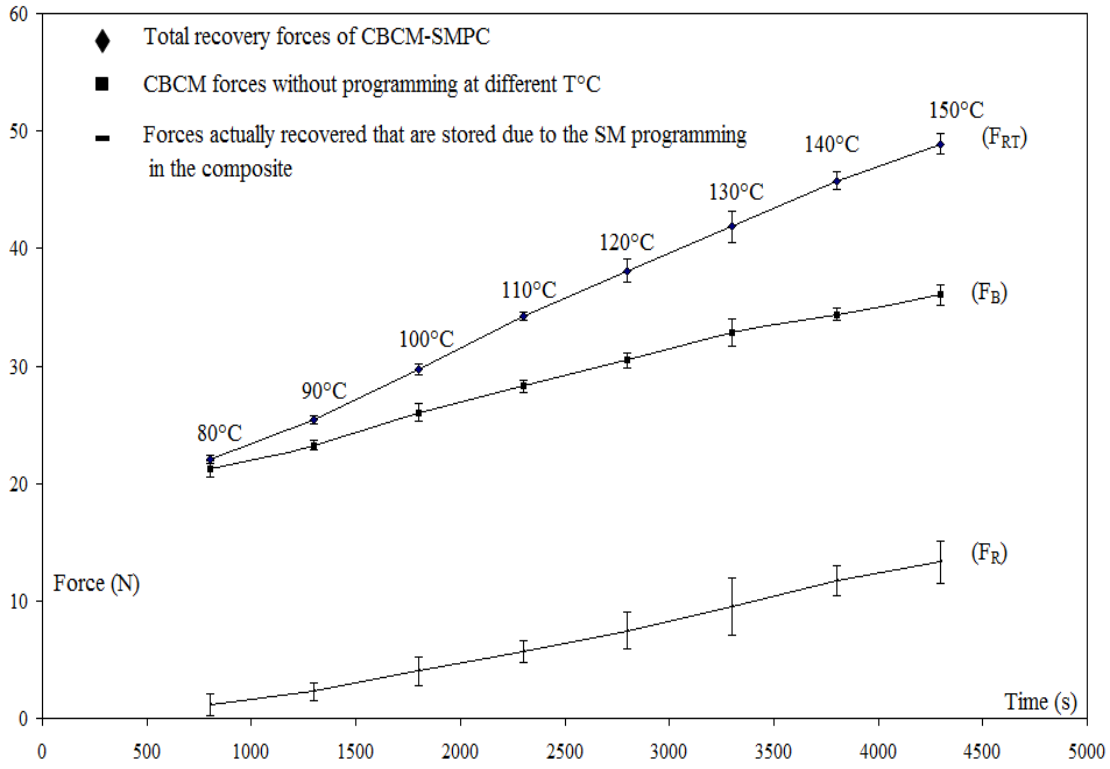

Figure IV.2.14. Different forces for CBCM at different temperatures; $F_R = F_{RT} - F_B$

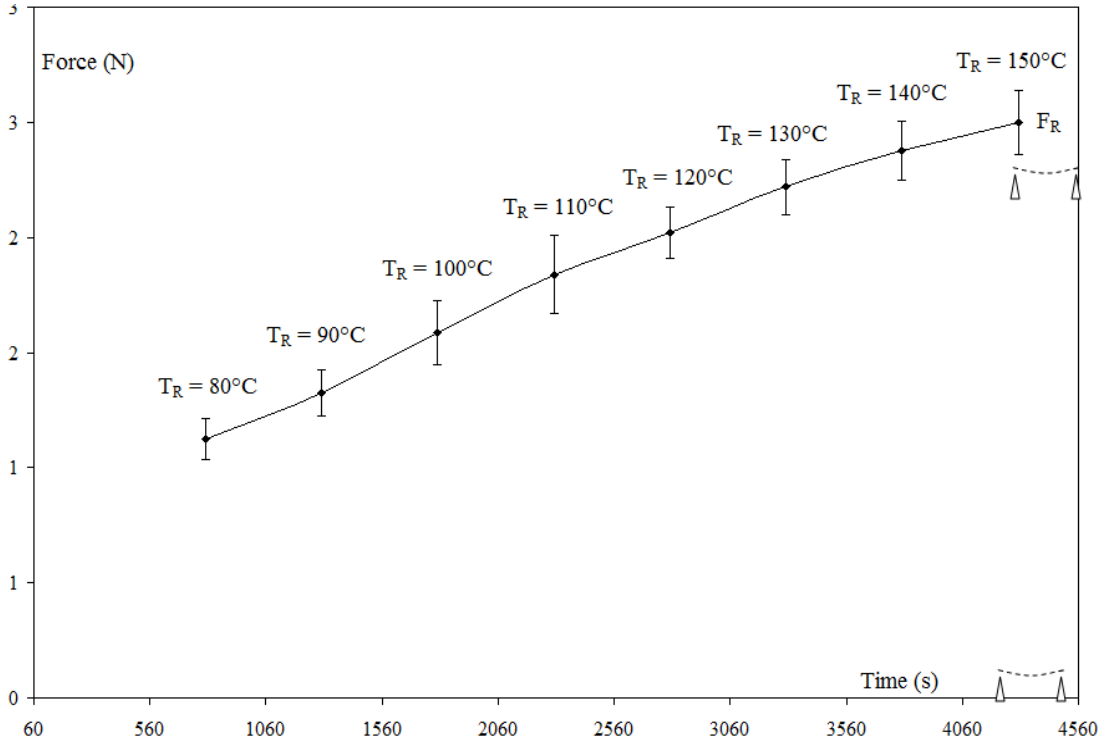

Figure IV.2.15. F_R for SYM at different T_R

The curves for one-step recovery for CBCM and SYM are given in Appendix-E. During multi-step recovery, like one-step recovery, it is possible to calculate W_R, in reference to d_F^I, during the step-wise recovery activation for each T_R. Table IV.2.9 gives W_R at each step (i.e. at different T_R) during multi-step recovery for CBCM and Table IV.2.10 gives W_R of SYM at each step (i.e. at different T_R) during multi-step recovery. If W_R at $T_R = T_D = 150°C$ is compared during one-step recovery and multi-step recovery, they are almost equal for CBCM and SYM. This demonstrates that W_R during multi-step recovery gives equal W_R even giving W_R at different lower T_R than T_D.

Work (J)	**T_R (°C)**							
	80	90	100	110	120	130	140	150
W_{RT}	0.08±0.02	0.11±0.03	0.15±0.03	0.21±0.04	0.26±0.04	0.32±0.05	0.41±0.04	0.48±0.05
W_A	0.07±0.01	0.08±0.01	0.11±0.01	0.14±0.01	0.16±0.01	0.18±0.01	0.20±0.01	0.23±0.01
$W_R = W_{RT} - W_A$	0.01±0.01	0.02±0.02	0.04±0.02	0.07±0.03	0.10±0.03	0.14±0.03	0.20±0.04	0.25±0.04

Table IV.2.9. W_R for CBCM during multi-step recovery

Work (J)	**T_R (°C)**							
	80	90	100	110	120	130	140	150
W_R	$2.03\times10^{-4} \pm 3.26\times10^{-5}$	$2.97\times10^{-4} \pm 1.3\times10^{-4}$	$4.53\times10^{-4} \pm 1.11\times10^{-4}$	$7.77\times10^{-4} \pm 1.54\times10^{-4}$	$1.07\times10^{-3} \pm 2.64\times10^{-4}$	$1.54\times10^{-3} \pm 4.15\times10^{-4}$	$1.99\times10^{-3} \pm 5.06\times10^{-4}$	$2.28\times10^{-3} \pm 4.64\times10^{-4}$

Table IV.2.10. W_R for SYM during multi-step recovery

IV.2.4) Conclusion

CBCM shows more initial fixity than SYM when taken the initial position as a reference point for the deformation during the programming cycle. It is of course due to the more deformation of CBCM than SYM. However, the SMPCs (CBCM and SYM) have the ability to show the multi-step recovery instead of one-step recovery by providing different T_R below T_D. The initial fixity can be recovered step-wise instead of one-step recovery. This step-wise recovery can be clearly observed after each cooling associated with the step-wise heating. After every step of heating and cooling, the initially fixity gradually decreases showing the recovery of the initial fixity. CBCM has the ability to show 2W-SME along with the multi-SME. CBCM while performing these effects, also changes its curvature during heating and cooling. This type of

2W-SME along with change of curvature is also shown by *Tobushi et al.* [67, 69]; however, they have used SMA reinforced Polyurethane SMPC. However, this type of 2W-SME along with the change of curvature is not possible for SYM. For CBCM, it is also possible to have infinite number of recovery positions during heating and cooling by providing infinite number of T_R from Ta to T_D. These effects ultimately lead to the fabrication of a strong 2W smart actuator with infinitive number of fixities and activated positions fully controllable by T_R. Moreover, at a given T_R, a specific activated position during recovery heating and fixity during cooling can be obtained for a number of cycles.

Similarly, during multi-step constrained recovery for CBCM and SYM, the recovery forces increase with the increase of recovery temperature giving the linear behavior. The recovered work in reference to the initial position during each step gives the values of different works obtained during the step-wise recovery. It is found both for CBCM and SYM that the recovered work obtained at T_D equal to 150°C is found to be same obtained during one-step and multi-step recoveries.

Chapter V. Conclusion and Perspectives

In this work, it has been tried to find the solutions for the current problems in SMPs and their composites discussed in the introduction especially the large activated displacement, recovery to original position at a temperature lower than the deforming temperature, large recovery force, recovery to original position even under load and the 2W shape memory effect with the change of the curvature of the composite. These solutions have been found by coupling the two properties of CBCM composite: its active property due to CBCM-effect and shape memory property due to its shape memory effect (SME). This study has been conducted mainly by normal programming cycle with two types of recoveries (one-step recovery and multi-step recovery). One-step recovery has been studied under unconstrained recovery, constrained recovery and recovery under load. Also, under one-step recovery, the effect of stress relaxation on shape properties has also been studied. Moreover, the effect of change in position and orientation of unidirectional glass layers on the shape memory properties have also been studied under one-step recovery. Similarly, multi-step recovery has been studied under unconstrained multi-step recovery and constrained multi-step recovery.

It is found that the total recovery displacement (during one-step unconstrained recovery) obtained due to two effects (CBCM-effect and shape memory effect) is larger than the individual displacements that results in overall higher activation. Hence, the reduced recoverable displacement of CBCM composite due to its rigidity is compensated by its free displacement. Also, during the activation of the total recovery displacement, recovery to original position is obtained at a temperature equal to 90°C. It proves that full recovery is possible at a temperature lower than the deforming temperature (T_D = 150°C). It is mainly due to the combination of two effects that is not possible otherwise as in the case of SYM. SYM cannot recover to its original position at a temperature lower than T_D. It recovers to its original position only when temperature becomes equal to T_D. Similarly, the total recovery force (during one-step constrained recovery) for CBCM is the combination of two effects (CBCM-effect and shape memory effect). The total recovery force is higher than the two individual forces (blocking force and recovery force). Also, when a temperature equal to T_D is provided for more recovery cycles, the force produced during heating is stabilized. Moreover, during cooling, a

residual force is observed; however, it is very less than the total recovery force showing that the major part of the force is always available when heated. This leads to the development of a strong CBCM actuator that can perform a number of cycles. SYM produces less recovery force than CBCM as SYM has no CBCM-effect. The recovery under load is possible for CBCM. It can recover close to full recovery under a load equal to its blocking force (F_B); however, under loads less than its F_B, it recovers beyond its original position showing recovery under load that is not possible otherwise as in case of SYM. SYM cannot give full recovery under any load. It is all due to the combination of two effects (CBCM-effect and SME).

It is further found that the stress relaxation during the programming cycle increases the initial fixity although the residual displacement during the recovery cooling is more than with the normal programming cycle. However, overall performance of the composites (CBCM and SYM) is not affected.

The effect of position and orientation of unidirectional glass layers in the composites affect the overall properties including the shape memory properties. The position and orientation of these layers affect the active properties (free displacement and blocking force) as well as rigidity of the composite. The increase in rigidity increases total force required to deform the composite to the same displacement during the programming cycle. It also affects the stabilization force (F_S). High rigidity degrades the initial fixity and thus it is lowest for the composite having the highest rigidity. During recovery, the total recovery displacement is lowest for the more rigid structure as it has less free displacement. Similarly, the total recovery force is also lowest for the more rigid structure as it has less blocking force F_B. Therefore, it is found that the composite having more asymmetry gives higher actuation properties than the other composites.

In multi-step recovery, during unconstrained recovery, for the recovery temperature (T_R) lower than T_D, it is found that the composite plate is not fully deprogrammed and the SME remains in the composite until T_R equal to T_D is provided. For CBCM, at a lower T_R than T_D, mainly CBCM-effect tends to move the composite plate upward; however, during cooling; SME tends to move it downward, back to the initial fixity. At T_R equal to 80°C, CBCM recovers to its original position and during cooling it goes back close to initial fixity by giving an fixity lesser

than the initial fixity. This indicates the recovery of initial fixity due to the heating at T_R equal to 80°C. For the next step, if T_R is increased (e.g. 90°C), CBCM will give more recovery; however, during cooling, it will also go back towards the initial fixity and the fixity associated to this cooling will be less than the cooling associated with 80°C. This indicates that as T_R increases, the initial fixity recovers and thus decreases during the associated cooling. This process continues until T_R becomes equal to T_D during which CBCM gets maximum total recovery displacement and after cooling it comes to its original position (the initial position before the start of the test). This shows the step-wise deprogramming of CBCM which results in gradual decrease (recovery) of initial fixity. During this process, CBCM performs 2W-SME (with the change of curvature during heating and cooling) along with the multi-SME. CBCM gives stabilized positions during heating and cooling for a number of cycles at a certain T_R. SYM also gives step-wise decrease of initial fixity performing multi-SME; however, it cannot perform 2W-SME. This shows that the composites are fully controllable with T_R. During multi-step constrained recovery, the composites give step-wise recovery forces that increase with the increase of T_R and show linear behavior.

The recovered work in reference to the initial position during each step gives the values of different works obtained during the step-wise recoveries (multi-step unconstrained and constrained recoveries). It is found both for CBCM and SYM that the recovered work obtained at T_D equal to 150°C is found to be same as obtained during one-step and multi-step recoveries.

In future, it would be interesting to carry out the following work:

- To increase the strain, it would be interesting to use a soft polymer although it will decrease the recovery forces. So, to optimize it, a knitting or 3D fabric with reinforcement in the direction of its thickness can be used to avoid its delamination etc.
- A rheological model can be developed in order to understand the effect of reinforcement on the shape memory properties.
- It would also be interesting to study recovery under load for a number of recovery cycles to observe the capability of the composites for recovery under cyclic loading.

- It would also be interesting to study F_{RELAX} for different composites to observe whether it is affected (like F_S) by the asymmetry or not.

References

[1] Postnote, "Smart Materials and Systems," Parliamentary Office of Science and Technology, London, U.K 2008.

[2] J. Ouellette, "How Smart are Smart Materials?," *American Institute of Physics,* 1996.

[3] Available: http://strlab.iitd.ac.in/SSDL/smart.pdf Accessed on 06/09/2012).

[4] P. Gaudenzi, *Smart Structures: Physical Behaviour, Mathematical Modelling and Applications,* 2009.

[5] C. A. Rogers, "Workshop Summary," in *proceedings of U.S. Army Reasearch Office Workshop on Smart Materials, Structures and Mathematical issues*, Virginia Polytechnic Institute & State University, pp. 1-12, 1988

[6] C. A. Rogers, "Intelligent Material Systems and Strucures," in *proceedings of U.S.-Japan Workshop on Smart / Intelligent Materials and Systems*, honolulu, Hawaii, pp. 11-33, 1990.

[7] L. Sun, *et al.*, "Stimulus-responsive shape memory materials: A review," *Materials & Design,* vol. 33, pp. 577-640, 2012.

[8] J. A. Hiltz, "Shape Memory Polymers Literature Review," Defence R&D Canada 2002.

[9] C. Liu, *et al.*, "Review of progress in shape-memory polymers," *Journal of Materials Chemistry*, vol. 17, 2007.

[10] T. Chung, "New shape memory effects in semicrystalline polymeric networks," PhD, Materials Molecular Science and Engineering Case western reserve university, Ohio, USA, 2009.

[11] J. Leng, *et al.*, "Shape-memory polymers and their composites: Stimulus methods and applications," *Progress in Materials Science,* vol. 56, pp. 1077-1135, 2011.

[12] C. Liang, *et al.*, "Investigation of Shape Memory Polymers and Their Hybrid Composites," *Journal of Intelligent Material Systems and Structures,* vol. 8, pp. 380-386, April 1, 1997.

[13] A. Lendlein and S. Kelch, "Shape-Memory Polymers," *Angewandte Chemie International Edition,* vol. 41, pp. 2034-2057, 2002.

[14] S. Madbouly and A. Lendlein, "Shape-Memory Polymer Composites:Shape-Memory Polymers." vol. 226, A. Lendlein, Ed., ed: Springer Berlin / Heidelberg, pp. 41-95, 2010.

[15] S.-H. Lee, *et al.*, "Dual Morphology of Islands and Fractal Holes in Block Copolymer Thin Films," *Macromolecules,* vol. 34, pp. 8405-8408, 2001.

[16] P. T. Mather, *et al.*, "Strain recovery in POSS hybrid thermoplastics," *Polymer Preprints,* vol. 41, p. 528, 2000.

[17] T. Takahashi, *et al.*, "Structure and properties of shape-memory polyurethane block copolymers," *Journal of Applied Polymer Science,* vol. 60, pp. 1061-1069, 1996.

[18] D. Ratna and J. Karger-Kocsis, "Recent advances in shape memory polymers and composites: a review," *Journal of Materials Science,* vol. 43, pp. 254-269, 2008.

[19] D. Zhang, *et al.*, "Shape memory polymer networks from styrene copolymer," Harbin, China, pp. 642360-6, 2007.

[20] B. Xu, *et al.*, "Polystyrene based shape memory nanocomposites," presented at the 17th ICCM conference, Edinburgh, UK 2009.

[21] I. A. Rousseau and T. Xie, "Shape memory epoxy: Composition, structure, properties and shape memory performances," *Journal of Materials Chemistry,* vol. 20, 2010.

[22] J. Leng, *et al.*, "Effect of a linear monomer on the thermomechanical properties of epoxy shape-memory polymer," *Smart Materials and Structures,* vol. 18, 2009.

[23] W. B. Song, *et al.*, "Synthesis and thermomechanical research of shape memory epoxy systems," *Materials Science and Engineering: A,* vol. 529, pp. 29-34, 2011.

[24] Available: http://mmrc.caltech.edu/FTIR/FTIRintro.pdf accessed on 05/09/2012).

[25] Available:http://www.perkinelmer.com/CMSResources/Images/44-132088APP_CharacterizationofPolymersUsingTGA.pdf Accessed on 07/09/2012).

[26] P. Gabbott, "A Practical Introduction to Differential Scanning Calorimetry," in *Principles and Applications of Thermal Analysis*, ed: Blackwell Publishing Ltd, pp. 1-50, 2008.

[27] K. P. Menard, *Dynamic Mechanical Analysis: A Practical Introduction*. Boca Raton London New York Washington, D.C.: CRC Press, 1999.

[28] G. P. Tandon, *et al.*, "Durability Assessment of Styrene- and Epoxy-based Shape-memory Polymer Resins," *Journal of Intelligent Material Systems and Structures*, vol. 20, pp. 2127-2143, November 1, 2009.

[29] J. Xu and J. Song. *Thermal Responsive Shape Memory Polymers for Biomedical Applications, Biomedical Engineering*, 2011.

[30] W. Sokolowski, "Medical Applications of Shape Memory Polymers," Jet Propulsion Laboratory, California Institute of Technology.

[31] F. Castro, *et al.*, "Time and Temperature Dependent Recovery of Epoxy-Based Shape Memory Polymers," *Journal of Engineering Materials and Technology*, vol. 133, pp. 021025-9, 2011.

[32] I. A. Rousseau, "Challenges of shape memory polymers: A review of the progress toward overcoming SMP's limitations," *Polymer Engineering & Science*, vol. 48, pp. 2075-2089, 2008.

[33] Q. Meng and J. Hu, "A review of shape memory polymer composites and blends," *Composites Part A: Applied Science and Manufacturing*, vol. 40, pp. 1661-1672, 2009.

[34] K. K. Westbrook, *et al.*, "Two-way reversible shape memory effects in a free-standing polymer composite " *Smart Materials Structure*, vol. 20, p. 065010, 2011.

[35] T. Chung, *et al.*, "Two-Way Reversible Shape Memory in a Semicrystalline Network," *Macromolecules*, vol. 41, pp. 184-192, 2008.

[36] S. Chen, *et al.*, "Properties and mechanism of two-way shape memory polyurethane composites," *Composites Science and Technology*, vol. 70, pp. 1437-1443, 2010.

[37] S. Chen, *et al.*, "Two-way shape memory effect in polymer laminates," *Materials Letters*, vol. 62, pp. 4088-4090, 2008.

[38] T. H. Kang, *et al.*, "Two-way actuation behavior of shape memory polymer/elastomer core/shell composites," *Smart Materials and Structures*, vol. 21 p. 035028, 2012.

[39] M. Behl, *et al.*, "One-Step Process for Creating Triple-Shape Capability of AB Polymer Networks," *Advanced Functional Materials*, vol. 19, pp. 102-108, 2009.

[40] I. Bellin, *et al.*, "Dual-shape properties of triple-shape polymer networks with crystallizable network segments and grafted side chains," *Journal of Materials Chemistry*, vol. 17, pp. 2885-2891, 2007.

[41] T. Xie, *et al.*, "Revealing Triple-Shape Memory Effect by Polymer Bilayers," *Macromolecular Rapid Communications*, vol. 30, pp. 1823-1827, 2009.

[42] T. Pretsch, "Durability of a polymer with triple-shape properties," *Polymer Degradation and Stability*, vol. 95, pp. 2515-2524, 2010.

[43] J. Li and T. Xie, "Significant Impact of Thermo-Mechanical Conditions on Polymer Triple-Shape Memory Effect," *Macromolecules*, vol. 44, pp. 175-180, 2011.

[44] I. Bellin, *et al.*, "Polymeric triple-shape materials," *Proceedings of the National Academy of Sciences*, vol. 103, pp. 18043-18047, November 28, 2006.

[45] J. M. Cuevas, *et al.*, "Triple-shape memory effect of covalently crosslinked polyalkenamer based semicrystalline polymer blends," *Soft Matter*, vol. 8, pp. 4928-4935, 2012.

[46] I. S. Kolesov and H.-J. Radusch, "Multiple shape-memory behavior and thermal-mechanical properties of peroxide cross-linked blends of linear and short-chain branched polyethylenes," *eXPRESS Polymer Letters*, vol. 2, pp. 461–473, 2008.

[47] T. Xie, "Tunable polymer multi-shape memory effect," *Nature*, vol. 464, pp. 267-270, 2010.

[48] K. Yu, *et al.*, "Mechanisms of multi-shape memory effects and associated energy release in shape memory polymers," *Soft Matter*, 2012.

[49] L. Sun and W. M. Huang, "Mechanisms of the multi-shape memory effect and temperature memory effect in shape memory polymers," *Soft Matter*, vol. 6, pp. 4403-4406, 2010.

[50] K. Gall, *et al.*, "Shape memory polymer nanocomposites," *Acta Materialia,* vol. 50, pp. 5115-5126, 2002.

[51] T. Ohki, *et al.*, "Mechanical and shape memory behavior of composites with shape memory polymer," *Composites Part A: Applied Science and Manufacturing,* vol. 35, pp. 1065-1073, 2004.

[52] Z. G. Wei and R. Sandstrom, "Shape-memory materials and hybrid composites for smart systems:Part I Shape-memory hybrid composites," *Journal of Materials Science,* vol. 33, p. 3743-3762, 1998.

[53] Z. G. Wei, *et al.*, "Shape memory materials and hybrid composites for smart systems: Part II Shape-memory hybrid composites," *Journal of Materials Science,* vol. 33, pp. 3763-3783, 1998.

[54] Y. Liu, *et al.*, "Thermomechanics of shape memory polymers: Uniaxial experiments and constitutive modeling," *International Journal of Plasticity,* vol. 22, pp. 279-313, 2006.

[55] H. Tobushi, *et al.*, "Shape Fixity and Shape Recovery in a Film of Shape Memory Polymer of Polyurethane Series," *Journal of Intelligent Material Systems and Structures,* vol. 9, pp. 127-136, 1998.

[56] V. A. Beloshenko, *et al.*, "The shape memory effect in polymers," *Russian Chemical Reviews* vol. 74, pp. 265 - 283, 2005.

[57] H. Tobushi, *et al.*, "Thermomechanical Constitutive Modeling in Shape Memory Polymer of Polyurethane Series," *Journal of Intelligent Material Systems and Structures,* vol. 8, pp. 711-718, 1997.

[58] S. A. Madbouly and A. Lendlein, "Shape-memory polymer composites," *Advanced Polymer Science,* 2009.

[59] M. Nishikawa, *et al.*, "Effect of fiber arrangement on shape fixity and shape recovery in thermally activated shape memory polymer-based composites," *Composites Part A: Applied Science and Manufacturing,* vol. 43, pp. 165-173, 2012.

[60] I. S. Gunes, *et al.*, "Evaluation of nanoparticulate fillers for development of shape memory polyurethane nanocomposites," *Polymer,* vol. 49, pp. 2223-2234, 2008.

[61] S. Mondal and J. L. Hu, "Shape Memory Studies of Functionalized MWNT-reinforced Polyurethane Copolymers," *Iranian Polymer Journal,* vol. 15, pp. 135-142, 2006.

[62] J. M. Cuevas, *et al.*, "Shape memory composites based on glass-fibre-reinforced poly(ethylene)-like polymers," *Smart Materials and Structures* vol. 21, p. 035004, 2012.

[63] M. Nishikawa, *et al.*, "Thermomechanical experiment and analysis on shape recovery properties of shape memory polymer influenced by fiber reinforcement," *Journal of Materials Science,* vol. 45, pp. 3957-3960, 2010.

[64] C.-S. Zhang and Q.-Q. Ni, "Bending behavior of shape memory polymer based laminates," *Composite Structures,* vol. 78, pp. 153-161, 2007.

[65] X. Luo and P. T. Mather, "Triple-Shape Polymeric Composites (TSPCs)," *Advanced Functional Materials,* vol. 20, pp. 2649-2656, 2010.

[66] H. Tamagawa, "Thermo-responsive two-way shape changeable polymeric laminate," *Materials Letters,* vol. 64, pp. 749–51, 2010

[67] H. Tobushi, *et al.*, "Two-Way Bending Properties of Shape Memory Composite with SMA and SMP " *Materials,* vol. 2, pp. 1180-1192, 2009.

[68] H. Tobushi, *et al.*, "Three-way actuation of shape memory composite," *Archives of Mechanics,* vol. 63, pp. 443–457, 2011.

[69] H. Tobushi, *et al.*, "Performance of shape memory composite with SMA and SMP," *Solid State Phenomena,* vol. 154, pp. 65-70, 2009.

[70] H. Tobushi, *et al.*, "Novel Shape Memory Actuators," *Theoretical and Applied Mechanics,* vol. 49, pp. 927-943, 2011.

[71] K. Jonnalagadda, *et al.*, "Local displacements and load transfer in shape memory alloy composites," *Experimental Mechanics,* vol. 37, pp. 78-86, 1997.

[72] H. M. Wache, *et al.*, "Development of a polymer stent with shape memory effect as a drug delivery system," *Journal of Materials Science: Materials in Medicine,* vol. 14, pp. 109-112, 2003.

[73] W. Barvosa-Carter, *et al.*, "Reversibly expandable energy absorbing assembly utilizing shape memory foams for impact management and methods for operating the same," USA Patent 7267367, 2007.

[74] V. R. Buravalla, *et al.*, "Tunable vehicle structural members and methods for selectively changing the mechanical properties thereto," USA Patent 7669918, 2006.

[75] A. L. Browne, *et al.*, "Electrostatically releasable fastening system and method of use," USA Patent 6944920, 2005.

[76] G. P. McKnight, *et al.*, "Airflow control devices based on active materials," USA Patent 7854467, 2010.

[77] A. L. Browne, *et al.*, "Adaptive head light and lens assemblies," USA Patent 7275846 Oct 2, 2007.

[78] T. Margraf, *et al.*, "Reflexive composites: integrated structural health management," presented at the 49th AIAA/ASME/ASCE/AHS/ASC Structures, Structural Dynamics, and Materials Conference, Schaumburg, 2008.

[79] X. Lan, *et al.*, "Fiber reinforced shape-memory polymer composite and its application in a deployable hinge," *Smart Materials and Structures*, vol. 18, p. 024002, 2009.

[80] H. Lu, *et al.*, "Sensing and actuating capabilities of a shape memory polymer composite integrated with hybrid filler," *Smart Materials and Structures*, vol. 19, p. 065014, 2010.

[81] G. Akovali, Ed., *Handbook of composites fabrication*. Rapra technology limited, 2001.

[82] *Module-1: General Introduction, Introduction to composites*. Available:http://nptel.iitm.ac.in/courses/Accessed on 10/09/2012

[83] K. Gall, *et al.*, "Internal stress storage in shape memory polymer nanocomposites," *Applied Physics Letters*, vol. 85, pp. 290-292, 2004.

[84] X. Luo and P. T. Mather, "Conductive shape memory nanocomposites for high speed electrical actuation," *Soft Matter*, vol. 6, 2010.

[85] A. McClung, *et al.*, "Deformation rate-, hold time-, and cycle-dependent shape-memory performance of Veriflex-E resin," *Mechanics of Time-Dependent Materials*, pp. 1-14, 2011.

[86] A. McClung, *et al.*, "Strain rate- and temperature-dependent tensile properties of an epoxy-based, thermosetting, shape memory polymer (Veriflex-E)," *Mechanics of Time-Dependent Materials,* pp. 1-17, 2011.

[87] I. A. Rousseau and T. Xie, "Shape memory epoxy: a systematic study of their performance," San Diego, CA, USA, 2009, pp. 72890X-12.

[88] D. M. Feldkamp and I. A. Rousseau, "Effect of the Deformation Temperature on the Shape-Memory Behavior of Epoxy Networks," *Macromolecular Materials and Engineering,* vol. 295, pp. 726-734, 2010.

[89] X. Wu, *et al.*, "Investigation of mechanical behavior of epoxy shape memory polymers," San Diego, CA, USA, 2009.

[90] Y. Liu, *et al.*, "Organic-montmorillonite modified shape memory epoxy composite," *Polymers for Advanced Technologies,* vol. 22, pp. 2017-2021, 2011.

[91] V. Beloshenko and Y. Voznyak, "Shape memory effect in the epoxy polymer composites with aggregated filler," *Polymer Science Series A,* vol. 51, pp. 416-423, 2009.

[92] H. Deng, *et al.*, "Tailoring of Thermal Transition Temperature and Toughening of Shape Memory Epoxy Polymer," *Applied Mechnaics and Materials,* vol. 182-183, pp. 93-98, 2012.

[93] Y. Liu, *et al.*, "Thermal, mechanical and shape memory properties of shape memory epoxy resin," *Materials Science and Engineering: A,* vol. 527, pp. 2510-2514, 2010.

[94] T. Xie and I. A. Rousseau, "Facile tailoring of thermal transition temperatures of epoxy shape memory polymers," *Polymer,* vol. 50, pp. 1852-1856, 2009.

[95] V. A. Beloshenko, *et al.*, "Shape memory effect in the epoxy polymer–thermoexpanded graphite system," *Composites Part A: Applied Science and Manufacturing,* vol. 33, pp. 1001-1006, 2002.

[96] M. A. Di Prima, *et al.*, "Thermo-mechanical behavior of epoxy shape memory polymer foams," *Smart Materials and Structures,* vol. 16, pp. 2330–2340, 2007.

[97] M. A. Di Prima, *et al.*, "Cyclic compression behavior of epoxy shape memory polymer foam," *Mechanics of Materials,* vol. 42, pp. 405-416, 2010.

[98] M. Di Prima, *et al.*, "Deformation of epoxy shape memory polymer foam. Part I: Experiments and macroscale constitutive modeling," *Mechanics of Materials,* vol. 42, pp. 304-314, 2010.

[99] M. A. Di Prima, *et al.*, "Deformation of epoxy shape memory polymer foam: Part II. Mesoscale modeling and simulation," *Mechanics of Materials,* vol. 42, pp. 315-325, 2010.

[100] H Drobez et al., "A new active composite," *Smart Materials and Structures,* vol. 18, p. 025020, 2009.

[101] K. B. Gautier, *et al.*, "Mechanical performances of a thermal activated composite," *Composites Science and Technology,* vol. 69, pp. 2633-2639, 2009.

[102] J.-M. Freyburgera, *et al.*, "Identification du comportement d'un matériau composite thermiquement actif," presented at the 2ème Conférence interdisciplinaire sur les matériaux Dijon, France, 2006

[103] A. Imbert, *et al.*, "Activation thermique pour le contrôle vibratoire de structures composites," presented at the 20ème Congrès Français de Mécanique, Besançon, France, 2011.

[104] H. Drobez, *et al.*, "Composite actif avec fonction d'assemblage," in *Comptes Rendus des JNC 16 -Toulouse,* Toulouse , France, 2009.

[105] A. Collaine, *et al.*, "The controlled behaviour of composite material model for control," *Experimental Techniques,* vol. 33, pp. 44-49, 2009.

[106] C. MAUPOINT, *et al.*, M3C, matériau composite à comportement contrôlé. *Technique de l'ingenéur* Available: http://www.techniques-ingenieur.fr/base-documentaire/materiaux-th11/materiaux-actifs-et-intelligents-surfaces-fonctionnelles-42126210/m3c-materiau-composite-a-comportement-controle-re82/ 2007 Accessed on 10/09/2012

[107] G. L'Hostis, *et al.*, "Matériaux et structures composites intelligents," presented at the 18ème Congrès Français de Mécanique, Grenoble, France, 2007.

[108] G. L'Hostis, *et al.*, "Modélisation de structures composites à géométrie variable," presented at the 20ème Congrès Français de Mécanique, Besançon, France, 2011.

[109] M. Hasson, *et al.*, "Optimization of the heating of a thermal activated composite," presented at the 11th world Textile conference Autex 2011 Mulhouse, France, Mulhouse, France, 2011.

[110] H. Drobez, *et al.*, "Thermomechanical Modelization of a New Active Material," *Journal of Intelligent Material Systems and Structures,* vol. 20, pp. 1541-1552, 2009.

[111] A. Fosbury, *et al.*, "The interlaminar interface of a carbon fiber polymer-matrix composite as a resistance heating element," *Composites Part A: Applied Science and Manufacturing,* vol. 34, pp. 933-940, 2003.

[112] H. Monner, "Smart material for active noise and vibration reduction," in *Proceedings of Noise and Vibration Emerging Methods, Saint Raphael, France,* 18-21 April 2005.

[113] H. Asanuma, *et al.*, "Proposal of an active composite with embedded sensor," *Science and Technology of Advanced Materials,* vol. 3, pp. 209-216, 2002.

[114] S. Rapp and H. Baier, "Determination of recovery energy densities of shape memory polymers via closed-loop, force controlled recovery cycling," *Smart Materials and Structures,* vol. 19, p. 045018, 2010.

[115] N. Lakhera, *et al.*, "Partially constrained recovery of (meth)acrylate shape-memory polymer networks," *Journal of Applied Polymer Science,* vol. 126, pp. 72-82, 2012.

[116] Available: http://shop.perkinelmer.com/content/technicalinfo/tch_ftiratr.pdf Accessed on 09/09/2012

[117] T. L. James, "Fundamentals of NMR," ed San Francisco, CA 94143-0446 U.S.A, 1998.

[118] F. Castro and H. J. Qi, "Investigation of Thermo-Mechanical Behavior of Shape Memory Polymers," in *Proceedings of the SEM Annual Conference,* New Mexico USA, 2009.

[119] H. Tobushi, *et al.*, "Shape recovery and irrecoverable strain control in polyurethane shape-memory polymer," *Science and Technology of Advanced Materials*, vol. 9, 2008.

[120] A. Basit, *et al.*, "Multi-shape memory effect in shape memory polymer composites," *Materials Letters*, vol. 74, pp. 220-222, 2012.

Appendices

Appendix-A

Chemical characterization

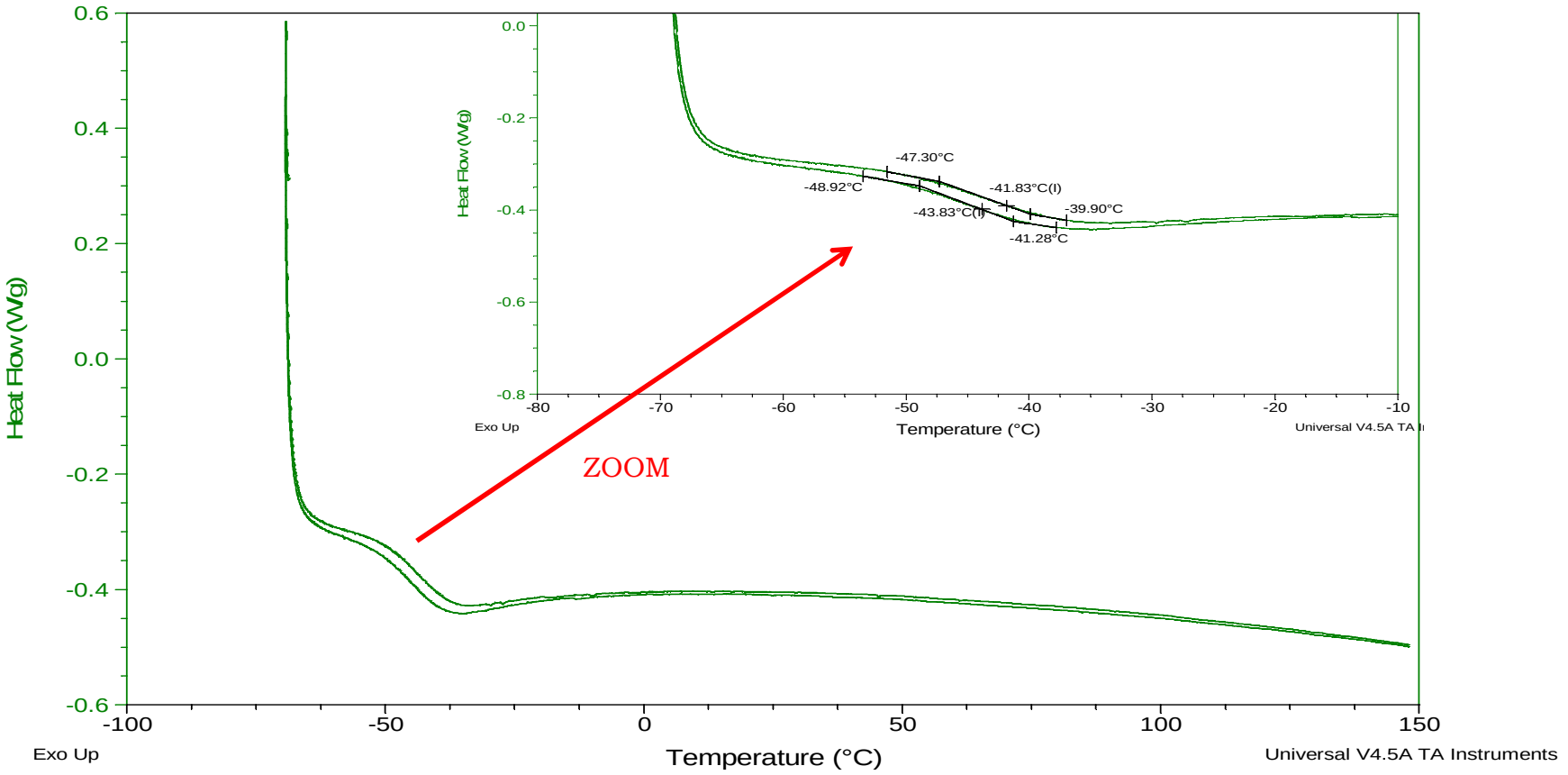

Figure A.1. DSC for Epoxy Resin

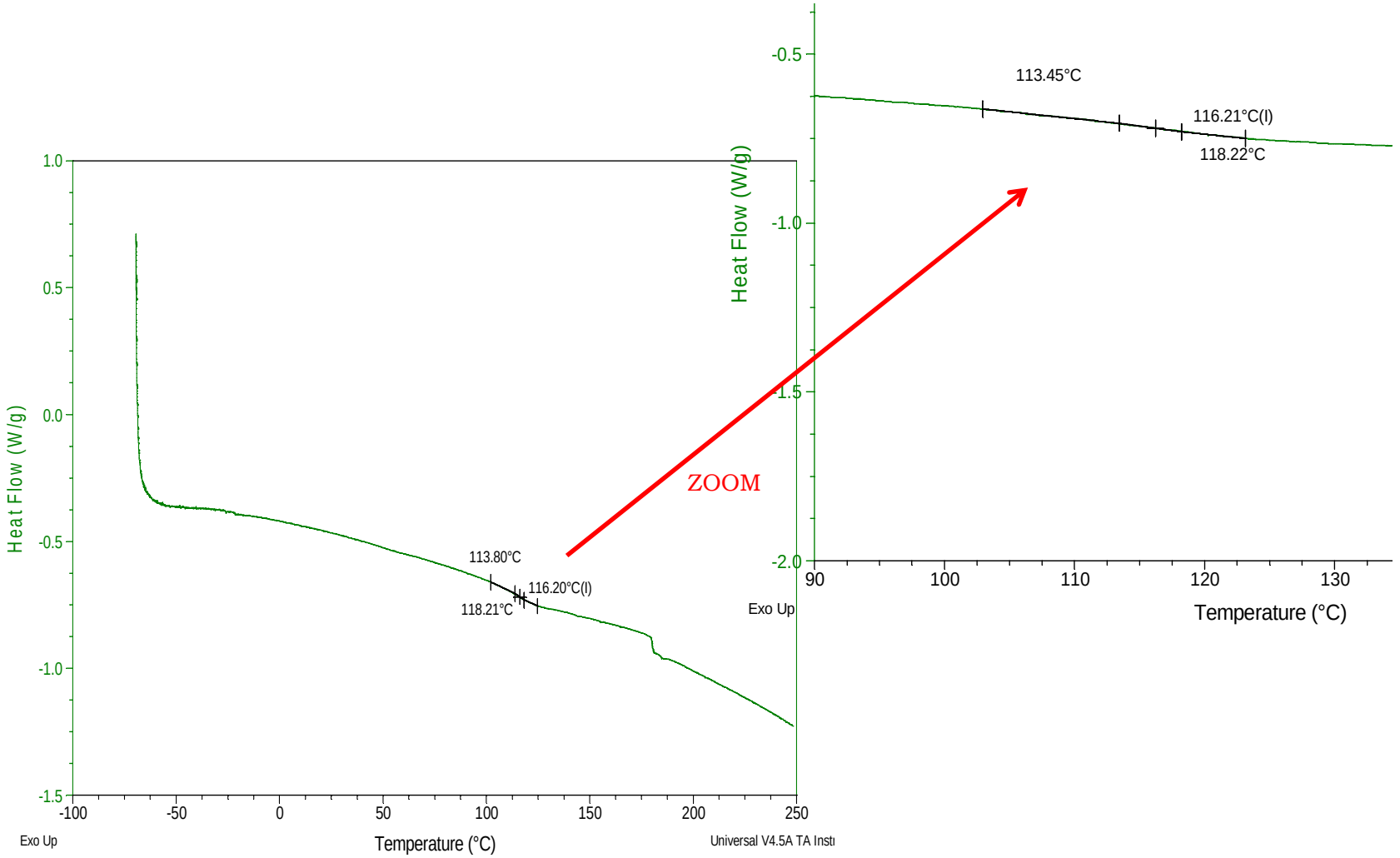

Figure A.2. DSC for cross-linked Epoxy composite

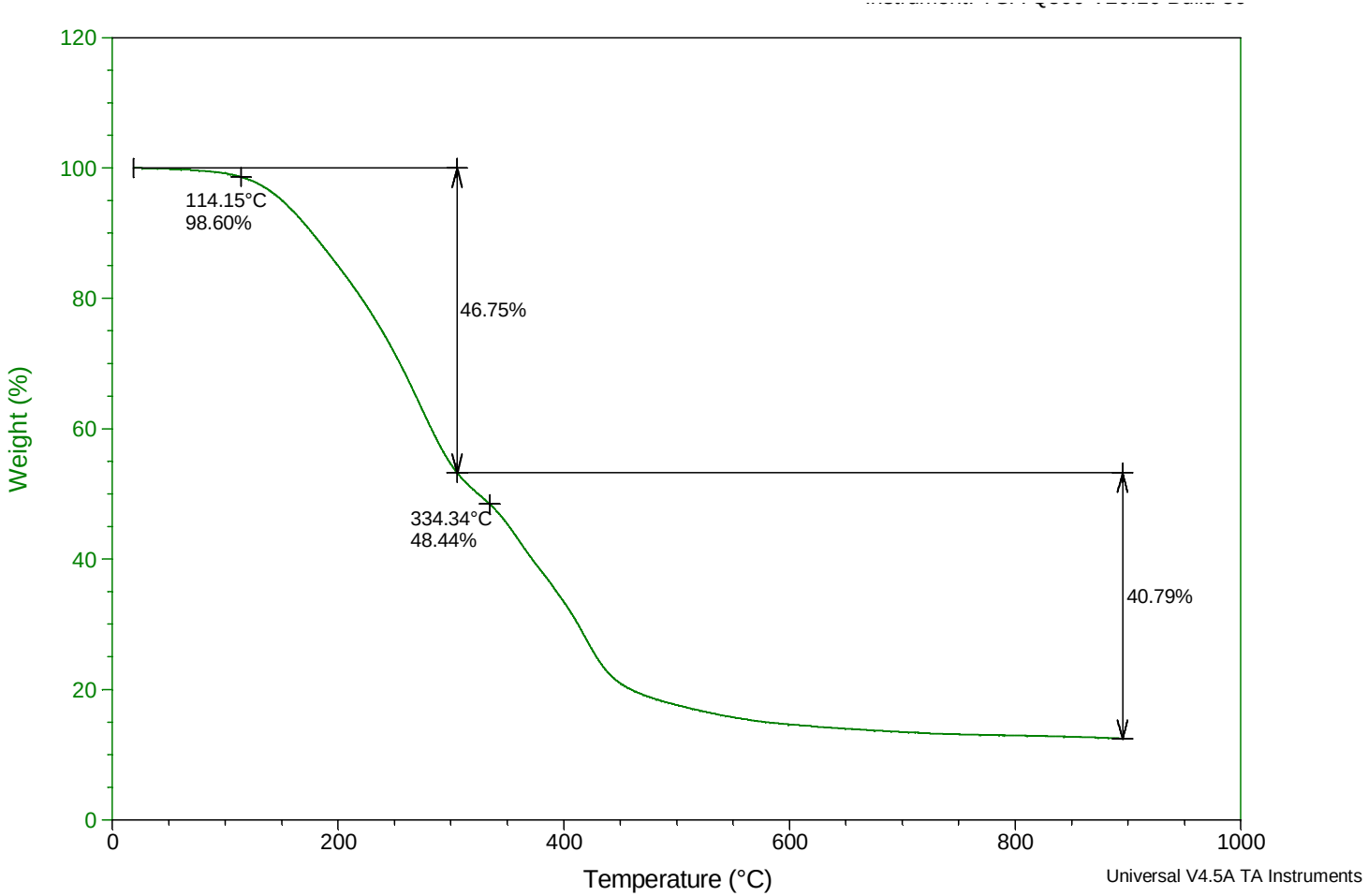

Figure A.3. TGA for Epoxy resin

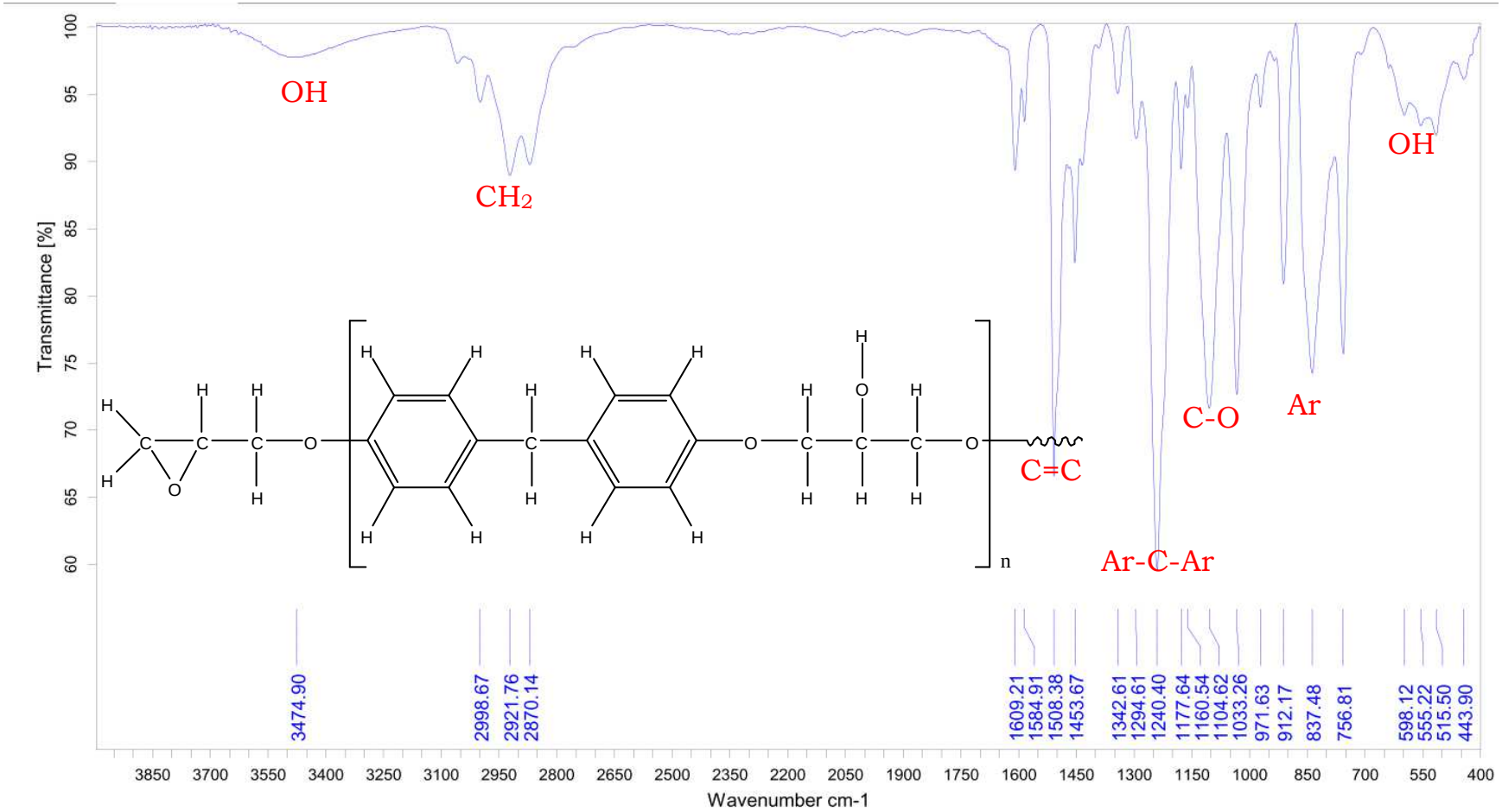

Figure A.4. ATR spectrum for Epoxy resin

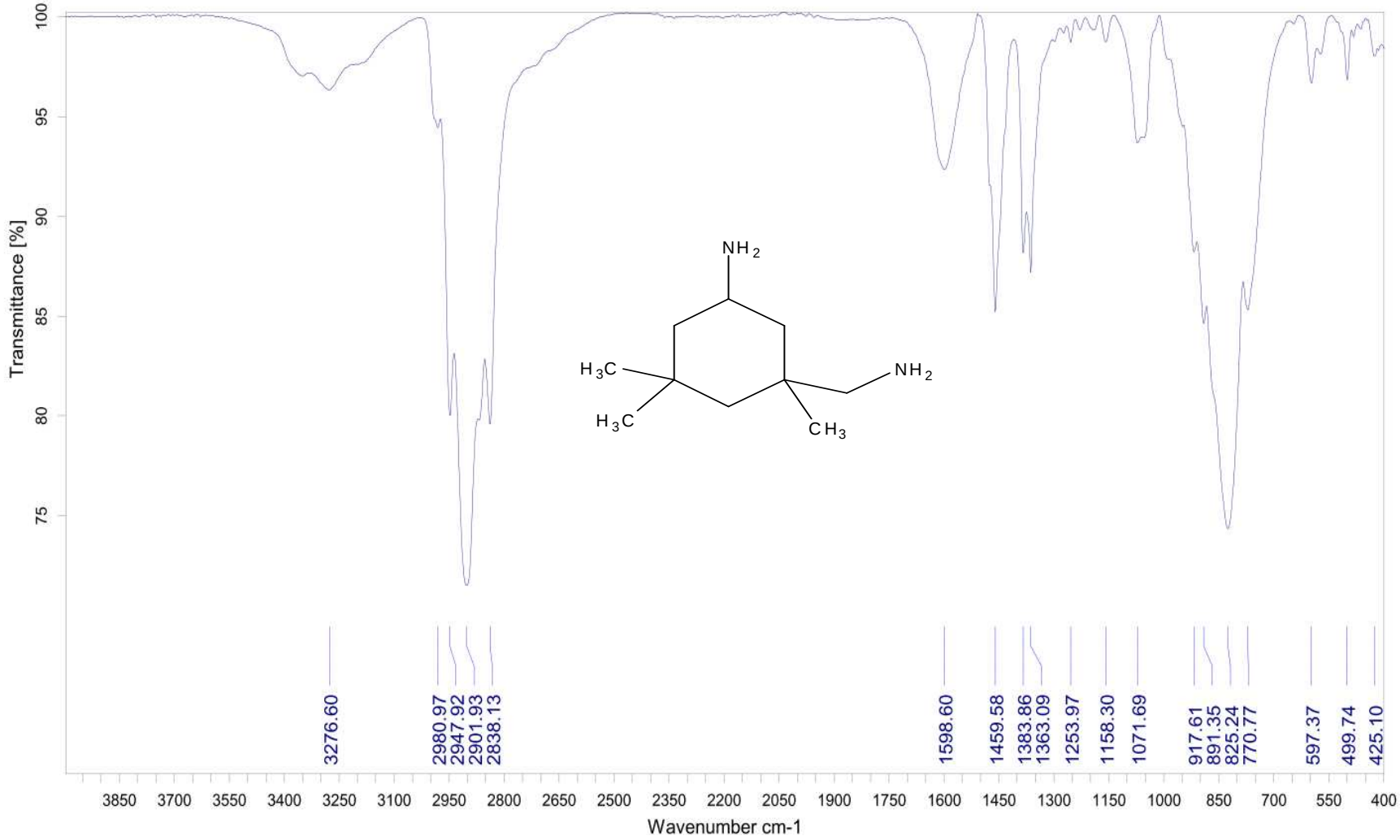

Figure A.5. ATR for Epoxy resin

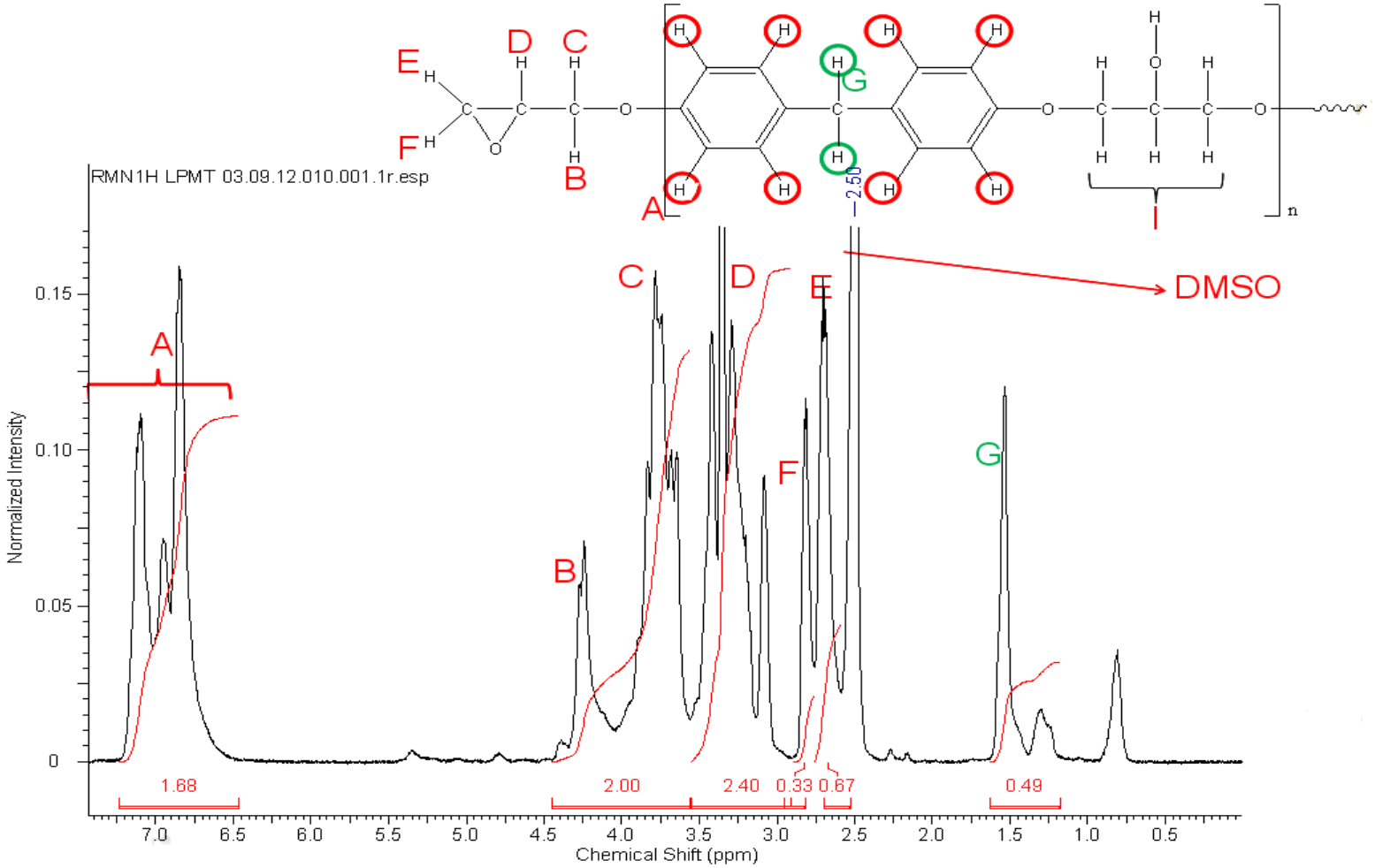

Figure A.6. RMN ^{1}H on Epoxy resin

Appendix-B

Recovery under load

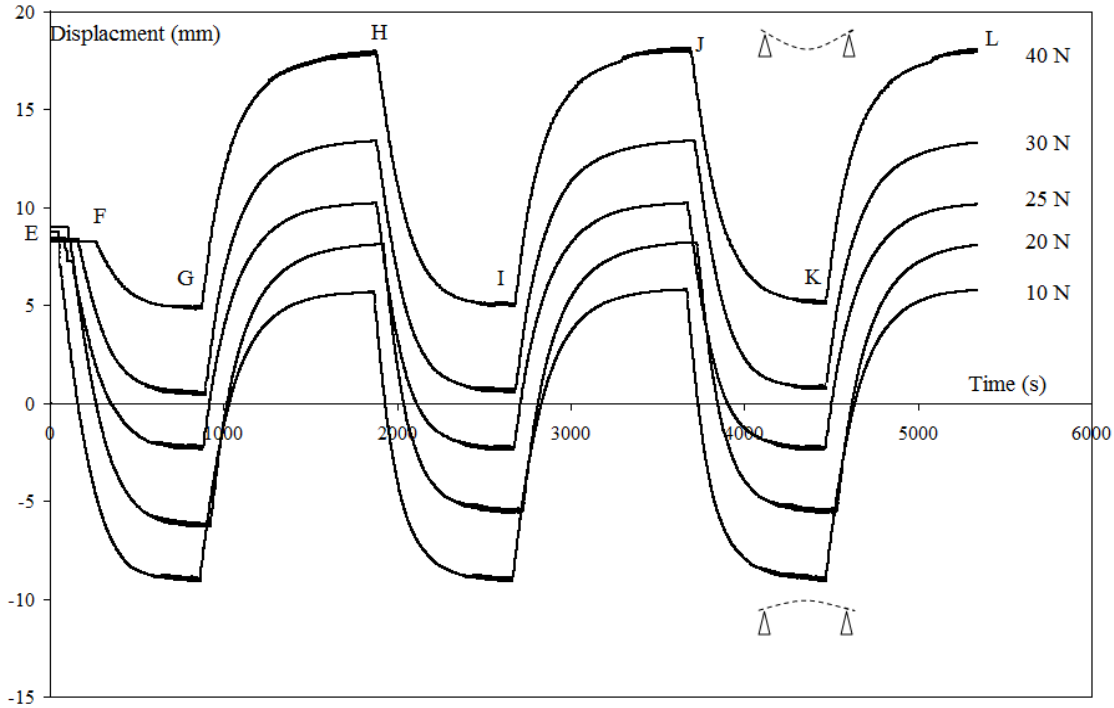

Figure B.1. CBCM recovery under different loads

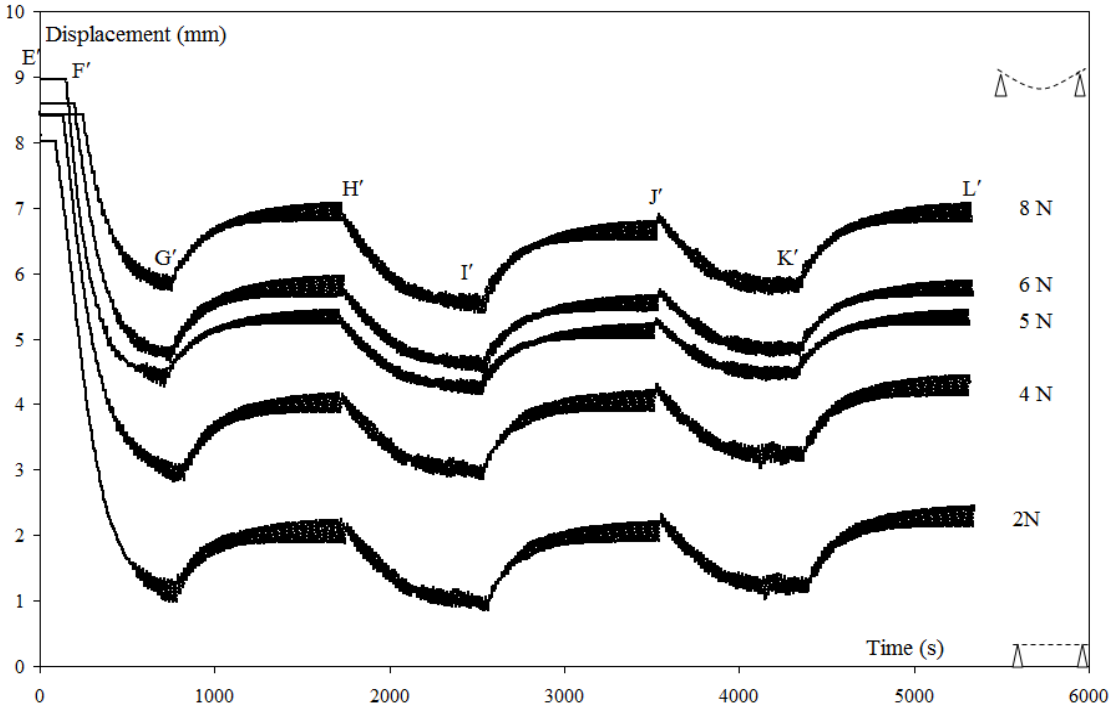

Figure B.2. SYM recovery under different loads

Appendix-C

Stress relaxation tests for SYM (and CBCM)

C.1) Unconstrained recovery

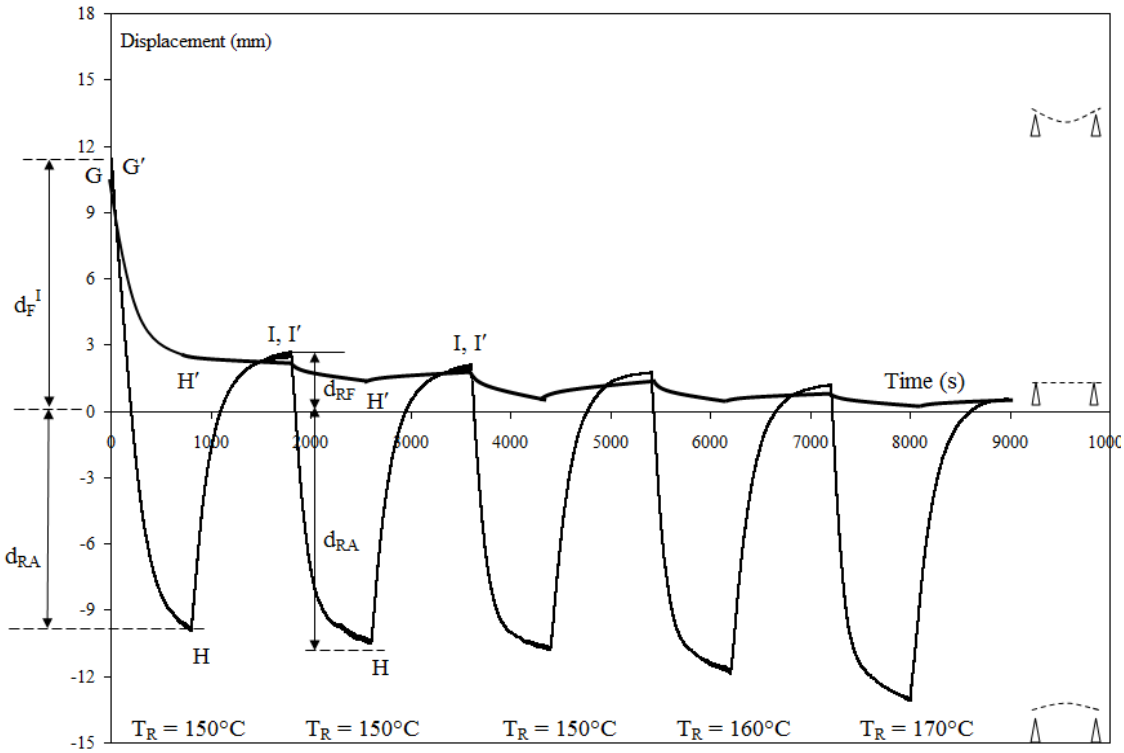

Figure C.1. CBCM and SYM Unconstrained recovery for stress relaxation tests

Figure C.1 shows the unconstrained recovery of CBCM and SYM (see also Table C.1) for 5 recovery cycles. The first 3 cycles are performed at T_R of 150°C that is equal to T_D (point H, H′); however, 4th cycle is at T_R of 160°C and the 5th cycle is at T_R of 170°C. After each given T_R, cooling is also performed. After the first cooling, it can be clearly observed from the Figure C.1 that the composite plates have a residual strain (point I, I′). This residual strain is more than the residual strain for normal programming cycle. The residual strain is induced in the composites due to the effect of stress relaxation performed during the programming cycle. The residual strain decreases as the composite is reheated at the same T_R for more than one cycle. However, it further decreases as T_R is increased to 160°C and then to 170°C. It demonstrates that with the addition of step of stress relaxation in the programming cycle, the residual strain is

observed which is named as irrecoverable residual strain by [119]. They have demonstrated that the residual strain is irrecoverable and it gives a new geometry to the composite plate. However, in this work, it is shown that it is recoverable if the composite plate is reheated at T_R higher than T_D.

Furthermore, it can be observed that the initial fixity increases due to the addition of stress relaxation step during the programming of the composite. CBCM gets 24% and SYM gets 19% more initial fixity with stress relaxation programming than the normal programming cycle respectively. For CBCM, ε_{RT} with stress relaxation programming (ε_{RT} = 7.23%) remains the same as compared to the normal programming (ε_{RT} = 7.28%). Similarly, for SYM, ε_{RT} with stress relaxation programming is 2.94%, and with normal programming is 3.05%. For SYM, the initial fixity increases with stress relaxation programming; however, due to the induction of more residual strain with stress relaxation programming, ε_{RT} remains almost the same as obtained with normal programming cycle.

Composite plates	**Deformations (%)**	**Recovery cycles**				
		1	2	3	4	5
		150°C	150°C	150°C	160°C	170°C
SYM	ε_{RA}	0.59±0.2	0.46±0.08	0.42±0.05	0.34±0.01	0.23±0.07
	ε_{RF}	0.69±0.16	0.62±0.09	0.58±0.06	0.45±0.03	0.31±0.07
CBCM	ε_{RA}	−3.4±0.13	−3.9±0.37	−4.08±0.44	−4.4±0.45	−4.7±0.39
	ε_{RF}	1.03±0.17	0.82±0.2	0.68±0.16	0.51±0.14	0.32±0.14

Table C.1. Recovery deformations for CBCM and SYM during unconstrained recovery with stress relaxation programming; ε_F^I for CBCM is 3.83±0.06; ε_F^I for SYM is 3.63±0.14

C.2) Constrained recovery

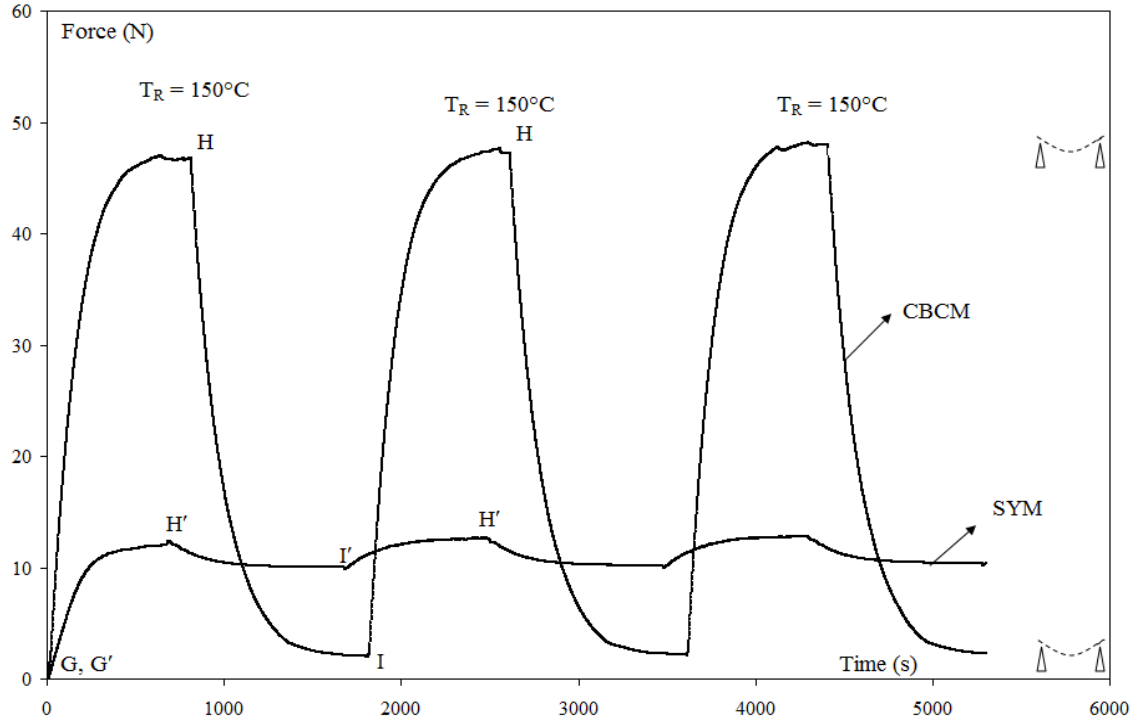

Figure C.2. Constrained recoveries with stress relaxation programming for CBCM and SYM

Similarly, Figure C.2 demonstrates the generation of recovery force during heating at T_R = 150°C (point H, H′) for SYM and CBCM during recovery cycles. Similarly, the residual forces (point I, I′) after the cooling increase with the increase of T_R. With stress relaxation programming, CBCM also produces higher forces than SYM as in the case with normal programming as given in the Table C.2.

Also, in comparison with normal programming cycle, SYM produces a little higher (11%) recovery force during heating and, similarly, a little higher (20%) residual force during cooling that demonstrates that, generally, stress relaxation does not affect the overall performance of the composite.

Composite plates	**Force (N)**	**Recovery cycles**		
		1	2	3
		150°C	150°C	150°C
SYM	F_{RT}	11.86±0.32	12.09±0.34	12.26±0.26
	F_{RES}	10.53±0.21	10.71±0.22	10.91±0.29
	$\delta F = F_{RT} - F_{RES}$	1.33±0.53	1.38±0.56	1.35±0.55
CBCM	F_{RT}	46.44±0.47	47.10±0.26	47.35±0.44
	F_{RES}	1.98±0.09	2.08±0.13	2.20±0.22
	$\delta F = F_{RT} - F_{RES}$	44.46±0.56	45.02±0.39	45.15±0.66

Table C.2. Recovery forces for CBCM and SYM during constrained recovery with stress relaxation programming; ε_F^I for CBCM is 3.73±0.08; ε_F^I for SYM is 3.69±0.17

Appendix-D

Programming cycles for different composites

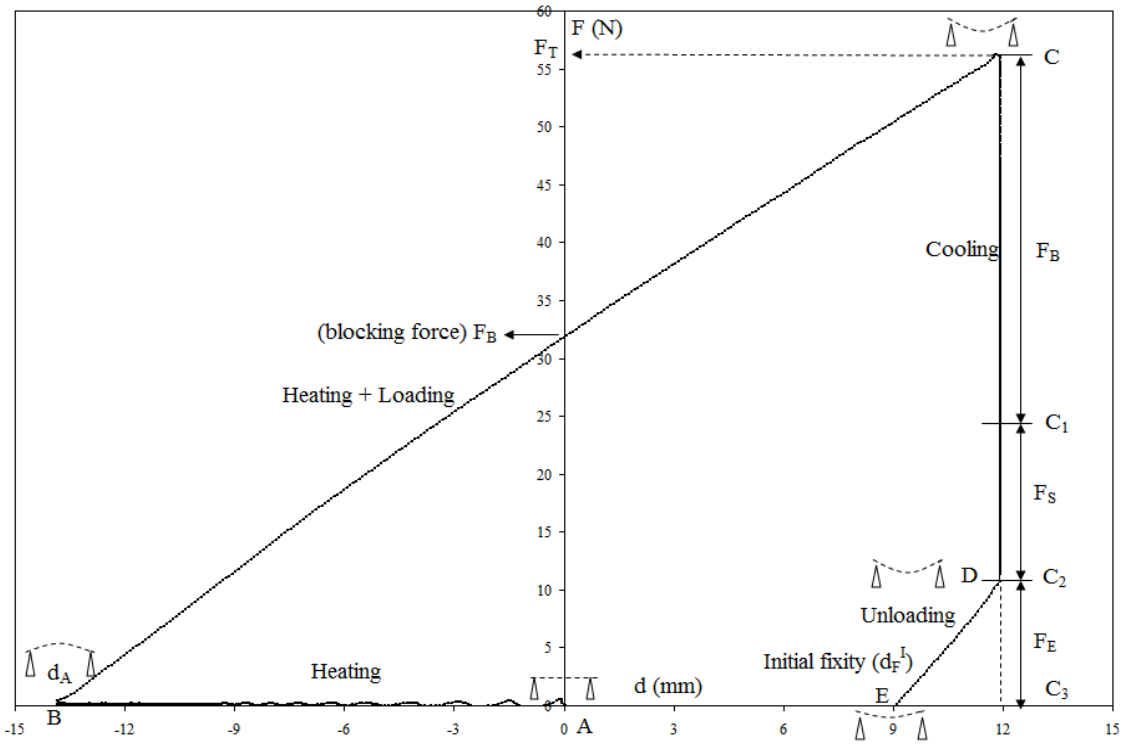

Figure D.1. Programming cycle for CBCM

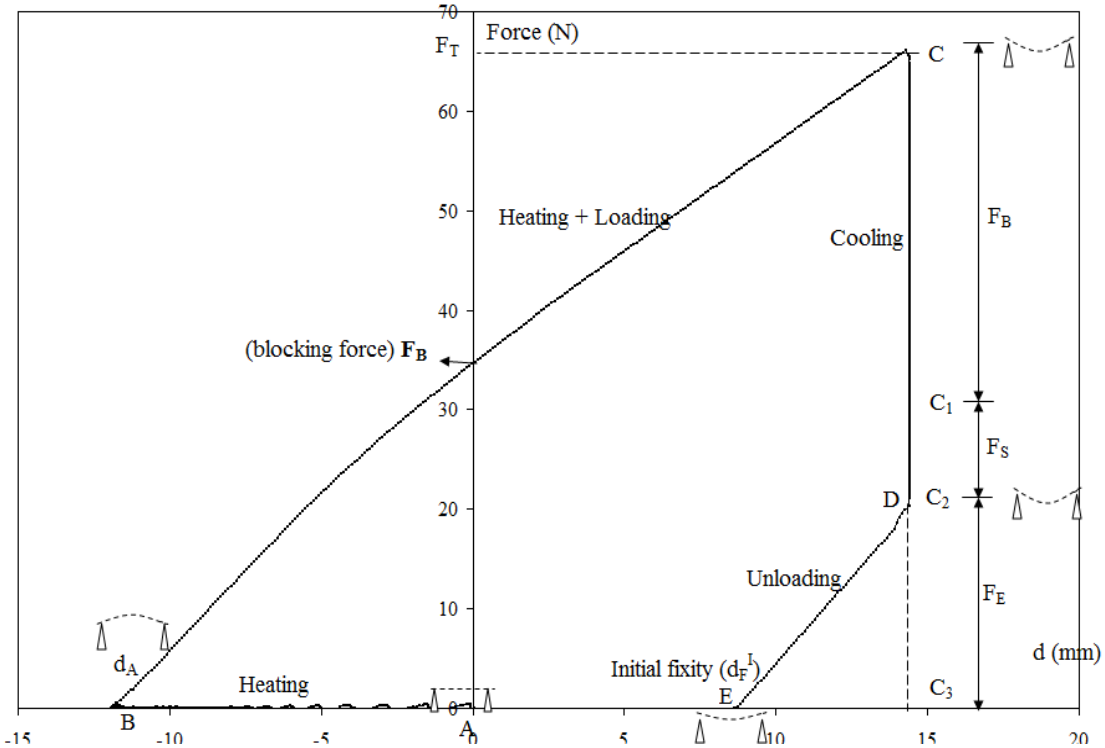

Figure D.2. Programming cycle for CBCM [1/2]

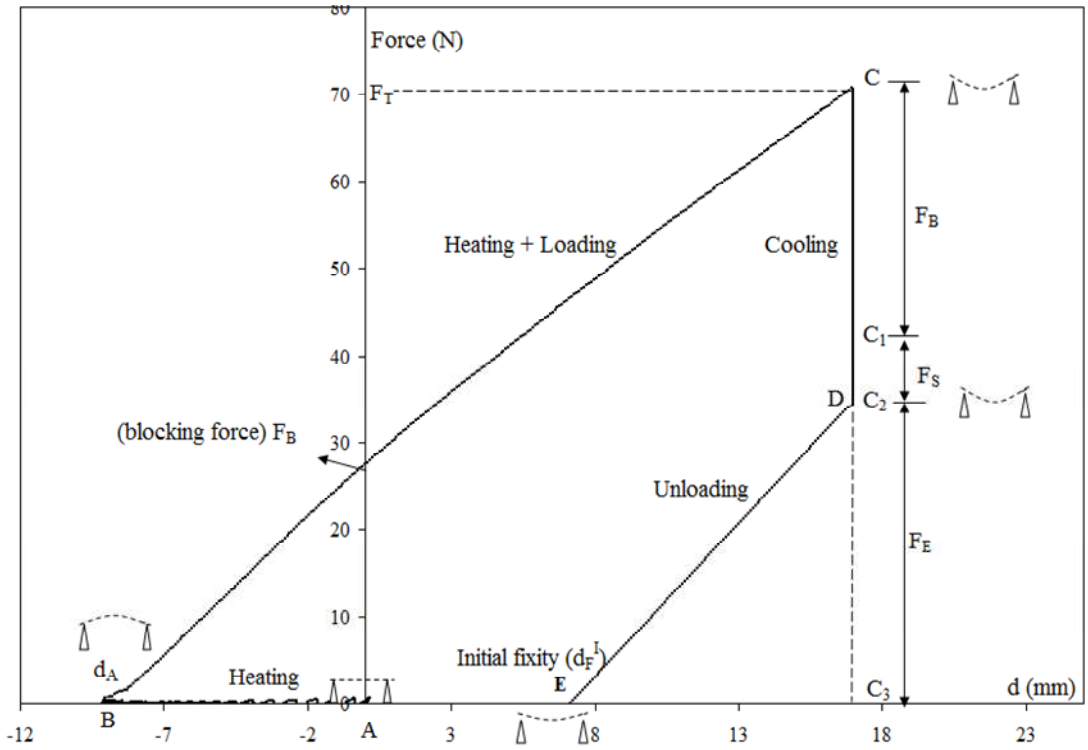

Figure D.3. Programming cycle for CBCM$_{1/2}$

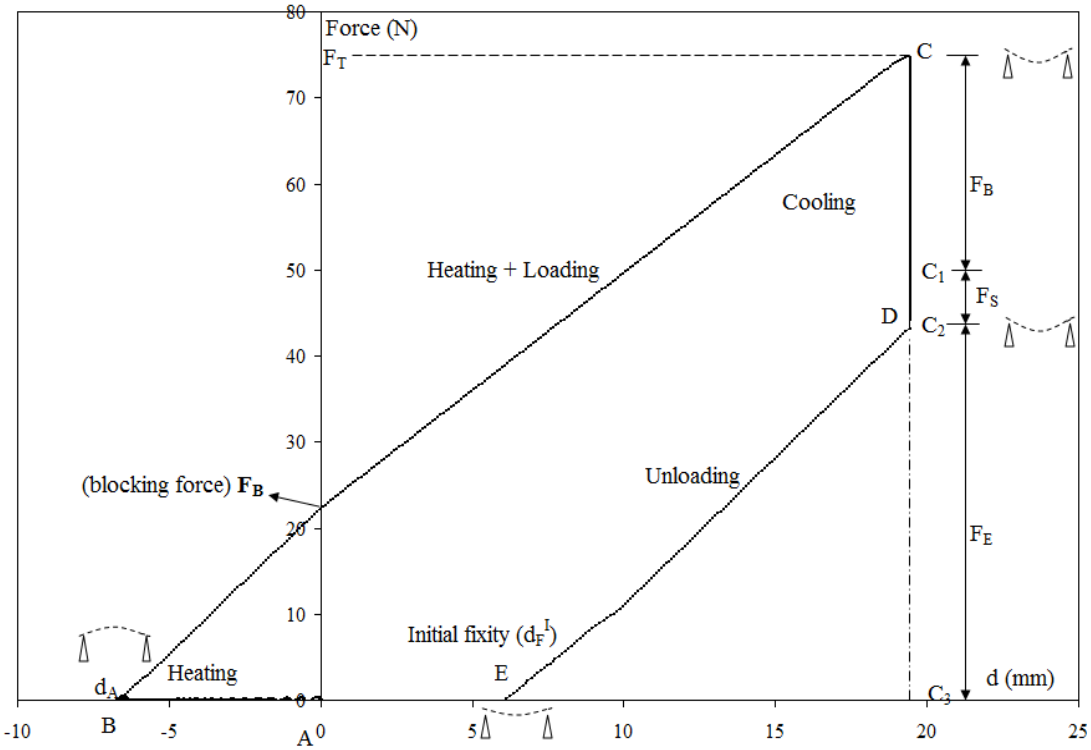

Figure D.4. Programming cycle for CBCM-L

Appendix-E

One-step recovery for CBCM

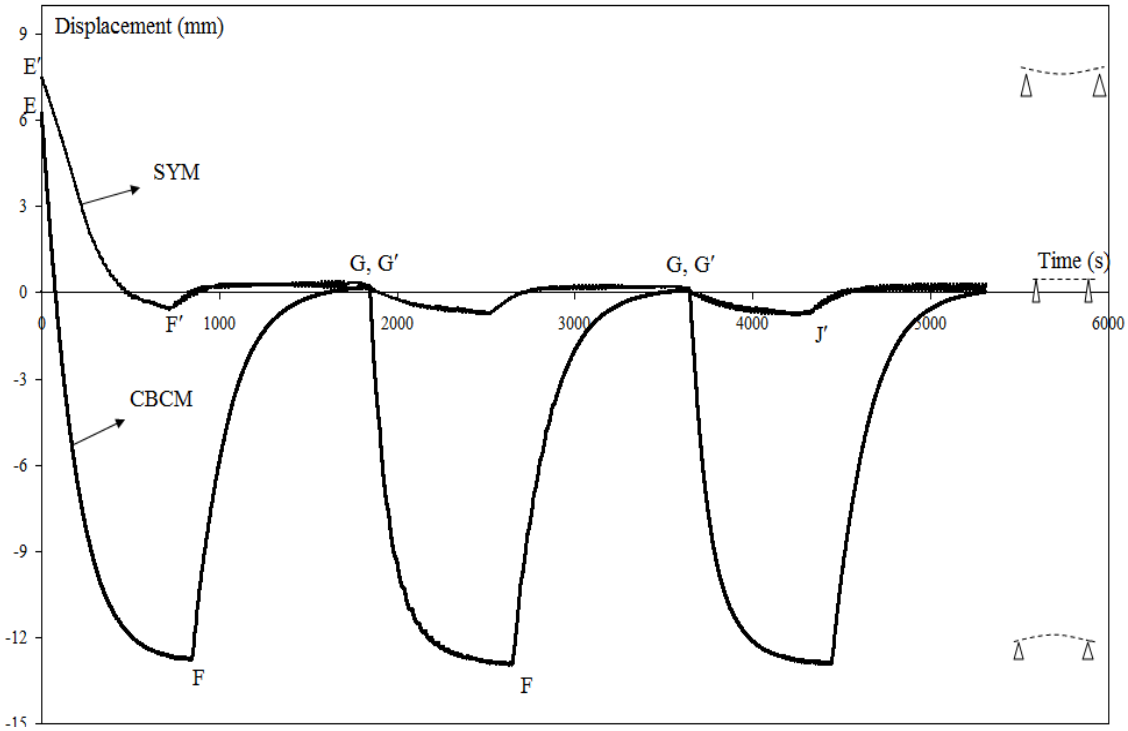

Figure E.1 One-step unconstrained recovery at 150°C for CBCM and SYM; (E, E′= Initial fixities; EF, GF = Heating during recovery; FG Cooling during recovery); d_{RT} for CBCM is 19.62 ± 0.33 mm and for SYM is 1.83 ± 0.18 mm

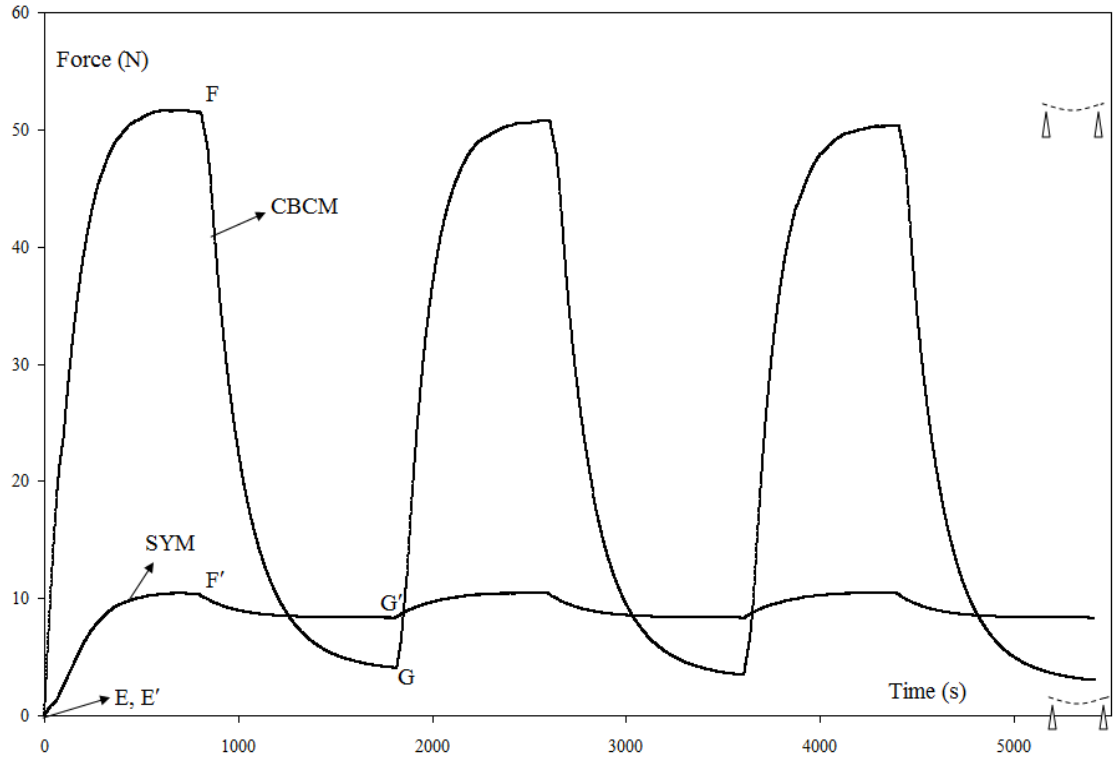

Figure E.2 Constrained recovery at 150°C; (E, E´= fixities; EF, GF = Heating during recovery; FG Cooling during recovery); F_{RT} for CBCM is 51.31 N ± 1.07 and for SYM is 2.56 ± 0.15 N